THERMODYNAMIC MEASUREMENTS BY GAS-LIQUID CHROMATOGRAPHY

by

A.B. SUNAL, B.Sc.

A Thesis submitted to the Faculty of Engineering of the University of Aston in Birmingham for the degree of Doctor of Philosophy.

Department of Chemical Engineering,
University of Aston in Birmingham.

October 1973.

1. SUMMARY.

The aim of the first part of this work was to provide solubility data for the large scale continuous and semi-continuous gas liquid chromatographs (G.L.C.) in operation in this department by using analytical G.L.C. equipment.

A commercial dual-channel chromatograph was modified to enable the partition coefficients of various solutes in polymer stationary phases to be measured at finite concentrations of the solute. The technique chosen was "Elution on a Plateau" in which the chromatographic column is first equilibriated by a carrier gas (nitrogen) containing the solute vapour. The partition coefficient of the solute is then calculated by measuring the elution volume of a small sample of the solute injected. The systems studied were:-

1. a) α-Pinene/Polypropylene Sebacate at 99.8, 120.0, 140.0, 150.0°C.
   b) β-Pinene/Polypropylene Sebacate at 100.3, 110.1, 120.0, 150.0°C.

2. a) Dichloro Methane/Silicone Oil MS 200 at 24.8, 29.1, 34.7, 39.8°C.
   b) 112, Trichloro trifluoro Ethane (Arklone-P)/Silicone Oil MS 200 at 24.8, 29.1, 34.7°C.
   c) 111, Trichloro Ethane (Genklene-P)/Silicone Oil MS 200 at 34.7, 45.1, 60.5, 74.0°C.

A limited amount of ternary data was also obtained whereby the infinite dilution partition coefficient of a third component was measured in the presence of the finite concentrations of the other two components, one of which was the stationary phase. In each case the partition coefficients were found to increase linearly with the gas phase concentration of the solute within the gas phase concentration ranges studied ($0\text{-}3\times10^{-4}$ g/cm^3 for Systems 1 and $0\text{-}5\times10^{-4}$ g/cm^3 for Systems 2).

Activity coefficients were calculated from the partition coefficients by using the known molecular weights of the solutes and the stationary phases and the vapour pressures of the solutes. For the binary systems the activity coefficients were correlated by means of the single and two-parameter Flory-Huggins Equation, the parameters being evaluated in this work. In each case the fit was very good, suggesting that this equation is adequate in describing the behaviour of these polymer solutions where polar interactions are moderate or small. The data of Systems 2 was also correlated by the binary Heil Equation with a similar accuracy to that of the Flory-Huggins Equation.

The ternary form of the Flory-Huggins equation was fitted to the ternary data and by using the previously calculated binary parameters the solute-solute interaction parameters were estimated.

The second part of this work was concerned with studying the separating efficiency of a rotating gas liquid chromatographic unit. This consisted of 44 20cm long, 2.5 cm ID tubes arranged in a circular bundle that rotated in the opposite direction to the flow of the carrier gas. The liquid feed, commercial turpentine with α and β pinenes as the major components, was continuously fed somewhere in the middle and the gas flow rate and the speed of rotation were adjusted so that the least absorbed component (α-pinene) moved with the gas phase, while the other component (β-pinene) was carried along with the packing. This second component was then stripped off in a different section of the bundle.

The inlet and off-take operations relied on the seal between stationary graphlon rings and the rotating surface of the bundle. A complete seal was found to be impossible to achieve with a minimum of 5% carrier gas leakage, while up to 50% of the feed was lost. Therefore, only a few runs could be conducted which showed that a steady state

operation was impossible under these circumstances. Although this meant a partial defeat of the objective of the first part of the work, some valuable information was gained about the operation of this type of semi-continuous countercurrent equipment.

ACKNOWLEDGEMENTS

The Author wishes to express his grateful thanks to the following:

Professor G.V. Jeffreys and the Department of Chemical Engineering for providing research facilities.

Professor P.E. Barker, who supervised the work, for his assistance and encouragement.

The technical staff of the department for providing technical assistance.

Sümerbank of Turkey for the provision of a scholarship.

My parents for their encouragement and financial support.

CONTENTS

2. INTRODUCTION.

With the discovery of gas chromatography by James and Martin (2), scientists almost immediately saw the possibility of extending this important analytical technique to preparative separations. In contrast to analytical chromatography, the primary consideration in preparative chromatography is throughput. The high efficiency of the former process is made possible to a large extent by the minute sample size required. Direct scale-up of analytical systems to handle preparative size samples, although common, always results in a significant deterioration of the quality of separation, leading to impure fractions and negating many of the advantages assumed for gas chromatography over the other separation methods.

In considering the efficiency of preparative gas chromatography, two points are relevant; 1) excess feed volume, 2) high solute concentration in the stationary phase that may lead to a non-linear partition isotherm. The second point is particularly important because not only does it cause band broadening with consequent overlapping, but it may also effect the value of the separation factor (α), defined as the ratio of the partition coefficients. In fact, theoretical studies by Sawyer and Hargrove (183) indicated that the maximum sample size that can be used without adversly effecting the intrinsic theoretical plate height of the column is limited by the solution considerations rather than the feed volume considerations.

From the preceding arguments it is obvious that a knowledge of vapour liquid equilibria is essential to the design and operation of a preparative gas liquid chromatography equipment as in other unit operations. Such information can be obtained from analytical scale gas chromatography (G.L.C) in the first place. This possibility has been appreciated since the early days of gas chromatography (2,184,185). Martin and Synge (186) in their pioneering work on gas-liquid

chromatography, developed an expression relating the retention volume of a solute (V_R) to its partition coefficient (K) by using a theoretical plate model

$$V_R = V_g + KV_L \qquad (2.1)$$

where V_g is the gas hold up of the column

V_L is the liquid volume in the column

Partition coefficients obtained from equation (2.1) have been shown to be consistent with the partition coefficients obtained from static measurements (187, 188).

The GLC technique has also been applied to the determination of other thermodynamic quantities such as activity coefficients, excess enthalpies and entropies of solution etc., in all of which the starting point is the measurement of the partition coefficient, but equation (2.1) is strictly confined to infinite dilution conditions and so the thermodynamic properties at other concentrations must be calculated from predicting equations such as Van Laar and Margules. Implicit in such a procedure is the assumption that the particular equation used applies to the system under study.

The realisation was soon made, however, that the GLC technique need not be limited to the infinite dilution conditions. The work of several authors, notably of Conder and Purnell (12,33), has led to the development of accurate theoretical equations as well as several experimental techniques that can be used at finite concentrations of the solute. Since the first priority in any such development is the establishment of the validity of the method, until very recently most of the work had been confined to the systems for which the data was available from other sources for comparison. This invariably meant the exclusion of such complex systems as polymer solutions for which the theoretical treatment is

difficult and the data is scarce, as they are hardly ever used in other unit operations.

The present work was initiated with the aim of providing vapour-liquid equilibrium data for the preparative scale chromatographs used in this work as well as by other workers in this department. As the liquid phases employed were highly polymeric in nature, the data obtained also made it possible to test the applicability of some of the solution theories specifically proposed for mixtures whose components greatly differ in size.

Over the past two decades the attempts at improving the throughputs of preparative scale chromatographs have concentrated on two distinctive processes. The first process is a direct scale up of the analytical technique with the accompanying problem of reduced efficiencies as a result of increased diameter. The second is a continuous countercurrent process whose advantage lies in fuller utilisation of the packing. The binary mixture to be separated is fed continuously into the middle of the column. The relative flow rates of the two phases are adjusted so that the less soluble component travels in the direction of the gas flow and the other is carried with the liquid phase. The more soluble component is then stripped off the liquid phase in a different section of the column assisted by heat or an excess gas flow rate. A most common means of achieving this operation has been the moving bed principle where the packing is allowed to fall through a vertical column under gravity (167-169, 177).

The rotating chromatograph used in this work is an extension of the above principle and one which eliminated the problems of solid handling encountered in moving bed techniques and also offered the advantage of compactness. However, it proved to be mechanically unreliable and the objective of the experimental work was limited to a greater understanding

of the principle of its operation. For this purpose a small section is provided at the end of the text where the theoretical and practical implications of the sequencing nature of the operation is discussed.

PART 1

THERMODYNAMIC MEASUREMENTS BY GLC

3. LITERATURE SURVEY.

In the last two decades gas chromatography (GC) has established itself as a powerful analytical technique. In addition to this, in recent years considerable research and development has been channelled into two other fields. The first one is a logical development of analytical GC through scale-up and automation in order to separate materials on a preparative and production scale. Since the separation of a mixture depends on the thermodynamic properties of the materials involved and kinetic processes in the column, there arises the second possibility, the measurement of physical properties.

The subject of physical measurements by GC can be divided into two general areas of study, (1) kinetic processes, (2) equilibrium processes. Kinetic processes (mass transfer between the phases, diffusion etc.) have been investigated primarily to improve the efficiency of the chromatographic separation. The very complex nature of the chromatographic process has necessarily forced simplifications on the various rate equations proposed. Therefore, it is impossible at this stage of development to measure the kinetic factos involved with any degree of reliability.

Since the basic process of chromatography is an equilibriation of one or more solutes between two immiscible phases, GC may be used to measure physical parameters normally measured by vapour pressure, solubility or compressibility measurements. Activity coefficients, second virial coefficients of gas mixtures, partition and adsorbtion isotherms are the most commonly measured thermodynamic quantities by GC. Other properties such as excess enthalpies, entropies and free energies of solutions can be measured by studying the temperature dependence of the activity coefficient.

It is the purpose of this review to show how these thermodynamic properties can be measured and interpreted by gas chromatography, and particularly gas-liquid chromatography (GLC). A review of the literature

shows that most of the early work was done at conditions approximating to infinite dilution. Finite concentration work was, and to some extent still is, concentrated on gas-solid chromatography with the main purpose of measuring surface areas of solid catalysts. In the GLC work the aim has been to establish GLC as a valid method with its obvious advantage of speed. Most of the work, therefore, is concentrated on systems where static data is available or on simple systems such as alkane mixtures where the well tested solution theories are known to apply. Consequently there is almost a complete absence of work on systems containing polymers which are possibly the most commonly used stationary phases both in the analytical and preparative field.

3.1 Sorption Isotherm from Retention Data.

According to several GC theories (1,2) the relationship between the partition coefficient (K) of a solute between a non-soluble gas and a solvent and the solute's retention volume (V^o_N) is given by,

$$V^o_N = J_3^2 V_N = J_3^2 (V_R - V_g) = KV_L \qquad (3.1.1)$$

where V^o_N = corrected net retention volume

V_R is the total retention volume = $F^o t_R$

F^o is the flow rate of the mobile phase measured at the column outlet

t_R is the retention time

J_3^2 is the James-Martin compressibility factor and is given according to the general formula

$$J_n^m = \frac{n}{m}\left[\frac{(pi/po)^m - 1}{(pi/po)^n - 1}\right]$$

pi and po are the column inlet and outlet pressure respectively

The partition coefficient is defined as:

$$K = \frac{q}{c} = \frac{\text{concentration of solute in stationary phase}}{\text{concentration of solute in mobile phase}}$$

There are several assumptions in the derivation of the above equation that must be recognised and if possible removed in order to carry out accurate measurements of the thermodynamic properties:

1. Non-linearity of the sorption isotherm.
2. Sorption effect.
3. Gas phase non-ideality and compressibility.
4. Liquid surface and solid surface adsorption.

These assumptions and their implications are briefly discussed in the following sections.

3.1.1 Non-Linear Isotherm.

Although equation (3.1.1) holds true for a linear isotherm at all concentrations, Helferich (3) showed by mathematical and intuitive arguments that in the more general case, the retention volume must be related to the slope of the partition isotherm and not the partition coefficient itself. That is,

$$V^{o}_{N} = V_{L} \left(\partial q/\partial c\right)_{c} \qquad (3.1.2)$$

At infinite dilution equation (3.1.2) becomes identical with equation (3.1.1) as $\left(\partial q/\partial c\right)_{c \to o} = q/c$. But the difference may be appreciable at finite concentrations depending on the curvature of the isotherm.

If the skew ratio, R, is defined as the ratio of the magnitudes of the slopes of the trailing and leading edges of a chromatographic peak at their points of inflection, then one would expect R to be greater than unity (self sharpening trailing edge) for anti-Langmuir type isotherms and less than unity (self sharpening leading edge) for Langmuir type isotherms (1). Since anti-Langmuir type isotherms are usually associated with positive deviations from Raoult's law and vice-versa, the direction of the peak assymetry should provide a good guide to the

solution behaviour. In most GLC systems, however, where liquids of widely different molecular size are involved, the occurrence of skew ratios greater than unity is considered normal for all moderate deviations from Raoult's law (4,5).

3.1.2 Sorption Effect.

Equations (3.1.1) and (3.1.2) are based on the assumption that mobile phase (solute and carrier) velocity remains constant throughout the region of a solute boundary. The work of several authors (6-8) leads to the following equation for the variation of flow rate due to the movement of the solute molecules across the interface (sorption effect):

$$\frac{F(y)}{F(o)} = \frac{1+k}{1+k(1-y)} \qquad (3.1.3)$$

and for the retention volume

$$V^{o}_{N} = V_{L}(1-y)(\partial q/\partial c)_{c} \qquad (3.1.4)$$

where $F(y)$ is the total flow rate reduced to outlet pressure conditions

$F(o)$ is the carrier gas flow rate reduced to outlet pressure conditions

y is the mole fraction of the solute in the mobile phase at the concentration c

k is the mass ratio defined as:

$$\frac{\text{mass of solute in the stationary phase}}{\text{mass of solute in the gas phase}}$$

It is seen from equation (3.1.3) that the sorption effect causes an increase in the total flow rate with concentration. It is interesting to compare the influence of the sorption effect on the shape of a chromatographic boundary with that of a non-linear isotherm. While the sorption effect always causes the sharpening of the leading boundary ($R < 1$) as the regions of higher concentration move faster than those at lower

concentration, the non-linear isotherm augments or counteracts this depending on the conditions laid in the previous section. Since the effect of a non-linear isotherm is most likely to be $R > 1$, it is quite possible to observe symmetrical peaks with non-ideal systems.

The value of y used in the above equations is a mean value over the length of the column, as in a moving mobile phase zone of constant concentration it increases as the pressure falls along the length of the column. This is more fully dealt with in the next section.

3.1.3 Gas Phase Non-ideality and Compressibility.

To correct for the non-ideality of the mobile phase Desty et al (9) and Everett and Stoddard (10) assumed that the equation of state of a slightly imperfect gas could be expressed as:

$$P = \frac{nRT}{V} + \frac{RT}{V}\sum_{ij} B_{ij}\, y_{ij} \qquad (3.1.5)$$

where $\sum_{ij} B_{ij}\, y_{ij}$ is the second virial coefficient of the binary mixture (i+j)

The effect of pressure on the retention volume is then given by

$$\ln V^{o\infty}_{N}(P) = \ln V^{o\infty}_{N}(0) + \frac{(2B_{12} - \bar{V}_1^{\infty})}{RT} P_o\, J_3^2 \qquad (3.1.6)$$

where B_{12} is the second cross virial coefficient

$\bar{V}_1^{\infty}$ is the partial molar volume of the solute at infinite dilution

$V^{o\infty}_{N}(P)$ and $V^{o\infty}_{N}(0)$ are the corrected net retention volumes at pressure P and zero pressure respectively.

Everett (11), who further considered the effect of pressure on the partition coefficient, suggested that J_3^2 should be replaced by J_4^3. The difference is, however, negligible near atmospheric pressure. Conder and Purnel (12) carried out a similar treatment at finite concentration to arrive at the following equation,

$$V^{o}_{N} = V_L (1 - aJy_o) (\partial q/\partial c)_c, \; p = P \qquad (3.1.7)$$

where y_o is the mole fraction of solute in the gas as measured at the column outlet.

The exact forms of a and J are given in Appendix 1. It is sufficient to say that at small values of y_o and near atmospheric pressure the following approximations can be made without introducing a significant error into the calculations

$$J \rightarrow J_3^2 \qquad a \rightarrow 1 \qquad P \rightarrow p_o J_4^3 \qquad (3.1.8)$$

The factor of the form $(1 - y_o)$ arises from the sorption effect while the exact form of aJy_o arises from the mobile phase imperfection.

3.1.4 Liquid Surface and Solid Surface Adsorption.

In 1961 Martin (13) proposed that adsorption on the liquid phase - gas phase interface contributed to the net retention volume of a solute and proposed the following equation for the retention volume

$$V^{o\infty}_{N} = K^{\infty}_{L} V_L + K^{\infty}_{a} A_L \qquad (3.1.9)$$

where K^{∞}_{L} is the bulk liquid partition coefficient

V_L is the volume of the bulk liquid

K^{∞}_{a} is the Gibbs adsorption coefficient

A_L is the liquid surface area.

Subsequent studies (14-18) repeated the original work and confirmed the value of the bulk liquid partition coefficient, but some doubt remains about the true value of K^{∞}_{a}. The discrepancy is explained in terms of the different values of the liquid surface area measured by two different techniques. With the nitrogen adsorption technique there is no certainty that the surface areas measured are, in fact, the relevant values because of the different sizes of the nitrogen and the solute molecules (19). With surface tension measurements, on the other hand, there is some doubt

as to the applicability of the Gibbs adsorption formula, equation (3.1.10), to GLC

$$\Gamma_2^{(1)} = -\frac{1}{RT}\left(\frac{\partial \varphi}{\partial \ln a_L}\right) \qquad (3.1.10)$$

where $\Gamma_2^{(1)}$ is the excess liquid surface concentration

φ is the surface tension

a_L is the bulk liquid concentration.

Martire (20), for example, has pointed out that equation (3.1.10) is derived for plane interfaces and may be safely applied to curved interfaces provided that the thickness of the film is negligible with the radius of its curvature. In GLC, therefore, where a non-uniform film is spread throughout narrow poles of various contours, the case is ill-defined.

In each of the studies a "polar" stationary phase with non-polar solutes were used. The suggestion was originally made (13,14) that the Gibbs adsorption would be observed only with such systems where a preferential orientation of the solute molecule at the surface of the highly polar solvent might be expected. Later (16,17,19) this statement was generalised to include not only polar solvents but also any system where the solubility of the solute in the solvent is very low, that is a high activity coefficient. This generalisation is also supported by the earlier findings of Ashworth and Everett (21) and Cruinckshank et al (22) who, working with non-polar - non-polar systems, did not observe any Gibbs adsorption effects.

Gibbs adsorption is not, however, the only source of adsorption in GLC. Urone and Parcher (23,24) studied the retention volume behaviour of polar solutes in the non-polar solvent squalane and concluded that there was a substantial adsorption on the solid surface. At least two

mechanisms may be involved in the adsorption process: a) the support adsorbs some of the solute dissolved in the liquid surface, b) the support disturbs the physical state of the liquid inducing specially orientated dipoles thus increasing the value of the partition coefficient. The first effect may predominate at high liquid loadings, while the second would be more probable at liquid phase coverage up to 5 molecular layers.

In view of the experimental evidence presented it is obvious that in systems where both the liquid surface and the solid surface adsorption are present the use of equation (3.1.7) may cause large errors in the calculated values of the bulk partition coefficient (25,26). Purnell and co-workers (27,28) considered all possible causes and combinations of adsorption in GLC and proposed the following equation

$$V^{o\infty}_N = K^{\infty}_L V_L + K^{\infty}_a A_L + K^{\infty}_s A_s \qquad (3.1.11)$$

This equation can be arranged to give

$$V^{o\infty}_N / V_L = K^{\infty}_L + (K^{\infty}_a A_L / V_L) + (K^{\infty}_s A_s / V_L) \qquad (3.1.12)$$

where K^{∞}_s and A_s are solid surface adsorption coefficient and area respectively.

Thus, if a number of identical columns with different loadings are employed K^{∞}_L can be obtained from a plot of $V^{o\infty}_N / V_L$ against $1/V_L$. If A_L is measured independently then both K^{∞}_a and $K^{\infty}_s A_s$ can also be found.

Equations (3.1.9) and (3.1.11) both only apply at infinite dilution characterised by symmetrical peaks. If assymetric peaks are observed at the smallest practical sample size then one of the two methods can be applied depending on whether it is a solution dominated peak (anti-Langmuir type, $R > 1$), (29), or an adsorption dominated peak (Langmuir type, $R < 1$), (19,30). Both methods are, essentially, a graphical extra-

polation to $^{1}/V_{L} = 0$. A third method was proposed by Martire (31) which depends on the convergence of computer iterations. Though the results agree with the other two methods, the theoretical basis for it is not clear.

3.2 Experimental Techniques of Measuring Sorption Isotherms at Finite Concentrations.

Early workers in this particular field of GC limited their measurements to infinite dilution conditions. As more confidence built up in GC as a valid method of measuring thermodynamic properties, more attention was turned to the possibility of carrying out the same measurements at higher concentrations. As a result more realistic theories were developed and the experimental techniques became more refined. The former development was described in the previous sections. In this section a review of the most commonly used techniques is given.

The present day techniques can broadly be classifiied into two types a) frontal techniques, b) elution techniques. These are then sub-divided according to the method of calculation employed.

3.2.1 Frontal Analysis by Characteristic Point (FACP). (32-37)

The method was first described by Glueckauf (34,35) for measuring the partition isotherm in liquid-solid chromatography. Glueckauf's treatment, therefore, omits the particularly relevant factors to GC. For this reason the procedure adapted by Stock (36), who applied Glueckauf's equation to gas-solid chromatography, allows accurate measurements only at low concentrations.

Essentially, the pure carrier gas and the carrier gas containing the solute vapour are alternately fed into the column by means of a switching device. Switching results in the formation of positive or negative step-like concentration change. Experiments (32,33) have shown that the input

profile is not always sharp and therefore it is essential to take account of this fact when using this technique by employing a second detector at the inlet of the column. To measure the partition isotherm, a boundary covering the concentration range required is passed into the column. Referring to Fig.(3.2.1), several points X, each corresponding to a particular concentration c, are chosen, and lines XF parallel to the time axis are drawn. The liquid phase concentration q is then calculated from the numerical integration of the following equation,

$$q = \frac{1}{V_L} \int_0^c \frac{V^o N}{(1 - Jy_o)} \, dc \qquad (3.2.1)$$

A rough estimate can be obtained, however, by measuring the area HGEX (36). Conder and Purnell (33) have analytically integrated equation (3.2.1) for cases where the retention time is at least ten times greater than the gas hold-up, and the pressure drop is less than 5% of the inlet pressure.

3.2.2 Frontal Analysis (FA). (32,33,38-41)

Just as in the previous method the pure carrier gas and the carrier gas containing solute vapour is led into the column alternately until the equilibrium is achieved. Referring to Fig. (3.2.1) again, the mass balance over the column dictates that the shaded area A (A′ for the desorption boundary) represents the amount of solute sorped in the stationary phase. As in FACP this method is only approximate as it ignores the variation of flow rate as the boundary emerges from the column due to sorption effects. A better accuracy is achieved by the use of equation (3.2.1) by replacing c by $\bar{c}$, the plateau concentration. With this method a number of runs must be made at different carrier gas concentrations to cover the concentration range required.

3.2.3 Elution by Characteristic Point (ECP). (33,42-44)

In this method, first described by Cremer and Huber (42), a large elution peak is passed through a column. The emerging peak is regarded as composed of two separate boundaries, one diffuse and one self sharpening. The equation derived by Cremer and Huber (42) to calculate the adsorption isotherm from the diffuse side of the peak is

$$a = \int_0^{\bar{p}} V_G^\circ \, dp \qquad (3.2.2)$$

where a is the adsorbate concentration in adsorbent

p is the partial pressure of adsorbate in the mobile phase

V_G° is the retention volume per gram of adsorbent.

The integration in equation (3.2.2) corresponds to the shaded area in Fig. (3.2.2). Therefore, taking different heights on the boundary and measuring the appropriate area, the complete isotherm can be obtained from a single experiment. This treatment does not, however, take into account gas compressibility, sorption effect and non-sharp input profile. More accurate results are obtained through the use of equation (3.2.1). ECP is greatly limited by the concentration range covered by the emergent peak as this may be many orders of magnitude smaller than the input concentration. Furthermore, because the concentration change is small, non-ideality (diffusion, slow mass transfer) can greatly effect the accuracy of the results especially at low concentrations (44).

3.2.4 Elution on a Plateau (EP). (7,33,45-48)

In this method the column is first equilibrated with a carrier gas containing the solute vapour, at a constant concentration. The partition coefficients are then calculated from the retention volume of a small negative or a positive peak, depending on whether the sample concentration is smaller or greater than the plateau concentration, Fig. (3.2.3).

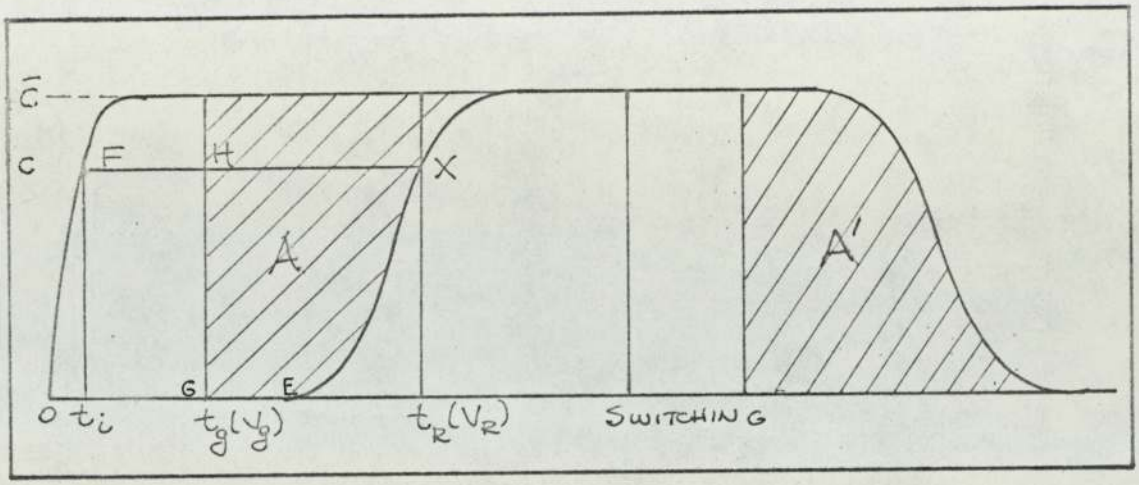

FIG. 3.2.1 - FRONTAL ANALYSIS AND FRONTAL ANALYSIS BY CHARACTERISTIC POINT

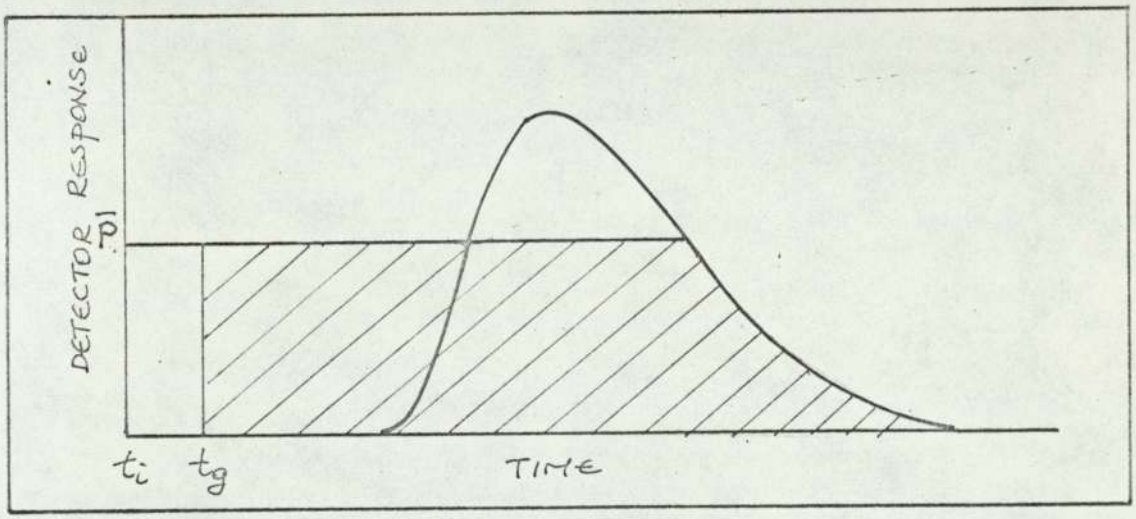

FIG. 3.2.2 - ELUTION BY CHARACTERISTIC POINT

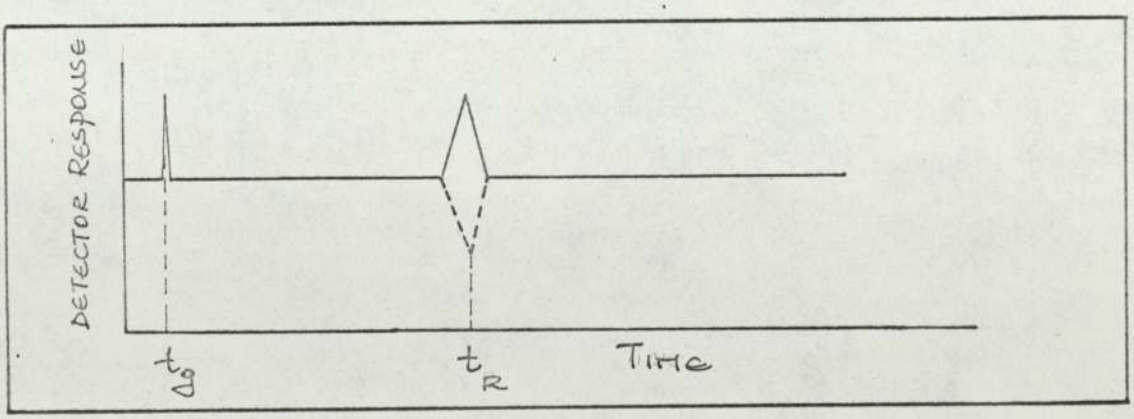

FIG. 3.2.3 - ELUTION ON A PLATEAU

Provided that the peak height is small compared with the plateau height, the partition coefficient calculated through the use of equation (3.2.1) corresponds to the plateau concentration. Of course, several runs must be performed to determine the partition isotherm in the concentration range required. This technique is particularly useful in the study of multi-component mixtures which can be achieved by simply changing the composition of the carrier gas (46,47).

3.2.5 Elution of Isotopes (EI). (3,7,46)

The experimental technique is exactly the same as in EP, but instead of the injected samples containing the solute under consideration, it contains an isotope of it. The partition coefficient, K, is then calculated from

$$V^{o}_{N} = KV_{L} \qquad (3.2.3)$$

The discrepancy between this equation and equation (3.2.1) arises from the fact that while the former describes the movement of individual molecules, the latter describes the movement of a disturbance created by the injection (3,7). Although the calculations are simpler than the other methods, the use is limited by the necessity to use special detectors and by the availability of suitable isotopes. This technique was used by Gilmer and Kobayashi (46) in the study of the adsorption behaviour of propane-methane mixtures on Silica Gel.

3.2.6 Analytical Method.

This technique differs from the others in that it does not depend on retention volume measurements, but rather makes use of the rapid and accurate analysing capability of GLC.

In a method described by Burnett (49), partition coefficients were calculated from the rate of removal of a solute from a known amount of diluted solution by an inert gas by analysing the gas stream every few

minutes. Katayama (50) and co-workers, on the other hand, used GLC to analyse the vapour phase concentration of a system equilibrated in a static apparatus.

3.2.7 Choice of Technique.

For all the methods described the common starting point for the calculation is equation (3.2.1) or a modification of it. Due to various approximations in its derivation, this equation is limited to a maximum value of y (mole fraction in the gas phase) in the range of 0.65 - 0.95 depending on the nature of the components (32). ECP and FACP methods also suffer from the effects of non-ideality on the shape of the boundary, especially at low concentrations. Even in FA, if the graphical method of calculation is used, considerable error may be introduced if the tailing is excessive, making it difficult to measure the area A in Fig. (3.2.1). Both EP and EI are free of these errors because the non-ideality causes symmetrical broadening of the peak without effecting the elution time of its maximum. Another difficulty with ECP, FA and FACP techniques, is the variation of the effluent flow rate as a peak or a single boundary progresses along the column. This is caused, in addition to sorption effects , by the difference in the viscosity between the pure carrier gas and the carrier gas and solute vapour inside the boundary. Several workers (37,51,52) have investigated this phenomenon and their treatments in general give qualitative agreement with their observations, though no exact theory has, so far, been developed.

One practical difficulty arises, in the case of frontal methods, from the need to keep the flow rate constant on switching. In practice elaborate precautions are taken in building dual circuits in an effort to match the flow resistances (32, 53). Even then a perfect matching is almost impossible mainly because of the viscosity change (53).

The highest accuracy is expected from EP, EI and FA techniques, but

they take considerably longer to apply as a separate run is required for each point on the isotherm.

The choice of the Elution-on-Plateau technique for this work was based on the foregoing arguments as well as on the considerations of the adaptability of the available Perkin Elmer F11 chromatograph. For example, it was found that the passage through the injection head caused considerable tailing, effectively ruling out the FACP technique.

3.3 Activity Coefficient.

The thermodynamic solution to the phase equilibrium was obtained many years ago by Gibbs (54) when he introduced the abstract concept of chemical potential (μ_i) which can be defined in terms of the Gibbs Free Energy as,

$$\mu_i \equiv \bar{g}_i \equiv \left(\frac{\partial G}{\partial n_i}\right)_{T,P,n_i \neq j} \qquad (3.3.1)$$

where $\bar{g}_i$ is the partial molar Gibbs Energy

n_i is the number of moles of component i

In attempting to simplify the abstract equation of chemical equilibrium, Lewis (55) first considered the chemical potential for a pure, ideal gas then generalised to all systems by defining a function f, called the fugacity, by writing for an isothermal change for any component in any system,

$$\mu_i - \mu_i^{o} = RT \ln f_i/f_i^{o} \qquad (3.3.2)$$

where 'o' refers to the standard state of i which is usually taken to be the pure state of i at the temperature and pressure of the system.

For a pure, ideal gas the fugacity is equal to the pressure (P), and for a component i in a gas mixture it is equal to its partial pressure, Py_i. Since all systems, pure or mixed, approach ideal gas behaviour at very low pressure, the definition of fugacity is completed by,

$$\frac{f_i}{y_i P} \rightarrow 1 \quad \text{as } P \rightarrow 0 \qquad (3.3.3)$$

Lewis called the ratio, f_i/f_i°, the activity, a. The activity coefficient of a component i is then defined as the ratio of its activity to its mole fraction.

$$\gamma_i = \frac{a_i}{x_i} = \frac{f_i}{f_i^{\circ} x_i} \qquad (3.3.4)$$

If an ideal solution is defined as one where the activity coefficient, γ_i, is unity, then this, combined with the present choice of standard state, makes the activity coefficient a criterion of non-ideality in the sense of deviations from the Raoult's Law of ideal solutions.

When two phases are at equilibrium the equilibrium criterion requires that the chemical potential of each component be the same in both phases. In the case of vapour-liquid equilibrium this gives,

$$\mu_i^L = \mu_i^V \qquad (3.3.5)$$

where L and V refer to the liquid and vapour phase respectively.

The substitutions of equations (3.3.2) and (3.3.4) thus gives

$$\gamma_i^L = \frac{f_i^V}{f_i^{\circ} x_i} \qquad (3.3.6)$$

where x_i is the mole fraction of component i in the liquid phase.

3.3.1 Correction for Vapour Phase Non-Ideality.

If the gas phase is assumed to obey the ideal gas laws it can be shown that equation (3.3.6) can be approximated by

$$\gamma_i^L = \frac{P y_i}{P_i^{\circ} x_i} \qquad (3.3.7)$$

The most accurate measurements are carried out, however, by using the virial equation of state along with extrapolation to zero pressure. Several authors (11,56,57) have shown that for a binary mixture at finite

concentration the activity coefficient reduced to zero pressure is given by

$$\ln \gamma_1(0) = \ln(Py_1/P_1^{\circ}x_1) + (P/RT)\left[B_{11} - (1-y_1)^2(B_{11} - 2B_{12} + B_{22}) - \bar{V}_1\right] - P_1^{\circ}/RT\,(B_{11} - V_1^{\circ}) \qquad (3.3.8)$$

where V_1° and $\bar{V}_1$ are the pure molar volume and partial molar volume of component 1 respectively.

The second term on the right hand side of equation (3.3.8) corrects for the non-ideality of the vapour mixture and for the effect of pressure, while the third term corrects for the deviation of the pure vapour of component 1 from the ideal gas laws. Equation (3.3.8) can also be written in terms of concentration, c. Noting that the equation of state is,

$$y_1P = P_1 = c_1\,RT\,(1 + \frac{BP}{RT}) \qquad (3.3.9)$$

$$\ln \gamma_1(0) = \ln(c_1RT/P_1^{\circ}x_1) + (P/RT)\left[2y_1B_{11} + 2(1-y_1)\,B_{12} - \bar{V}_1\right] - P_1^{\circ}/RT\,(B_{11} - V_1^{\circ}) \qquad (3.3.10)$$

At infinite dilution equation (3.3.10) reduces to, (10)

$$\ln \gamma_1^{\infty}(0) = \ln \gamma_1^{\infty *} + P/RT\,(2B_{12} - \bar{V}_1^{\infty}) - P_1^{\circ}/RT\,(B_{11} - V_1^{\circ}) \qquad (3.3.11)$$

where $\ln \gamma_1^{\infty *} = \ln\,(c_1RT/P_1^{\circ}x_1)_{x_1 \to o}$

3.3.2 Activity Coefficient from GLC.

In the GLC determination of partition coefficients the column pressure and consequently the mole fraction of the solute at constant concentration changes continuously along the length of the column due to expansion. For this reason P and y terms in the equation of the previous section represent mean values. In terms of the outlet values they can be approximated to (11,58),

$$P = p_oJ_4^3 \qquad y = y_oJ_4^3 \qquad (3.3.12)$$

If the liquid phase concentration (q) is defined in terms of a unit volume of the non-volatile solvent, from the definition of partition coefficient,

$$x_1 = \frac{c_1 K V_L}{q_1 V_L + n} \qquad (3.3.13)$$

where n is the total number of moles of non-volatile solvent in the column.

Substitution of equations (3.3.13) and (3.3.12) into equation (3.3.10) gives,

$$\ln \gamma_1(0) = \ln \frac{RT(qV_L+n)}{P_1^{o} K V_L} + \frac{p_o J_4^3}{RT}\left[2y_{10} J_4^3 B_{11} + 2(1-y_{10} J_4^3) B_{12} - \bar{V}_1\right] - \frac{P_1^{o}}{RT}(B_{11} - V_1^{o}) \qquad 3.3.14)$$

The ternary form of equation (3.3.8) was derived by Scatchard and Tickner (59)

$$\ln \gamma_1(0) = \ln \frac{Py_1}{x_1 P_1^{o}} + \frac{P}{RT}\left[(2B_{12}-B_{11}-B_{22})y_2(1-y_1) + (2B_{13}-B_{11}-B_{33})y_3(1-y_1) - (2B_{23}-B_{22}-B_{33})y_2y_3 + B_{11} - \bar{V}_1\right] - \frac{P_1^{o}}{RT}(B_{11} - V_1^{o}) \qquad (3.3.12)$$

A modified form of this equation for the case where component 1 is at infinite dilution is used in this work to calculate the activity coefficients in the ternary mixtures.

3.3.3 Effect of State Variables on Activity Coefficients.

The effects of temperature, pressure and composition are briefly summarised below.

3.3.3.1 Temperature Dependence of Activity Coefficients.

At constant pressure and composition the dependece of the activity coefficient on temperature is given by (60,61)

$$\left(\frac{\partial \ln \gamma_i}{\partial T}\right)_{P,x} = -\frac{\bar{h}_i - h_i^{o}}{RT^2} = -\frac{\bar{h}_i^{E}}{RT^2} \qquad (3.3.15)$$

where h_i is the partial molar enthalpy of component i in solution

h_i^{o} is the molar enthalpy of component i in pure state

h_i^{E} is the excess molar partial enthalpy of component i.

The equation (3.3.15) can be re-arranged to give

$$\left(\frac{\partial \ln \gamma_i}{\partial (1/T)}\right)_{P,x} = \frac{\bar{h}_i^{E}}{R} \qquad (3.3.16)$$

Therefore, provided that $\bar{h}_i^{E}$ does not vary with temperature, a plot of $\ln \gamma_1$ against 1/T at constant composition and pressure should give a straight line. The assumption of constant $\bar{h}_i^{E}$ has been investigated by many workers. While Colburn and Schoenber (62) found this to be true for a series of organic mixtures, Gainey and Young (63), working with benzene and n-alkane mixtures, found that $\bar{h}_i^{E}$ increased with decreasing temperature. Shaffer and Daubert (64) also confirmed the constancy of $\bar{h}_i^{E}$ for solutions of aldehydes, ketones and alcohols in water. This is in contradiction with the findings of Colburn and Schoenber who reported that the rule had failed when water was one of the components.

If $\bar{h}_i^{E}$ does vary with temperature, it can be calculated at a particular temperature by measuring the activity coefficient at a small distance on either side of the temperature of interest. This in turn, however, requires extreme precision in the measurements of the activity coefficients.

The error in partial entropy of mixing ($\bar{s}_i^{E}$), calculated from equation (3.3.17) is likely to be even larger as it depends on absolute as well as on relative retention measurements,

$$RT \ln \gamma_i = \bar{h}_i^{E} - T\,\bar{s}_i^{E} \qquad (3.3.17)$$

3.3.3.2 Pressure Dependence of Activity Coefficients.

When composition and temperature are constant the variation of activity coefficient with pressure is given by,

$$\left(\frac{\partial \ln \gamma_i}{\partial P}\right)_{T,x} = \frac{\bar{V}_i - V_i^{o}}{RT} = \frac{\bar{V}_1^{E}}{RT} \qquad (3.3.18)$$

where $\bar{V}_i^{E}$ is the excess partial molar volume of component i. Lloyd (48) reported that the excess volume of mixing of benzene, cyclohexane and methyl cyclohexane in polyoxyethylene 400 diricionoleate was too small to be measured. The same conclusion was reached by Ible and Dodge (65) for several hydrocarbon mixtures. Therefore, at low pressure and at constant temperature and composition the liquid activity coefficient can be regarded as being independent of pressure.

3.3.3.3 Composition Dependence of Activity Coefficients.

The dependence of the liquid activity coefficient on composition is usually expressed in terms of excess functions, in particular excess Gibbs function. Excess partial Gibbs function is defined as

$$\bar{g}_i^{E} = \bar{g}_i \text{ (real)} - \bar{g}_i \text{ (ideal)} \qquad (3.3.19)$$

Recalling the definition of fugacity,

$$\bar{g}_i^{E} = RT \ln \frac{f_i(\text{real})}{f_i(\text{ideal})} \qquad (3.3.20)$$

now for an ideal solution

$$f_i(\text{ideal}) = x_i f_i^{o} \qquad (3.3.21)$$

where o refers to the pure state

$$\bar{g}_i^{E} = RT \ln \frac{f_i(\text{real})}{f_i^{o} x_i} \qquad (3.3.22)$$

From the definition of activity coefficient, equation (3.3.4), equation (3.3.22) now becomes,

$$\bar{g}_i^E = \left(\frac{\partial G^E}{\partial n_i}\right)_{T,P,n_{j \neq i}} = RT \ln \gamma_i \qquad (3.3.23)$$

or for the excess molar Gibbs energy (G^E)

$$G^E = RT \sum_i x_i \ln \gamma_i \qquad (3.3.24)$$

At constant temperature and pressure, for all components in a mixture, the excess partial molar Gibbs energies and activity coefficients are related to one another by a fundamental relation known as the Gibbs-Duhem equation,

in terms of activity coefficients

$$\sum_i x_i \frac{d \ln \gamma_i}{dx_i} = 0 \qquad (3.3.25)$$

and in terms of excess partial molar Gibbs energies

$$\sum_i x_i \, d \, \bar{g}_i^E = 0 \qquad (3.3.26)$$

It is obvious from equation (3.3.25) that in a solution containing n components the activity coefficients of (n - 1) components can be used to calculate the activity coefficient of the n^{th} component.

3.4 Solution Theories.

The excess Gibbs energy consists of two parts, an excess enthalpy term and an excess entropy term,

$$G^E = H^E - TS^E \qquad (3.4.1)$$

The simplest assumption that can be made about G^E is to set it equal to zero; this leads to the equation for ideal solution. The next simplest assumption is to set either S^E or H^E equal to zero. The former assumption leads to the theory of regular solution as developed by Van Laar (66), Hildebrand (67,68) and Scatchard (69), while the other leads to the concept of athermal solution first introduced by Flory (70) and Huggins (71) independently.

These two theories and their developments with the resultant

expressions for the activity coefficient are briefly described in the proceeding sections.

3.4.1 Regular Solutions.

a) Van Laar Equation (66).

Based on the assumption of zero volume of mixing and entropy of mixing, Van Laar constructed a thermodynamic cycle for forming a liquid mixture from the pure liquids at constant temperature. The resultant expression for the activity coefficient in a binary mixture is,

$$\ln \gamma_1 = \frac{A_{12}}{\left[1 + \frac{A_{21} x_1}{A_{12} x_2}\right]^2} \qquad (3.4.2)$$

The constants are related to the end values by

$$A_{12} = \ln \gamma_1^{\infty} \qquad A_{21} = \ln \gamma_2^{\infty} \qquad (3.4.3)$$

b) The poor agreement of Van Laar's equation with experimental work is mainly a result of the use of Van der Wall's equation of state in its derivation. Hildebrand (67,68) and Scatchard (69) removed this limitation to arrive at the expression,

$$RT \ln \gamma_1 = V_1 (\delta_1 - \delta_2)^2 \phi_2^2 \qquad (3.4.4)$$

where V_1 is the volume of pure liquid

δ is the solubility parameter

and ϕ_2, volume fraction of component 2, is defined as

$$\phi_2 = \frac{x_2 V_2}{x_1 V_1 + x_2 V_2}$$

The solubility parameters, δ_1 and δ_2, are functions of temperature, but the difference $(\delta_1 - \delta_2)$ is often nearly independent of temperature (61).

c) Margule's Equation (72).

The original derivation of Margule's Equation was purely empirical,

based on the assumption that S^E is zero and that H^E could be written as a polynomial expansion in the mole fraction. The two-constant Margule's equation is then given as

$$\ln \gamma_1 = \left[A_{12} + 2(A_{21} - A_{12})x_1\right] x_2^2 \qquad (3.4.5)$$

The constants are related to the end values in the same manner as in the Van Laar's equation.

Multi-constant binary equations for the prediction of activity coefficients can be obtained by additional terms in the expression for the excess Gibbs energy function.

The three-constant Margule's equation is given by

$$\ln \gamma_1 = x_2^2 \left[A_{12} + 2(A_{21} - A_{12} - D)x_1 + 3Dx_1^2\right] \qquad (3.4.6)$$

d) Extension to Multi-component Mixtures.

The regular solution theory is easily extended to solutions containing more than one component, in which case the activity coefficient is given by the expression,

$$RT \ln \gamma_i = V_i (\delta_i - \bar{\delta})^2 \qquad (3.4.7)$$

where $\bar{\delta} = \sum_1^m \phi_i \delta_i$

and $\phi_i = \dfrac{x_i V_i}{\sum_1^m x_i V_i}$

The multi-component forms of Van Laar and Margules equations can be obtained from the general form assumed by Wohl (73,74) by suitable assumptions.

Ternary Van Laar equation:

$$\ln \gamma_1 = \frac{x_2^2 A_{12}\left(\frac{A_{21}}{A_{12}}\right) + x_3^2 A_{13}\left(\frac{A_{31}}{A_{13}}\right) + x_2 x_3 \frac{A_{21}}{A_{12}} \frac{A_{31}}{A_{13}} \left(A_{12} + A_{13} - A_{32}\left(\frac{A_{13}}{A_{12}}\right)\right)}{x_1 + x_2\left(\frac{A_{21}}{A_{12}}\right) + x_3\left(\frac{A_{31}}{A_{13}}\right)} \qquad (3.4.8)$$

with the limitation that $\frac{A_{12}}{A_{21}} \frac{A_{23}}{A_{32}} = \frac{A_{13}}{A_{31}}$ (3.4.9)

Ternary Margules equation:

$$\ln\gamma_1 = x_2^2\left[A_{12}+2x_1(A_{21}-A_{12})\right]+x_3^2\left[A_{13}+2x_1(A_{31}-A_{13})\right]$$
$$+ x_2 x_3\left[\tfrac{1}{2}(A_{21}+A_{12}+A_{31}+A_{13}-A_{23}-A_{32})\right.$$
$$\left.+ x_1(A_{21}-A_{12}+A_{31}-A_{13})+(x_2-x_3)(A_{23}-A_{32})-C(1-2x_1)\right] \quad (3.4.10)$$

The Margules equation does not have the limitation, equation (3.4.9), of the Van Laar equation, but it contains an extra constant, C, which can only be obtained from ternary data. Since such data are scarce it is either set to zero or it can be estimated from the relationship (75)

$$C = \tfrac{1}{2}(A_{31}-A_{12}+A_{31}-A_{13}+A_{32}-A_{23}) \quad (3.4.11)$$

The regular solution theories always predict $\gamma_i > 1$. This is a direct consequence of the geometric mean assumption for the interaction of two dissimilar molecules in the mixture. For many non-polar solutions, however, they give a good semi-quantitative representation of activity coefficients (61).

3.4.2 Athermal Solutions.

In considering the thermodynamic properties of solutions containing widely different size molecules, it has been found advantageous to assume, at least at first, that the enthalpy of mixing is zero and to concentrate on the entropy of mixing, using the concept of a quasicrystalline lattice of Guggenheim and Miller (76). Their treatment leads to the expression for the activity coefficient in a binary mixture

$$\ln\gamma_1 = \ln\left[1-(1-\tfrac{1}{r})\phi_2\right] - \frac{z}{2}\ln\left[1-(1-\tfrac{1}{r})\frac{2\phi_2}{z}\right] \quad (3.4.12)$$

where ϕ is the volume fraction

z is the number of nearest neighbour sites to a given segment of the large molecule

r is the size ratio of molecules.

The equation (3.4.12) is not very sensitive to the numerical value of z (77,78). When $z \longrightarrow \infty$ the result corresponds to the Flory-Huggins equation (70,71).

$$\ln \gamma_1 = \ln \left[1-(1 - \frac{1}{r}) \phi_2\right] + (1 - \frac{1}{r}) \phi_2 \qquad (3.4.13)$$

3.4.3 Non-Athermal Solutions.

a) Real solutions are neither truly regular nor athermal. Their behaviour is better represented if an extra term is added to the Flory-Huggins equation for the contribution of excess enthalpy to excess Gibbs energy. This usually takes the form of the theory of regular solutions in which the excess enthalpy is proportional to the volume of solution and the product of the volume fractions. The differentiation of this equation then gives the following expression for the activity coefficient

$$\ln \gamma_1 = \ln \left[1 - (1 - \frac{1}{r}) \phi_2\right] + (1 - \frac{1}{r}) \phi_2 + \chi \phi_2^2 \qquad (3.4.14)$$

The dimensionless parameter χ is a characteristic of the interaction between the molecules of the solution. According to the theory both r and χ should be independent of composition, but experiments have shown (79) that a much better fit to the data is obtained if they are both regarded as adjustable parameters.

The addition of an enthalpy term to the theoretical result for athermal mixtures is essentially an empirical modification in order to obtain a reasonable expression for the excess Gibbs energy. The implicit assumption in equation (3.4.14) that the molecular interaction does not contribute to the excess entropy term is not always supported by experimental evidence (80,81).

b) Wilson's Equation.

Based on semi-empirical arguments, Wilson (82) extended the Flory-Huggins equation to include solutions where molecules not only differ in size but also in their intermolecular forces,

$$\ln\gamma_1 = -\ln(1-A_{21}x_2)+x_2\left[\frac{x_2A_{12}}{1-A_{12}x_1} - \frac{x_1A_{21}}{1-A_{21}x_2}\right] \qquad (3.4.15)$$

and $$A_{ij} = 1- \frac{V_i}{V_j} \exp\left[-(\lambda_{ij} -\lambda_{ii})/RT\right] \qquad (3.4.16)$$

where λ_{ij} is related to the potential energies of the i-j pair of molecules.

One major advantage of the Wilson equation is that it has a built-in temperature dependence through equation (3.4.16) as $(\lambda_{ij} -\lambda_{ii})$ is, to a good approximation, independent of temperature. Orye and Prausnitz (83) analysed the available data for a number of systems including hydrocarbons, alcohols, esters and halogen containing compounds, and concluded that the Wilson equation was as good and in many cases much better than Van Laar's and the two-constant Margule's equation in representing the data.

c) Non-Random Two-Liquid (NRTL) Equation.

Following the concept of local volume fractions of Wilson, Renon (84) derived the following three-parameter equation.

$$\ln\gamma_1 = x_2^2\left[\tau_{21}\left(\frac{G_{21}}{x_1+x_2G_{21}}\right)^2 + \frac{\tau_{12}G_{12}}{(x_2+x_1G_{12})^2}\right] \qquad (3.4.17)$$

where $$\tau_{ij} = \frac{(g_{ij}-g_{jj})}{RT} \quad \text{with } g_{ij} = g_{ji}$$

$$G_{ij} = \exp(-\alpha_{ij}\tau_{ij})$$

The parameter g_{ij} is similar to λ_{ij} in the Wilson equation in that it is a characteristic of the molecular interactions between the i-j pair. The third parameter α_{12} is related to the non-randomness of the mixture. When α_{12} is zero, equation (3.4.17) reduces to the two-constant Margules equation. By choosing an appropriate value of α_{12}, the equation can be made to describe many types of systems (84).

d) The Heil Equation.

In 1966 Heil and Prausnitz (85) presented a semi-empirical equation for the excess Gibbs energy that gave a very good representation of the properties of a variety of polymer solutions including those in which there are strong specific interactions. Their equation for the activity coefficient is

$$\ln(\gamma_1 x_1) = s_1 \frac{x_1}{x_1+G_{21}x_2} + s_1 G_{21} \frac{x_2}{x_1+G_{21}x_2} - s_2 G_{12} \frac{x_2}{G_{12}x_1+x_2}$$

$$+ (1-s_1)\ln \frac{x_1 V_1}{x_1 V_1+x_2 V_2} + (1-s_1) \frac{x_2 V_2}{x_1 V_1+x_2 V_2}$$

$$+ (s_2-1) \frac{x_2 V_2}{x_1 V_1+x_2 V_2} + \frac{s_1 G_{21} \tau_{21} x_2}{(x_1+G_{21}x_2)} - \frac{s_1 x_1 G_{21} \tau_{21} x_2}{(x_1+G_{21}x_2)}$$

$$+ \frac{s_2 G_{12} \tau_{12} x_2}{(G_{12}x_1+x_2)} - \frac{s_2 G_{12}^2 x_1 x_2}{(G_{12}x_1+x_2)} \qquad (3.4.18)$$

where the parameters are defined as

s = number of segments per polysegmented molecule

$$G_{21} \equiv \frac{V_2}{V_1}\left[\exp -(g_{12}-g_{11})/RT\right]$$

$$G_{12} \equiv \frac{V_1}{V_2}\left[\exp -(g_{12}-g_{22})/RT\right]$$

$$\tau_{12} \equiv (g_{12}-g_{22})/RT \qquad \tau_{21} \equiv (g_{12}-g_{11})/RT$$

The interaction energy g_{ij} represents the energy between an i-j pair. It is assumed that these energies are independent of polymer molecular weight and are only a weak function of temperature. As the difference between the interaction energies become small compared with the thermal energy, RT, equation (3.4.18) reduces to the Flory-Huggins equation with

$$\chi = \frac{2g_{12}-g_{11}-g_{22}}{RT}$$

Wiek et al (86) compared the Heil equation with the Flory-Huggins equation of the form used by Everett and co-workers (77,78) for solutions containing high molecular weight polymers and found that the Flory-Huggins equation gave a slightly better fit, but the Heil's equation was superior with polymer solutions containing associated solvents where chemical effects were dominant.

e) Extension to Multi-component Systems.

For a ternary system containing a polymer, component 3, the Flory-Huggins equation becomes (86),

$$\ln\gamma_1 = \ln\frac{1}{z} + 1 - \frac{1}{z} - \frac{\chi_{23}}{2}\phi_2\phi_3 + (\chi_{12}\phi_2+\chi_{13}\phi_3)(1-\phi_1) \qquad (3.4.19)$$

where $z = \frac{1}{r_1}x_1 + \frac{1}{r_2}x_2 + x_3$

and r is the ratio of the size of the polymer molecule to the size of the solute molecule.

The multi-component form of the Wilson equation is (82)

$$\ln\gamma_i = -\ln(1-\sum_j x_j A_{ji}) + 1 - \sum_j\left[x_j(1-A_{ij})/(1-\sum_k x_k A_{kj})\right] \qquad (3.4.20)$$

The multi-component form of the NRTL equation is (84)

$$\ln\gamma_i = \frac{\sum_j \tau_{ji}G_{ji}x_j}{\sum_k G_{ki}x_k} + \sum_j \frac{x_j G_{ij}}{\sum_k G_{kj}x_k}\left(\tau_{ij} - \frac{\sum_L x_L\tau_{Lj}G_{Lj}}{\sum_k G_{kj}x_k}\right) \qquad (3.4.21)$$

3.5 Correlations for Infinite Dilution Activity Coefficient.

With any two-constant binary equation, the knowledge of γ^∞ for each component of the mixture makes it possible to calculate the activity coefficients over the entire concentration range. Therefore, many attempts have been made to predict the end values. Some of these are reviewed below.

According to the regular solution theory of Hildebrand (68)

$$\ln \gamma_1^{\infty} = \frac{V_1(\delta_1-\delta_2)^2}{RT} \qquad (3.5.1)$$

The solubility parameter, δ, can be calculated from vapour pressure data according to the equation,

$$\delta^2 = \frac{2.303\ RB}{V}\left(\frac{T}{t+c}\right)^2 - \frac{RT}{V}$$

where t is the temperature in ^{o}c

V is the molar volume

B and c are the constants in the Antoin equation.

For non-athermal mixtures, the contribution of size effects to the activity coefficient has, generally, been assumed to be of the Flory-Huggins type and the main effort has been directed towards correlating the interaction parameter χ. According to the regular solution theory,

$$\chi = \frac{V_1(\delta_1-\delta_2)^2}{RT} \qquad (3.5.2)$$

This has been used by several workers (87,88) in discussing GLC results including a detailed study by Cruickshank and co-workers for systems in n-octadecane (89). Other, more involved, correlations have been proposed (89,90) for mixtures containing n-alkanes and branched alkanes and also for solutions of benzene in n-alkanes with reasonable success (90).

For more troublesome polar systems Blank and Prausnitz (91) proposed to split the solubility parameter into a non-polar (λ) and a polar part (τ), so that

$$\delta^2 = \lambda^2 + \tau^2 \qquad (3.5.3)$$

τ is defined to be the solubility parameter of a non-polar molecule having the same size and shape as the polar molecule under consideration. Thus if the size effects are ignored, for a mixture containing a polar component 1 and a non-polar component 2,

$$\ln\gamma_1^{\infty} = \frac{V_1}{RT}(\lambda_1 - \delta_2)^2 + \frac{T^*}{T}(\lambda_1^2 - 2\psi) \qquad (3.5.4)$$

$$\ln\gamma_2^{\infty} = \frac{V_2}{RT}(\lambda_1 - \delta_2)^2 + \frac{T^*}{T}(\tau_1^2 - 2\psi) \qquad (3.5.5)$$

and when both components are polar

$$\ln\gamma_1^{\infty} = \frac{V_1}{RT}(\lambda_1 - \delta_2)^2 + \frac{T^*}{T}(\tau_1 - \tau_2)^2 \qquad (3.5.6)$$

where T* is the temperature at which τ_1 is calculated, and ψ is an empirical constant. Slightly more improved versions of equations (3.5.4)-(3.5.6) are given by Helpinstil and Van Winkle (92).

A most extensive study on the correlation of infinite dilution activity coefficients with molecular structure has been made by Pierotti et al (93). They have published correlations of values of γ^{∞} for homologous series hydrocarbons in various specific solvents and sometimes in a homologous series of solvents. A homologous series is defined to be a series of compounds that differ from each other only by the number of methylene groups.

For a homologous series of solvents

$$\ln\gamma_1^{\infty} = A_{12} + \frac{B_2 n_1}{n_2} + \frac{c_1}{n_1} + D(n_1 - n_2)^2 + \frac{F_2}{n_2} \qquad (3.5.7)$$

All the constants, except D, are characteristics of the functional group (part of the molecules that is common to all in the series) of the component indicated by the subscript. They are all temperature dependent. For a particular solvent A_{12} and F_2/n are combined to form one constant.

In real systems, where there may be many types of interactions, Null and co-workers (94,95) proposed that various contributions to γ^{∞} are additive. Extensive tabulations are given (95) for the contribution terms due to heat of mixing, polar energy, volume effects, free energy of broken polymer bonds etc. This approach has the advantage that one or more of the terms can be taken to suit a particular system and that any future development on other types of interactions can be simply added on.

3.6 Other Measurements by GC.

In addition to the measurement of activity coefficients and the study of solutions, GC has been frequently used to determine two other properties: cross second virial coefficient, and the surface area of solid support. The first one employs high pressure chromatography and is essentially a method of comparing the gas fugacity correction to the liquid activity coefficient at different pressures. The second, although not a thermodynamic property of the system, is directly calculated from retention volume measurements.

Some of the work done in these two fields are reviewed in the proceeding sections.

3.6.1 Measurement of the Second Cross Virial Coefficients.

High pressure chromatography has been used to determine the second cross virial coefficients (B_{12}). The GLC method involves studying the effect of carrier gas pressure on the partition coefficient. The equation (3.1.6) can be rearranged to give for the net retention volume,

$$\ln V_N^{o\infty}(P) = \ln V_N^{o\infty}(0) + \beta p_o J_3^4 \qquad (3.6.1)$$

where $$\beta = 2(B_{12} - V_1^{\,o})/RT \qquad (3.6.2)$$

$$\ln V_N^{o\infty}(0) = \ln \frac{n_1 RT}{\gamma_1^{\infty} P_1^{\,o}} - \frac{(B_{22}-V_1^{\,o})P_1^{\,o}}{RT} \qquad (3.6.3)$$

Thus from the slope of a plot of $\ln V_N$ versus $p_o J_4^3$ a value of B_{12} can be obtained. Cruickshank et al (96) measured B_{12} of various hydrocarbons, including benzene and hexane, in hydrogen and argon with squalane and dinonylphthalate as the liquid phases. The main sources of error were the assumptions that $\bar{V}_1^{\infty}$ could be approximated to $V_1^{\,o}$ (an error of $\mp$ 10 cm^3 $mole^{-1}$) and that the solubility of the carrier gas in the liquid phase could be neglected (an error of $\mp$ 5 cm^3 $mole^{-1}$ for argon). The

results obtained were compared with those calculated from the second virial coefficients of the pure solutes using the McGlashen and Potter equation of state (97). The agreement was very good when the combining rules of Hudson and McCoubrey (98) were employed for the pseudo-critical temperatures and pressures.

Gainey and Young (63) and Cruickshank, Gainey and Young (89) determined B_{12} for the benzene + nitrogen mixture by GLC with various n-alkanes as the liquid phases. A correction term was applied to account for the effect of carrier gas solubility in the liquid phase. The result is to change the value of β in equation (3.6.3) to β'

where $$\beta' = \frac{2B_{12} - \bar{V}_1^{\infty}}{RT} + \lambda \left[1 - \left(\frac{\partial \ln \gamma_1}{\partial x_2} \right) \right] \qquad (3.6.4)$$

x_2 is the mole fraction of the carrier gas in the stationary phase and λ_1 is defined by the expansion of x_2 as a series in local carrier gas pressure

$$x_2 = \lambda p + Vp^2 + \ldots\ldots \qquad (3.6.5)$$

The results were in reasonable agreement with the theoretical values calculated from the McGlashen-Potter equation (97).

Hicks and Young (99) measured B_{12} for the systems (c_4 - c_7) hydrocarbons + nitrogen and compared them with the theoretically calculated values. The agreement was found to be within the estimated experimental error of $\pm$ 10 cm^3 $mole^{-1}$.

Everett et al (100), working in the pressure range of 1.5-6 atm., chromatographically measured B_{12} of benzene, n-octane in eight different carrier gases. With H_2, N_2, A , and CH_4 the values of B_{12} estimated using the Hudson-McCoubrey rule (98) were in close agreement with the experimental data, while the systems He + benzene, O_2 + benzene, CO + octane the differences were just outside the experimental error. In all cases

geometric-mean relationship gave values of B_{12} which fell far below those obtained experimentally. Where independently measured B_{12} values were available, these agreed with the experimental data better than the theoretical calculations.

Dantzler et al (101), using a static method determined the excess second virial coefficients ($B_{12} = B_{12} - 0.5(B_{11}+B_{22})$) for a number of hydrocarbons. The measurement of B_{12} by this method relies on the knowledge of the second virial coefficients of the pure components and, therefore, the accuracy of the results are often no better than those directly measured chromatographically. However, the results compared reasonably well with the available chromatographic data (96).

Pecsok and Windsor (102) measured B_{12} for various hydrocarbon + hydrocarbon mixtures at two temperatures, 25 and 50°C, with an experimental accuracy of $\pm$ 25 cm^3 $mole^{-1}$. The carrier gas (methane and ethane) solubility was corrected for by roughly estimating the correction factor in equation (3.6.4). The results, when compared with the available static data, showed that provided that the solubility correction factor is calculated accurately, GLC presents a valid and a quick method of measuring second cross virial coefficients.

Coan and King (103), using a non-chromatographic method, measured B_{12} of benzene in a series of gases ranging in complexity from helium to ethylene, and the results were found to agree within the experimental error with values obtained by GLC (63,96,100).

Conder and Langer (104), who measured the specific retention volumes of various aliphatic and aromatic hydrocarbons in di-n-butyl tetrachloro-terephthalate, concluded that the difference arising from the use of two different carrier gases (helium and nitrogen) could adequately be explained in terms of the factor $\beta p_o J_3^4$ in equation (3.6.1). In

estimating the second virial coefficients, they followed the suggestion of Guggenheim and Wormal (105) that all hydrocarbons obey the McGlashen-Potter equation, provided a suitable value is chosen for the number of carbons in each hydrocarbon.

3.6.2 Measurement of Solid Surface Areas.

The standard method for the determination of the surface area of solids is the adsorption of an inert gas such as hydrogen. In the conventional techniques the adsorption isotherm is determined by pressure-volume measurements and the surface area is calculated from the standard BET equation (106)

$$\frac{\bar{P}}{V(\bar{P}-P^{o})} = \frac{1}{V_m C} + \frac{C-1}{V_m C} \cdot \frac{\bar{P}}{P^{o}} \qquad (3.6.6)$$

where $\bar{P}$ is the pressure of the gas in equilibrium with the sorbed gas

P^{o} is the saturation pressure of the gas

V is the volume of the gas adsorbed

V_m is the volume of the gas adsorbed when the surface of the adsorbent is covered with a single layer of molecules

C is a constant roughly equal to $e^{(E_1-E_2)/RT}$, where E_1 and E_2 are the heat of adsorption and the heat of condensation respectively.

Thus a plot of $\bar{P}/V(\bar{P}-P^{o})$ against P/P^{o} should be a straight line with slope $(C-1)/V_m C$ and intercept $1/V_m C$. From the known molecular diameter and assuming close packing in the unimolecular layer, the surface area of the adsorbent can be calculated. Since GC has been proved to be an accurate method of measuring distribution isotherms, Gas-Solid Chromatography should provide a convenient way of measuring the surface area of adsorbents. Some of the work done in this field is reviewed below.

The first known work that was specifically aimed at measuring surface

areas is that of Nelson and Eggerton (107), who devised a technique whereby a mixture of helium and nitrogen was passed through a column of the adsorbent. As the column was cooled by dipping it into liquid nitrogen, a kathorometer placed at the outlet of the column produced a peak corresponding to the adsorption of nitrogen. A similar peak but opposite in direction was produced when the nitrogen desorbed as the column was allowed to warm up. By calibrating the detector against the amount of nitrogen in the mixture, the distribution isotherm could be determined and the surface area calculated from the BET equation. The results of the experiments with various adsorbents (firebrick, alumina powder, etc.) were found to be in good agreement with the conventional measurements.

Roth and Ellwood (108) used the Nelson-Eggerton method with a slightly different apparatus for better control of the gas flow rates. The surface areas of four samples, namely copper chromite, two samples of alumina and chromium, whose surface areas had been determined conventionally, were measured. For the first three samples the agreement was 1% or better in spite of the difference in the out-gassing procedure used in the two techniques. A similar technique was employed by Farey and Tucker (109) on a number of adsorbents with surface areas ranging from 0.1 to 70 m^2/g.

The method is not confined to the use of permanent gases as was demonstrated by James and Phillips (39) who measured the distribution isotherm of benzene and cyclohexane on charcoal by frontal analsis. It should be pointed out, however, that the effective area so determined may depend on the nature of the adsorbate. Thus Purnell and Perett (38) found that their measurements on fire brick supports gave half to two thirds the

values found by other workers using low temperature nitrogen adsorption. Since the discrepancy is most likely caused by the difference in molecular size, the former result is more relevant to chromatographic studies with these particular chemicals.

4. DESIGN AND CONSTRUCTION OF EQUIPMENT.

The accuracy of the thermodynamic data measurements by the method of 'Elution on a Plateau (EP)' is critically governed by the operating conditions. When high boiling liquids such as pinenes are used as the solute in the chromatographic column added difficulties arise in preventing the condensation of the solute in the lines leading to the column and in the techniques used in the measurements of concentration levels.

The main components of the apparatus were:

1. Gas Chromatograph
2. Equipment for flow rate control and measurement
3. Equipment for generation of constant concentration
4. Gas sampling unit.

The general design features of the apparatus were dictated by the linearity range of the flame ionization detectors (FID) used.

Preliminary studies showed that with both the pinenes and the halocarbons, the FID's were well outside their linear ranges at the concentration levels covered by this work. This meant that the concentration levels could not be measured directly from the height of the plateau as registered on a recorder without sacrificing accuracy at the upper end of the concentration range. Furthermore, at these concentrations it was found that the response of the FID's were more sensitive to changes in carrier flow rates than the concentration of the carrier gas. At very high concentrations the detector is fully saturated and fails to respond to any further increase in the gas concentration, a phenomenon that was also reported by Hilmi (57). It was, therefore, decided to use the second FID on the F11 to measure concentrations independently. This arrangement enabled a wide range of carrier gas flow rates to be used for elution volume measurements without the necessity of calibrating the first FID

for every flow rate. It also reduced errors in the calculated elution volumes due to small fluctuations in the carrier flow rate in the course of a run.

The apparatus was slightly modified after the ∝-pinene runs. Figs. 4.1,4.2 show the general layout of the equipment before and after the modifications respectively.

Essentially, a nitrogen stream carrying solute vapour was split up into two streams. One stream was passed through column A setting up a constant concentration plateau. The second stream was vented to the atmosphere after passing through a gas sampling valve and a trap to condense out the solute. The carrier gas to column B was supplied by a separate line. All the lines carrying solute vapour were heated by heating tapes, connected to and controlled by a variac. The temperature of the gas stream was measured at various points in the circuit by iron-constantan thermocouples connected to a temperature indicator calibrated for iron-constanton, through a multi-pole switch.

With the exception of a few brass fittings, the lines carrying solute vapour were constructed from stainless steel tubing and, in certain places, from teflon tubing to allow for the lifting of the F11 analyser head for access to the columns.

4.1 Gas Chromatograph

The gas chromatograph used was a standard "Model F11 Perkin-Elmer Chromatograph", with the following component parts:

A - Oven

B - Analyser Unit

C - Flame Ionization Amplifier

D - Recorder

E - Pressure and Flow Control Units

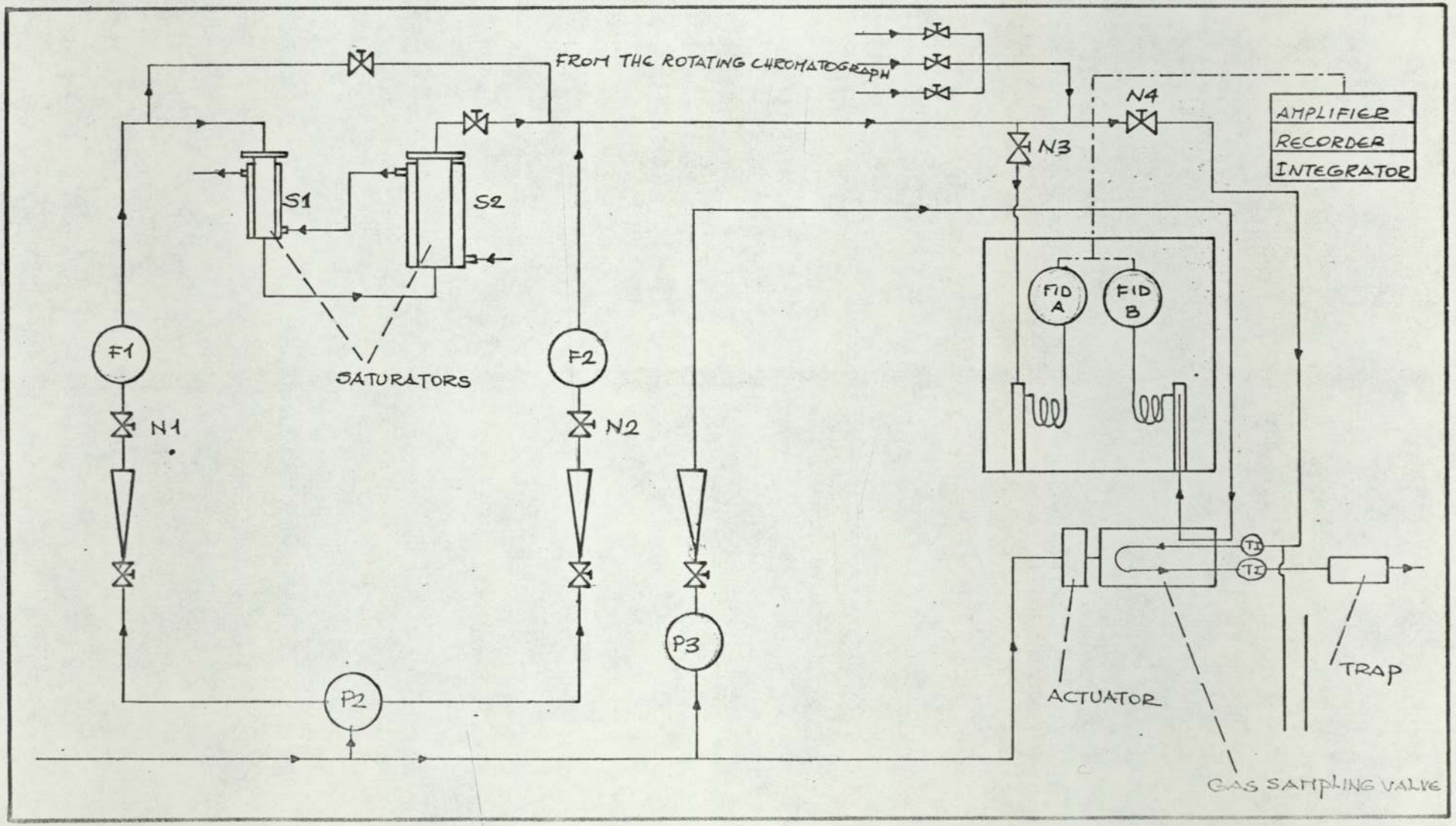

FIG. 4.1. LAY-OUT OF EQUIPMENT FOR α-PINENE RUNS

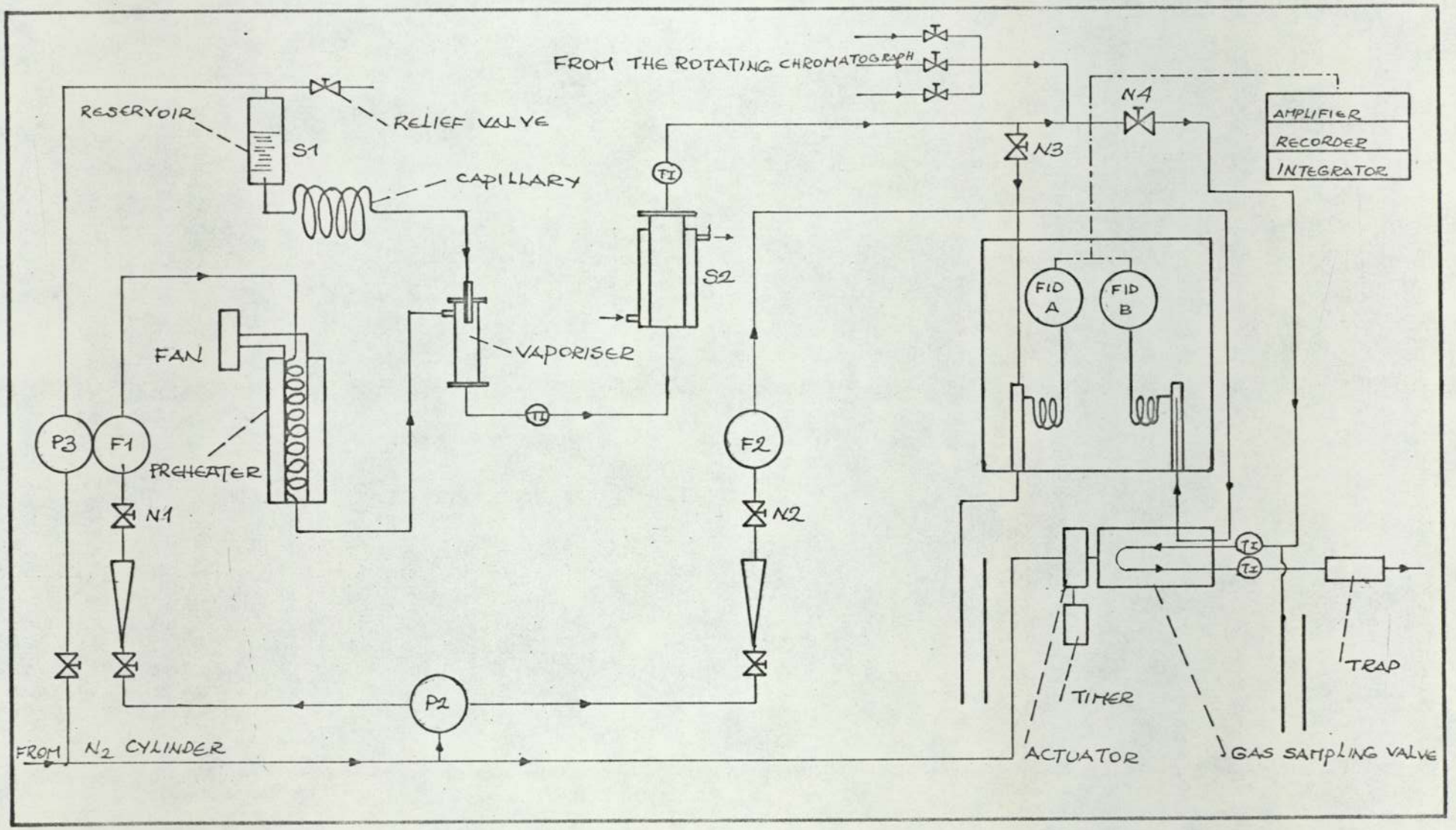

FIG. 4.2 - LAY-OUT OF EQUIPMENT FOR β-PINENE AND HALOCARBON RUNS

A - Oven.

The temperature of the oven, set by a dial calibrated in degrees centigrade, was controlled to $0.1^{\circ}C$. Although a direct read-out of the oven and injection block temperatures were provided such that a full scale deflection on a potentiometric recorder corresponds to $500^{\circ}C$, the oven temperature was measured by a mercury-in-glass thermometer graduated in $0.1^{\circ}C$.

B - Analyser Unit.

The analyser unit contains two flame ionization detectors (FID), two injection blocks and is designed to take two 0.318 mm (1/8 in.) OD columns. The response does not vary with the temperature of the detector and consequently good accuracy is achieved without the need for temperature control of the detectors. By using a selector switch at the back of the unit, the FID channels were used alternately.

C - Flame Ionization Amplifier.

The ionization amplifier is designed to amplify the small current from the FID and convert it into a millivolt signal suitable for a potentiometric recorder. The amplified signal is then fed through an attenuater with seventeen steps ranging from 1 to 20×10^4. Facilities are provided for flame ignition and polarity reversal of the FID.

D - Recorder.

The recorder used was a "Hitachi - Perkin-Elmer Model 159" giving a full scale deflection at 2.5 mV. A front panel switch is provided for selecting one of three chart speeds.

E - Pressure and Flow Control Units.

These were also obtained from Perkin-Elmer Ltd. and contained the flow controllers and pressure regulators described in the proceeding

Plate 4.1. Front View of the Apparatus

A. Integrator
B. Flow Control Unit
C. Pressure Control Unit
D. FID Analyser Head
E. F11 Oven
F. Recorder
G. Gas Sampling Unit
H. Monometer for Column Pressure Drop Measurements
I. Sample Lines from the Rotating Chromatograph.

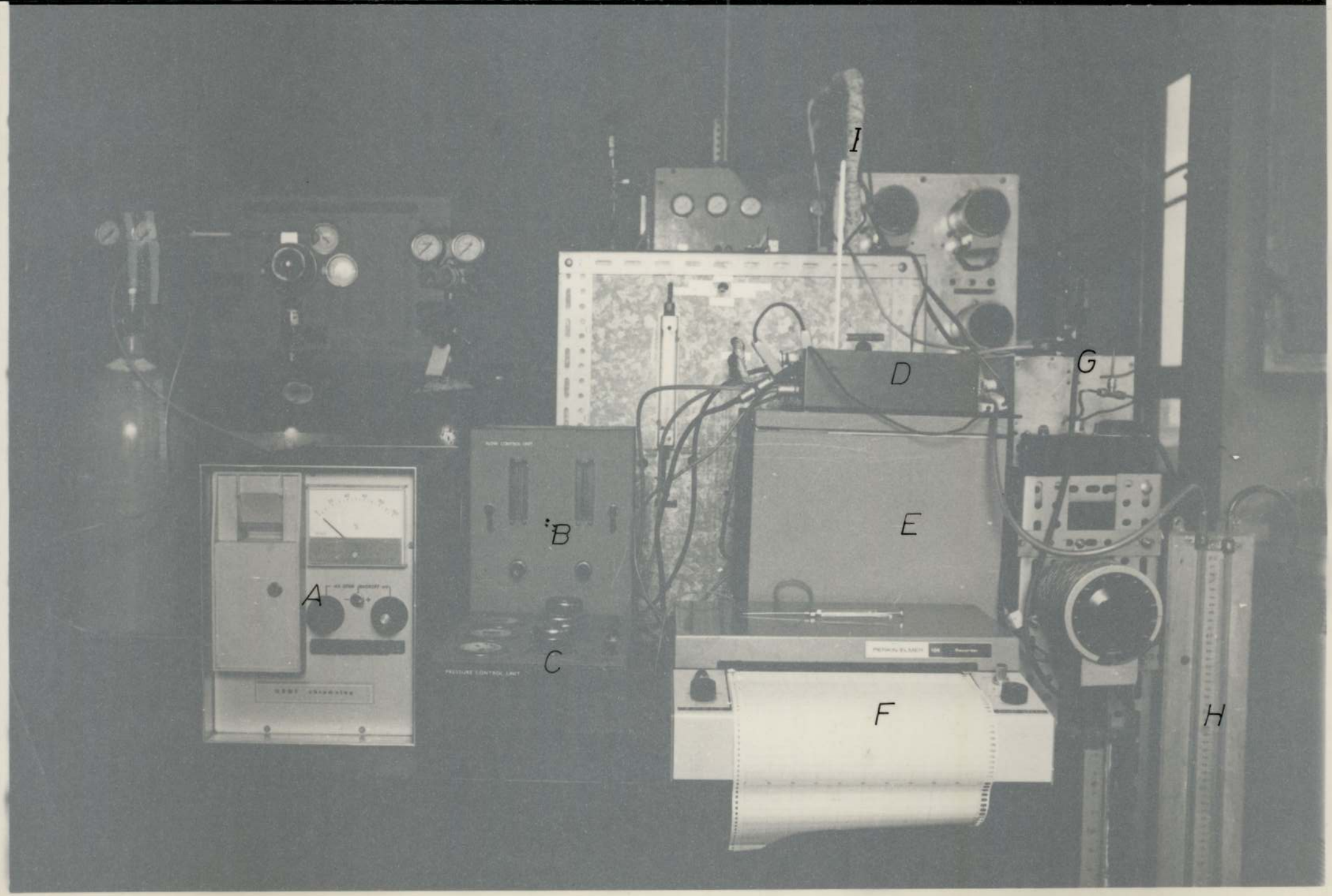
A
B
C
D
E
F
G
H
I

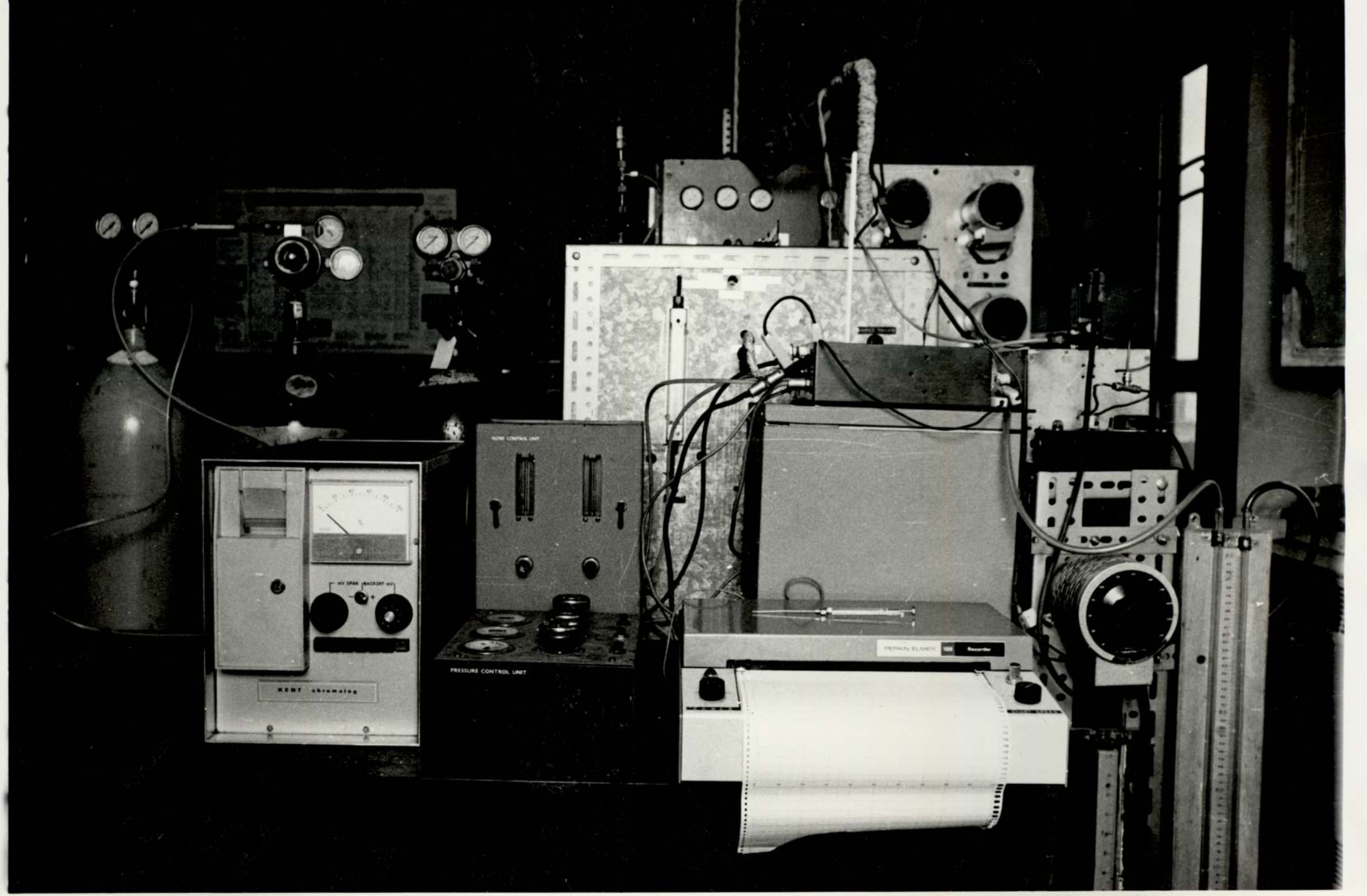
KENT chromalog
PRESSURE CONTROL UNIT

sections.

An electronic integrator "Kent Chromolog 1" was connected in parallel with the amplifier for direct integration. The sensitivity is 2000 counts per minute and no automatic base line correction is provided.

4.2 Flow Rate Measurement.

4.2.1 Flow Rate Control of the Carrier Gases.

For accurate measurements of elution volumes it was essential that the carrier flow rate to column A be kept constant during the elution of a peak. Also, because of the high sensitivity of FID to carrier flow rate, the nitrogen flow rate to the second FID had to be reproduced very closely over long periods of time. To accomplish this flow controllers and pressure regulators were used in various parts of the carrier flow lines. However, limitations were imposed by their materials of construction on their position in that they could not be placed in the lines carrying hot solute vapour.

A. Flow Controllers.

Flow controllers used were Brook's self contained, differential regulators (type 8944), designed to control downstream mass flow rate for constant up stream pressure. The material of construction of the body was brass and that of the diaphragm, Buna-N. The flow rate was adjusted by a needle valve at the inlet to the controller and integral with it (N1-N2). Toggle valves were provided before each controller for shut-off without effecting the settings of the needle valves. Day to day reproducibility of flow rates were found to be better than 2%. The flow rates used during the course of this work were well within the range of flow controllers (0 to 200 cm^3/min at NTP).

The ratio of the solute vapour containing nitrogen streams going to column A to that going to the gas sampling valve was adjusted by the

needle valves N3 and N4. These precision needle valves, provided with micrometer handles for reproducible and very fine metering, were obtained from Clockhouse Engineering and Instrument Co. They are designed to handle flow rates of 3 to 3000 cm^3/min with extreme accuracy. All the parts in contact with the gas stream were made of 316 stainless steel and teflon.

No detrimental effects of the hot solute vapours were observed during their usage.

B. Pressure Regulators.

Pressure regulator P1 at the nitrogen cylinder head was of a double stage diaphragm type with two bourdon type pressure gauges attached to it for inlet and outlet pressure readings. The down stream pressure could be varied from 0 - 1135 KN/m^2(150 psig). Pressure regulators P2 and 3 were of single stage diaphragm type. P2 was permanently set at 454 KN/m^2(51 psig) and was used to provide constant inlet pressure to the flow controllers. P3 has a 0-515 KN/m^2(60 psig) Bourdon type pressure gauge connected to it. During α-pinene runs it was used to provide constant flow rate to column B and in subsequent runs to regulate pressure in the solute reservoir.

4.2.2 Flow rate Measurement of the Carrier Gases.

A 6 cm scale 'Brooks' rotameter was placed between pressure regulator P2 and each flow controller, thus always operating at the set pressure of P2(454 KN/m^2). Another rotameter of 10 cm scale was placed in the line after P3. Although all the rotameters were calibrated using a soap bubble meter, they were not considered accurate enough for retention data measurements. Instead they were used for rough setting of flow rates and for the purpose of checking for leaks in the lines. This was done by

blocking the end of the relevant line and then observing the position of the rotameter float when the line was fully pressurised.

A. Flow Rate Measurement for Column A.

Several methods of measuring flow rates are conventionally available, however for accurate retention data it was desirable that the method chosen should fulfil two requirements:

1. It must be accurate for small flow rates as a maximum flow rate of 30 cm^3/min was anticipated.
2. It must be able to measure the flow rate during the elution of a peak without disturbing the flow.

A capillary flow meter would meet these requirements and would be relatively easy to construct. But, as mentioned in earlier sections, it was not possible to control accurately the temperature of the lines carrying solute vapour, thus introducing appreciable error as a result of the variations in viscosity with temperature. It would also have been necessary to construct a thermostated unit for the capillary flow meter.

It was, therefore, decided to take advantage of the good temperature control of the F11 oven by basing the calibration on the differential pressure across the chromatographic column.

The pressure drop for the flow of an incompressible fluid through porous media is given by, (110)

$$\frac{p1-p2}{L} = \frac{\alpha \mu v}{g} + \beta \rho \frac{\bar{u}^2}{g} \qquad (4.2.1)$$

where p1 and p2 are the upstream and downstream absolute pressures respectively

L is the thickness of the medium

$\bar{u}$ is the superficial velocity of fluid (based on total cross section).

ρ is the fluid density

μ is the fluid viscosity

α is a viscous resistance coefficient

β is an inertial resistance coefficient

g is the gravitational constant

For purely viscous flow the second term on the right hand side of equation (4.2.1) becomes negligible. The resulting equation is known as Darcy's equation of flow through porous media. In this case it can be seen that provided viscosity and, therefore, the temperature are constant, a straight line is obtained from a plot of pressure drop against volumetric flow rate (v), i.e.

$$\Delta p \propto v \qquad (4.2.2)$$

In fact, the viscosity of nitrogen is slightly modified by the presence of solute vapour needing a correction to the carrier rate measured at a particular concentration of the solute. The nature of this correction is fully discussed in later chapters.

The inlet pressure of the column was measured by a 100 cm long U tube, the outlet pressure being atmospheric. Preliminary studies showed that at the expected flow rates, a maximum pressure drop of about 10 cm Hg would result requiring a manometer fluid with a density of about 1.5 g/cm^3 for maximum variation in manometer level with flow rate. A red-coloured, carbon tetrachloride fluid was used for this purpose. One end of the U tube was connected to the injection head through the injection septum with a thin capillary tube.

B. Flow Rate Measurement for Column B.

In α-pinene runs the flow rate to column B was controlled by the pressure regulator P3 which had to be reset for each temperature. In the subsequent runs the flow controller F2 was connected to column B. With this arrangement it was found that the flow rate was kept constant over a column temperature range of more than 50°C and therefore did not need any resetting.

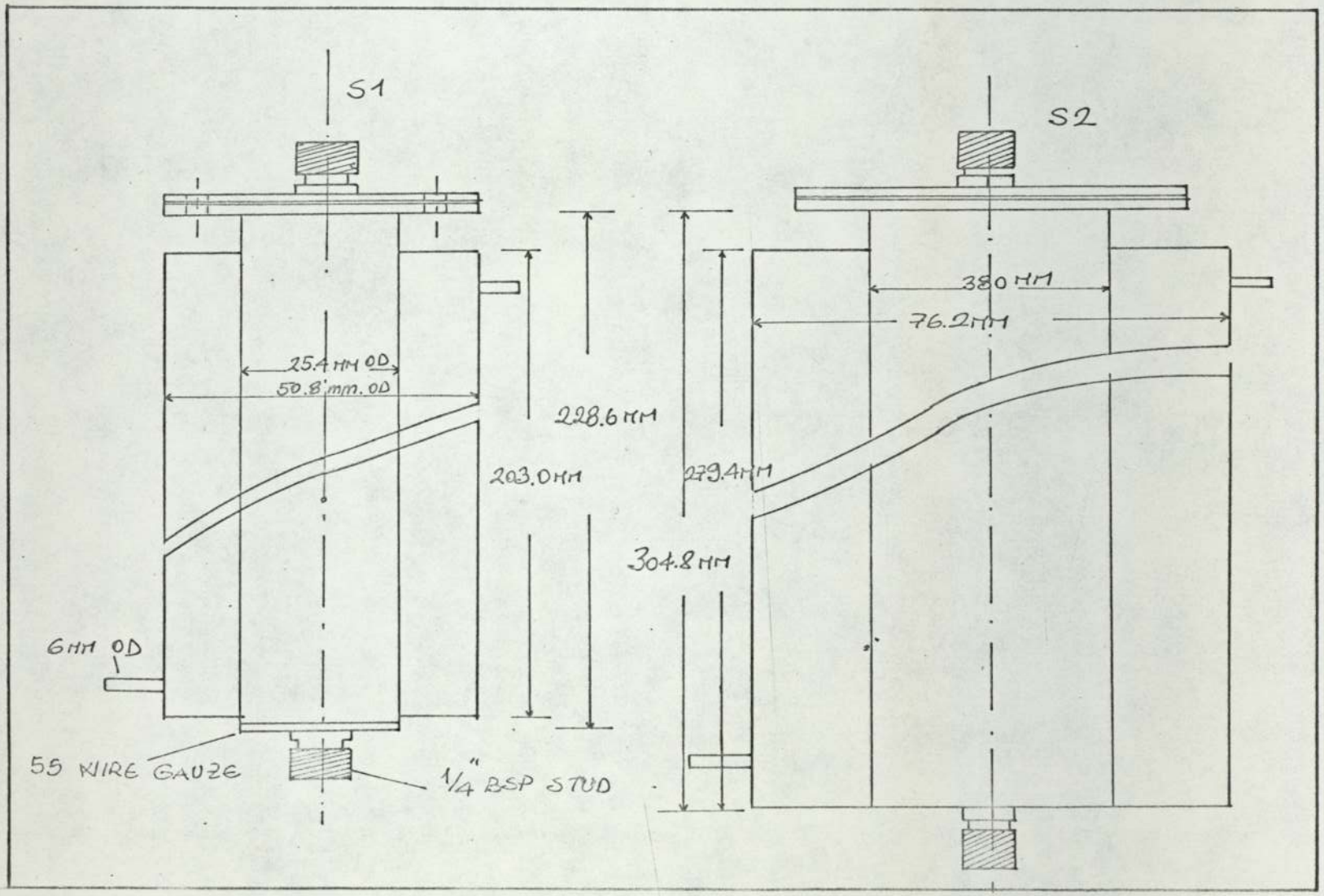

FIG. 4.3.1 - SATURATORS

4.2.3 Flow Control and Measurement of Auxiliary Gases.

Hydrogen flow rates to both FID's were controlled independently by pressure regulators similar to P2 coupled with built-in restrictions at the F11 analyser head. Each line had a toggle valve before their respective pressure regulator.

The oxygen line was split into two at the analyser head and the flow rate was controlled by a pressure regulator at the head of the oxygen cylinder. Each oxygen line also had built-in restrictions.

The flow rates of the auxiliary gases could not be measured easily as the construction of the FID's was such that they were not gas tight. No attempt was made to measure them by placing rotameters before the restrictions as this would have required lengthy calibrations. Since these flow rates did not come into retention volume calculations, all the settings were done according to the readings of 0- 515 KN/m^2 (60 psig) pressure gauges attached to each regulator.

4.3 Equipment for the Generation of Constant Concentration Levels.

4.3.1 Lay-out of Equipment for α-Pinene Runs.

Dimensions of the saturators are shown in Figure 4.3.1. The jackets were made of copper, all the other parts were of stainless steel. Initially only the saturator S1 was used, but to obtain concentrations greater than 1.5×10^{-4} g/cm^3 a second saturator, S2, had to be connected in series with it. Fire brick pieces of approximately 0.5 cm size were thoroughly soaked in purified α-pinene and packed into the saturators. Nitrogen from a high pressure cylinder was dried by passing it through a filter containing silica-gel. This dry nitrogen was split up after the pressure regulator P2. One stream was passed through the saturators via the flow controller F1 creating a concentrated gas stream. To obtain lower concentrations the second stream from F2 was joined with the first stream

after the saturators. A plug of glass wool was inserted in the line at this point to prevent any entrainment of the liquid. A by-pass line was provided across the saturators for infinite dilution measurements.

The saturators were heated by circulating hot oil through their jackets from a constant temperature bath. The bath was made to the following dimensions:

Width = 25.4 cm (10.0 in), Depth = 20.4 cm (8.0 in) and Length = 45.5 cm (18.0 in).

The bath was insulated with 0.95 cm ($\frac{1}{4}$ in) compressed asbestos sheets all round in addition to 1.6 cm (5/8 in) thick block-board which formed the casing of the bath. A tight fitting stainless steel lid was also provided to reduce oil fumes as considerable cracking and darkening of the oil, Shell's Valdatla Oil 79, was observed at temperatures above 90°C. It also helped to reduce vapourisation when water was the heating medium. The thermostat unit, a 1 KW 'Tempunit' obtained from Tecne Ltd., was equipped with a stirrer and a centrifugal pump capable of pumping water at a rate of 6000 cm^3/min at a head of 120 cm. Temperature control is achieved by a bimetallic helix operating a pneumatic capsule. The unit was initially set to operate in the range ambient to 95°C but was adjusted to operate up to 130°C.

B. Layout of Equipment for β-pinene and Halocarbon Runs.

The design outlined in the preceding section was adequate for α-pinene whose purity was better than 99%, the main impurity being β-pinene. Provided that the saturators were regularly replenished, the composition of the α-pinene vapour could be kept almost constant. β-pinene, however, could not be purified to better than 98% with more volatile α-pinene and camphene making up the rest. Because of the difference in their boiling points when nitrogen was first passed through the freshly loaded saturators, the amount of α-pinene and camphene in

Plate 4.2. Back View of the Apparatus. (B-Pinene and Halocarbon Runs)

S1 - Reservoir
S2 - Large Capacity
PH - Preheater
VP - Vaporiser
C - Trap
CP - Cappilary Tube.

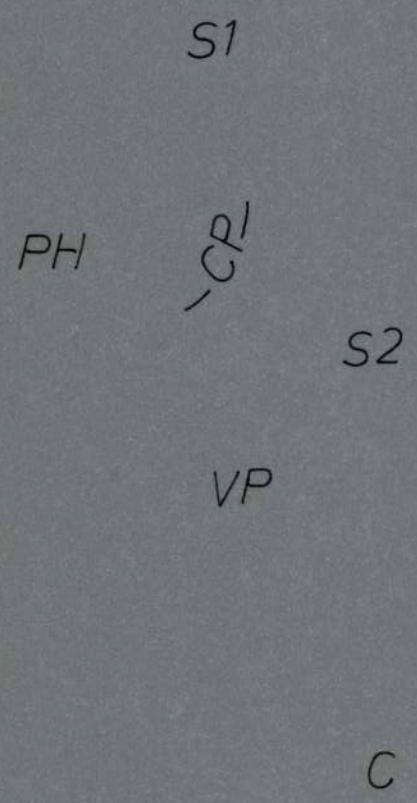
S1
PH
CP1
S2
VP
C

C

25

AV

BH

12

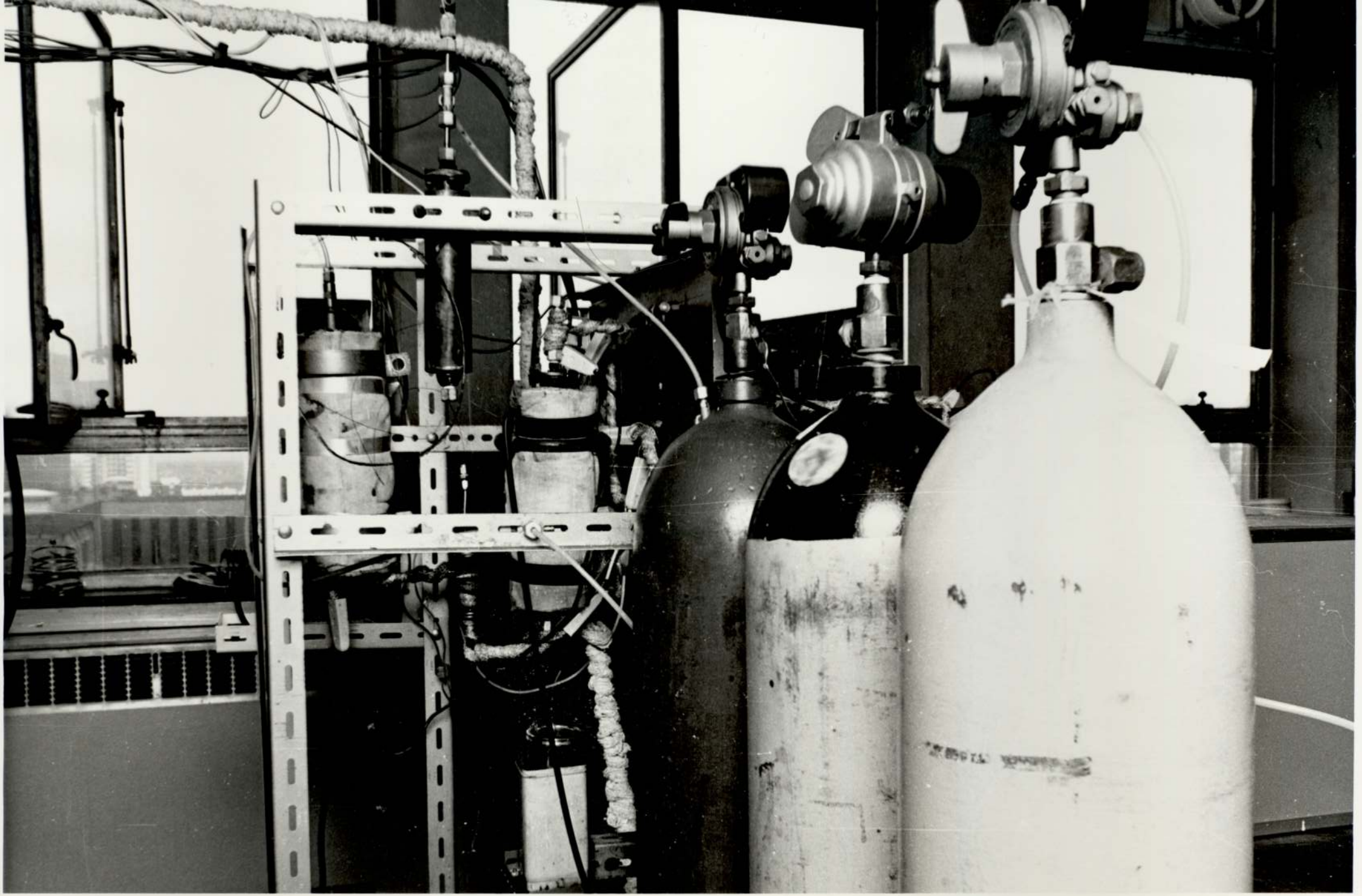

the solute vapour was increased to nearly 10% due to fractionation. It was obvious from this that another method which would maintain solute vapour composition constant had to be found. A capillary pump system shown in Fig. 4.2 satisfied this requirement and also helped to minimise the consumption of β-pinene which was important in view of the limited amount available.

Various sizes of stainless steel capillary tubes ranging from 31 gauge (ID = 0.1 mm) to 26 gauge (ID = 0.25 mm) were investigated. It was found to be almost impossible to prevent the blockage of small diameter tubes. To obtain good regulation of liquid flow while at the same time to minimise the risk of blockage, two coils, one 8 m long of 0.2 mm ID and the other 10 m long of 0.25 mm ID, were prepared from 2 m lengths by joining two ends in a short sleeve of larger diameter capillary tube and cementing it with araldite. In spite of careful filtering of the liquid blockages were not entirely eliminated which usually necessitated the removal of the blocked section with the result that the lengths of the coils were not kept constant during the course of the work. However, this did not effect the results as it was not necessary to know the flow rate of the liquid once the detector B was calibrated. One end of the coil was connected to a liquid reservoir through a septum sandwiched between two stainless steel washers with holes just large enough to take the capillary. The other end was connected to a vapouriser again by sealing it with a septum. The septums, which were made of silicone rubber, had to be changed frequently to maintain the seal as they swelled both in β-pinene and in halocarbons.

By varying the pressure in the reservoir the liquid rate and hence the gas concentration could be changed. The same effect could also be achieved by varying the carrier flow rate to the vaporiser. The top end of the reservoir was connected to the pressure regulator P3 via a toggle valve for quick depressurisation.

The reservoir used was the saturator S1 described in the previous section. A diagram of the vaporiser is shown in Fig. 4.3.2. All parts were made of stainless steel and it was packed with stainless steel wire mesh to increase its heat capacity and to facilitate uniform vaporisation. Heating was supplied by wrapping it with heating tape and the temperature of the gas leaving was measured by a thermocouple at the outlet. The nitrogen system prior to entering the vaporiser was preheated by passing it through 60 cm long coiled tube placed in a heater. The preheater was made up of a 30.3 cm (1 ft) long, 3.5 cm (1 in) ID steel tube heated by resistance wire wrapped round and insulated from it by a glass tube 0.2 cm thick. The insulation on the outside was provided by an asbestos cylindrical shell. To promote heating a small fan was used to blow air down the inside of the preheater.

Preliminary studies indicated that because of the small capacity of lines between the vaporiser and column A, any fluctuations caused either by non-uniform vaporisation or variations in liquid flow rate effected immediately, especially at high nitrogen rates, the concentration plateau in the chromatographic column. This was overcome by placing the saturator S2 after the vaporiser to act as a large capacity. It was packed with stainless steel wire mesh and heated by circulating either oil or water from the constant temperature bath described in the previous section.

In halocarbon runs below 35°C because of the small difference between the ambient and the oven temperatures, the control of the oven temperature was not up to its specification of 0.1°C. To overcome this problem the F11 oven was replaced by the temperature bath described above. The heating medium was water and with the laboratory windows opened to keep the ambient temperature at about 15°C, a precision of 0.1°C could again be achieved. In these cases with the temperature bath out of the flow circuit, the capacitor S2 was also taken out.

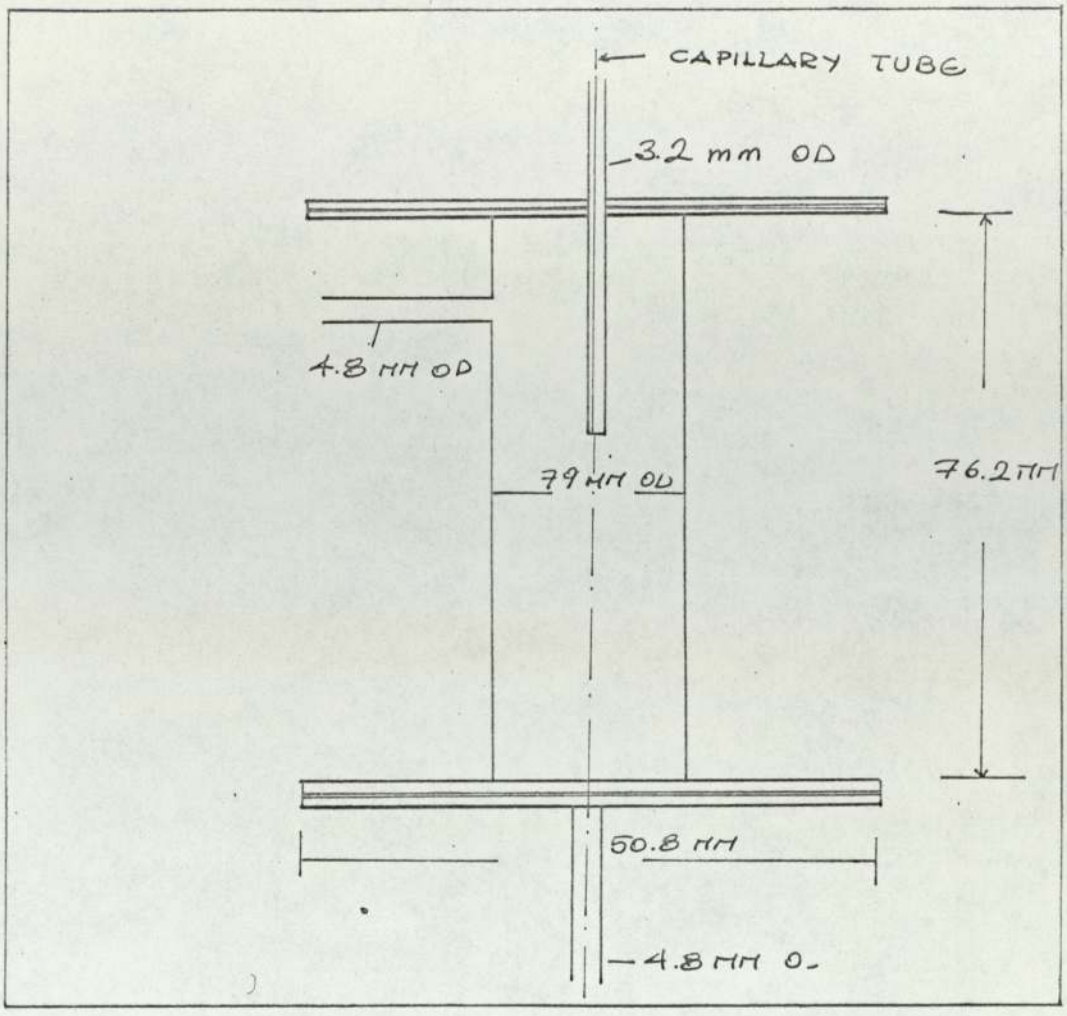

FIG. 4.3.2 - VAPORISER

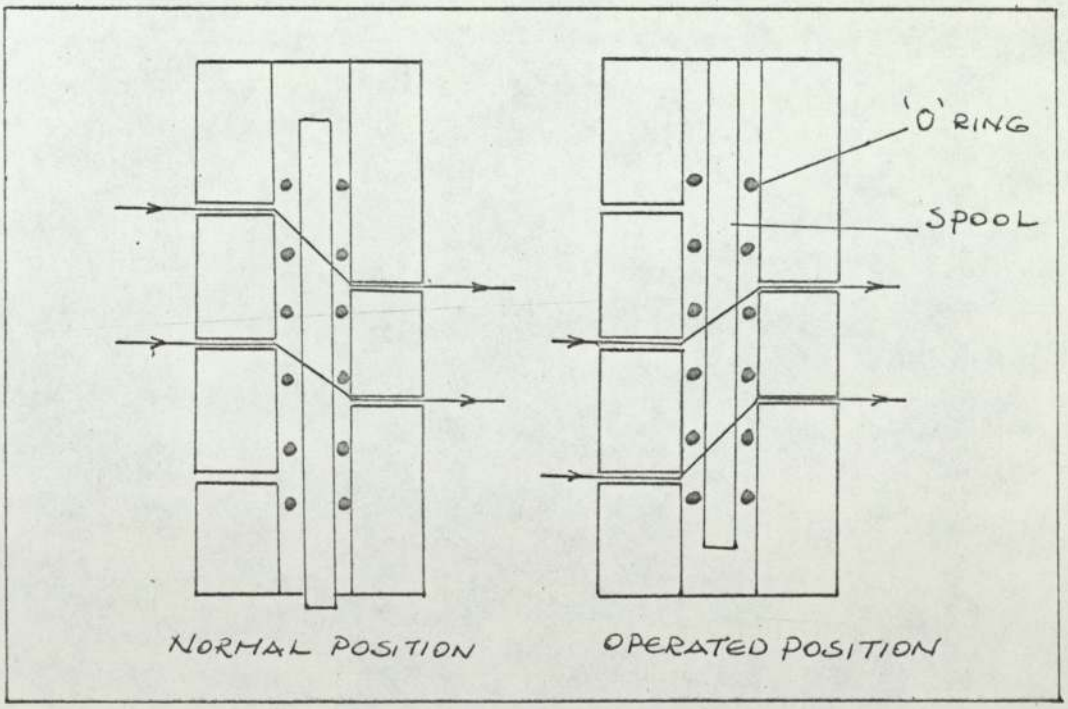

FIG. 4.4.1 - PRINCIPLE OF OPERATION OF A 5 PORT SPOOL VALVE

With these arrangements a very flexible operation with good control of the gas concentration was achieved.

4.4 Gas Sampling Unit.

High boiling points of α and β pinenes, 155°C and 158°C respectively, meant that a gas tight syringe could not be used for sampling as it would have to be heated to above 50°C to prevent condensation at high concentrations. Even with low boiling liquids like acetone it was found to be very difficult to obtain a reproducibility of better than 5%. Because of the high cost of commercial gas sampling valves it was decided to build one using a 5-port spool valve obtained from A. Schrader & Son Ltd. The principle of operation of such a valve is shown in Fig. 4.4.1.

A hard chrome plated piston floats in static viton 'O' rings which are retained by a series of perforated shells. The position to which the groves of the piston are moved determines which exit port is open to the supply. Two of these valves were connected to each other as shown in Fig. 4.4.2 to form the gas sampling valve. When in the normal position carrier passes along the solid lines to column B, while the solute carrying stream enters through the other port and leaves the valve via a sample loop of approximately 1 cm^3 in volume. When the valve is actuated the carrier stream sweeps away the contents of the loop while the solute stream is transferred along the broken lines. Theoretically the size of the sample injected should be determined solely by the volume of the sample loop. However, in practice it was found that the longer the duration of actuation the greater was the sample size and the tailing on the trailing edge of the peak produced. Three seconds was chosen as the actuation time on the basis of its being capable of being timed accurately and producing little or no tailing.

The gas sampling valve was enclosed in a box made up of 0.95 cm (5/8 in) thick compressed asbestos sheets. The internal dimensions of

the box were:

Width = 15.2 cm (6 in), Height = 14.0 cm (5½ in), Length = 20.4 cm (8 in).

The heating was provided by two 60W, 120V steel jacketed "Cressall" heaters mounted on the side walls and connected to a variac. The temperature of the incoming and outgoing solute streams were measured by two thermocouples just outside the box. A mercury U manometer was also connected at this point to the inlet side to measure the pressure drop across the sample loop as the pressure drop in the lines after the valve was negligible. The carrier outlet port was connected to column B by a 0.8 mm (1/32 in) ID tube through the injection septum at the analyser head.

In earlier work the actuation of the valve was achieved pneumatically, the return being by springs at the other end of the valve. The on-off operation of pneumatic pressure was effected by a manually actuated 3-port spool valve which when in one position let the supply pressure act on the pistons of sample valve and in the other exhausted the lines while at the same time cutting of the supply pressure. As the gas sampling valve operated free of any lubricating grease, frequent sticking of the spools were caused by insufficient spring pressure. This was overcome by replacing the spring by pneumatic heads thus achieving the arrangement shown in Fig. 4.4.2. In this case the actuation was provided by a solenoid-actuated, pilot-operated 5-port spool valve. This is similar in operation to the other 5-port spool valves, but the actuation is achieved by the solenoid's opening a small hole connecting the supply pressure port to the pneumatic head. The timing of the actuation was done automatically by an electronic timer connected to the solenoid which could repeat the operation at preset time intervals. A circuit diagram of the timer is shown in Fig. 4.4.3.

The design of the trap, used to condense solutes from the gas leaving

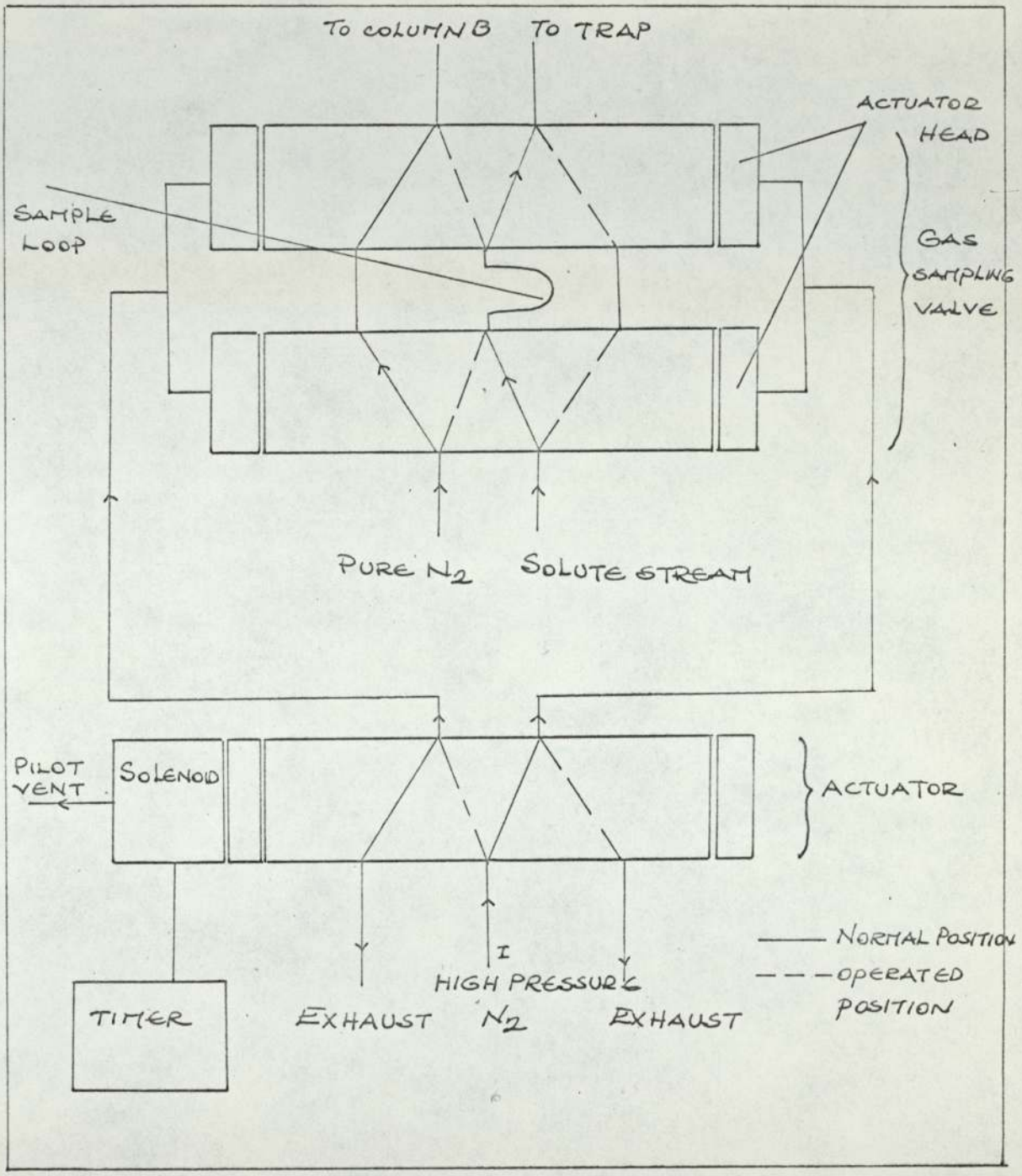

FIG. 4.4.2 - GAS SAMPLING UNIT

Plate 4.3. Gas Sampling Unit

GSV - Gas Sampling Valve
SL - Sample Loop
SV - 5-Port Spool Valve
S - Solenoid.

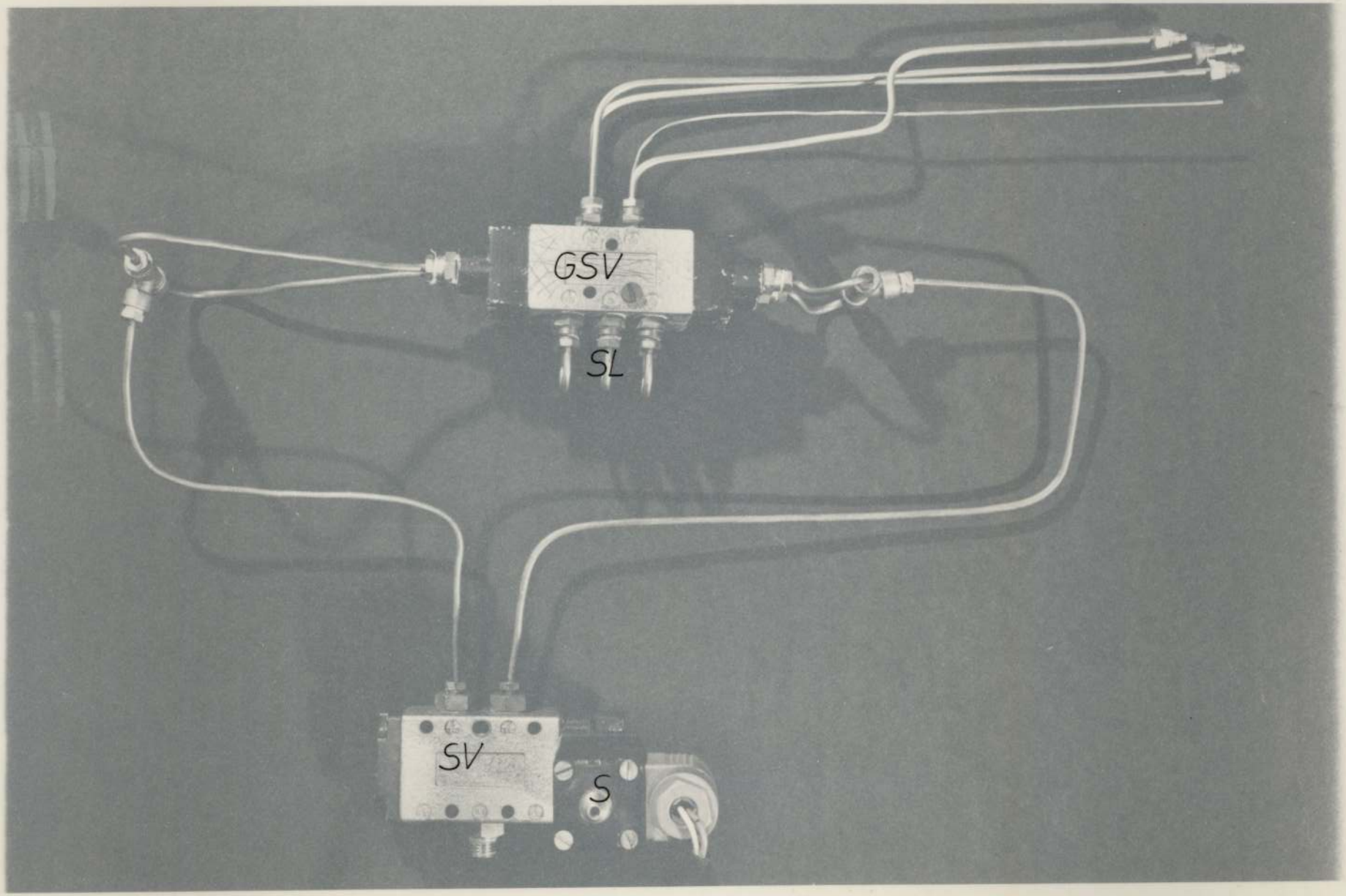
GSV
SL
SV
S

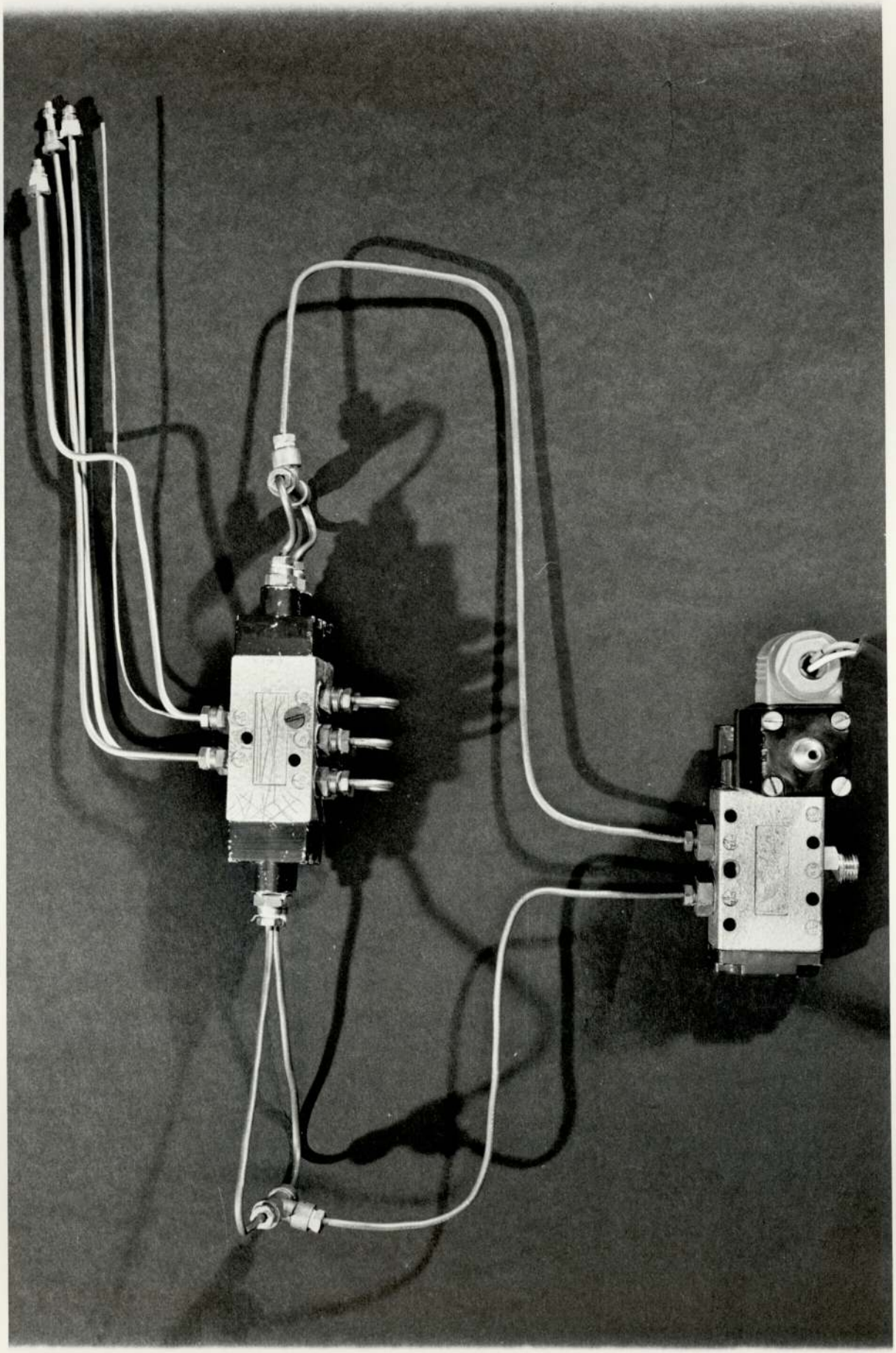

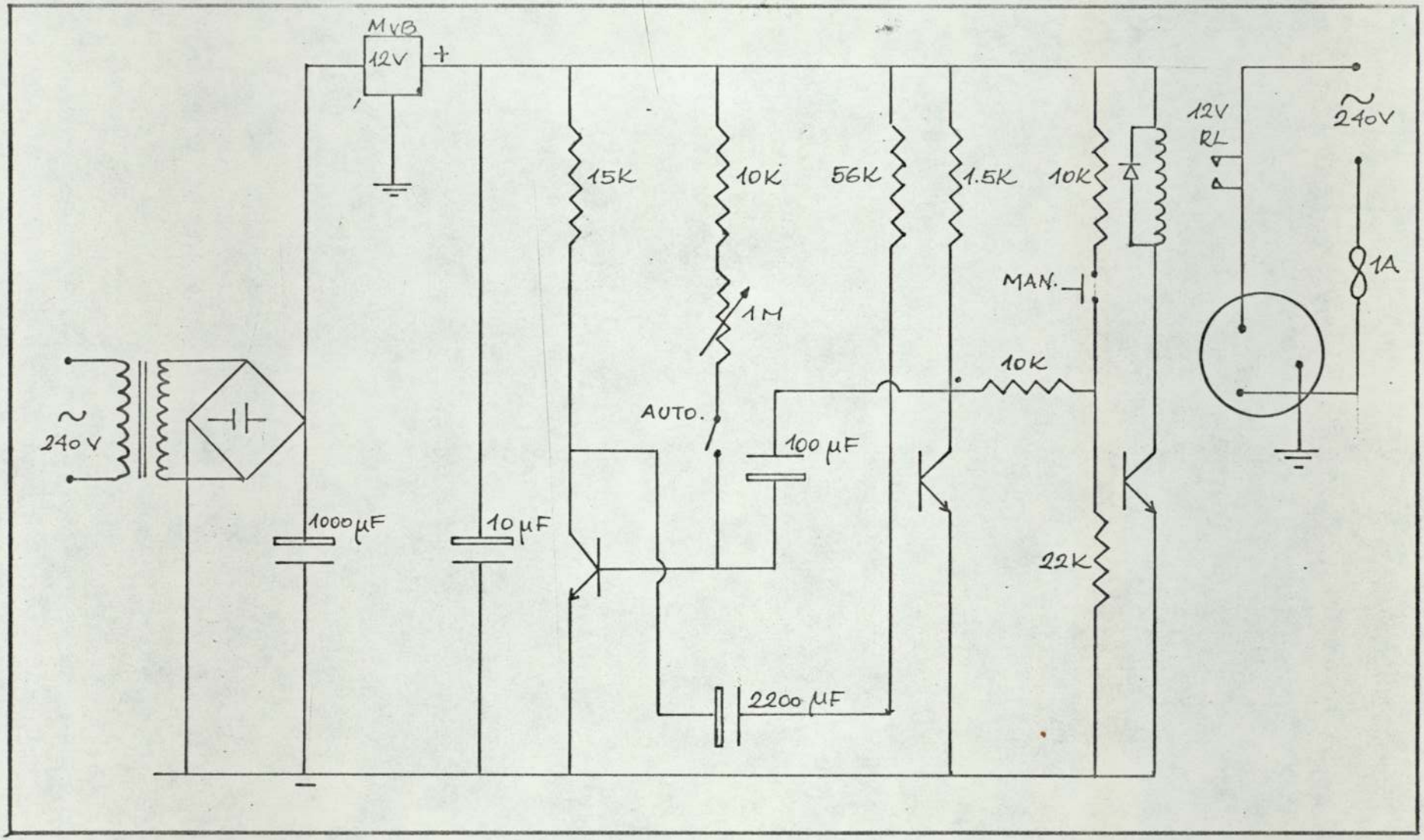

FIG. 4.4.3 CIRCUIT DIAGRAM OF THE TIMER

the gas sampling valve, was the same as those used on the outlets from the continuous chromatograph and is shown in Plate (11.4). The cooling medium was ice which proved to be ineffective for halocarbons.

5. EXPERIMENTAL WORK.

The experimental work was conducted to investigate the thermodynamic behaviour of the polymer solutions as well as to provide data for the large scale chromatographs in operation in this department. For the latter reason the systems chosen were those currently investigated in the large scale chromatographs:

A. Binary Systems

1. α-Pinene/Polypropylene Sebacate.
2. β-Pinene/Polypropylene Sebacate.
3. Dichloromethane/Silicone Oil MS 200.
4. 1,1,2 Trichloro - 1,2,2 Trifluoroethane (Arklone-P)/Silicone Oil MS 200.
5. 1,1,1 Trichloroethane (Genklene-P)/Silicone Oil MS 200.

B. Ternary Systems

1. α-Pinene/ β-Pinene/Polypropylene Sebacate.
2. Dichloromethane/Arklone-P/Silicone Oil MS 200.
3. Dichloromethane/Genklene-P/Silicone Oil MS 200.
4. Arklone-P/Genklene-P/Silicone Oil MS 200.

The chromatographic method of measuring thermodynamic properties and investigating solution behaviour has become well established over the past 10-15 years, though experiments involving polymers are very few due to the complexity of such systems with the consequent difficulty of interpreting the results. The starting point in the measurement of any thermodynamic quantity by a chromatographic method is the elution volume measurement. From this the thermodynamic quantities such as partition coefficients and activity coefficients can be calculated. By investigating the variations of these quantities at different temperatures and solution compositions, other thermodynamic quantities such as heat of mixing or entropy of mixing

can be calculated or the validity of the various solution theories can be tested.

The results and their interpretations with the above systems are given in the following chapters. This chapter is concerned with the experimental techniques and procedures involved and the effects of various operational variables on the results.

5.1 Measurement of Carrier Flow Rates.

5.1.1 Flow Rate to Detector 'B'.

Detector 'B' was used to measure the concentration of the plateau on the other channel of the chromatograph. Since the flame ionization detector is very sensitive to the carrier flow rate and also to the ratio of the carrier rate to the hydrogen rate, it was essential that its carrier rate be measured accurately and kept constant throughout the experiments.

The flow rate measurements were carried out by a soap bubble meter made from a 50 cm^3 burette graduated in 0.1 cm^3. The gas entered the burette from a side arm which extended into the burette upwards forming a small jet. A small amount of dilute soap solution was kept in a rubber holder attached to the base of the burette. By squeezing the rubber a soap film could be created at the tip of the jet which then travelled up the vertical burette. The rate of travel of the soap film was timed with a stop watch. The burette was thoroughly washed with chromic acid and rinsed with distilled water before the introduction of the soap solution.

The flow rates were corrected for the vapour pressure of the soap solution at the ambient temperature (assumed to be equal to the vapour pressure of water at the same temperature). To ensure that the gas was saturated with water vapour a 12.7 cm (5 in) long, 0.795 cm (5/16 in) ID glass tube, packed with small pieces of wet fire brick, was inserted in the line just before the soap-bubble meter. All the flow rates were

converted to 101.33 KN/m^2 and 15.5°C.

To measure the flow rate the soap-bubble meter was connected to the detector end of the column via a length of 0.318 cm (1/8 in) OD stainless steel tube that passed through a hole drilled in the analyser head. During α-pinene runs where the flow rate was controlled by a pressure regulator this procedure assumed that there was no pressure drop across the FID itself that could alter the flow rate once the column was reconnected to the detector. This, in fact, was found to be true when a pressure tapping was inserted between the column and the detector. Although the oven did not require more than 10 minutes (slightly longer at temperatures below 50°C) to reach a required temperature, at least 30 minutes was allowed before taking a measurement to ensure that the column had also reached the same temperature. At least 5 or 6 readings were taken over a period of time and the mean is reported.

In the α-pinene runs where the carrier gas was supplied from a pressure regulator the above procedure was repeated at each of the four temperatures and the inlet pressure was reset to obtain the original flow rate.

In the β-pinene and halocarbon runs the flow controller F2, Fig.4.2, was found to be very adequate in compensating for any change in the back pressure through the temperature ranges employed. This was not surprising in view of the fact that whereas the pressure drop was only 69-103 KN/m^2 between 100-150°C at the flowrate of 41.75 cm^3/min. the flow controller could supply up to 454 KN/m^2 as set by the pressure regulator P2.

5.1.2 Flow Rate to Detector 'A'.

Since the sensitivity of this detector was of no consequence, the only requirements were that the carrier flow rate be kept constant during a single elution run and that its value be known accurately.

Two different experimental and computational procedures were employed.

1. ∝-Pinene Runs:

In these runs the flow rates were measured individually at each concentration. First the column was allowed to equilibriate at the required gas concentration as observed by a smooth recorder trace. The analyser head was then lifted, the column was quickly disconnected from the detector and connected to the soap bubble meter. The oven was allowed to attain its original temperature and the flow rate was measured. To prevent the ∝-pinene vapour from condensing in the soap-bubble meter, an ice-cooled glass trap, see Plate (11.4), was placed in the line just before the glass tube containing wet fire brick. In the course of the runs conducted on the continuous chromatograph this type of trap was measured to be over 95% efficient in removing pinene vapours from nitrogen gas.

The effective flow rate, F(y), was calculated (6-8) from equation (5.1.1)

$$F(y) = F(o) \frac{1+k}{1+k(1-y)} \qquad (5.1.1)$$

where F(o) is the solute vapour free gas flow rate as measured by the soap bubble meter

k is the capacity ratio given by $\frac{q}{c}\frac{V_L}{V_g} = K \frac{V_L}{V_g}$

Although k changes with concentration, the second term on the right-hand side of equation 5.1.1 is not very sensitive to concentration as it contains k both in the numerator and in the denominator. In the calculations the infinite dilution value of k was used to calculate the flow rate at the next heighest concentration. The newly found value of k was then used to calculate the flow rate at the next concentration, and

so on up the concentration range.

2. β-Pinene and Halocarbon Runs:

The technique described for α-pinene, although accurate, was very laborious and lengthy. The opening of the oven top and disconnecting the column from the detector inevitably upset the flow conditions in the whole system and as a result the concentration level took a long time to settle back to its original value. This proved to be a major disadvantage, especially at high concentrations when initial stabilisation times werevery long (2-3 h). It was also found in some runs that the flow rate had changed more than the accepted 1% and the run had to be repeated.

To overcome these problems it was decided to devise a means of monitoring the flow rate continuously during the course of the run. One of the most common ways of doing this is to measure the pressure drop across a capillary tube kept at a constant temperature. The only available constant temperature bath was the F11 oven which was too small to take any extra fittings. Therefore the calibration was based on the pressure drop across the chromatographic column (see Section 4.2.2). The experimental calibration data at each of the temperatures used is presented in Tables A.2.1, A.2.2 and plotted in Figures A.2.1 and A.2.2 of Appendix A.2. The data was originally plotted on a scale twice as large as that of Figs. A.2.1 and A.2.2. The manometer used was a 100 cm long U tube fitted with coloured carbontetrachloride, whose density is presented in Table A.3.1 of Appendix A.3. A scale attached to the U tube enabled the pressure drop to be read to 0.05 cm.

According to equation 4.2.1 the pressure drop across a packed column is proportional to viscosity. Since the calibration was carried out with pure nitrogen a correction had to be made to the measured flow rate for the presence of solute vapour, according to equation 5.1.2,

$$F(y) = F(o) \quad \frac{\mu(o)}{\mu(y)} \qquad (5.1.2)$$

where y is the mole fraction in gas phase

F(y) is the corrected flow rate

F(o) is the flow rate read off from the calibration chart

$\mu(o)$ is the viscosity of nitrogen

$\mu(y)$ is the viscosity of the nitrogen-solute vapour mixtures.

In the absence of any experimental data the vapour viscosities of the systems employed were calculated from the equations available in the literature. A summary of the equations are given below. A more detailed discussion together with the calculated results are presented in Appendix A.4.

1. β-Pinene:

The viscosity of β-pinene was calculated from Arnold's equation (111)

$$\mu = \frac{27.0 \cdot M^{\frac{1}{2}} T^{3/2}}{V_b^{2/3} (T+1.47\ T_b)} \qquad (5.1.3)$$

2. Dichloromethane (DCM)/Arklone-P (A-P)/Genklene-P (G-P):

The viscosities of these halocarbons were calculated from the Bromley-Wilke equation (112)

$$\mu = \frac{33.3\ (M\ T_c)^{\frac{1}{2}}}{V_c^{2/3}} \quad f(1.33\ T) \qquad (5.1.4)$$

3. Nitrogen:

The viscosity of nitrogen was also calculated from equation (5.1.4).

4. Nitrogen-Solute Mixtures:

The mixture viscosities were calculated from the individial viscosities according to the equation, (113-a)

$$\mu(y) = \frac{\sum y_i \mu_i (M_i)^{\frac{1}{2}}}{\sum y_i (M_i)^{\frac{1}{2}}} \qquad (5.1.5)$$

Because of the small gas phase concentrations involved in this work the maximum correction was about 6%.

5.2 Auxiliary Gases.

A combination of pressure regulators and flow restrictors on the lines before the detectors were used to control the flow rates of both hydrogen and oxygen. Since the FIDs were not designed to be gas tight the only way to measure these flow rates would have been to place a rotameter on the line after the appropriate pressure regulator. However, this would have necessitated the calibration of the rotameter for each pressure setting. Since these flow rates did not come into the calculations they were not measured and the pressures were set according to the considerations of detector performance.

5.3 Detector Performance.

It is known that the sensitivity of a flame ionization detector depends on various factors of which the most important are:

1. The voltage applied across the electrodes.
2. The distance between the electrodes.
3. The ratio of hydrogen flow rate to carrier flow rate.
4. The flow rate of hydrogen.
5. The flow rate of oxygen.

The first two variables on the F11 are fixed by the manufacturer. Therefore the only way to alter the sensitivities of the detectors was to alter the three flow rates. These were set according to different criteria for the two detectors, dictated by the different duties they had to perform.

5.3.1 Performance of Detector 'B'.

In setting the flow rates to this detector the following points had to be considered:

1. The need to maximise the detector performance.
2. The limitation imposed on the carrier flow rate by the gas sampling valve (G.S.V.).

The detector performance with regard to the three flow rates was investigated by injecting 0.6m cm^3 of α-pinene at 130°C and by measuring the height and the area of the peak produced. The results are shown in Tables 5.3.1 and 5.3.2 and Figs. 5.3.1 and 5.3.2. Owing to the poor reproducibility of liquid sample injection only the mean of the results at each hydrogen pressure is plotted in Figs. 5.3.1 and 5.3.2. As can be seen from the former graph at constant oxygen pressure the detector response initially increased sharply with the hydrogen pressure and then levelled off and even slightly dropped. The actual point of level-off was determined by the nitrogen flow rate, changing from 253 KN/m^2 of H_2 pressure at the nitrogen rate of 23.15 cm^3/min to 336 KN/m^2 at 64.1 cm^3/min. The higher the nitrogen rate the higher is the maximum sensitivity. If the detector performance is measured by the peak area rather than the peak height then an entirely different picture emerges as shown in Fig.5.3.2. This is due to the fact that the lower the carrier flow rate the shorter and broader are the peaks. Again the maximum response is obtained between the hydrogen pressures of 253-336 KN/m^2. This is, of course, a better representation of the detector response as the amount injected is measured not by peak height but by peak area . One important conclusion that can be drawn from this graph is that the maximum response is determined by the hydrogen flow rate whatever is the carrier flow rate.

The actual carrier flow rate chosen was influenced by the operation of the gas sampling valve (G.S.V). At low flow rates appreciable tailing

Table 5.3.1. Response of Detector 'B' to Carrier and Hydrogen Flow Rates at the Oxygen Pressure of 240 KN/m^2.

Carrier Flow Rate at NTP cm^3/min	Hydrogen Pressure KN/m^2	Peak Height cm	Peak Area cm^2
35.7	170	5.9	7.95
	170	6.1	8.09
	198	13.4	17.1
	198	13.35	17.0
	253	19.1	23.7
	253	19.25	23.0
	281	20.2	23.7
	281	19.65	24.8
	308	19.65	23.5
	308	19.4	23.1
	336	19.5	23.4
	336	19.7	23.3
	364	18.0	20.2
	364	19.6	22.0
23.15	170	5.3	9.64
	170	5.3	9.52
	198	12.35	20.0
	198	12.2	19.4
	226	15.8	23.3
	226	16.0	23.95
	226	16.6	24.5
	253	16.2	23.05
	253	16.7	23.25
	253	15.6	23.4
	308	15.5	23.4
	308	16.0	23.6
	308	16.75	25.25
	308	16.10	23.45
	336	15.8	21.7
	336	16.2	22.9

Table 5.3.1 Continued.

Carrier Flow Rate at NTP cm^3/min	Hydrogen Pressure KN/m^2	Peak Height cm	Peak Area cm^2
64.1	170	5.9	4.55
	170	5.1	3.76
	170	5.0	3.74
	170	4.75	3.42
	198	11.9	11.2
	198	12.05	11.25
	226	17.9	16.95
	226	16.95	16.65
	226	17.7	17.53
	253	19.8	17.95
	253	20.6	19.83
	308	24.1	23.6
	308	22.2	20.9
	308	23.65	23.5
	336	24.6	23.6
	336	24.5	23.6
	336	29.16	23.3
	364	22.4	22.55
	364	24.1	22.5
	364	25.3	22.6
	364	23.6	21.7

Other operating conditions:

Oven temperature: 130.0°C

Oxygen pressure: 240 KN/m^2

Sample size: 0.6 m cm^3

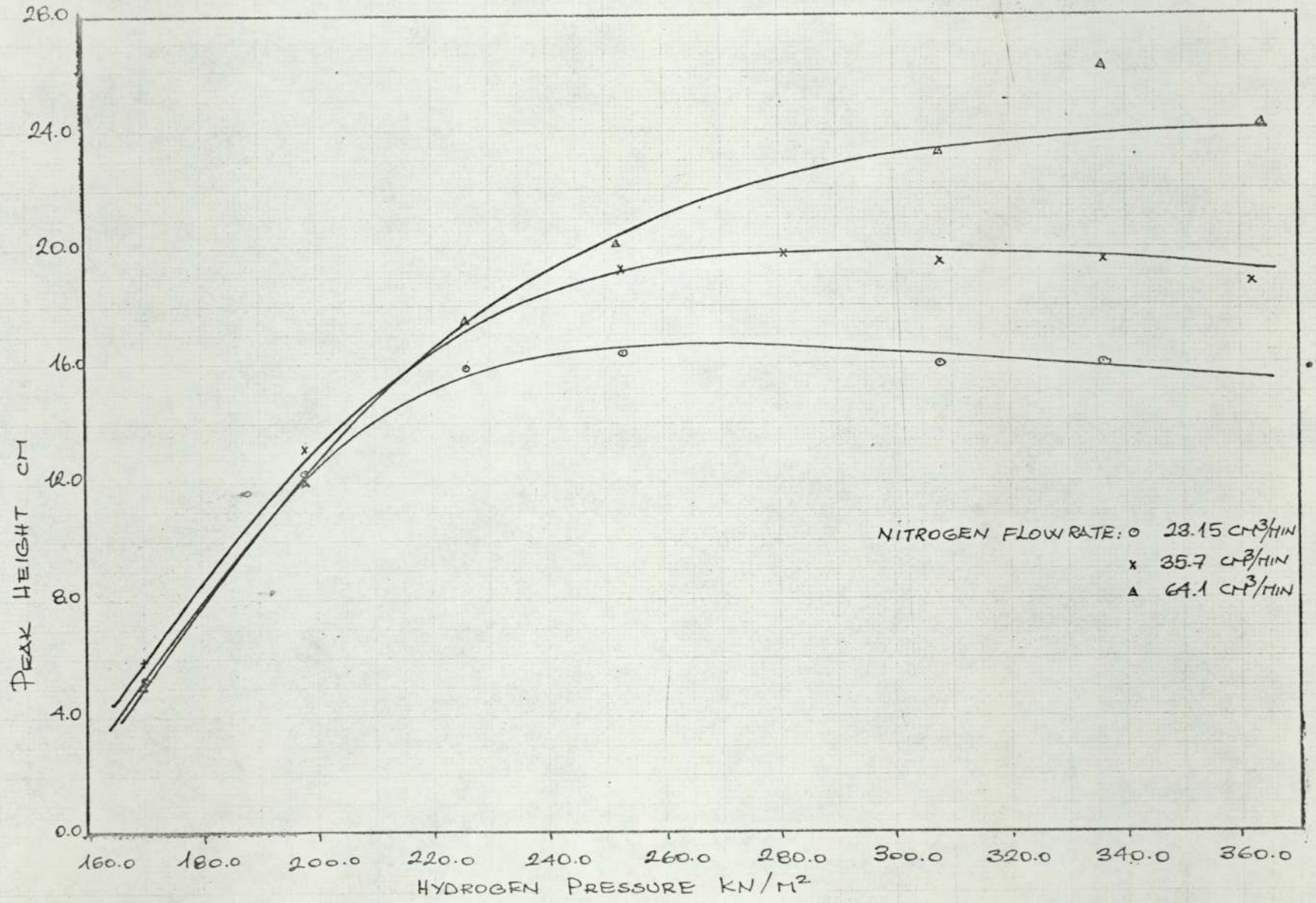

FIG. 5.3.1 RESPONSE OF DETECTOR 'B' TO HYDROGEN AND CARRIER FLOW RATES

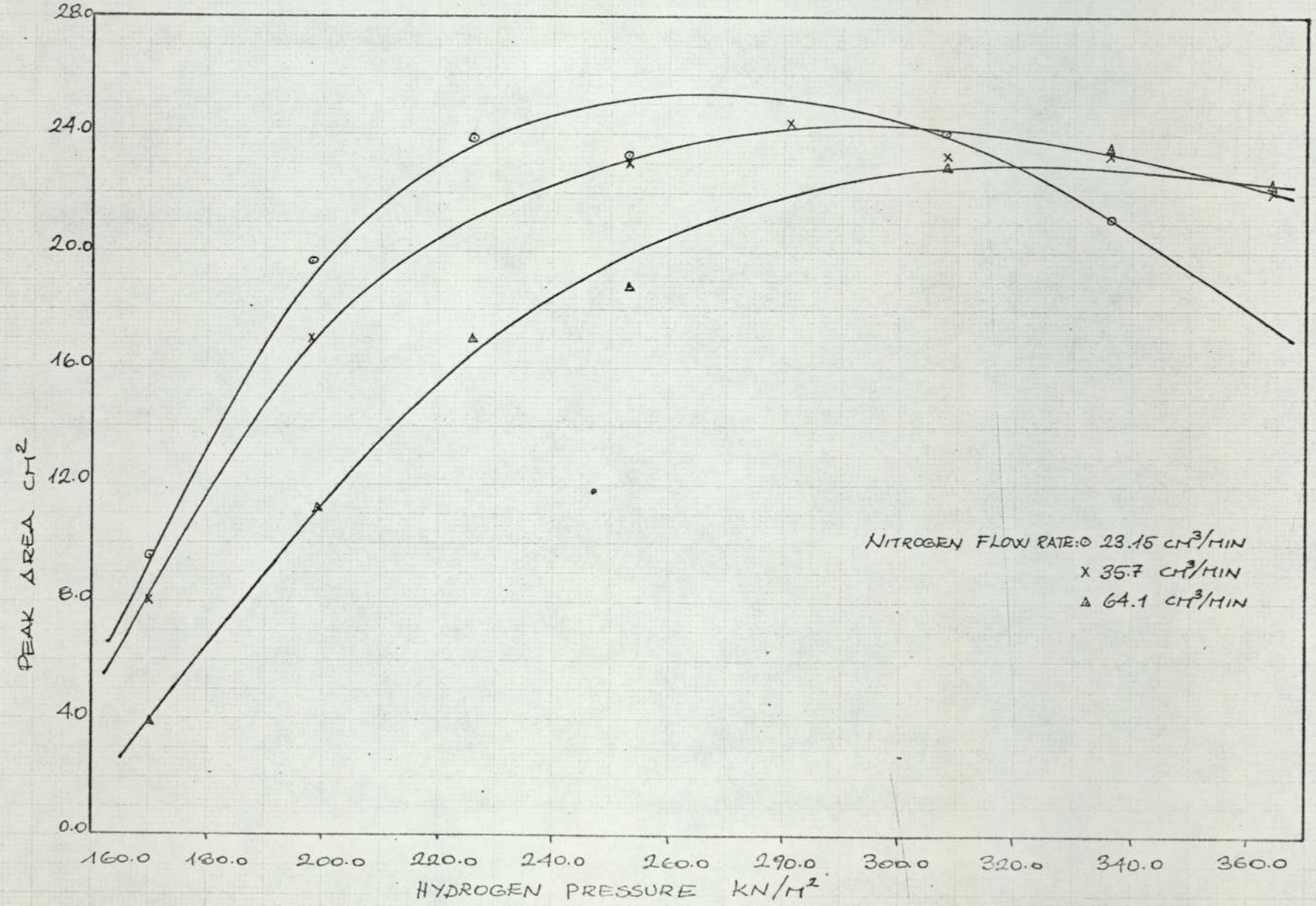

FIG. 5.3.2 RESPONSE OF DETECTOR 'B' TO HYDROGEN AND CARRIER FLOW RATES

was observed. This was thought to be caused by diffusion and mixing in the lines from the G.S.V. to the top of the chromatographic column. On the other hand, at high flow rates, the stability of the flame was upset. This is probably due to the fact that while the sample loop operated at atmospheric pressure the carrier gas that swept it was at much higher pressure. At much above 240 KN/m^2 it was even observed to upset the concentration plateau in the other detector.

In the case of the pinenes another point of consideration was the resolution of the peaks, as the same detector was used to analyse the vapour phase concentration in the continuous chromatographic runs.

Preliminary studies with various flow rates showed that 40-50 cm^3/min at the hydrogen pressure of 308 KN/m^2 would satisfy the above requirements.

Oxygen was used to aid combustion instead of air for higher sensitivity, but the experiments showed that, Table 5.3.2, the oxygen flow rate had no effect on the detector response and, therefore, it was arbitrarily set to 240 KN/m^2. This finding is in contrast to the work of some other authors (57) who found that the sensitivity increased with oxygen flow rate.

Table 5.3.2. Detector Response Versus O_2 Rate at Nitrogen Flowrate of 641 cm^3/min and H_2 Pressure of 240 KN/m^2.

Oxygen Pressure KN/m^2	Peak Height cm	Peak Area cm^2
170		18.75
240	209	19.75
240	19.85	19.3
240	20.1	18.9
308		18.75
378		18.5

At no point during these experiments was any background noise observed. Only at the carrier rate of 23.15 cm^3/min and a hydrogen pressure of 364 KN/m^2 was there a slight base line drift. It is suspected that the same phenomenon might be observed at the other carrier rates if the hydrogen rate is raised sufficiently. The flow conditions are summarised below.

Table 5.3.3. Flow Rates to Detector 'B'.

Runs	Nitrogen Flow Rate at NTP, cm^3/min	Hydrogen Pressure, KN/m^2	Oxygen Pressure, KN/m^2
α-Pinene/β-Pinene	41.75	308	240
DCM/A-P/G-P	47.70	308	240

5.3.2 Performance of Detector 'A'.

The carrier flow rate to detector 'A' was set individually for each run to obtain reasonably long retention times for accurate timing but not too low so that the peaks were not excessively broad. When the carrier gas contained solute vapour, the detector was very sensitive to the carrier flow rate,its response increasing with the flow rate. This, in fact, was a good check on whether the flow rate had altered during a run.

In the presence of solute vapour the detector response was also found to increase with the hydrogen flow rate. The response of this detector was not required to be kept constant, indeed it was impracticable to keep it constant because of the need to vary the carrier flow rate. Therefore, the hydrogen pressure was altered to suit a particular run. At low concentration it was increased to get a high response while at some high concentrations it was decreased to keep the recorder trace within the chart paper. Generally the pressure was 205-308 KN/m^2.

The oxygen pressure was the same as in the other detector, i.e. 240 KN/m^2 as it could not be set independently.

5.4 The Chromatographic Column.

5.4.1 Preparation of Solid Support.

Since one of the aims of this research was to provide data for the large scale chromatographs, the same types and sizes of solid supports were used in the analytical columns.

1. α-Pinene/β-Pinene Runs:

The solid support used was 30-44 BS mesh Celite obtained from Johns-Manville Ltd. This was first washed with distilled water to remove fines. It was then placed in a flask with concentrated nitric acid and boiled under total reflux conditions for 30-45 minutes. The acid was decanted off and the Celite washed several times with distilled water until all the traces of the acid were removed as checked by pH paper. It was then dried at 80-100°C. The acid washing of Celite is known to reduce active sites that cause adsorption and hence tailing of the eluted peak (38,114).

2. DCM/A-P/G-P Runs:

The solid support was 30-44 mesh fire brick that was available in this department. This was also washed with distilled water to remove fines but no acid-wash treatment was given. This was partly because it was used untreated in the large scale chromatograph and partly because the acid washing of pink diatomaceous supports is of doubtfull value (38).

5.4.2 Stationary Phase.

The stationary phases were also those used in the large scale chromatographs, namely Polypropylene Sebacate (PPS) for the pinenes and Silicone Oil MS 200 for the halocarbons. They were chosen for their good separating qualities. Their molecular weights (or rather molecular weight ranges as both are highly polydisperse compounds) were of special interest as they entered the activity coefficient calculations. The molecular

weight of PPS was measured by the method of intrinsic viscosity, explained in detail in Appendix A.5. Its molecular weight was also checked by gel permeation chromatography by the Rubber and Plastics Research Association of Great Britain. The molecular weights of Silicone Oil MS 200 was supplied by its manufacturer, Dow Corning Ltd. These values are summarised below:

Table 5.4.1. Molecular Weights of the Stationary Phases.

Stationary Phase	Wt Average MW	Number Average MW	Z Average MW	MW Range
PPS	3,160	1,620	4,980	-
MS/200	7,100	-	-	1,600-25000

The number average molecular weight of PPS measured by the intrinsic viscosity measurements were 1,630 and 1900 in benzene and chloroform respectively.

5.4.3 Coating of the Solid Supports and Packing of the Columns.

The loadings of the packings were the same as in the large scale chromatographs, i.e. 20% w/w PPS on Celite and 25.0% Silicone Oil MS 200 on fire brick. These high loadings were intially chosen to facilitate high throughputs in the large scale chromatographs, but they also help to eliminate solid support adsorption and to reduce the contribution of Gibbs adsorption to the overall partitioning process. In other words, the partition coefficients measured under these conditions can be taken as being equal to the bulk liquid partition coefficient as would be measured by the conventional techniques.

To coat the support the required amount of the stationary phase was carefully weighed and dissolved in about ten times its own volume of an

appropriate solvent. The solvents used were acetone for Polypropylene Sebacate and dichloromethane for Silicone Oil MS 200. A weighed amount of solid support was added to this solution. The whole mixture was then carefully transferred to the flask of a rotary evaporator. A combination of a water bath at slightly above ambient temperature and a water pump connected to the rotary evaporator helped to slowly remove the solvent while the rotating action ensured that the mixture was thoroughly mixed and a uniform coating was obtained. When all the solvent evaporated the contents were further dried at about 50°C.

To check the effectiveness of the coating procedure it was decided to reverse the above operation and strip the packing of its stationary phase and measure the amount removed. These experiments were carried out on a batch of 20.00% w/w Polypropylene Sebacate on Celite prepared for the pinene runs. A small amount of packing was put in a Buckner funnel with an oversize, very fine, filter paper that covered the sides of the funnel to prevent fines escaping. The Buckner funnel was connected to a water pump and its contents thoroughly washed with about 500 cm^3 of acetone. The packing was then transferred to an oven where it was allowed to dry at 50°C for about one hour and weighed. The results are shown in Table 5.4.2.

Table 5.4.2. Checking of the Packing Loading.

Run No.	Sample wt before washing g	Expected wt of stationary phase, g	Measured wt of stationary phase, g	% Error
1	2.00032	0.40006	0.40289	+0.71
2	2.0010	0.40020	0.40765	+1.86

Considering the small amounts that had to be measured the agreement is good.

The sign of the error, positive, indicates that perhaps the drying operation was not complete.

The column material used in all cases was 0.476 cm (3/16 in) OD, 0.317 mm (1/8 in) ID stainless steel tube obtained from Frank Stacey & Co. Ltd. The column lengths chosen were roughly 60 cm for Channel 'A', chosen with the aim of minimising the pressure drop while obtaining reasonably long retention times, and 250 cm for Channel 'B', chosen to obtain a good resolution of the peaks though this was not very important in the case of the three halocarbons.

Before packing a column, it was thoroughly washed with acetone and dried with dry filtered nitrogen. It was then packed by adding a small amount of the packing at a time and gently tapping the side of the column until the packing level stopped dropping. When this happened both ends of the column were sealed by a small plug of glass wool.

The particulars of the columns are summarised in Table 5.4.3. Different sets of columns had to be used for α-pinene and β-pinene runs as the columns 1-A and 1-B were destroyed when the oven overheated (to over 400°C) caused by an electrical fault.

Table 5.4.3. Chromatographic Columns.

Column No	System	Stationary Phase	Total wt of Packing, g	Wt of Stationary Phase, g	wt % loading
1-A 1-B	α-Pinene	Polypropylene Sebacate	1.34752 8.44900	0.26950 1.68980	20.00%
2-A 2-B	β-Pinene	Polypropylene Sebacate	1.10985 6.6390	0.22197 1.32780	20.00%
3-A	DCM/A-P/G-P	Silicone Oil MS 200	2.7350 11.1678	0.68411 2.79345	25.01%

5.4.4 Measurement of the Column Gas Hold-up.

There are three standard methods of measuring the column hold-up when a flame ionization detector is used:

1. Using a standard.

2. Estimating it from the column dimension and packing density.

3. From the elution time of a methane peak.

The first one requires that the partition coefficient of a compound in the particular stationary phase is known. Unfortunately no solubility data was available in these particular stationary phases. Furthermore, since they are polymers their characteristics are likely to change from one manufacturer to another, even from one batch to another.

The second method was also not considered reliable because of the presence of various fittings between the column and the analyser head.

The third method, used in this work, is sometimes considered unreliable as a generally applicable method because of the solubility of methane in organic solvents (115,116). This claim is not borne out by the values in Table 5.4.4 which gives the average gas hold-up at different temperatures. If methane were soluble in these stationary phases then one would expect a progressive decrease in the calculated gas hold-up with increase in temperature, and this is obviously not so. Considering the elution times that had to be measured, 10-20 seconds, they are very consistent except for two, Column 1-B at 120°C and Column 2-B at 150°C. In all cases the length of the gas syringe needle was the same as that used to inject the solutes, i.e. 12.7 cm (5 in). The amount injected was kept below 0.2 cm^3 to prevent it from making a significant contribution to the carrier flow rate.

Hilmi (57) in his work with volatile hydrocarbons reported a fourth method in which a small negative peak is produced when air is injected into the carrier stream containing solute vapour. This could not be observed in this work. It may be that it is submerged in the disturbance

created by the injection action which persisted right up to the methane peak. Increasing the size of the injection was no help as it also increased the size of the disturbance.

Table 5.4.4. Calculated Column Hold-up at Different Temperatures.

Column No	Temperature ^{o}C	V_g cm^3
1-B	99.8	6.086
	120.0	5.302
	1110.0	6.150
	150.0	5.760
2-B	100.35	5.60
	110.1	5.658
	120.0	5.611
	150.0	6.340
3-B	24.8	5.695
	29.1	5.802
	34.7	5.707
	39.8	5.814
	45.1	6.010
	60.5	5.793
	74.0	5.828

5.5 Effects of Variables on Retention Data.

5.5.1 Effect of Pressure Drop and Flow Rate.

The effect of flow rate on the elution volume is caused by the non-ideality and compressibility of the gas phase. Since the condition of zero pressure drop can never be attained the gas flow rate increases down the column as the gas expands. It is sometimes stated tha gas phase diffusion at too low a flow rate and resistance to mass transfer in either phase at too high a flow rate would prevent the establishment of equilibrium in the column and thus effect the elution volume. Chromatographic theories clearly show that these kinetic processes only

cause band broadening and do not affect the position of the peak maximum. In other words, the peak maximum is always at equilibrium.

Conder and Purnell (12) derived a correction factor for the pressure drop at finite concentrations. According to this the corrected retention volume (V_R') is given by

$$V_R' = J V_R = J t_R F(y) \qquad (5.5.1)$$

where t_R is the elution time

$F(y)$ is the effective flow rate

and the form of the correction factor J is given in Appendix 1 (equation A.1.1 to A.1.4).

At small solute concentrations and near atomospheric pressure J can be approximated J^3_2 without any significant loss of accuracy.

The form of equation A.1.2 suggests that a plot of V_R' versus $\frac{(p_i/p_o)^3-1}{(p_i/p_o)^2-1}$ should be a straight line with a slope equal to $(2/3)V'_R$. Testing this requires the measurement of V_R through a wide range of pressure drops which was not possible with the present apparatus. The results of one set of experiments, Table 5.5.1, carried out with the three halocarbons at 45.1°C with a limited range of flow rates, were inconclusive as might be expected.

5.5.2 Effect of Sample Size.

The technique of Elution on a Plateau (EP) used in this work to measure the partition coefficients at finite concentrations of a solute, assumes that the concentration of the sample injected is small compared to the concentration of the plateau. If this condition is not fulfilled, then the partition coefficient measured does not correspond to the concentration of the plateau but to some higher concentration. Therefore, it is essential that the maximum size of the sample that can be used without violating the above condition is known. This point, in fact, proved to be a major limitation of the EP technique for two reasons.

Table 5.5.1. Effect of the Carrier Flow Rate on the Elution Volume at Infinite Dilution.

Solute	Flow Rate cm^3/min	V_R cm^3	J_3^2	V_R' cm^3
DCM	16.35	46.20	0.968113	44.73
	21.09	45.38	0.959400	43.54
	25.18	46.22	0.951410	43.97
	28.53	46.38	0.945976	43.88
	33.24	46.78	0.937667	43.58
		Mean=46.19 RMSD=0.46 (0.99%)		Mean=43.94 RMSD=0.43 (0.98%)
A-P	16.35	51.79	0.968113	50.14
	21.11	50.16	0.95940	48.12
	25.50	51.43	0.951410	48.93
	28.50	51.49	0.945976	48.71
	33.22	51.98	0.937667	48.74
		Mean=51.37 RMSD=0.64 (1.24%)		Mean=48.92 RMSD=0.66 (1.35%)
G-P	16.37	126.51	0.967784	122.43
	21.22	128.73	0.959116	123.47
	25.47	127.55	0.951410	121.36
	28.39	126.19	0.946189	119.40
	33.08	126.99	0.946091	120.65
		Mean=127.19 RMSD=0.89 (0.70%)		Mean=121.46 RMSD=1.11 (0.92%)

1. At high solute concentrations FID response became increasingly non-linear and insensitive to concentration. This meant that either the sample size had to be increased with concentration to get a large enough peak, or that the sample size was kept constant at the expense of accurate timing. It was also observed that the peaks became flat topped at high concentrations. This is also thought to be a function of the FID response.

2. With all the systems studied in this project the partition coefficients and thus the elution times were found to increase with concentration. Since the longer the elution time the broader the peaks are, it became increasingly difficult to locate the peak maximum as the solute concentration increased.

The result of both phenomena was to place a limit on the concentration level at which the partition coefficients could be measured accurately. These limits, which were also a function of column temperature and carrier flow rates, were decided individually for each run.

Table 5.5.2 and Fig. 5.5.1 show the effect of sample size on the elution volume of α-pinene and β-pinene at 110.1°C. All the points are mean of 3-4 injections. It is seen, particularly from the α-pinene figures, that up to about 0.1 m cm^3 the change in the elution volume is not measurable within the present experimental accuracy. From 0.1 to 0.2 m cm^3 the change is very small, if any, and after that increases linearly. The limit for these runs was, therefore, taken as 0.2 m cm^3, but most of the runs were conducted with sample sizes less than 0.1 m cm^3. Where bigger samples were needed these were compared with those obtained with 0.1 m cm^3 samples for any significant change. Unfortunately, these comparisons were not always conclusive because of the difficulty in timing small peaks. When this happened the average of all the injections was taken.

Of the three halocarbons, Genklene-P was chosen to investigate the effect of sample size. This was because:

1. The partition coefficients of Genklene-P increased with concentration more than the other two.
2. Its elution volume was very much higher, particularly at low temperatures, thus giving broader peaks and consequently needing bigger samples than DCM and A-P.

The results at 34.7°C are tabulated in Table 5.5.3 and plotted in Fig. 5.5.2. No change could be observed up to about 0.8 m cm^3 after which the elution volume increased sharply. In the actual runs the limit for G-P was set at 0.6 m cm^3 at which a maximum of 0.3 m cm^3 was quite adequate for DCM and A-P.

With all the 5 compounds trace amounts (less than 0.01 m cm^3) were sufficient to produce sizeable peaks at infinite dilution where lower amplifier attenuation could be used.

5.6 Calibration of Detector 'B'.

For the calibration of the detectors for the vapour phase concentration two experimental stages are required:

1. The creation of a vapour mixture of known concentration.
2. The injection of a sample of this mixture into the chromatograph and area measurement.

5.6.1 Measurement of the Concentration.

A survey of the literature revealed three techniques for the execution of the first step.

1. A known amount of the solute is injected through a septum into a flask containing the carrier gas. By measuring the volume of the flask and the pressure of its contents and the concentration of the mixture can be calculated. For high boiling point compounds the flask would have to be

Table 5.5.2. Effect of Sample Size on the Elution Volumes of α-Pinene and β-Pinene.

Solute	Sample Size m cm^3	V'_R cm^3
α-Pinene	0.02	40.87
	0.04	40.87
	0.06	40.88
	0.08	40.79
	0.10	40.67
	0.30	41.29
	0.60	41.97
	1.0	42.61
	2.0	44.78
β-Pinene	0.04	61.09
	0.1	61.45
	0.5	63.45
	1.0	65.80
	2.0	70.28

Table 5.5.3. Effect of Sample Size on the Elution Volume of Genklene-P.

Sample Size m cm^3	V'_R cm^3
0.6	175.82
0.8	175.78
1.0	178.21
2.0	183.53
4.0	191.40
6.0	198.24
8.0	208.95

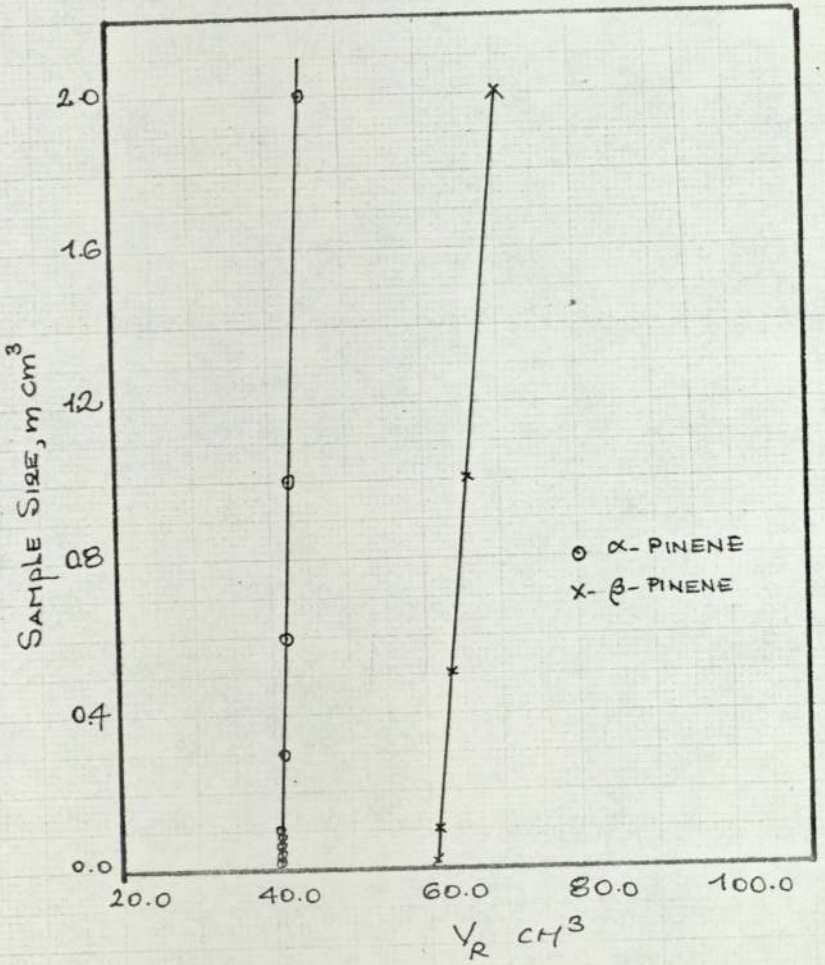

FIG.5-5-1 EFFECT OF SAMPLE SIZE ON THE ELUTION VOLUMES OF α AND β-PINENE

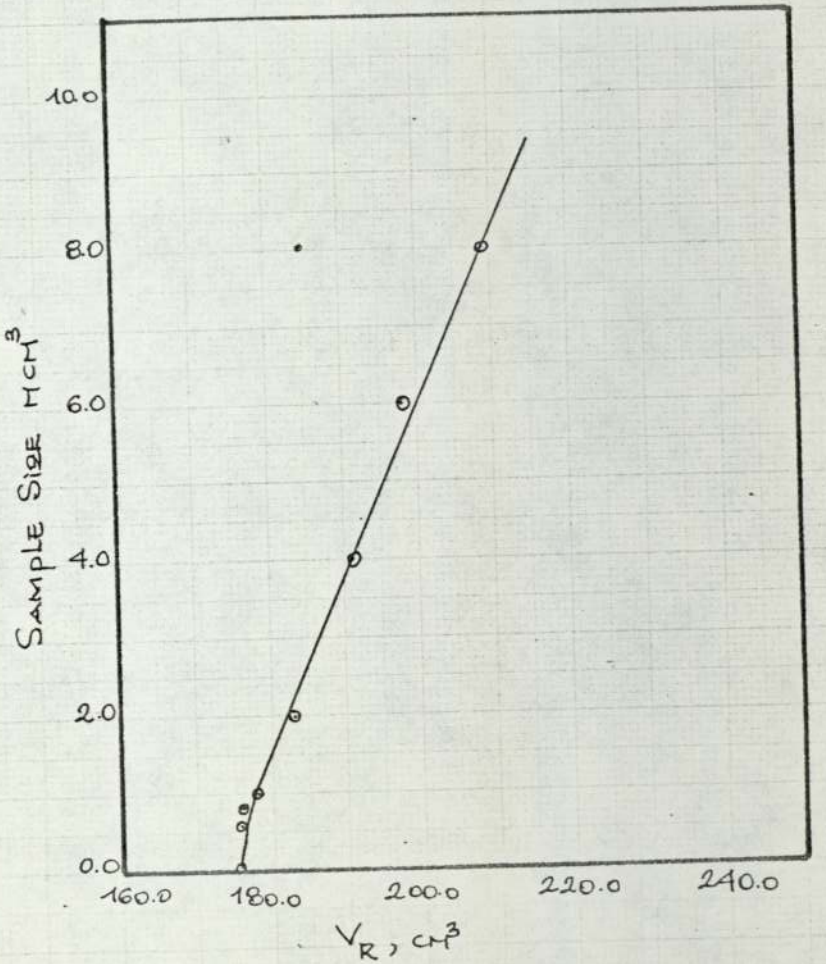

FIG.5-5-2 EFFECT OF SAMPLE SIZE ON THE ELUTION VOLUME OF GENKLENE-P

kept at an elevated temperature for high concentrations.

2. A carrier gas stream is passed through a saturator, or a number of them, containing the solute. If it is assumed that the gas is saturated at the temperature of the saturator, the concentration can be calculated from the vapour pressure of the solute and the flow rate of the carrier gas.

3. This is similar to the second technique except that the assumption of saturation is removed by calculating the concentration by determining the amount of the solute removed from the saturator in a given time (49).

Two different techniques were employed for ∝-pinene and for the rest of the systems. These are explained in detail below.

A. ∝-Pinene Runs.

For this compound the first technique was considered unsuitable as the only practical way of drawing samples from such a flask is by a gas syringe. This was considered inaccurate for the reasons given in the next section. The second technique was also considered unsuitable as an independent method is need to check the accuracy of the assumption of saturation. Therefore, a modified version of the third method was used. Instead of measuring the amount removed from the saturator, the amount collected on a bed of adsorbent was determined. The adsorbent used was granular charcoal, activated for gas adsorption, obtained from Hopkin & Williams Ltd. This was packed into a glass tube of the dimensions given below:

Length = 20.3 cm (8 in), outside diameter = 0.635 cm ($\frac{1}{4}$ in), inside diameter 0.397 cm (5/32 in).

One end of the tube was dimpled to hold the charcoal in its place and a small plug of glass wool was placed at both ends to prevent any fines dropping. The open end of the glass tube was joined to the 0.635 cm ($\frac{1}{4}$ in)

SS tube leading out of the sample loop of the gas sampling valve, see Plate (4.3). Heating tape was wrapped round right to the end of the SS tube to prevent the condensation of α-pinene until it reached the charcoal bed.

The efficiency of the charcoal was checked by placing two beds in series and weighing the amount collected in each one. It was found that until α-pinene reached $4/5^{th}$ of the first bed, as observed by the wetness of the charcoal due to the adsorption of α-pinene, nothing was collected in the second bed. In the actual experiments wetness was never allowed to pass the half-way mark.

In carrying out the calibration, the flow rates were set to achieve the desired concentration. The conditions were allowed to stabilise with a dummy bed in line as this introduced a certain back pressure (about 1.5 cm Hg) into the system. When the concentration became steady a freshly packed and carefully weighed bed was quickly exchanged with the dummy bed and the stop-watch started. The flow rate of the carrier gas was measured by the soap-bubble meter connected to the free end of the bed and the concentration was periodically checked by injecting samples into the chromatograph. After a certain period lasting from 20 to 50 minutes depending on concentration, the bed was disconnected and reweighed. The weighing was done to 5 decimal places, an average bed weighed about 8g. The pressure of the sample loop was measured by a mercury-manometer and the temperature was taken as the average of the inlet and outlet temperatures as measured by two thermocouples. The peak areas were then normalised at 101.33 KN/m^2 and 120.0°C according to the ideal gas law.

The results are tabulated in Table 5.6.1 and plotted in Fig.5.6.1. The relatively high scatter below a concentration of about $0.6 \times 10^{-4} g/cm^3$ suggests that this method is not very accurate for very low concentrations.

Table 5.6.1. Calibration of Detector 'B' for α-Pinene.

Amount Collected g	N_2 Flow Rate at NTP, cm^3/min	Concentration at NTP, $g/cm^3 \times 10^4$	Peak Area Integrator Units
0.04270	77.9	0.0995	85.8
0.05402	51.4	0.263	131.6
0.11369	67.00	0.356	166.7
0.18027	67.0	0.598	275.0
0.19343	60.7	0.797	410.2
0.15454	50.3	1.230	736.7
0.22691	46.3	1.634	987.8
0.22817	46.4	1.640	1046.9
0.31096	45.8	2.260	1516.0
0.23105	27.2	2.880	1900.0
0.3334	50.5	3.300	2172.7

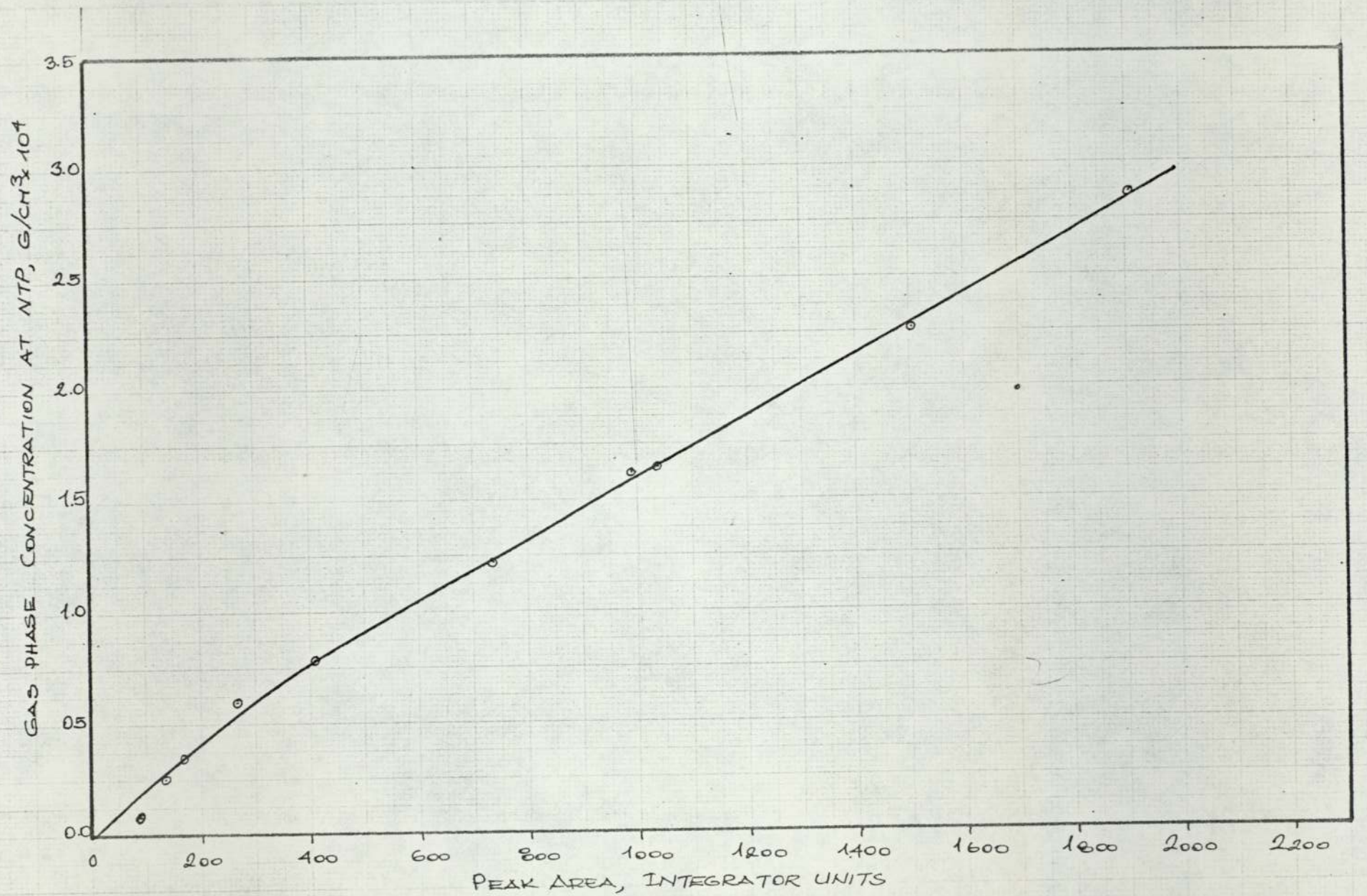

FIG. 5.6.1 CALIBRATION OF DETECTOR 'B' FOR α-PINENE

This is almost certainly caused by the fact that at these concentrations the weight of solute that had to be measured was very small compared to the total weight of the bed. However, this did not affect the accuracy of the thermodynamic measurements as in the whole of the α-pinene runs only one run was carried out at a concentration between this concentration and the infinite dilution value. An unexpected phenomenon, which was also observed with β-pinene, that used a different calibration technique, is the slight curvature below a concentration of about 0.8×10^{-4} g/cm^3, as shown in Figs. 5.6.1 and 5.6.2. It seems that below this concentration the sensitivity of the detector progressively decreases.

B. β-Pinene/DCM/A-P/G-P Runs.

The capillary pump incorporated in the design of the apparatus for these runs was capable of metering very small amounts of liquid. This greatly facilitated the measurement of concentration as the amount of solute in the carrier stream could now be easily calculated from the discharge rate of the capillary pump.

The flow rate of the liquid solute was measured by collecting it in a small sample bottle, weighing about 10g, over a period of time. To reduce the losses due to the vapour pressure of the solute the capillary was fed through a minute hole in the cap of the bottle which was immersed in an ice-salt mixture. The capillary was then reconnected to the vaporiser and the nitrogen flow rate was set to achieve a particular concentration. When the conditions had stabilised 4 or 5 samples were injected into the chromatograph for the peak area determination. Other concentrations were obtained simply by readjusting the nitrogen flow rate which was measured by the soap-bubble meter. The liquid flow rate was periodically checked and if it had altered more than 1% the runs were repeated. The sample loop pressure and temperature were again measured at each concentration and the peak areas were normalised at 101.33 KN/m^2

Table 5.6.2. Calibration of Detector 'B' for β-Pinene.

Liquid Solute Flow Rate g/hr	Nitrogen Flow Rate at NTP cm^3/min	Concentration at NTP, $g/cm^3 \times 10^4$	Peak Area Integrator Units
0.79676	496.8	0.267	129.8
	430.4	0.308	159.8
	352.5	0.377	198.2
	305.2	0.435	232.3
1.99085	514.30	0.645	335.6
	428.6	0.7742	409.5
	401.5	0.826	441.9
	368.15	0.901	503.9
	319.8	1.037	577.4
	298.9	1.110	637.0
	245.4	1.352	768.7
	195.5	1.697	972.3
	167.0	1.986	1182.9
	163.3	2.032	1275.0
	131.8	2.517	1554.0
	126.4	2.625	1600.2

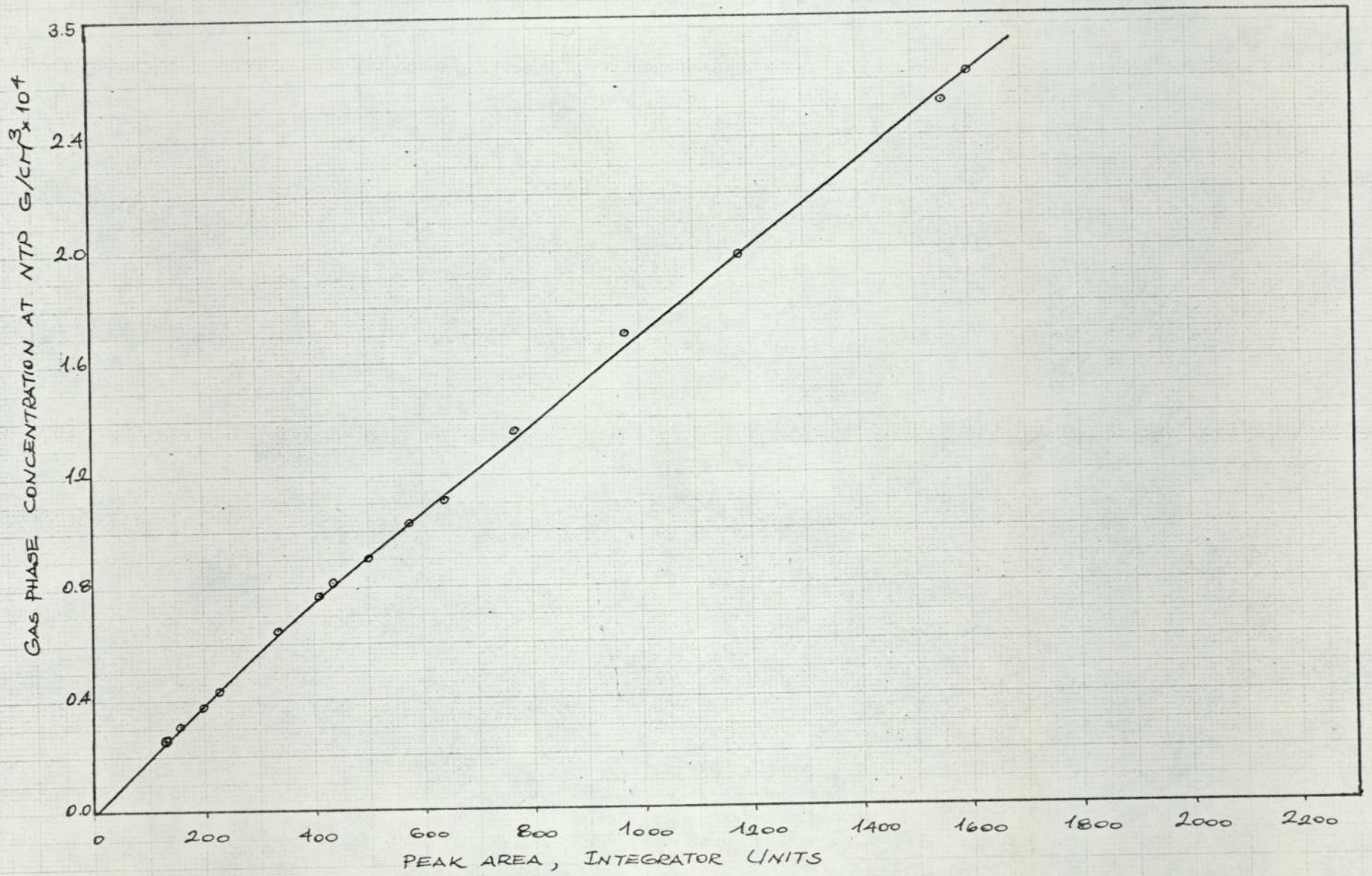

FIG. 5-6.2· CALIBRATION OF DETECTOR 'B' FOR β - PINENE

Table 5.6.3. Calibration of Detector 'B' for Genklene-P.

Run No	Liquid Solute Flow Rate g/hr	Nitrogen Flow Rate at NTP, cm^3/min	Concentration at NTP, $g/cm^3 x10^4$	Peak Area Integrator Units
1	1.9601	250.6	1.303	454.0
2		176.4	1.852	678.0
3	1.9800	109.9	3.003	1083.0
4	1.9601	108.65	3.006	1073.0
5	1.9800	86.6	3.810	1357.0
6		63.2	5.220	1862.0
7		58.65	5.630	2090.0
8		50.20	6.570	2517.0

Table 5.6.4. Calibration of Detector 'B' for Arklone-P.

Run No	Liquid Solute Flow Rate g/hr	Nitrogen Flow Rate at NTP cm^3/min	Concentration at NTP, $g/cm^3 x10^4$	Peak Area Integrator Units
1	2.0700	330.8	1.043	208.0
2		253.1	1.363	276.4
3		171.2	1.970	394.5
4		141.3	2.440	510.0
5		109.6	3.147	659.0
6		94.105	3.668	753.0
7		81.60	4.230	881.0
8		75.20	4.586	953.0
9		67.90	5.080	1068.0
10		61.35	5.620	1206.0

Table 5.6.5. Calibration of Detector 'B' for Dichloromethane.

Run No	Liquid Solute Flow Rate g/hr	Nitrogen Flow Rate at NTP cm^3/min	Concentration at NTP, $g/cm^3 \times 10^4$	Peak Area Integrator Units
1	3.29616	532.2	1.031	206.3
2		359.5	1.523	381.3
3		264.3	2.0787	486.4
4		193.0	2.8459	675.1
5	3.42800	172.5	3.312	787.7
6		152.7	3.741	884.5
7		129.3	4.419	1028.6
8		107.0	5.337	1268.0

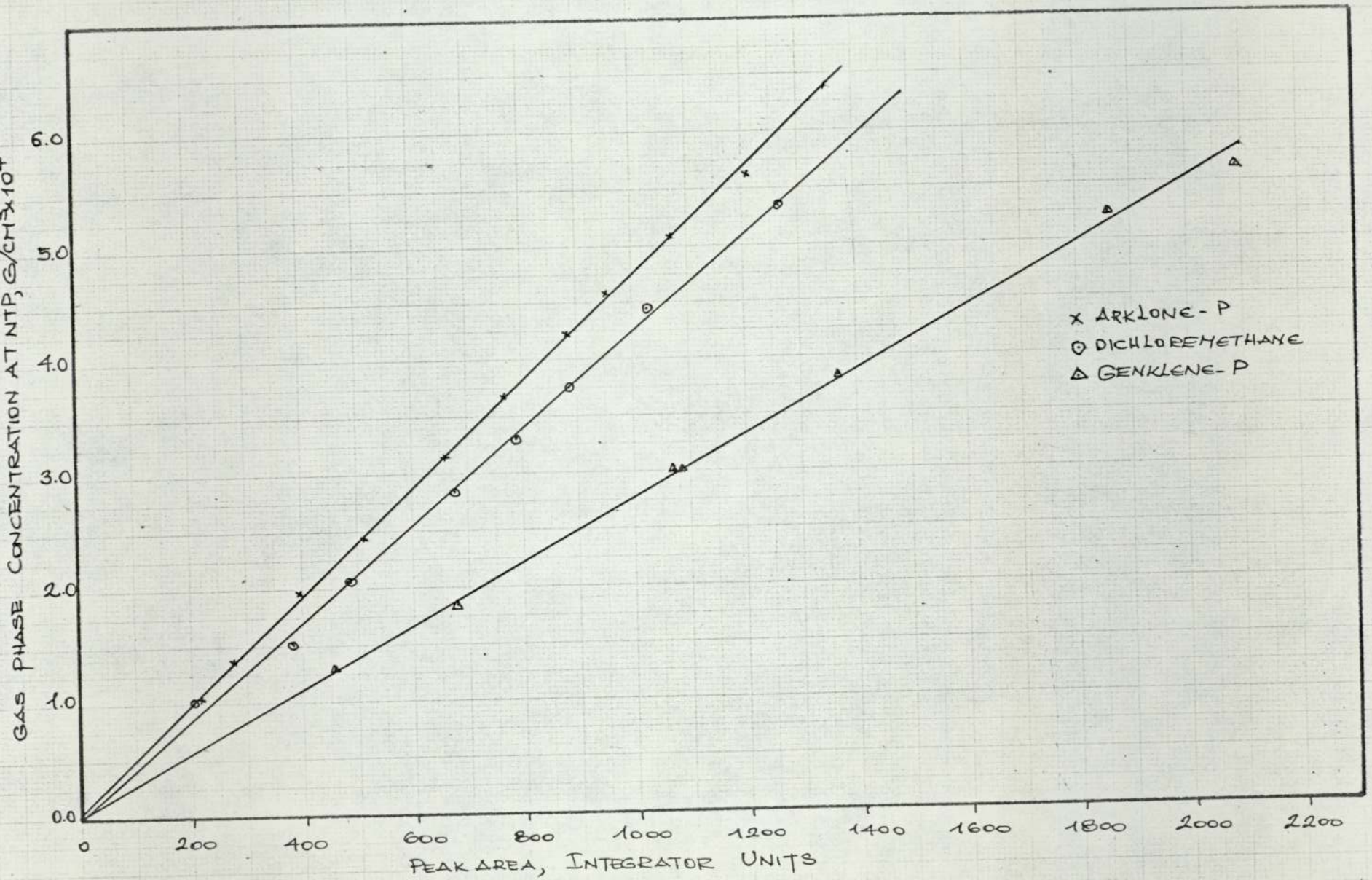

FIG. 5.63 CALIBRATION OF DETECTOR 'B' FOR DICHLORO METHANE, ARKLONE-P AND GENKLENE-P

and 75°C, 50°C, 35°C, 39°C for β-pinene, G-P, A-P and DCM respectively.

The results are shown in Tables 5.6.2, to 5.6.5 and Figs. 5.6.2 and 5.6.3.

5.6.2 Injection of the Gas Sample and the Measurement of the Peak Area.

The most commonly used gas sampling device is a gas tight syringe. The major drawback of this instrument is its confinement to low boiling compounds, i.e. those whose vapour pressure at ambient temperature is higher than its partial pressure at a particular concentration, otherwise condensation will occur. Heating the syringe will not overcome this problem as it will render the actual amount injected uncertain. Even with volatile compounds it is very difficult to get reproducible results as preliminary experiments with acetone showed that even the mode of injection affected the size of the peak. With α-pinene and β-pinene, whose saturation points are 64.5°C and 69.5°C respectively at the concentration of $3 \times 10^{-4} g/cm^3$ at NTP, which is the maximum used in this work, the use of a gas syringe was clearly impossible. Therefore, a gas sampling valve of the design explained in Section 4.4 was constructed.

Since the calibrations were carried out in terms of concentration rather than the actual amount of the solute, the volume of the sample loop was not required to be known, but it was estimated to be about 1 cm^3 from the dimensions of the sample loop tube. Ideally the sample loop should be kept at a constant temperature, but in the present design extensive temperature gradients were found to exist in the box that housed the gas-sampling valve. This could have been overcome by inducing circulation by a small fan. However, it was found that the temperature of the stream leaving the gas-sampling valve was very much dependent on the temperature of the stream entering it. Since the latter was produced by heating tapes connected to a variac it could not be controlled with any

precision. Instead, the temperatures of the incoming and outgoing streams were measured by two thermocouples and the peak areas were corrected to some datum temperature.

With the present set-up the reproducibility of the gas sampling valve injections could not be isolated from the fluctuations that might occur in the stream it was sampling. Throughout this work 2% variation about the mean was set as the maximum, though in the majority of the runs the reproducibility was better than this. A typical reproducibility is shown in Table 5.6.6 which gives the peak areas obtained at the β-pinene concentration of $0.774 \times 10^{-4} g/cm^3$.

Table 5.6.6. Reproducibility of Gas Sample Injections.

Run No	Peak Area Integrator Units
1	404
2	406
3	403
4	406
5	409
6	411
7	413
8	413
9	413
Mean = 408.7 RMSD = 3.7 (0.90%)	

In some of the preliminary work the peak areas were measured by cutting the peaks out with a scalpel blade and weighing them. The observed variations in the weight per unit area of graph paper meant that this had to be measured in the immediate vicinity of each peak to obtain a reproducibility of about 2%. Later, however, an electronic integrator,

a Kent Chromolog II, was acquired which was found to be very satisfactory for the purposes of this work. Provided that the integrator base line was zeroed after each peak, its reproducibility was about 0.2% which is the same as the maximum precision with which the peak heights could be measured.

5.7 Experimental Procedure.

The experimental procedure was composed of two parts:

1. The measurement of the elution volumes (Channel 'A').
2. The measurement of the solute vapour concentration in the carrier gas (Channel 'B').

These are described in detail below.

5.7.1 Measurement of the Elution Volumes.

The part of the experimental procedure employed prior to the actual measurement of the elution volumes was slightly different with the two designs described in Chapter 4.

A. α-Pinene Runs.

The flow rate of nitrogen from the saturators and that of the pure nitrogen stream were adjusted to give the required concentration and the carrier flow rate. The concentration could also be adjusted by varying the temperature of the saturators. Although this was a lengthier operation, it was sometimes preferred when the carrier rate was wanted to be kept the same as in the previous run. In these runs the analyser head had to be lifted to gain access to the chromatographic column for the flow rate measurement. Once the flow rate was measured the column was reconnected to the detector and the conditions were allowed to return to their set values.

B. β-Pinene and Halocarbon Runs.

Since the design of the apparatus in these runs had the capability of monitoring the carrier flow rate continuously, the oven was left on permanently once the required temperature was obtained. Only slight adjustments had to be made for the day to day variations. The concentration was invariably adjusted by altering the pressure in the solute reservoir.

When the conditions had stabilised, as observed by the constancy of the concentration plateau height in detector 'A' as well as the constancy of the peaks produced by detector 'B', the elution volume measurements were started. A small liquid sample was injected onto the column and the appearance of the peak maximum was timed with a stop-watch. Two stop-watches, one capable of timing to 0.2 second and the other to 0.05 second, were used. At least 3 or 4 injections of each solute were timed. A typical chromatogram is shown in Fig.5.7.1. As mentioned before, the peaks became broader and flatter at high concentrations. In these instances the peak maximum could not be located immediately. Instead the beginning and the end of the peak plateau were timed with the second stop-watch, which had two second hands, and the arithmetic mean was computed. The syringe used was a 1 m cm^3 Hamilton syringe equipped with a 12.7 cm (5 in) long needle which enabled the injections to be made directly above the column.

The major difficulty experienced in this work was the problem of condensation and adsorption on the injection septum. This was held in a septum cap about 2.5 cm away from the heated injector block, which meant that the septum was at a considerably lower temperature than the carrier stream. Condensation showed itself by a sudden increase in the plateau height, thought to be caused by the entrainement of the condensed solute. The effect of adsorption was the appearance of unexpectedly big peaks even

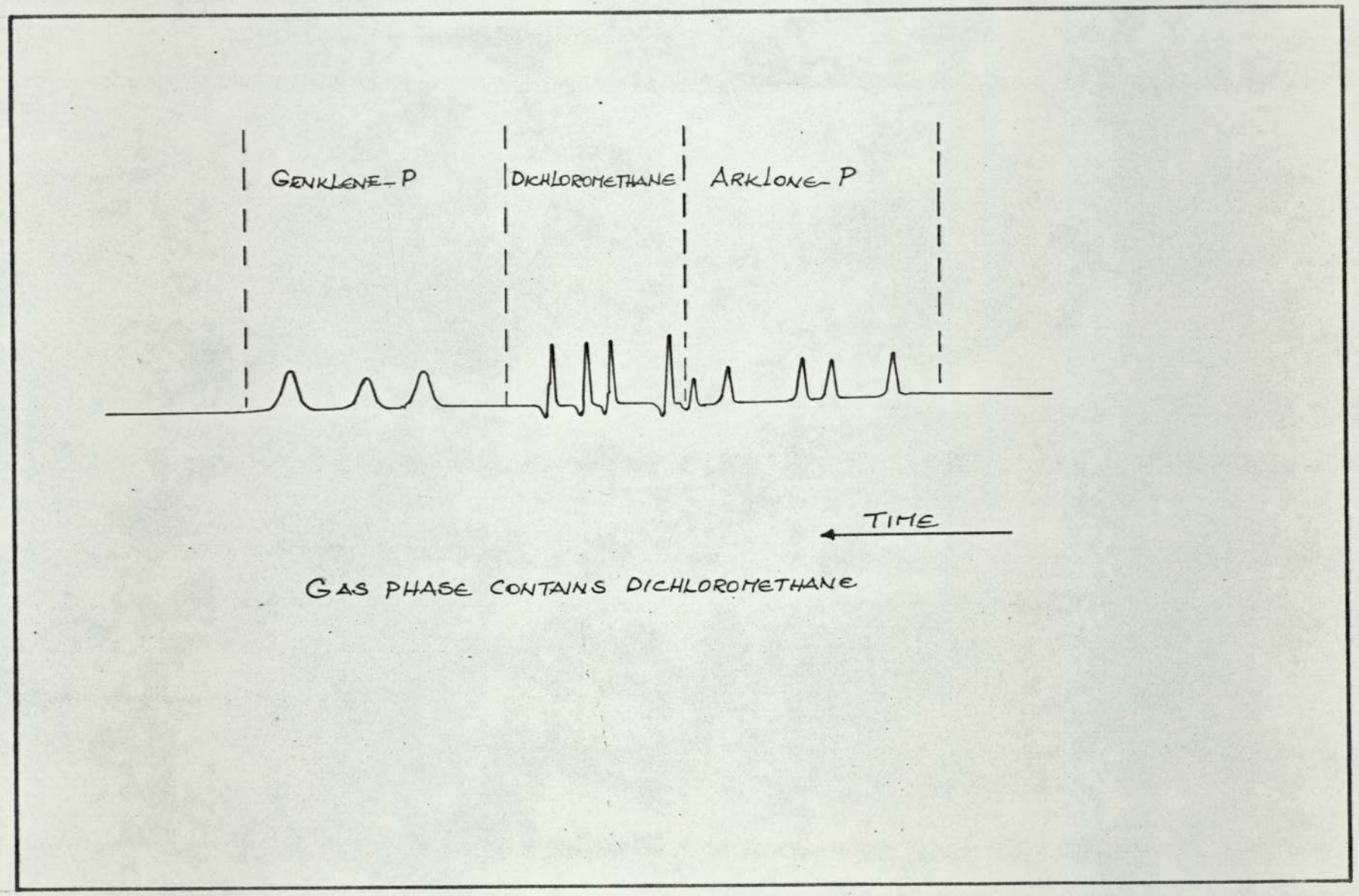

FIG. 5.7.1- ELUTION VOLUME MEASUREMENTS

when the syringe was thought to be free of any solute. The piercing action of the needle is thought to have the effect of injecting the solute adsorbed in the septum. Condensation was prevented by wrapping heating tape round the septum cap at the expense of shortening the septum life. Adsorption on the other hand could not be prevented. Several types of septums were tried but were found to swell considerably in all the compounds used. A material that is resistant to these solutes is teflon which is too hard as a septum but is available as a thin backing on conventional septums, or in tape form which can be wrapped around the septums. Both forms were tried, but were found to be useless in protecting the septum after a few injections.

The only way round this problem was to conduct the runs as quickly as possible before the solute built up in the septum. This, of course, was not always possible and some runs had to be abandoned to change the septum. As a result, while the duration of most runs was 2 to 4 hours, those at very high concentrations took up to two days to complete successfully.

5.7.2 Measurement of Concentration.

The concentration of the plateau was determined by measuring the peak area produced by a sample of the carrier solute stream injected by the gas sampling valve. The sample loop temperature and pressure was measured and the peak area corrected to the conditions of the particular calibration. At least three or four samples were injected before the start of the elution volume measurements and the same was done at the end of the run to check for any variations in the concentration level. The mean of the peak areas was computed and the concentration was read off from the appropriate calibration chart.

5.8 Purity of Materials

Very high purity pinenes are prohibitively expensive. Although some 99%+ α and β pinenes were obtained in the course of the experiments with the rotating chromatograph, the quantities obtained were not enough to safisfy the needs of the equilibrium studies. Therefore, it was decided to purify the relatively pure and commercially available α and β pinenes on a batch distillation column. The column consisted of two 1 m long, 2.5 cm (1 in.) i.d. glass tubes with a 1 litre round bottom flask as the still. The packing was made up of rolls of 2.5 cm (1 in.) diameter multi-strand, stainless steel knitted mesh.

The chromatograms of the commercial pinenes and the products of the distillation are shown on Fig. 5.8.1. Both mixtures were distilled several times, retaining the middle fraction in each time. The purities are summarised below.

Table 5.8.1. Purity of the Pinene Mixtures.

	Purity of α-Pinene Mixture, %		Purity of β-Pinene Mixture, %	
	Commercial	Distilled	Commercial	Distilled
Lights	0.5	-	-	-
α-Pinene	94.3	99.6	6.9	1.02
Camphene	2.3	0.4	0.7	0.58
β-Pinene	2.9	-	83.7	98.4
Heavies	-	-	8.7	-

Arklone-P and Genklene-P were quoted by their manufacturer, Imperial Chemical Industries, to be better than 99% pure. Dichloromethane was also specified by its manufacturer (Koch-Light Lab. Ltd.) to be purer than 99%. The chromatograms of these halocarbons are shown in Fig. 5.8.2.

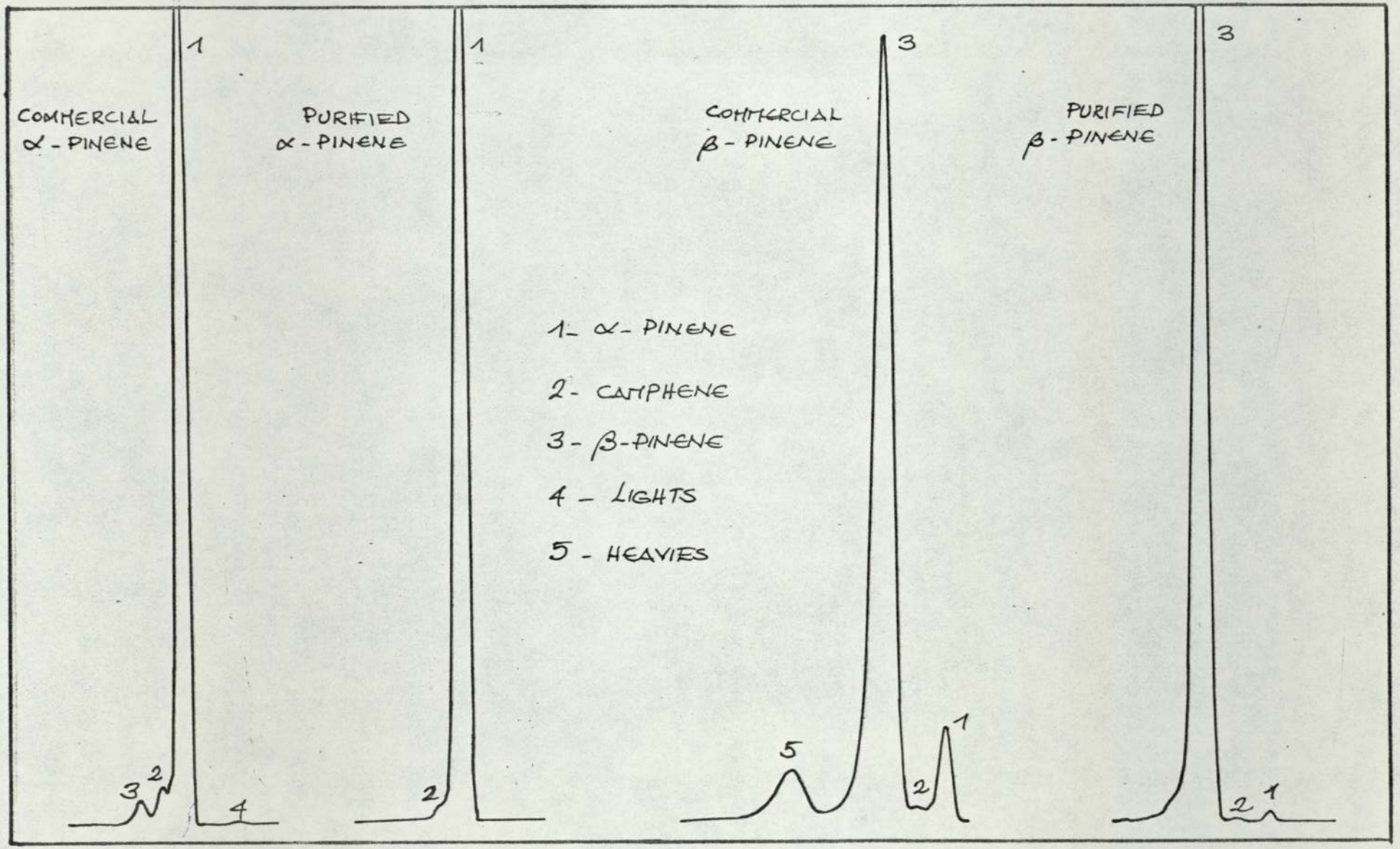

FIG. 5.8.1 - DISTILLATION OF PINENE MIXTURES

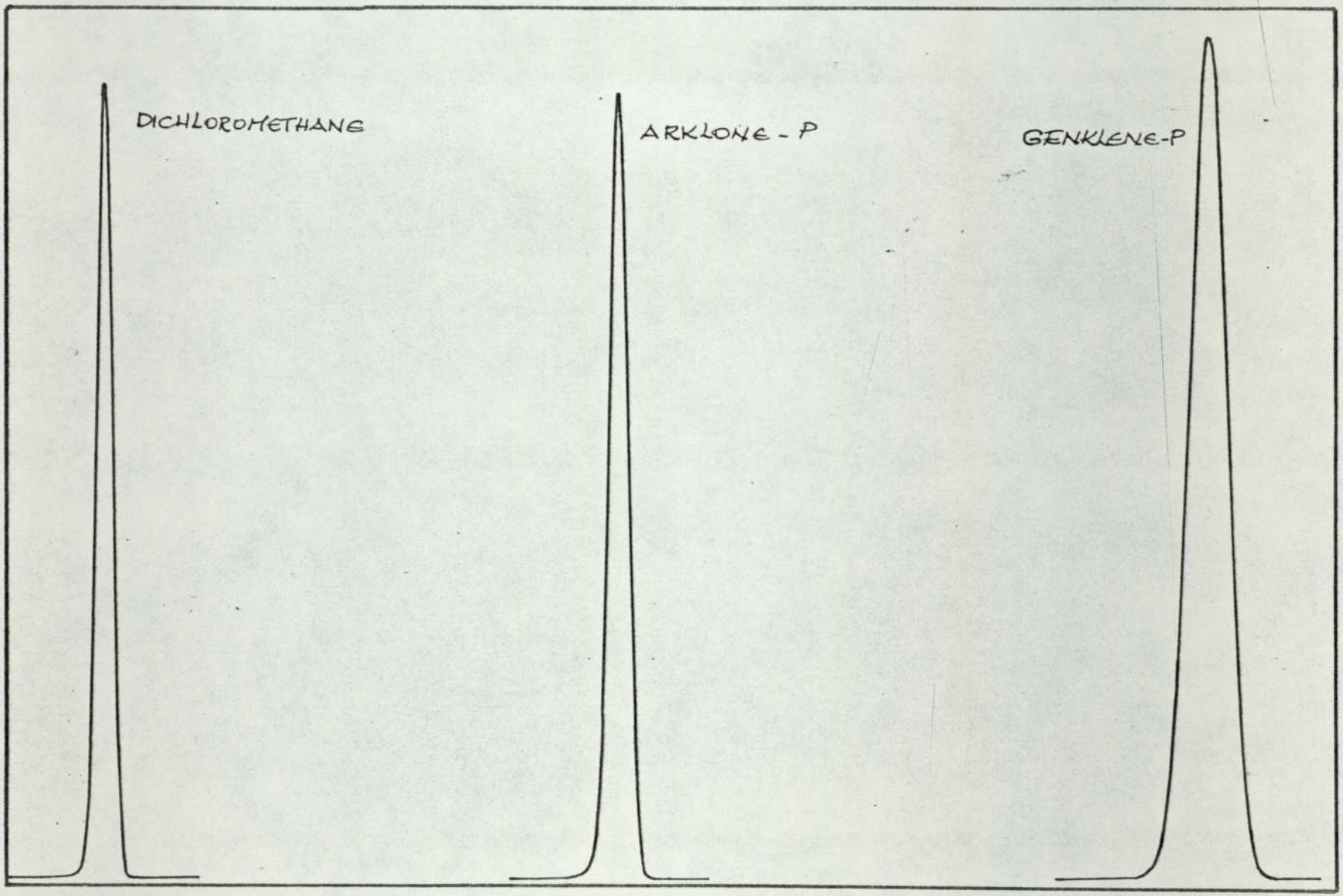

FIG. 5.8.2 - HALOCARBONS

6. CALCULATION OF BINARY DATA.

6.1 Calculation of the Partition Coefficients.

6.1.1 The Approximations due to Theoretical Assumptions.

The partition coefficients were calculated from the retention data according to the equation 3.2.7 which can be rewritten in the form of

$$q = \frac{1}{V_L} \int_0^c \frac{j(V_R - V_g)}{(1-aJy_o)} \, dc \qquad (6.1.1)$$

The assumptions and limitations involved in the derivation of the above equation are summarised below.

1. The contribution of liquid surface and solid surface adsorption to the measured partition coefficient is negligible compared with the bulk liquid partition coefficient.
2. The pressure drop and the mean pressure in the column is small.

The effect of the first assumption would be expected to be most accute at infinite dilution. This is due to the fact that the adsorption isotherms are usually of the Langmuir type (the adsorption coefficient decreasing with increasing concentration), while the bulk partition coefficients are, most commonly, anti Langmuir in type (the partition coefficient increasing with increasing concentration) (27,30), as is the case with all the five systems studied in this work. Furthermore, the curvatures of the isotherms for both type of surface sorption is often one or two orders of magnitude greater than that for bulk solution which means that the latter reaches infinite dilution condition before the adsorption processes. These would then lead to the observation that with decreasing the sample sizes from a high value the retention volume would at first decrease, reach a minimum and then increase at very small sample sizes. while the peak shapes would change from one having a diffuse leading boundary and sharp trailing boundary to the opposite (29,31). Sample size

retention volume plots of Figs.5.5.1 and 5.5.2 , coupled with the observation that the peaks remained symmetrical at small sample sizes in all the systems, confirms the validity of the first assumption. This was to be expected in view of high liquid loadings and high solubilities involved with the former helping to reduce solid surface adsorption while the latter decreasing the contribution of liquid surface adsorption.

The maximum value of mean column pressure, $J_3^2\, p_o (\simeq J_4^3 p_o)$, for which equation 6.1.1 is valid depends on the extent of the gas phase non-ideality, characterised by the numerical value of B_{22}, and the gas phase concentration of the solute, y. Conder and Purnell (12) derived the following equation for the maximum permissible value of $p_o J_3^2$

$$p_o\, J_3^2 \simeq \left(\frac{V_R}{V_R}\right)\left(\frac{RT(1-y_o J_3^2)^{\frac{1}{2}}}{B_{22}(y_o J_3^2)^2}\right) \qquad (6.1.2)$$

where V_R is the tolerable error in V_R

p_o is in atmospheres.

In this work only the second virial coefficients of the halocarbons could be calculated. With these solutes the maximum B_{22} was about -1500 cm^3/g mole and the maximum gas phase mole fraction, $y_o J_2^3$, was about 0.15. The substitution of these values into equation 6.1.2 gives a value of 7 atm for one percent error in V_R at $T = 307.7^oK$. This is well above the mean column pressures achieved in this work which were only slightly above atmospheric pressure.

6.1.2 The Method of Calculation.

As can be seen from equation (6.1.1) the partition coefficient, $K = q/c$, cannot be calculated directly from a single retention volume measurement. The solute concentration in liquid, q, needs to be calculated first from the integration of equation (6.1.1),

$$q = \int_{o}^{c} \frac{j(V_R - V_g)}{V_L(1-aJy_o)} \qquad (6.1.3)$$

The following steps were carried out in the calculation of K.

1. The uncorrected retention volume, V_R, was calculated from the total flow rate, F(y) and the retention time, t_R

$$V_R = \frac{t_c}{2885} \frac{760}{p_o} F(y)\ t_R \qquad (6.1.4)$$

where t_c is the column temperature

and F(y) refers to NTP (155^0C and 760 mm Hg) condition.

F(y) itself was measured directly in the case of halocarbon and β-pinene runs and calculated from equation 3.1.3 in the case of α-pinene runs as explained in earlier chapters.

The gas hold-up, V_g, was calculated in a similar manner from the retention time of a methane peak. The liquid volume, V_L, was calculated from the known weight of the stationary phase and its density at the column temperature. The compressibility factor, j, was approximated by the James-Martin correction factor J_2^3.

2. The solute mole fraction in gas phase at column outlet pressure, y_o, was calculated from

$$y_o = \left(\frac{cRT}{M_1 p_o}\right)\left(1 + \frac{B\ p_o}{RT}\right) \qquad (6.1.5)$$

where c is defined in terms of g/cm^3 of gas phase

M_1 is the molecular weight of the solute

B is the second virial coefficient of the mixture, given by

$$B = y^2 B_{11} + 2y(1-y)B_{12} + (1-y)^2 B_{22} \qquad (6.1.6)$$

With the pinenes, where the second virial coefficients, B_{22}, could not be calculated, y_o was approximated by the first term in the brackets on the

right hand side of equation 6.1.5. With the halocarbons this first term was taken as a first approximation and a value for y was calculated from

$$y = J_3^2 \, y_o \qquad (6.1.7)$$

This value for y was then used to calculate B from equation (6.1.6), which in turn was used in equation (6.1.5) to find a new value for y_o. Since the difference between the first and the second approximations was very small, the latter was taken as the true value of y_o.

The term a (see Appendix A1) also involves terms containing B_{22} and therefore was approximated to unity for the pinenes.

3. Since all the calculations were performed on a digital computer, it was convenient to carry out the integration in equation (6.1.3) by first expressing $(\partial q/\partial c)$ as a polynomial in terms of c, and then integrating the resultant equation analytically to obtain q, i.e.

$$(\partial q/\partial c) = A + Bc + C\,c^2 + \ldots\ldots \qquad (6.1.8)$$

$$\text{and } q = Ac + \frac{B}{2} c^2 \frac{C}{3} c^3 + \ldots\ldots \qquad (6.1.9)$$

In all cases the coefficient C was found to be zero, i.e. a linear relationship existed between $(\partial q/\partial c)$ and c.

The partition coefficient was then calculated by dividing equation (6.1.9) by c, i.e.

$$K = q/c = A + \frac{B}{2} c \qquad (6.1.10)$$

The results are tabulated in Tables 6.1.1 to 6.1.5 and the plots of partition coefficient versus concentration are presented in Figs. 6.1.1 to 6.1.5.

Table 6.1.1. Partition Coefficient of ∝-Pinene in Polypropylene Sebacate.

Temperature °C	c x 10^4 g/cm^3 at NTP	J_2^3 V_R cm^3	K
99.8	0.0	61.7	206.7
	0.78	65.6	216.6
	0.92	66.1	218.1
	1.51	69.0	224.5
	1.61	68.6	225.6
	1.91	72.2	228.9
	2.77	75.2	238.4
120.0	0.0	38.7	123.7
	0.625	39.8	126.1
	1.06	40.2	127.7
	1.325	40.6	128.7
	1.51	40.5	129.4
	1.575	41.0	129.7
	2.06	41.2	131.6
140.0	0.0	27.1	76.5
	0.40	28.2	77.4
	0.71	28.0	78.1
	0.95	27.9	78.63
	1.20	28.0	79.2
	1.71	28.4	80.3
	1.76	28.2	80.4
	2.60	28.9	82.30
	4.18	30.3	85.8
150.0	0.0	21.4	58.8
	0.70	22.8	59.2
	0.912	22.4	59.3
	1.24	22.3	59.5
	1.95	21.9	60.0
	2.46	21.7	60.3

Table 6.1.2. Partition Coefficient of β-Pinene in Polypropylene Sebacate.

Temperature °C	c x 10^4 g/cm^3 at NTP	J_2^3 V_R cm^3	K
100.35	0.0	80.9	336.1
	0.64	85.31	349.2
	0.90	87.8	354.5
	1.13	90.0	359.2
	1.76	91.5	372.2
	1.83	92.4	373.6
	1.91	95.1	375.2
	2.20	95.8	381.2
	2.35	97.9	384.3
110.1	0.0	61.1	248.6
	0.63	64.1	257.0
	0.95	65.2	261.3
	1.14	65.6	263.8
	1.48	67.2	268.4
	1.51	67.1	268.8
	1.86	69.4	273.4
	2.01	70.4	275.4
	2.09	70.7	276.5
	2.19	73.3	277.9
120.0	0.0	48.4	193.4
	0.69	49.9	198.3
	1.21	50.6	202.0
	1.59	51.4	204.2
	1.92	52.3	207.0
	2.28	54.6	209.6
	2.33	53.7	209.9
150.0	0.0	26.6	88.2
	0.52	26.9	90.6
	0.69	27.4	91.3
	1.16	28.2	93.5

Table 6.1.3. Partition Coefficient of Dichloromethane in Silicone Oil MS 200.

Temperature ^{o}C	c x 10^4 g/cm^3 at NTP	$J_2^3 V_R$ cm^3	K
24.8	0.0	77.4	99.8
	1.15	80.5	105.1
	1.8625	82.9	108.4
	2.675	85.5	112.1
	3.075	88.3	114.0
	3.775	92.8	117.2
	4.475	97.5	120.4
29.1	0.0	70.9	90.6
	1.2375	72.2	94.3
	1.885	74.0	96.2
	2.625	75.7	98.5
	3.625	77.8	101.5
	4.025	78.2	102.7
	4.975	83.1	105.6
34.7	0.0	58.8	73.6
	1.875	59.9	77.1
	2.5125	60.9	78.3
	3.050	61.9	79.4
	3.975	62.3	81.1
	4.825	63.6	82.7
	5.35	63.9	83.7
39.8	0.0	50.3	61.8
	1.425	51.0	63.6
	1.9375	51.1	64.3
	2.1375	51.1	64.6
	2.6375	51.9	66.5
	4.525	52.5	67.7
	5.00	52.2	68.3

Table 6.1.4. Partition Coefficient of Arklone-P in Silicone Oil MS 200.

Temperature ^{o}C	$c \times 10^{4}$ g/cm^{3} at NTP	$J_2^3 V_R$ cm^3	K
24.8	0.0	87.0	116.5
	0.6125	89.2	117.1
	1.3375	91.9	117.8
	1.7001	92.6	118.2
	2.750	96.9	119.3
	3.6625	105.5	120.2
29.1	0.0	79.2	102.8
	1.1625	80.5	105.2
	2.8125	83.7	108.6
	3.825	85.9	110.7
	4.20	88.3	111.5
34.7	0.0	66.4	84.6
	1.300	68.3	86.5
	2.150	69.1	87.7
	2.975	69.7	88.9
	3.025	70.5	88.9
	3.825	70.8	90.1
	4.7125	72.1	91.4

Table 6.1.5. Partition Coefficient of Genklene-P in Silicone Oil MS 200.

Temperature ^{o}C	$c \times 10^{4}$ g/cm^{3} at NTP	$J_2^3 V_R$ cm^3	K
34.7	0.0	174.7	234.2
	0.900	184.2	245.6
	1.950	200.1	259.0
	2.675	214.5	268.2
	3.100	219.3	273.6
	3.750	227.8	281.9
	4.500	237.6	291.5
45.1	0.0	122.6	160.8
	0.975	125.0	166.0
	1.525	128.4	168.9
	2.463	135.3	173.9
	3.375	139.7	178.8
	4.150	143.9	182.9
60.5	0.0	78.6	99.3
	1.5125	80.6	102.4
	2.1875	81.7	103.7
	2.3375	82.1	104.4
	3.175	83.4	105.7
	4.025	84.2	107.5
74.0	0.0	55.1	66.5
	0.9875	56.2	67.7
	1.650	56.8	68.5
	2.400	56.8	69.5
	3.2125	57.2	70.5
	4.500	58.7	72.1

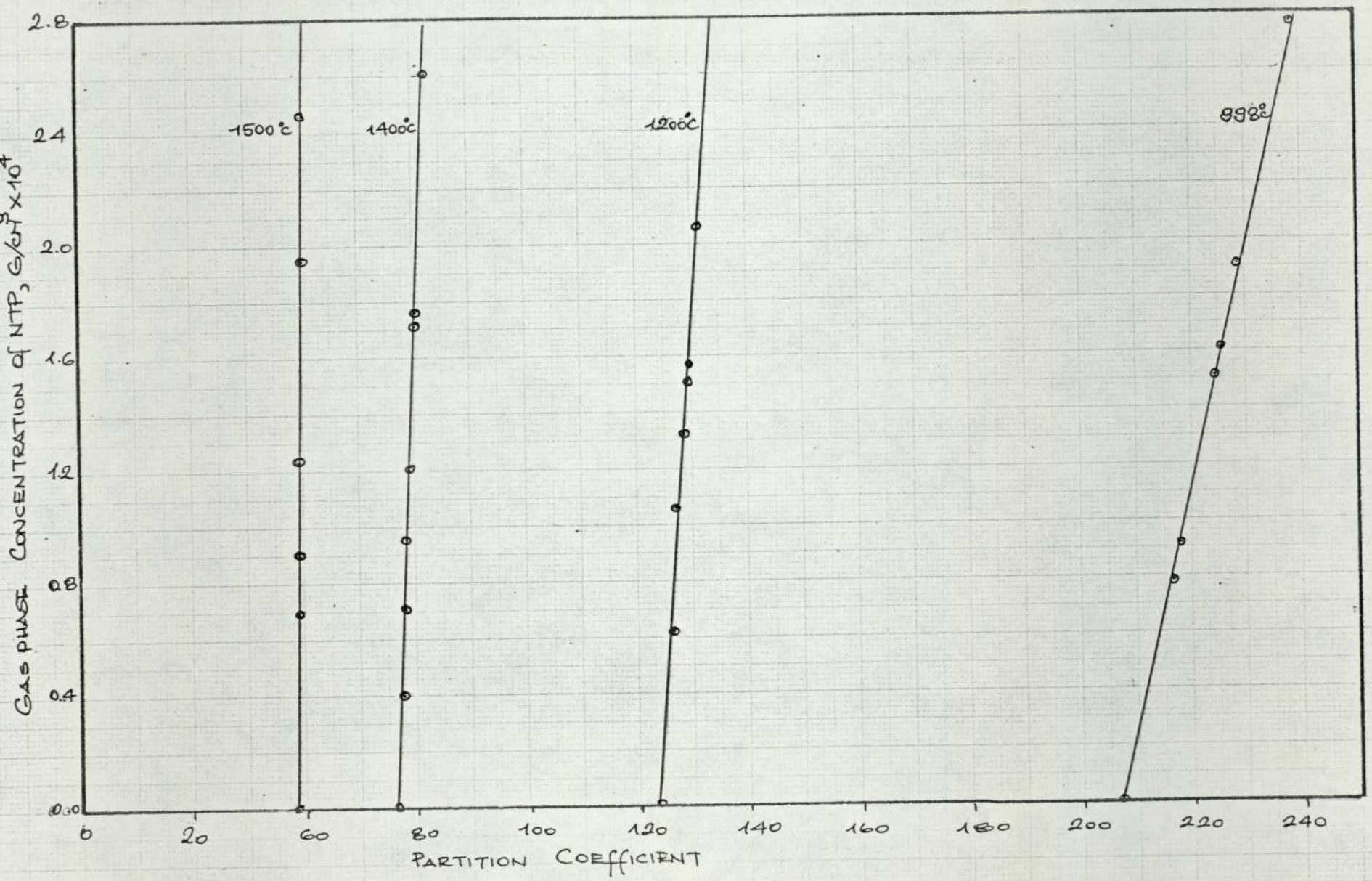

FIG.G.1.1 PARTITION COEFFICIENT of α-PINENE IN POLYPROPYLENE SEBACATE

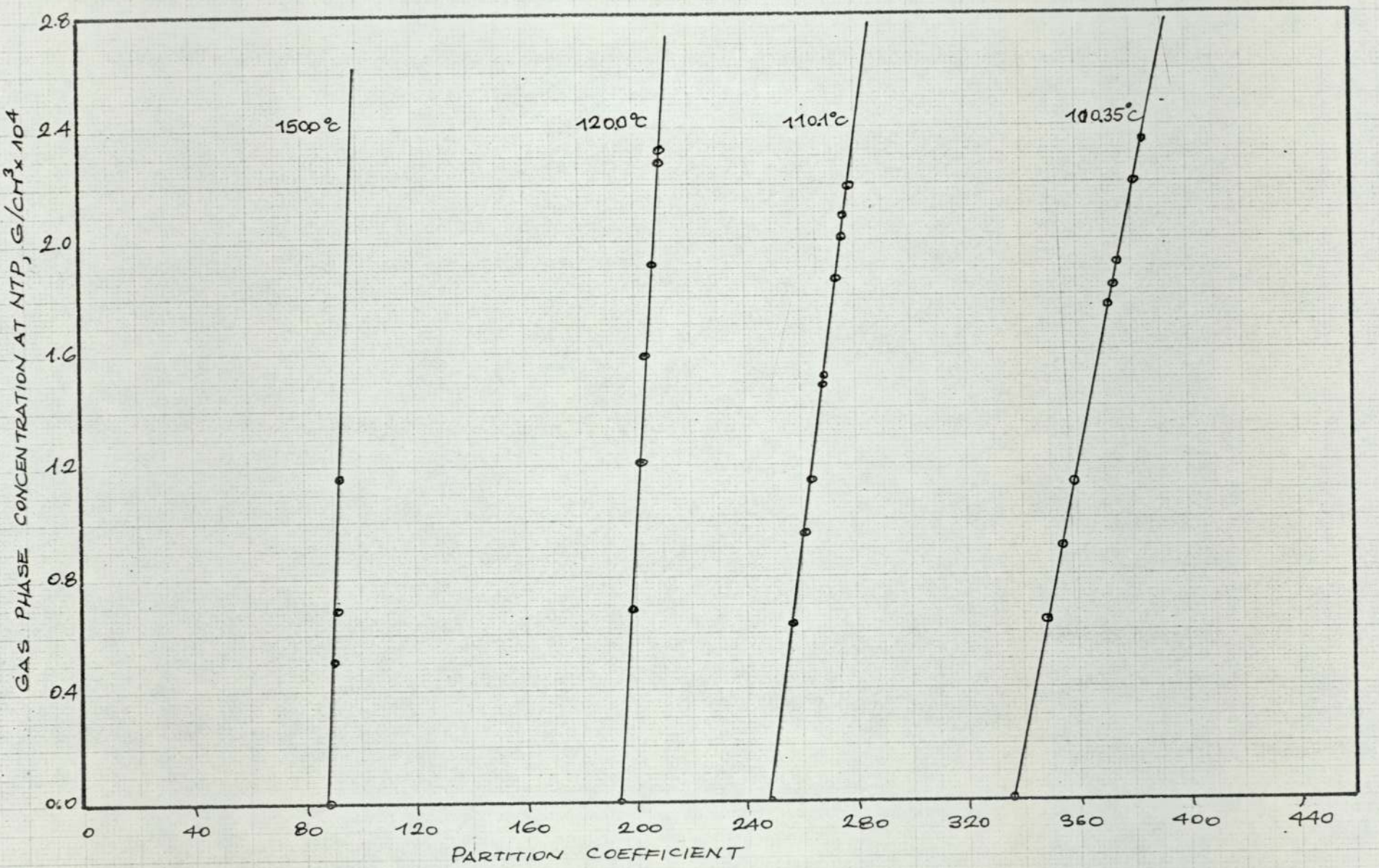

FIG. 6.1.2 PARTITION COEFFICIENT OF β-PINENE IN POLYPROPYLENE SEBACATE

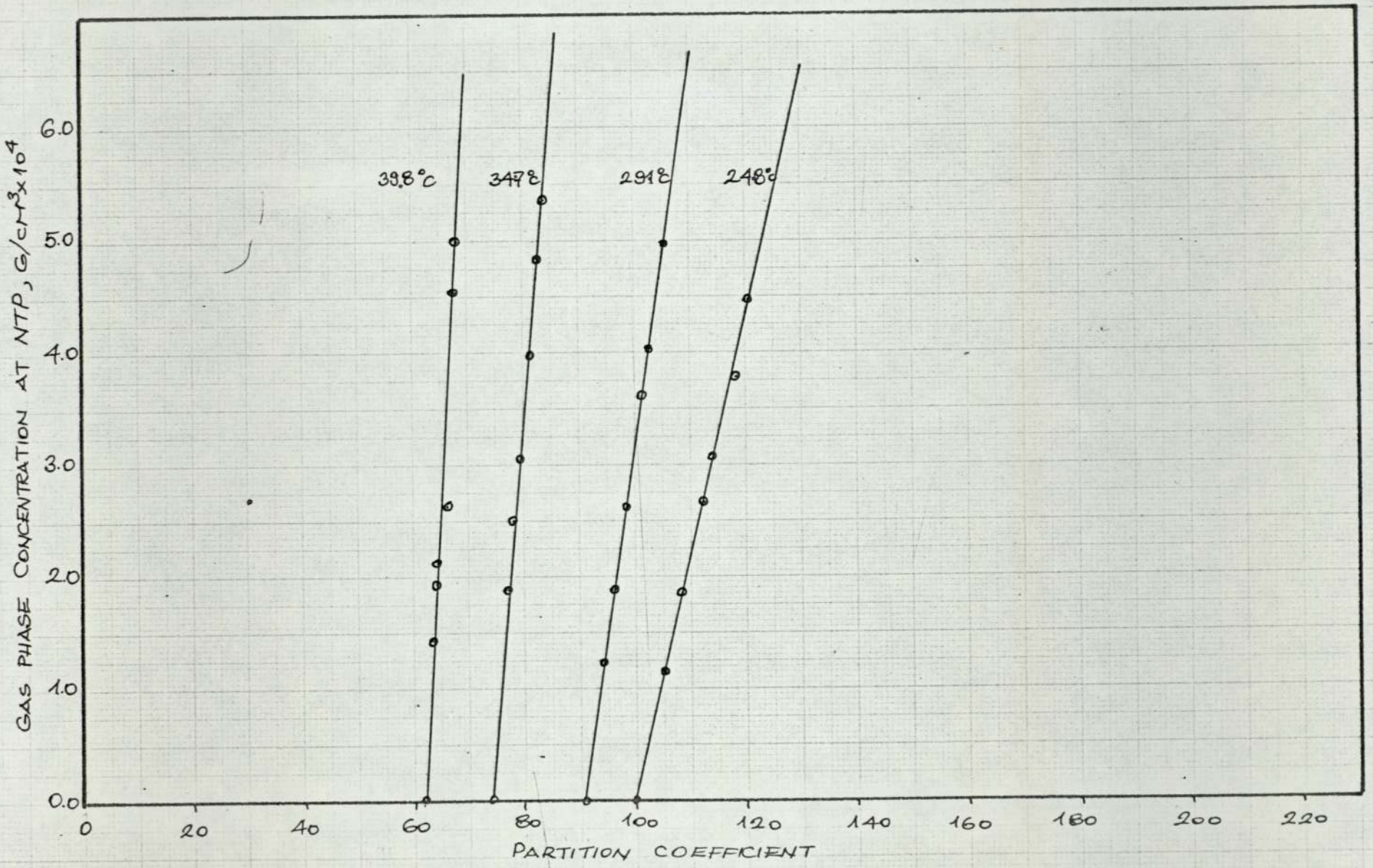

FIG. 6.1.3 PARTITION COEFFICIENT OF DICHLOROMETHANE IN SILICONE OIL MS 200

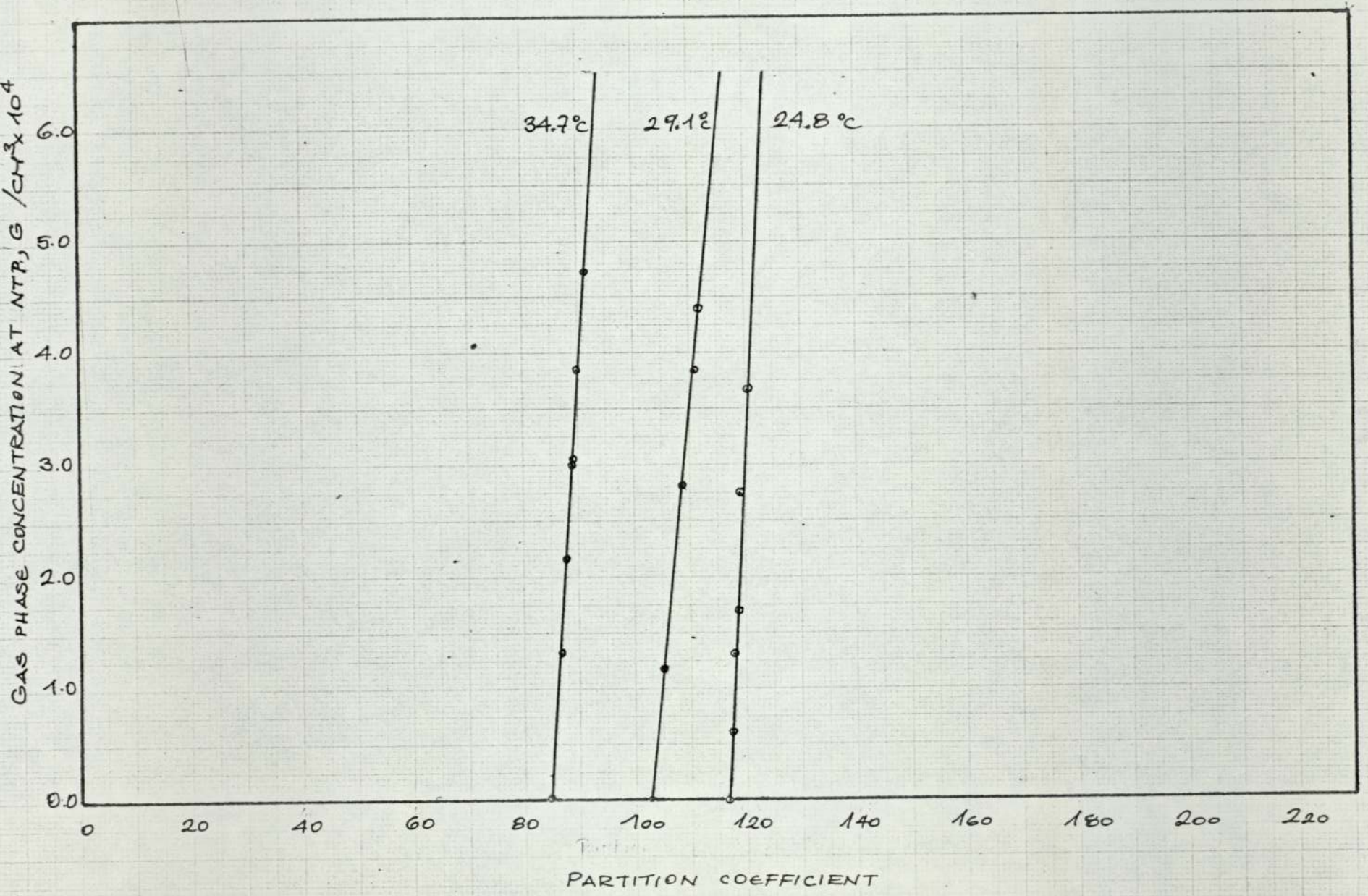

FIG. 6.1.4. PARTITION COEFFICIENT OF ARKLONE-P IN SILICONE OIL MS 200

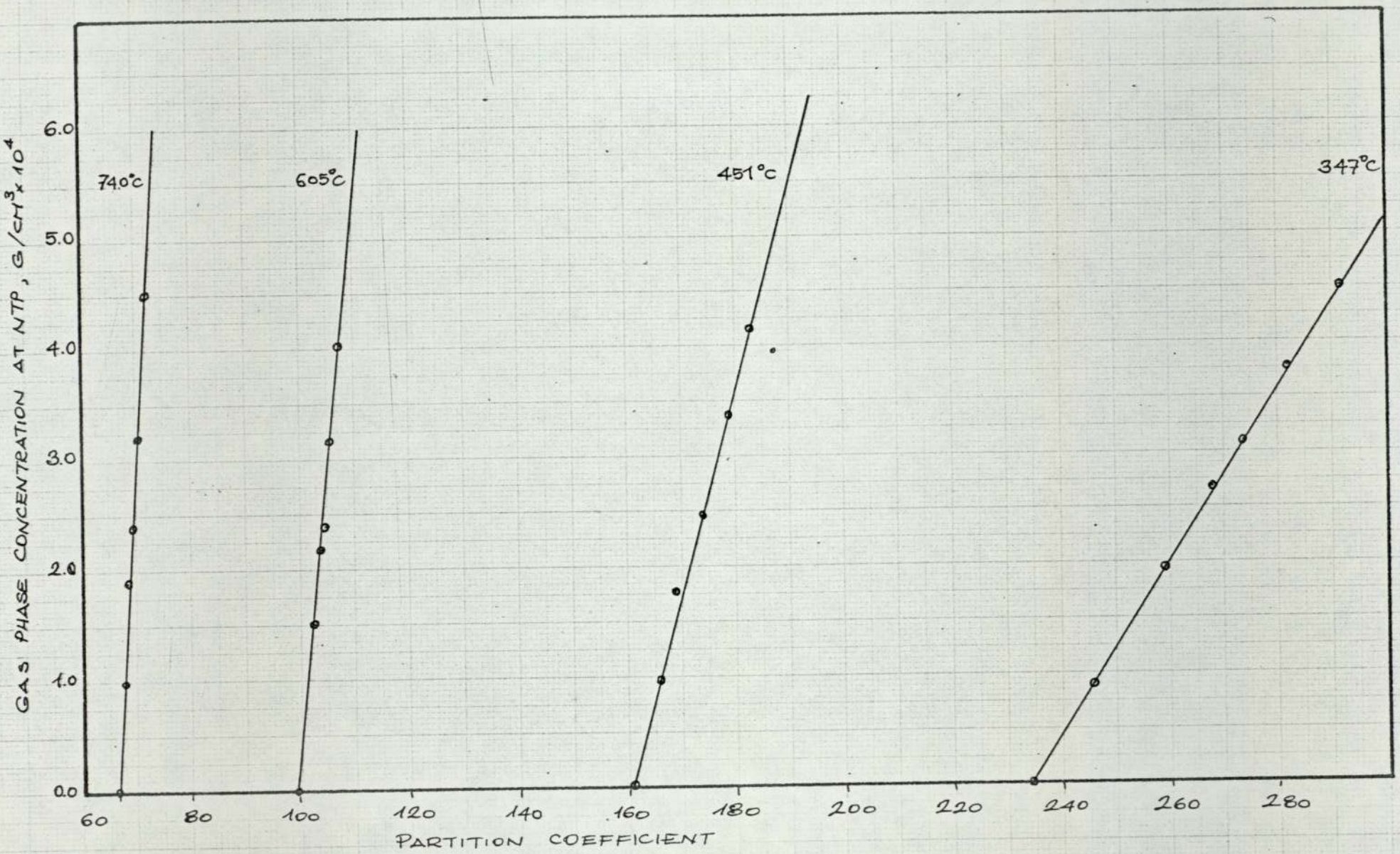

FIG. 6.1.5. PARTITION COEFFICIENT GENKLENE-P IN SILICONE OIL MS 200

6.2 Calculation of Activity Coefficients from Retention Data.

Very recently several workers drew attention to the anomilies arising in the numerical value of the activity coefficient of a substance in a polymer when it is based on mole fraction and to the need to know the molecular weight of the polymer to be able to calculate it. Hartkopf (117) in his work relating specific retention volumes to relative retention data cancelled out the molecular weight dependence of γ by assuming γ for hydrocarbons in Apiezon L to be the same (0.7) as in lighter paraffins and used this as a standard of reference for other stationary phases. Roberts and Hawkes (118), who considered the assumptions underlying Raoult's law, suggested that the use of volume fractions instead of mole fractions might be more appropriate. This definition of γ also obviates the need to know the polymer molecular weight, although it requires that the densities of both the solute and the stationary phase be known. When these are not available Brockmeir et al (119) and Paterson et al (120) recommend the use of weight fractions. The latter authors, however, concluded that the choice of a mole fraction, weight fraction or volume fraction in the calculation of the activity coefficient is purely arbitrary while showing preference for the weight fraction.

Most recently a completely new approach was developed by Fritz and Kovatz (121). They proposed the use of molarity as a measure of composition and the normalisation of the activity coefficient by its value in a standard stationary phase. They showed that the specific retention volume decreases on homologous stationary phases of increasing molecular weight and approaches a finite limiting value, and that the most convenient data should be those converted to hypothetical solvents of infinite molecular weight. These findings are particularly important as

they point out the difficulty of obtaining reproducible thermodynamic data by different workers when polymer stationary phases are involved.

In this work the data was based on mole fractions as it was intended to utilise them in evaluating the efficiencies of large scale chromatographs for which the use of mole fractions is common practice.

When the concentrations c and q are expressed as g/cm^3 of gas phase and stationary phase, equation (3.3.14) gives

$$\ln \gamma_1(o) = \ln \frac{RT(V_L q_1/M_1+n)}{P_1^{\,o}\, KV_L} + \frac{P_o J_4^{\,3}}{RT}\left[2y_{o1}J_4^{\,3}B_{11}+2(1-y_{o1}J_4^{\,3})B_{12}-\bar{V}_1\right] - \frac{P_1^{\,o}}{RT}(B_{11}-V_1^{\,o}) \qquad (6.2.1)$$

and the mole fraction was calculated from

$$x_1 = \frac{(c_1/M_1)KV_L}{(q_1/M_1)V_L+n} \qquad (6.2.2)$$

The number of moles of stationary phase n was based on weight average molecular weights given in Table 5.4.1 , and the partial molar volume of the solute $\bar{V}_1$ was assumed to be equal to the molar volume of the pure solute, $V_1^{\,o}$.

The non-logarithmic term on the right hand side of equation (6.2.1) is the fugacity correction for the gas phase requiring the values of the second virial coefficients of the pure components and of the mixture. As indicated earlier these values for the pinenes could not be found in the literature or calculated from other physical properties. Therefore, the gas fugacity correction to the activity coefficients of these compounds were ignored.

The second virial coefficients of the halocarbons, however, were available in the literature and were correlated by the equations given in a later section and explained in more detail in Appendix A.6. An inspection of Tables 6.2.6 to 6.2.8 shows that the contribution of the

fugacity correction to the logarithm of the activity coefficient is less than 1%.

The results are tabulated in Tables 6.2.4 to 6.2.8 and plotted in Figs. 6.2.1 to 6.2.5.

6.2.1 Calculation of the Vapour Pressures.

The vapour pressures of all the five solutes were calculated from an equation of the form

$$\log_{10} P^{o} = (-0.2185\ A/T) + B \qquad (6.2.3)$$

where P^{o} is in mm Hg

A is the molar heat of vaporisation in cal/g-mole

B is a constant

T is the temperature in ^{o}K.

The values for A and B given in Ref.(122) are listed in Table 6.2.1, but when the vapour pressures were calculated using these values they were found to deviate from the values available in the literature (113b). Therefore, it was decided to recalculate the constants by a least square analysis of the data of Ref. 113b. These are also shown in Table 6.1.1, together with the root mean square deviation of the data points from the best line.

Table 6.2.1. The values of the Constants in Equation 6.2.3.

Solute	Ref (27)		Best fit values		
	A cal/g-mole	B	A cal/g-mole	B	RMSD
α-Pinene	9813.6	7.898207	9698.36	7.83170	0.57
β-Pinene	10235.8	8.075933	10036.37	7.96490	1.2
Dichloromethane	7572.3	8.1833	7575.57	8.16293	7.0
Arklone-P	8012.7	7.955902	7110.48	7.72642	1.2
Genklene-P	7115.4	7.681107	7552.32	7.63580	1.8

6.2.2 Calculation of the Second Virial Coefficients.

The method of calculation of the second virial coefficients for pure vapours and the vapour mixtures are discussed in detail in Appendix A.6. A summary of these methods is given below and the calculated values are presented in Tables 6.2.2 and 6.2.3. The critical constants required in these methods were either obtained from literature or estimated by the methods discussed in Appendix A.7.

1. Pure Vapours.

Nitrogen.

The data for nitrogen (123) were correlated by the following equation developed by Pitzer and Curl (124),

$$\frac{P_c B}{R T_c} = B_o^*(T_r) + w B_1^*(T_r) \qquad (6.2.4)$$

where P_c and T_c are critical temperature and pressure respectively

T_r is the reduced temperature $\equiv T/T_c$

B_o^* and B_1^* are functions of T_r and given in Appendix A.7

w is the accentric factor and is related to the vapour pressure by

$$w \equiv \log_{10} P^o/P_c \Big|_{T_r = 0.7} - 1.0 \qquad (6.2.5)$$

Halocarbons.

The data for the three halocarbons used in this work were correlated by the method given by Halm and Stiel (125), which is an extension of the Pitzer-Curl equation to polar molecules

$$\frac{P_c B}{R T_c} = B_o^*(T_r) + w B_1^*(T_r) + X^* B_2^*(T_r) + X^{*2} B_3^*(T_r) + w^6 B_4^*(T_r) + w X^* B_5^*(T_r) \qquad (6.2.6)$$

where B_2^*, B_3^* and B_4^* are also functions of T_r (Appendix A.7)

X* is a polarity term and is calculated from

$$X^* \equiv \log P^o/P_c \Big|_{T_r} = 0.6 + 1.552 + 1.7\ w \qquad (6.2.7)$$

2. Nitrogen - Halocarbonsmixtures.

The cross second virial coefficients (B_{12}) of these mixtures were also calculated from the Halm-Stiel equation, but the parameters X*, w and the critical constants now refer to the mixture. The method of their calculations is also given in Appendix A.6.

Table 6.2.2. Second Virial Coefficients of Pure Vapours, $cm^3/mole$.

Temperature °C	Nitrogen	Dichloromethane	Arklone-P	Genklene-P
24.8	-4.27	-1085.2	-1036.2	-1377.5
29.1	-3.43	-986.9	-1021.7	-1330.9
34.7	-2.38	-880.2	-1000.7	-1287.8
39.8	-1.45	-800.4	-979.5	-1259.2
45.1	-0.533	-737.2	-956.1	-1235.7
60.5	1.955	-598.2	-883.0	-1177.2
74.0	3.93	-525.8	-818.1	-1119.8

Table 6.2.3. Cross Second Virial Coefficients of Nitrogen - Halocarbon Mixtures, $cm^3/mole$.

Temperature °C	Dichloromethane - N_2	Arklone-P - N_2	Genklene-P - N_2
24.8	-663.9	-89.5	-103.1
29.1	-614.1	-76.1	-88.7
34.7	-561.8	-58.2	-63.13
39.8	-523.4	-42.1	-40.0
45.1	-493.4	-17.8	-23.1
60.5	-427.2	10.1	43.3
74.0	-383.5	47.4	108.0

Table 6.2.4. Activity Coefficient of ∝-Pinene in Polypropylene Sebacate.

99.8°C			120°C		
x_1	γ_1	$\ln \gamma_1$	x_1	γ_1	$\ln \gamma_1$
0.0	0.2489	-1.390	0.0	0.2301	-1.469
0.2815	0.3307	-1.106	0.1549	0.2671	-1.320
0.3176	0.3457	-1.062	0.7395	0.2930	-1.224
0.4403	0.4094	-0.893	0.2841	0.3088	-1.175
0.4574	0.4202	-0.867	0.3126	0.3198	-1.140
0.5036	0.4527	-0.793	0.3221	0.3237	-1.128
0.6050	0.5465	-0.604	0.3867	0.3527	-1.042
140°C			150°C		
0.0	0.2085	-1.549	0.0	0.2097	-1.562
0.0682	0.2212	-1.508	0.0897	0.2286	-1.475
0.1158	0.2311	-1.465	0.1139	0.2344	-1.451
0.1501	0.2388	-1.432	0.1492	0.2433	-1.413
0.1834	0.2468	-1.399	0.2175	0.2626	-1.337
0.2451	0.2632	-1.335	0.2606	0.2764	-1.286
0.2507	0.2648	-1.329			
0.3359	0.2919	-1.231			
0.4588	0.3437	-1.068			

Table 6.2.5. Activity Coefficient of β-Pinene in Polypropylene Sebacate.

100.35°C			110.1°C		
x_1	γ_1	$\ln \gamma_1$	x_1	γ_1	$\ln \gamma_1$
0.0	0.1759	-1.756	0.0	0.1739	-1.749
0.3441	0.2580	-1.351	0.2743	0.2318	-1.462
0.4282	0.2916	-1.232	0.3668	0.2613	-1.342
0.4879	0.3213	-1.135	0.4124	0.2789	-1.277
0.6059	0.4030	-0.909	0.4810	0.3104	-1.170
0.6161	0.4121	-0.887	0.5427	0.3458	-1.062
0.6272	0.4225	-0.862	0.5637	0.3598	-1.022
0.6631	0.4603	-0.776	0.5742	0.3672	-1.002
0.6794	0.4798	-0.734	0.5868	0.3766	-0.977
120.0°C			150.0°C		
0.0	0.1657	-1.798	0.0	0.1533	-1.875
0.2407	0.2129	-1.547	0.1005	0.1662	-1.795
0.3616	0.2485	-1.392	0.1301	0.1705	-1.769
0.4293	0.2751	-1.291	0.2044	0.1824	-1.702
0.4794	0.2975	-1.212	0.2911	0.1988	-1.615
0.5254	0.3223	-1.132			
0.5313	0.3258	-1.121			

Table 6.2.6. Activity Coefficient of Dichloromethane in Silicone Oil MS 200.

Temperature °C	x_1	γ_1	$\ln \gamma_1$	
			Ideal Part	Non-ideal Part
24.8	0.0	0.0615	-2.788	-0.0174
	0.5119	0.1195	-2.124	-0.0187
	0.6366	0.1555	-1.861	-0.0195
	0.7224	0.1966	-1.626	-0.0204
	0.7525	0.2169	-1.528	-0.0208
	0.7933	0.2524	-1.377	-0.0216
	0.8238	0.2879	-1.245	-0.0224
29.1	0.0	0.0570	-2.846	-0.0180
	0.5041	0.1103	-2.185	-0.0191
	0.6125	0.1382	-1.959	-0.0196
	0.6925	0.1702	-1.751	-0.0202
	0.7622	0.2134	-1.524	-0.0211
	0.7827	0.2306	-1.445	-0.0214
	0.8207	0.2716	-1.281	-0.0223
34.7	0.0	0.0564	-2.857	-0.0178
	0.5593	0.1220	-2.085	-0.0188
	0.6333	0.1444	-1.916	-0.0192
	0.6798	0.1632	-1.793	-0.0194
	0.7388	0.1956	-1.612	-0.0199
	0.7778	0.2254	-1.469	-0.0204
	0.7971	0.2438	-1.391	-0.0707
39.8	0.0	0.0557	-2.869	0.0179
	0.4435	0.0972	-2.313	0.0183
	0.5227	0.1121	-2.170	0.0184
	0.5481	0.1179	-2.119	0.0185
	0.6802	0.1617	-1.803	0.0189
	0.7291	0.1875	-1.654	0.0191
	0.7501	0.2014	-1.583	0.0193

Table 6.2.7. Activity Coefficient of Arklone-P in Silicone Oil MS 200.

Temperature °C	x_1	γ_1	$\ln \gamma_1$	
			Ideal Part	Non-ideal Part
24.8	0.0	0.06738	-2.706	0.00876
	0.2200	0.08588	-2.463	0.00825
	0.3826	0.1078	-2.228	0.00764
	0.4414	0.1187	-2.131	0.00733
	0.5633	0.1503	-1.895	0.00645
	0.6338	0.1778	-1.727	0.00567
29.1	0.0	0.0653	-2.742	0.0130
	0.3256	0.0945	-2.237	0.0121
	0.5466	0.1360	-2.006	0.0106
	0.6256	0.1615	-1.833	0.0980
	0.6489	0.1709	-1.776	0.0948
34.7	0.0	0.06501	-2.752	0.0189
	0.3090	0.09196	-2.404	0.0178
	0.4286	0.1096	-2.228	0.0171
	0.5126	0.1267	-2.082	0.0164
	0.5169	0.1277	-2.074	0.0163
	0.5781	0.1443	-1.951	0.0156
	0.6313	0.1627	-1.831	0.0149

Table 6.2.8. Activity Coefficient of Genklene-P in Silicone Oil MS 200.

Temperature °C	x_1	γ_1	$\ln \gamma_1$	
			Ideal Part	Non-ideal Part
34.7	0.0	0.05883	-2.838	0.00509
	0.5516	0.1249	-2.084	0.00370
	0.7376	0.2021	-1.601	0.00206
	0.7997	0.2554	-1.366	0.00958
	0.8252	0.2866	-1.250	0.00268
	0.8547	0.3344	-1.095	0.00727
	0.8795	0.3896	-0.941	0.00190
45.1	0.0	0.05937	-2.837	0.0136
	0.4750	0.1094	-2.225	0.0121
	0.5902	0.1376	-1.995	0.0112
	0.7054	0.1856	-1.694	0.0098
	0.7713	0.23231	-1.468	0.0084
	0.8093	0.2719	-1.309	0.0072
60.5	0.0	0.05801	-2.877	0.0295
	0.4681	0.1055	-2.276	0.0291
	0.5632	0.1267	-2.092	0.0260
	0.5802	0.1314	-2.055	0.0258
	0.6561	0.1576	-1.872	0.0245
	0.7108	0.1842	-1.715	0.0231
74.0	0.0	0.05817	-2.891	0.0468
	0.278	0.07895	-2.584	0.0452
	0.394	0.09284	-2.421	0.0441
	0.489	0.1086	-2.263	0.0429
	0.466	0.1256	-2.116	0.0415
	0.651	0.1526	-1.919	0.0394

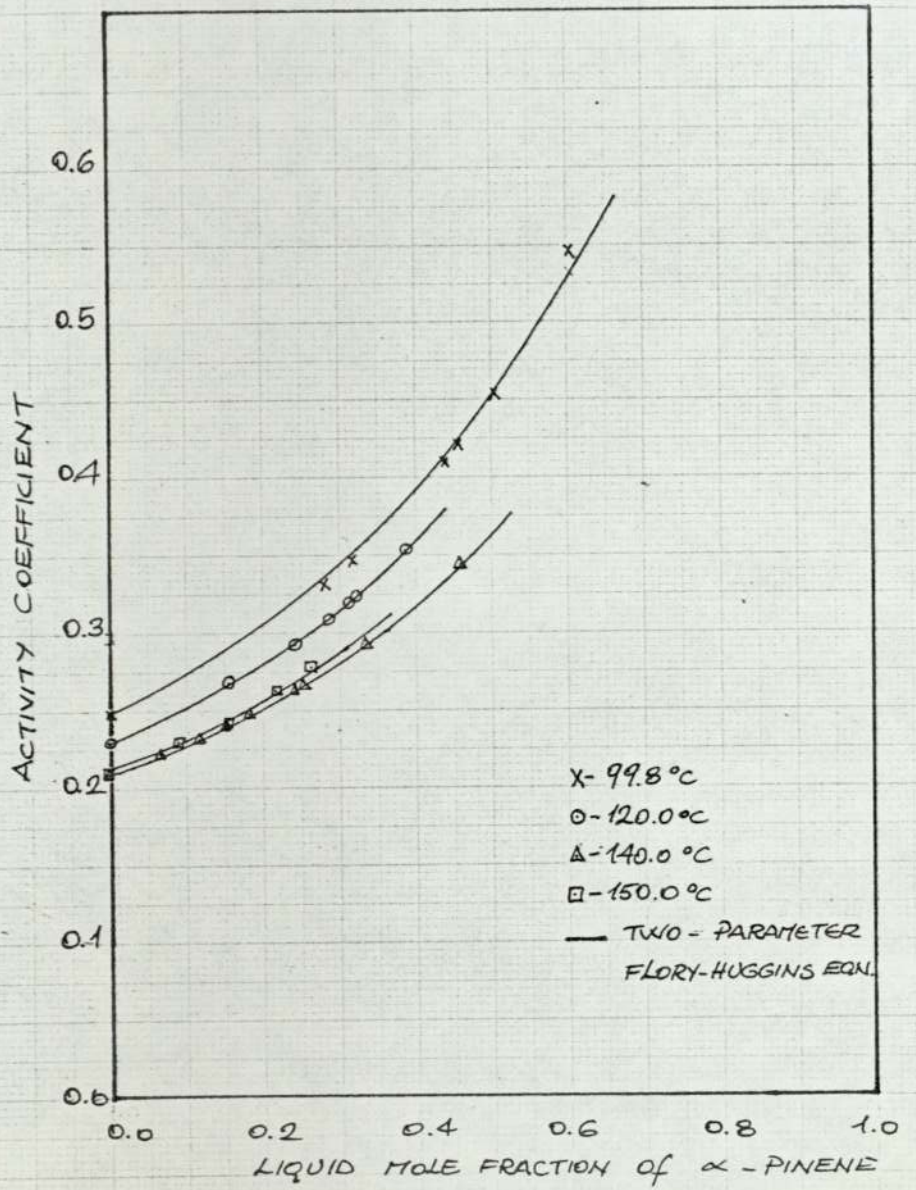

FIG. 6.2.1 - ACTIVITY COEFFICIENT OF α PINENE IN POLYPROPYLENE SEBACATE

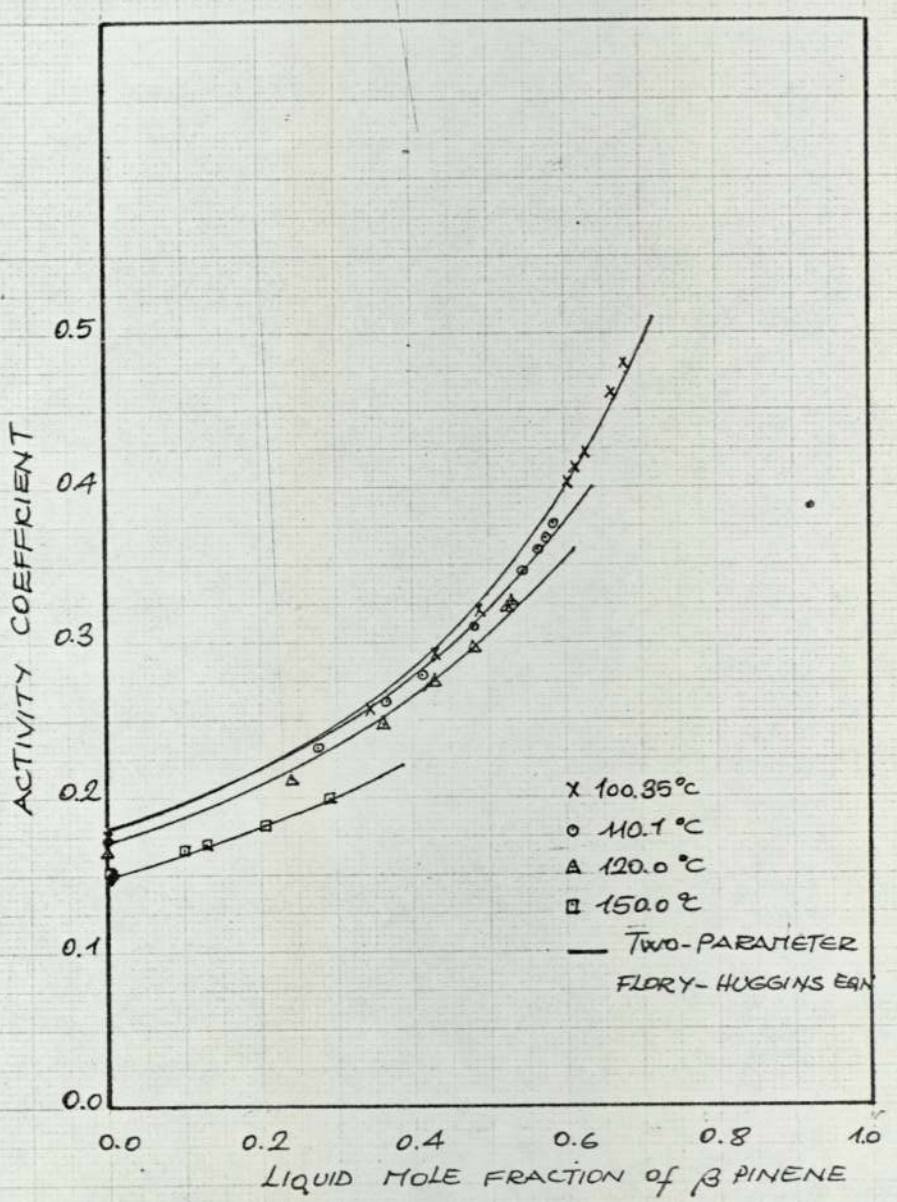

FIG 6.2.2 ACTIVITY COEFFICIENT of β-PINENE IN POLYPROPYLENE SEBACATE

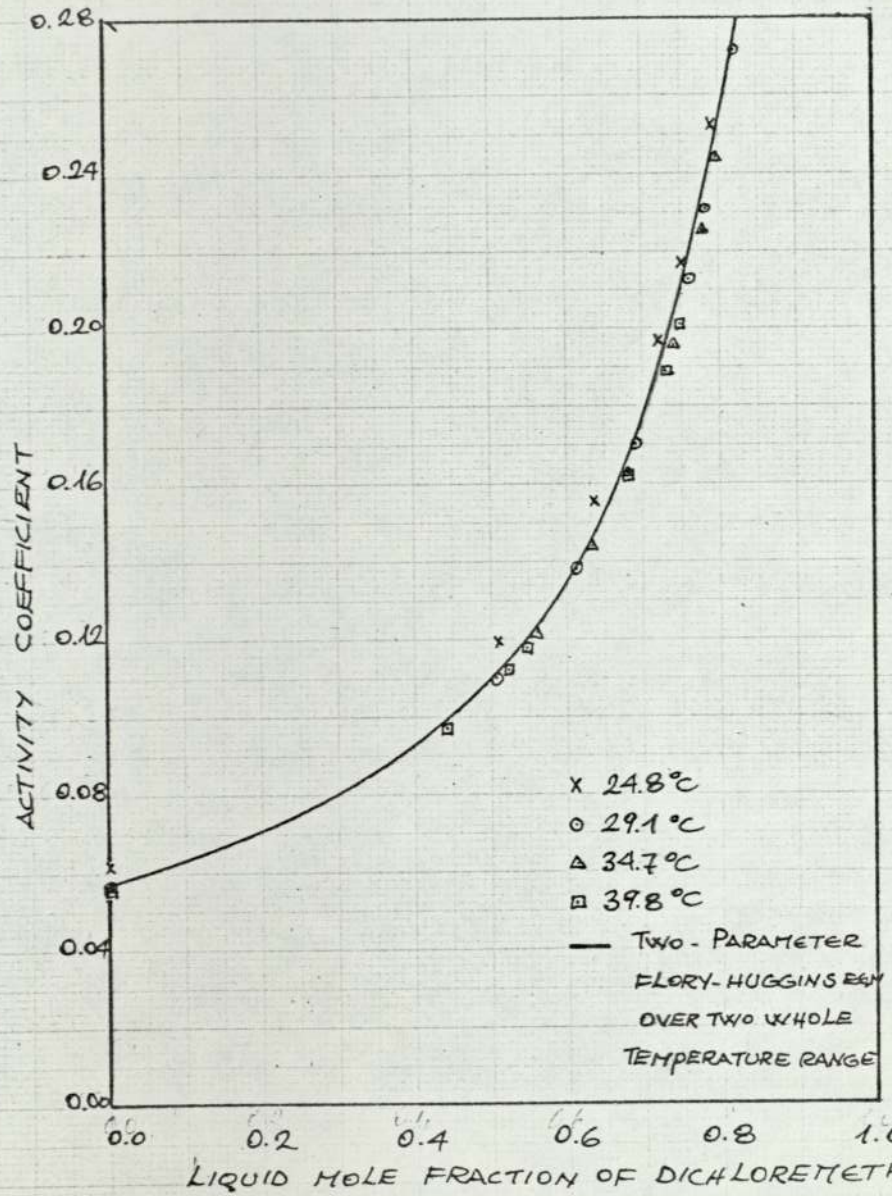

FIG. 6.2.3. ACTIVITY COEFFICIENT OF DICHLOROMETHANE IN SILICONE OIL MS 200

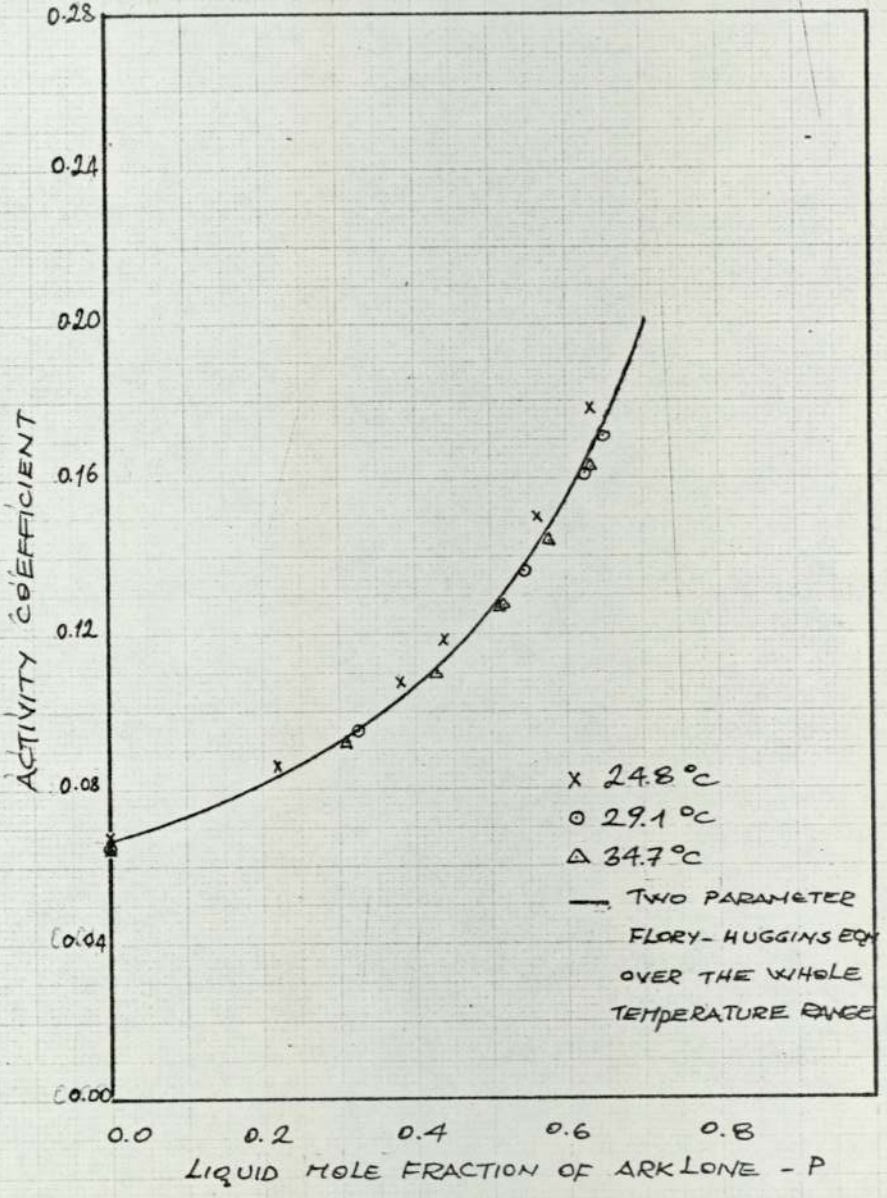

FIG. 6.2.4. ACTIVITY COEFFICIENT OF ARKLONE-P IN SILICONE OIL MS 200

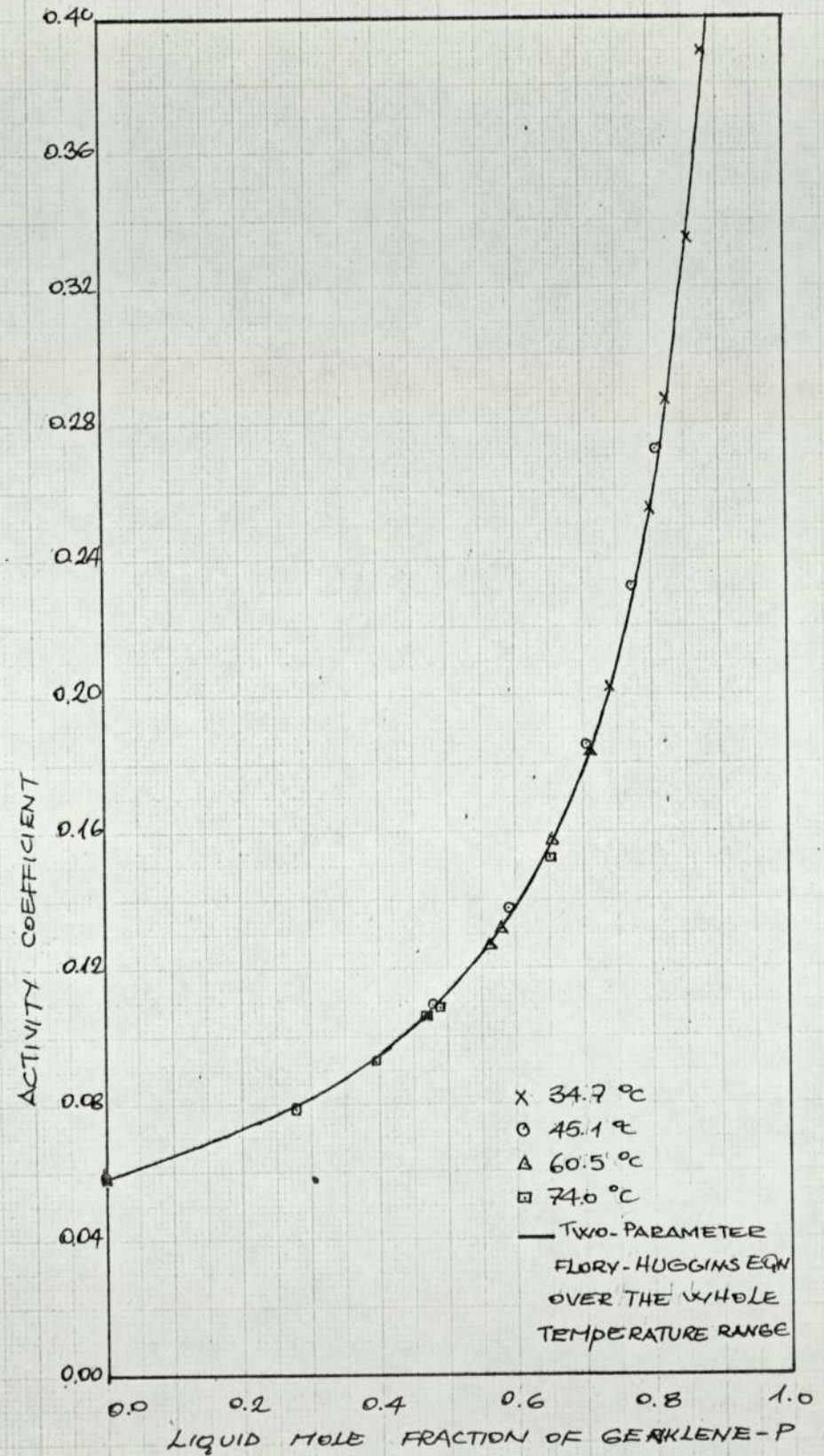

FIG. 6.2.5 ACTIVITY COEFFICIENT OF GENKLENE-P IN SILICONE OIL MS 200

6.3 Application of the Binary Flory-Huggins Equation.

Statistical theories of solution thermodynamics express the activity of a component as the sum of two contributions

$$\ln \gamma_1 = \ln \gamma_1 a + \ln \gamma_1 t \qquad (6.3.1)$$

a, the "athermal" activity coefficient is independent of temperature and arises from the differences in size between solute and solvent molecules. According to the Flory-Huggins equation (70,71) γa is given by

$$\ln \gamma_1 a = \ln \left[1-(1-\frac{1}{r})\phi_2\right] + (1-\frac{1}{r})\phi_2 = -\frac{\bar{s}a_1^E}{R} \qquad (6.3.2)$$

where ϕ_2 is the volume fraction of polymer

r is the ratio of molar volume of polymer to the molar volume of solute.

The thermal activity coefficient, γt, on the other hand, is temperature dependent and is characteristic of the solute-solvent interaction. According to the regular solution theory (68)

$$\ln \gamma_1 t = \chi_{12}\phi_2^2 = \frac{\bar{h}_1^E}{RT} \qquad (6.3.3)$$

where χ_{12} is the interaction parameter.

The modified Flory-Huggins equation thus becomes

$$\ln \gamma_1 = \ln \left[1-(1-\frac{1}{r})\phi_2\right] + (1-\frac{1}{r})\phi_2 + \chi_{12}\phi_2 \qquad (6.3.4)$$

Experimental results on polymer solutions, however, show that (126) the value of χ typically is in the range of 0.35-0.5 at the limit $x_2 \rightarrow o$ even for solutions that are nearly athermal ($\bar{h}^E \rightarrow o$). This indicates a large entropic contribution to γt_1, as a result of change of volume on mixing, i.e.

$$\ln \gamma t_1 = \frac{\bar{h}_1^E}{RT} - \frac{\bar{s}t_1^E}{R} \qquad (6.3.5)$$

In fact there is also a configurational contribution to $\bar{h}^E$ (120,126,127). This arises from the temperature dependence of **r** in equations (6.3.2)

through to (6.3.5) as the thermal expansion coefficients of the solute and the polymer solvent are usually different.

In this work the Flory-Huggins equation was expressed in terms of mole fractions through the following definitions

$$x_1 = \frac{\phi_1}{\phi_1+\phi_2} \qquad x_2 = \frac{\phi_2}{\phi_2+\phi_1} \tag{6.3.6}$$

and $\rho = \frac{1}{r}$

The equation (6.3.4) thus becomes

$$\ln \gamma_1 = \ln\left(\frac{\rho}{\rho x_1+x_2}\right) + \left(\frac{x_2(1-\rho)}{\rho x_1+x_2}\right) + \chi_{12}\left(\frac{x_2}{\rho x_1+x_2}\right)^2 \tag{6.3.7}$$

It should be pointed out here that the numerical value of the calculated interaction parameter does not change regardless of whether the activity coefficient is based on mole fraction or any other fraction.

6.3.1 Composition Dependence of the Interaction Parameter, .

The interaction parameters were calculated at each composition and the results are presented below:

1. α-Pinene/Polypropylene Sebacate and β-Pinene/Polypropylene Systems.

The results are tabulated in Tables 6.3.1 and 6.3.2 and Figs. 6.3.1 and 6.3.2. As can be seen from these tables the interaction parameter almost always increases with concentration, the only exception being the one for β-pinene polypropylene sebacate system at 150°C. This is in general agreement with the experimental observations of other workers (126,127) which indicates large contributions to χ from some source other than neighbour interactions, though no satisfactory theoretical explanation has yet been advanced.

2. Dichloromethane/Silicone Oil MS 200, Arklone-P/Silicone Oil MS 200, Genklene-P/Silicone Oil MS 200 Systems.

The experimental data are given in Tables 6.3.3 - 6.3.5 and plotted

Table 6.3.1. Variation of the Interaction Parameter with the Concentration of ∝-Pinene in Polypropylene Sebacate.

Temperature °c	x_1	χ_{12}	$\rho = \frac{V_1^o}{V_2^o}$
99.8	0.0	0.5841	0.05388
	0.2815	0.6028	
	0.3176	0.6079	
	0.4403	0.63171	
	0.4574	0.6361	
	0.5036	0.6499	
	0.6050	0.6951	
120.0	0.0	0.5157	0.05331
	0.1549	0.5256	
	0.2395	0.5332	
	0.2841	0.5382	
	0.3126	0.5418	
	0.3867	0.5531	
	0.3221	0.5431	
140.0	0.0	0.4324	0.05247
	0.0682	0.4316	
	0.1159	0.4312	
	0.1501	0.4310	
	0.1824	0.4319	
	0.2451	0.4311	
	0.2507	0.4311	
	0.3359	0.4322	
	0.4588	0.4383	
150.0	0.0	0.4475	0.05195
	0.0896	0.4545	
	0.1139	0.4567	
	0.1492	0.4604	
	0.2175	0.4678	
	0.2602	0.4738	

Table 6.3.2. Variation of the Interaction Parameter with the Concentration of β-Pinene in Polypropylene Sebacate.

Temperature °C	x_1	χ_{12}	$\rho = \frac{V_1^o}{V_2^o}$
100.35	0.0	0.2324	0.054132
	0.3441	0.2685	
	0.4282	0.2767	
	0.4879	0.2902	
	0.6059	0.3321	
	0.6161	0.3372	
	0.6272	0.3432	
	0.6631	0.3659	
	0.6795	0.3783	
110.1	0.0	0.2182	0.054302
	0.2743	0.2336	
	0.3668	0.2428	
	0.4124	0.2489	
	0.4811	0.2606	
	0.4864	0.2617	
	0.5427	0.2750	
	0.5637	0.2812	
	0.5742	0.2846	
	0.5868	0.2888	
120.0	0.0	0.1670	0.054473
	0.2407	0.1814	
	0.3616	0.1935	
	0.4293	0.2064	
	0.4795	0.2132	
	0.5255	0.2240	
	0.5313	0.2256	
150.0	0.0	0.08059	0.054969
	0.1006	0.06832	
	0.1301	0.06441	
	0.2045	0.05412	
	0.2912	0.04114	

Table 6.3.3. Variation of the Interaction Parameter with the Concentration of Dichloromethane in Silicone Oil MS 200.

Temperature ^{o}C	x_1	χ_{12}	$\rho = \frac{V_1^{o}}{V_2^{o}}$
24.8	0.0	0.9552	0.008780
	0.5119	0.9367	
	0.6366	0.9289	
	0.7227	0.9213	
	0.7525	0.9184	
	0.7933	0.9146	
	0.8238	0.9095	
29.1	0.0	0.8780	0.008799
	0.5040	0.8695	
	0.61247	0.8664	
	0.6925	0.8640	
	0.7622	0.8624	
	0.7827	0.8624	
	0.8207	0.8636	
34.7	0.0	0.8680	0.008791
	0.5592	0.8610	
	0.6333	0.8597	
	0.6798	0.8589	
	0.7388	0.8586	
	0.7778	0.8592	
	0.7971	0.8601	
39.8	0.0	0.8600	0.008751
	0.4435	0.8556	
	0.5226	0.9063	
	0.6802	0.8524	
	0.7291	0.8524	
	0.7501	0.8527	

Table 6.3.4. Variation of the Interaction Parameter with the Concentration of Arklone-P in Silicone Oil MS 200.

Temperature °C	x_1	χ_{12}	$\rho = \frac{V_1^o}{V_2^o}$
24.8	0.0	0.4365	0.01628
	0.2200	0.4438	
	0.3826	0.4527	
	0.4414	0.4572	
	0.5633	0.4707	
	0.6338	0.4880	
29.1	0.0	0.4017	0.01634
	0.3256	0.3993	
	0.5446	0.4023	
	0.6256	0.3986	
	0.6489	0.3988	
34.7	0.0	0.3970	0.01634
	0.3090	0.3943	
	0.4286	0.3931	
	0.5126	0.3924	
	0.5169	0.3925	
	0.5781	0.3922	
	0.6313	0.3921	

Table 6.3.5. Variation of the Interaction Parameter with the Concentration of Genklene-P in Silicone Oil MS 200.

Temperature ^{o}C	x_1	χ_{12}	$\rho = \frac{V_1^{o}}{V_2^{o}}$
34.7	0.0	0.4695	0.01372
	0.5516	0.4683	
	0.7376	0.4746	
	0.7997	0.4830	
	0.8252	0.4893	
	0.8547	0.5016	
	0.8795	0.6190	
45.1	0.0	0.4756	0.01376
	0.4750	0.4785	
	0.5902	0.4812	
	0.7054	0.4879	
	0.7713	0.4967	
	0.8093	0.5057	
60.5	0.0	0.4493	0.01381
	0.4681	0.4511	
	0.5632	0.4528	
	0.5802	0.4531	
	0.6561	0.4559	
	0.7108	0.4594	
74.0	0.0	0.4507	0.01383
	0.2778	0.4459	
	0.3941	0.4428	
	0.4896	0.4401	
	0.5657	0.4374	
	0.6551	0.4340	

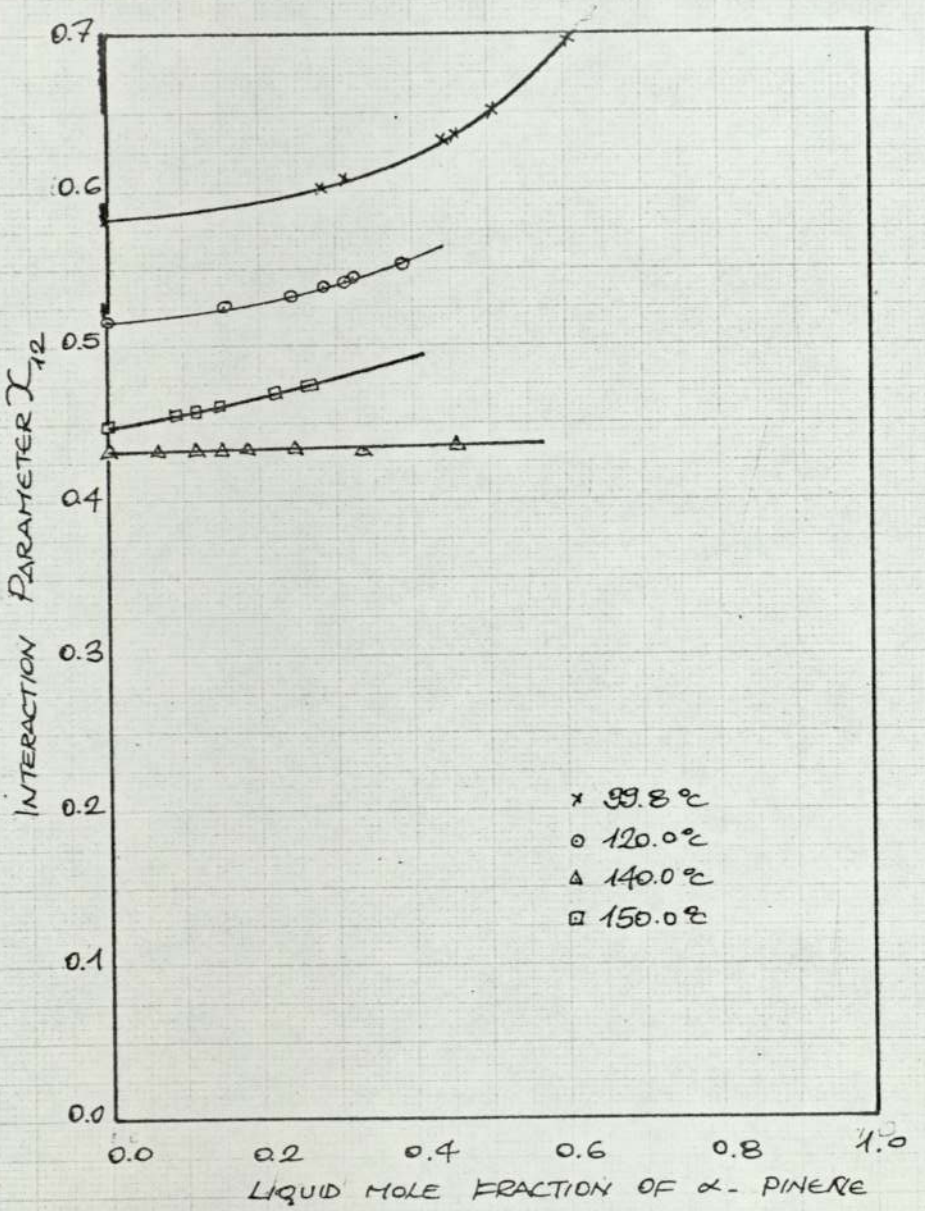

FIG. 6.3.1 CONCENTRATION DEPENDENCE OF THE INTERACTION PARAMETER

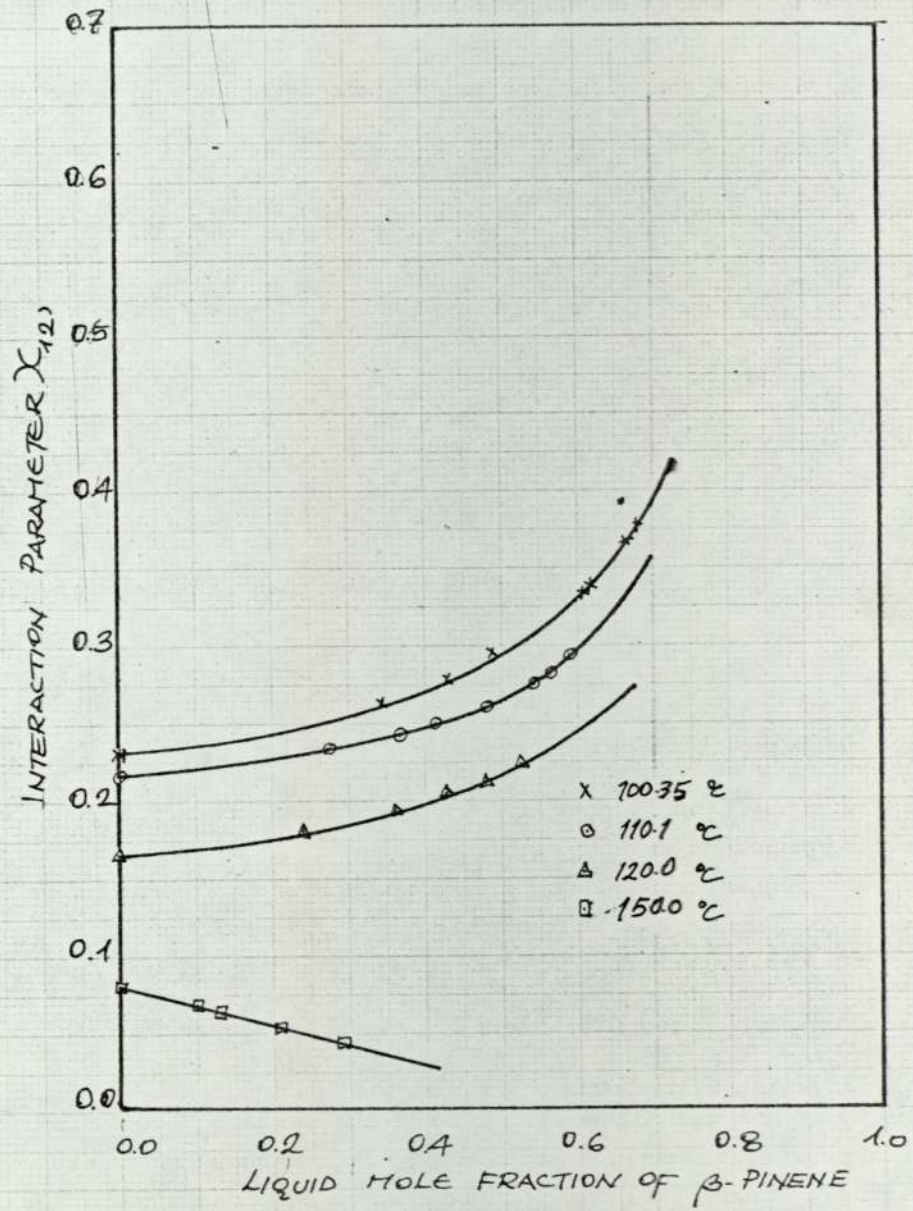

FIG. 6.3.2 - CONCENTRATION DEPENDENCE OF THE INTERACTION PARAMETER

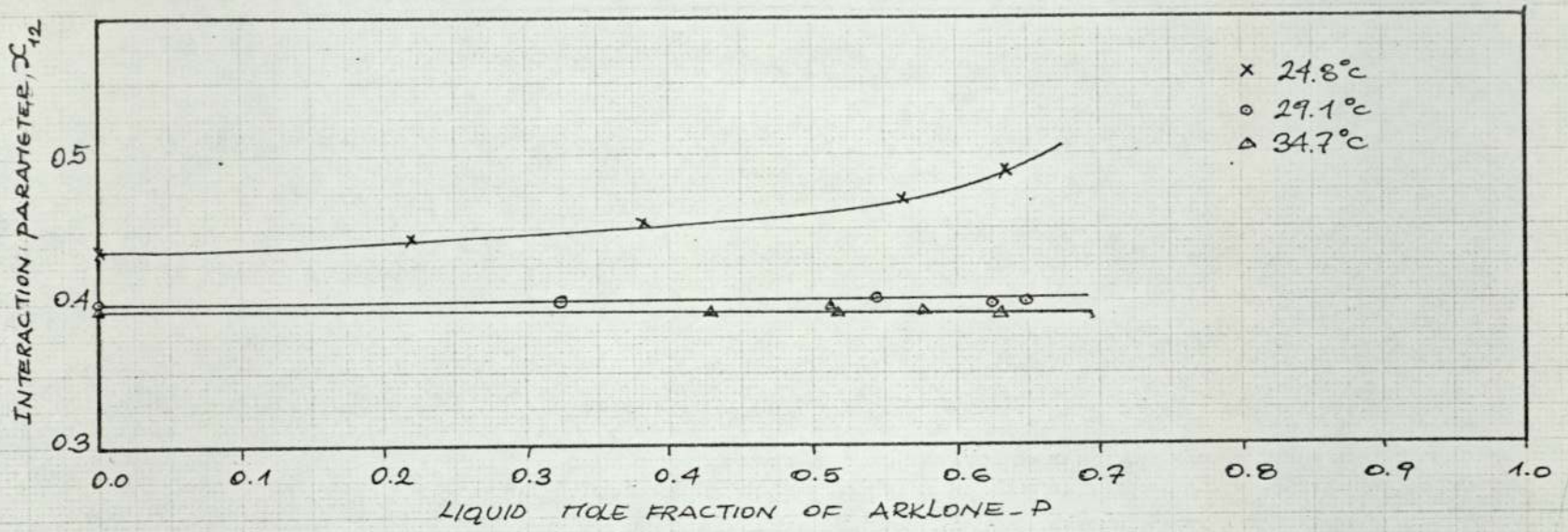

FIG. 6.3.4 CONCENTRATION DEPENDENCE OF THE INTERACTION PARAMETER

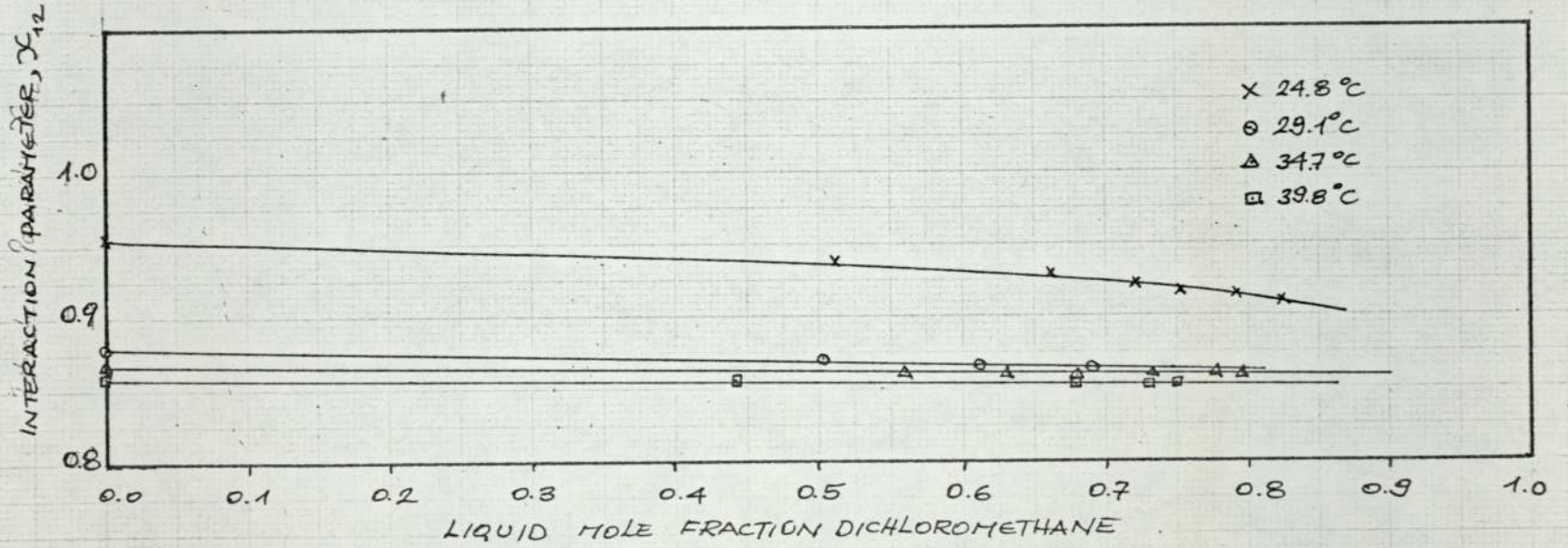

FIG. 6.3-3 CONCENTRATION DEPENDENCE OF THE INTERACTION PARAMETER

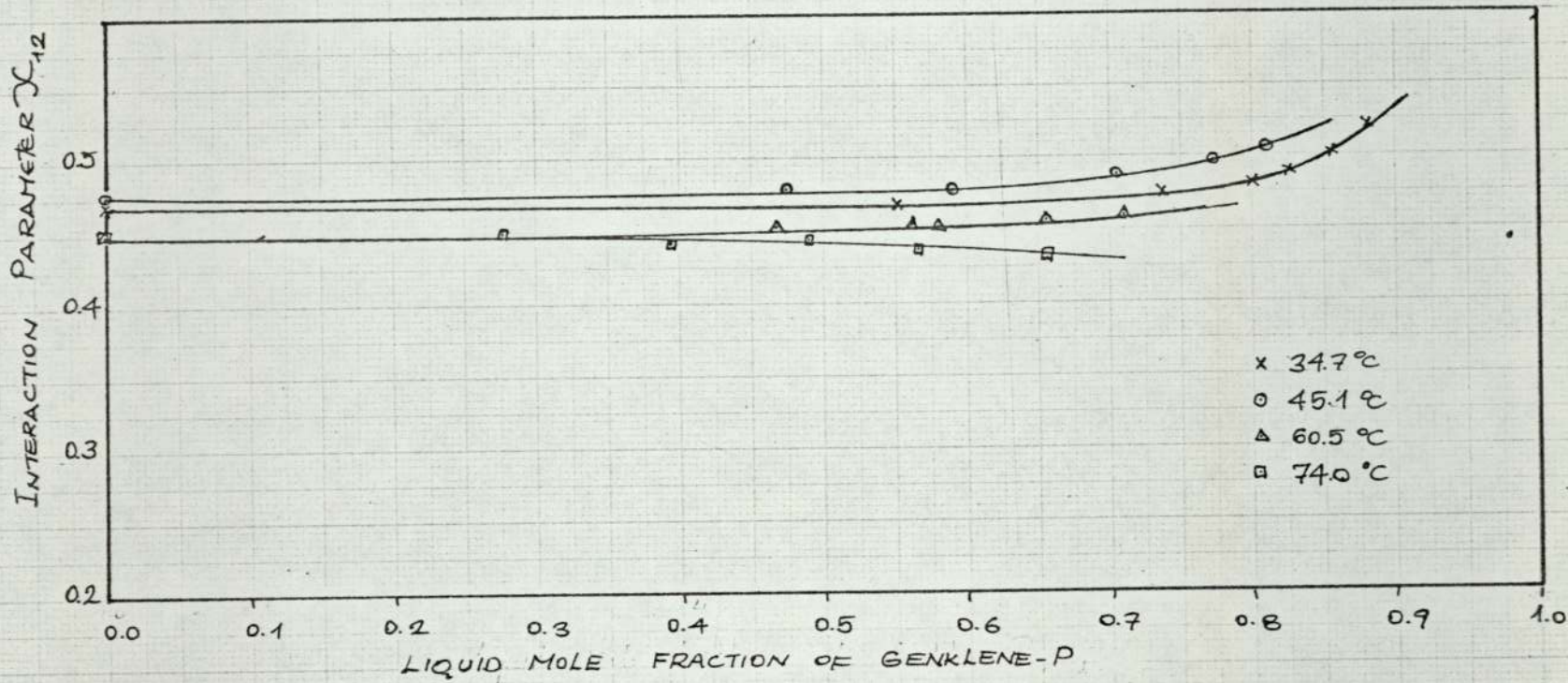

FIG. 6.3.5 CONCENTRATION DEPENDENCE OF THE INTERACTION PARAMETER

in Figs. 6.3.3 - 6.3.5. With these systems there does not seem to be a definite tendency in the variation of χ_{12} with the concentration. The change in either direction is small compared with the previous systems and in most cases well within the experimental precision. In fact, as will be seen later in this chapter, the activity coefficient-mole fraction data for these systems are very well correlated by the Flory-Huggins equation using only one value for χ_{12}.

6.3.2 Estimation of the Solubility Parameters.

At infinite dilution of the solute, $x_1 \rightarrow o$, equation (6.3.7) becomes

$$\ln \gamma_1^{\infty} = \ln \rho + (1-\rho) + \chi_{12}^{\infty} \qquad (6.3.8)$$

If, now, the non-configurational contribution to the entropy of mixing, $\bar{s}t_1^E$, is ignored, the combination of equations (6.3.5) and equation (6.3.8) gives

$$\chi_{12}^{\infty} = \frac{\bar{h}_1^{E\infty}}{RT} \qquad (6.3.9)$$

In this case according to the regular solution theory of Hildebrand

$$\frac{\bar{h}_1^{E\infty}}{RT} = \chi_{12}^{\infty} = \frac{\bar{V}_1^{\infty}}{RT} (\delta_2 - \delta_1)^2 \qquad (6.3.10)$$

where $\bar{V}_1^{\infty}$ is the partial molar volume of the solute at infinite dilution in the polymer

δ_1 and δ_2 are the solubility parameters of the solute and the polymer respectively and are a measure of the potential energy due to the attraction of the molecules in the pure liquid form.

For volatile compounds, δ, can be calculated from the heat of vaporisation, H_v, according to the equation, (128)

$$\delta^2 = \frac{H_v - RT}{V} \qquad (6.3.11)$$

For polymers and non-volatile compounds, δ may be evaluated in a number of

Table 6.3.6. Estimation of the Solubility Parameter of Polypropylene Sebacate from the Solubility Parameters of α and β Pinenes.

Solute	Temperature ^{o}C	χ_{12}^{∞}	ΔH_v cal/g-mole	V_1^{o} cm^3/g-mole	δ_1 $cal^{0.5}/cm^{1.5}$	$\delta_2 - \delta_1$ $cal^{0.5}/cm^{1.5}$	δ_2 $cal^{0.5}/cm^{1.5}$
α-Pinene	99.8	0.58409	9698.36	170.2	7.595	1.595	9.19
	120.0	0.51571		173.12	7.530	1.525	9.06
	140.0	0.43244		176.81	7.451	1.417	8.87
	150.0	0.44747		178.54	7.415	1.452	8.87
β-Pinene	100.35	0.23240	10036.37	169.27	7.580	1.018	8.86
	110.1	0.21816		170.9	7.545	0.985	8.53
	140.0	0.16701		172.56	7.505	0.870	8.38
	150.0	0.080595		177.68	7.398	0.6175	8.02

ways, such as swelling, intrinsic viscosity, additive group contribution method and solubility (129).

In this section the solubility parameters were either calculated from equation (6.3.11) using the available vapour pressure data, or taken from the literature. The solubility parameters for the polymers were then estimated from equation (6.3.10) using the experimental values of the interaction parameters. $\bar{V}_1^{\infty}$ was assumed to be equal to the molar volume of pure liquid, V_1^{o}.

1. α-Pinene/Polypropylene Sebacate, β-Pinene/Polypropylene Sebacate Systems.

In the absence of any values in the literature the solubility parameters of both pinenes were calculated from their respective heats of vaporisation as calculated from the clausius Clapeyron equation

$$\frac{d \ln P^{o}}{d(1/T)} = - \frac{\Delta H_v}{R} \qquad (6.3.12)$$

The calculated values for the solubility parameter of polypropylene sebacate are shown in Table 6.3.6 along with the values of the other parameters used in the calculations.

δ_2 is found to decrease with temperature changing from 9.19 to 8.87 from α-pinene runs and from 8.60 to 8.02 from β-pinene runs. Though no literature values are available for this polymer for comparison the solubility parameters of most polyesters are found to be in the range of 8.2 to 10.1 (128). However, the discrepancy between the values obtained from α-pinene and β-pinene runs points out to the anomaly created by the assumption of $\bar{s}t^{E} = 0$. Since they are isomers, their heats of vaporisation and molar volumes, and hence their solubility parameters, are very similar. The use of equation (6.3.9) would then suggest similar interaction parameters. This is obviously not the case, otherwise it would not be possible to separate them on this stationary phase.

Table 6.3.7. Estimation of the Solubility Parameter of Silicone Oil MS 200 from the Solubility Parameters of Dichloromethane, Arklone-P and Genklene-P.

Solute	Temperature °C	χ_{12}^{∞}	ΔH_v cal/g-mole	V_1° cm^3/g-mole	$\delta_{1(CLT)}$ $cal^{0.5}/cm^{1.5}$	$\delta_{1(LIT)}$ $cal^{0.5}/cm^{1.5}$	$(\delta_2 - \delta_1)$ $cal^{0.5}/cm^{1.5}$	$\delta_{2(CLT)}$ $cal^{0.5}/cm^{1.5}$	$\delta_{2(LIT)}$ $cal^{0.5}/cm^{1.5}$
Dichloro-methane	24.8	0.95517	7575.6	64.70	10.41	9.7 (12)	2.96	12.66	7.35 (S-68)
	29.1	0.8780		65.08	10.37		2.85	12.55	5.03 (VA-132)
	34.7	0.86804		65.35	10.34		2.85	12.55	6.2 (S-132)
	39.8	0.86003		65.35	10.33		2.86	12.56	7.7 (S-132)
					Mean = 10.36			Mean = 12.58	7.3 (AD-133)
Arklone-P	24.8	0.43653	7110.48	119.97	7.58	8.5 (12)	1.47	9.97	7.6 (S-134)
	29.1	0.40167		120.86	7.55		1.41	9.91	7.5 (S-135)
	34.7	0.39703		121.49	7.53		1.41	9.91	7.1 (VS-136)
					Mean = 7.55			Mean = 9.93	7.6 (VS-136)
Genklene-P	34.7	0.46946	7552.32	101.99	8.52	-	1.68	10.08	6.8 (VS-136)
	45.1	0.47565		103.27	8.46		1.71	10.11	
	60.5	0.44926		105.06	8.37		1.68	10.08	
	74.0	0.45069		106.56	8.30		1.71	10.11	
					Mean = 8.40			Mean = 10.1	

S - From Swelling Measurements

VA - From Vapour Pressure Measurements

VS - From Viscosity Measurements

AD - From Additive Group Contribution Method.

2. Dichloromethane/Silicone Oil MS 200, Arklone-P/Silicone Oil MS 200, Genklene-P/Silicone Oil MS 200.

The solubility parameters for these solutes were also calculated from their vapour pressure data using equations (6.3.11) and (6.3.12). When these values for Dichloromethane and Arklone-P are compared with those obtained from the literature (128), a significant discrepancy is found (Table 6.3.7). A large part of this difference is almost certainly due to the error in the value of ΔH_v. For instance, ΔH_v for Dichloromethane is known to change from 8200.9 cal/g-mole at 1.67°C to 7376.4 cal/g-mole at 37.8°C (122) as compared with 7602.37 cal/g-mole calculated from its vapour pressure data.

δ_2 was again calculated from the values of δ_1 (literature values where available) and χ_{12}^{∞} by equation (6.3.10). These values are listed in Table 6.3.7 together with those found in the literature. Although it seems that δ_2 for this polymer (a polydimethylsiloxane) varies considerably according to its molecular weight, the degree of cross-linking and the method of determination, the values found in this work are too high. This is most likely a result of neglecting the contribution of the entropy to χ_{12}^{∞}, $\chi_{\Delta s}$. Taking a value 7.3 for δ_2, $\chi_{\Delta s}$ was calculated from

$$\chi_{12}^{\infty} = \chi_{\Delta s} + \frac{V_1^{\circ}}{RT} (\delta_2 - \delta_1)^2 \qquad (6.3.13)$$

The mean values are 0.272, 0.126, 0.002, for Dichloromethane, Arklone-P and Genklene-P respectively (Table 6.3.8) which seem reasonable in view of the fact that $\chi_{\Delta s}$ for most systems are found to be in the range of 0.1 to 0.4. The rather small value for Genklene-P may have been caused by the uncertainty in its solubility parameter value.

6.3.3 Correlation of the Data by the One-Parameter Flory-Huggins Equation.

If the ratio of the molar volumes, $\frac{V_2^{\circ}}{V_1^{\circ}}$, is taken to represent the

Table 6.3.8. Entropy Contribution to the Interaction Parameter for $\delta_2 = 7.3$ cal$^{0.5}$/cm$^{1.5}$.

Solute	Temperature °C	$\chi_{\Delta s}$
Dichloromethane	24.8	0.325
	29.1	0.254
	34.7	0.252
	39.8	0.255
	Mean =	0.272
Arklone-P	24.8	0.145
	29.1	0.112
	34.7	0.111
	Mean =	0.126
Genklene-P	34.7	-0.0069
	45.1	0.0091
	60.5	-0.0035
	74.0	0.0095
	Mean =	0.002

ratio of the size of the molecules, ρ, as was done in the original treatment by Flory and Huggins, then one value of the interaction parameter, χ_{12}, should correlate the activity coefficient over the whole composition range. But, as was seen earlier, χ_{12} is, in fact, composition dependent. Therefore, the Flory-Huggins equation was fitted to the experimentally obtained activity coefficient - composition data to get the best value of χ_{12} at each temperature using a least square routine based on the Rosenbrock's constrained hill-climb method (130).

Table 6.3.9. Best Fit Values of the Interaction Parameter, χ_{12}, at Various Temperatures for the Systems α-Pinene/Polypropylene Sebacate and β-Pinene/Polypropylene Sebacate. $\rho = \frac{V_1^o}{V_2^o}$

Solute	Temperature °C	ρ	χ_{12}	$\chi_{12}T$ °K
α-Pinene	99.8	0.0539	0.6396	283.4
	120.0	0.0533	0.5380	211.4
	140.0	0.0525	0.4327	178.7
	150.0	0.0520	0.4614	195.2
β-Pinene	100.35	0.0541	0.3286	122.7
	110.1	0.0543	0.2658	101.8
	120.0	0.0545	0.2076	81.6
	150.0	0.0550	0.0595	25.2

These are tabulated in Tables 6.3.9 and 6.3.10 and the activity coefficients calculated using these values are given in Appendix A.8.

1. α-Pinene/Polypropylene Sebacate, β-Pinene/Polypropylene Sebacate Systems.

The fit obtained is good with a maximum scatter of about 5% Differentiating equation (6.3.13), and ignoring the slight dependence of the molar volume on temperature,

$$\frac{d(\chi_{12}T)}{dT} = T\frac{d(\chi_{\Delta s})}{dT} + \chi_{\Delta s} \qquad (6.3.14)$$

Theoretically $\chi_{\Delta s}$ should be independent of temperature, i.e. $\chi_{12}T$ should vary linearly with temperature with a slope equal to $\chi_{\Delta s}$. Fig. 6.3.6 does, in fact, show that for these systems $\chi_{12}T$ decreases linearly with temperature, though there is some scatter on the α-pinene/polypropylene sebacate plot.

Table 6.3.10. Best Fit Values of the Interaction Parameter, χ_{12}, at Various Temperatures for the Systems Dichloromethane/MS 200 Arklone-P/MS 200 and Genklene-P/MS 200. $\rho = \frac{V_1^o}{V_2^o}$

Solute	Temperature °C	ρ	χ_{12}	χ_{12} T °K
Dichloromethane	24.8	0.00878	0.9179	273.3
	29.1	0.00880	0.8640	261.0
	34.7	0.00879	0.8596	264.5
	39.8	0.00875	0.8586	268.5
Arklone-P	24.8	0.0163	0.4659	138.7
	29.1	0.0163	0.3997	120.7
	34.7	0.0163	0.3927	120.8
Genklene-P	34.7	0.0137	0.4970	152.9
	45.1	0.0138	0.4985	158.6
	60.5	0.0138	0.4553	151.8
	74.0	0.0138	0.4389	152.3

2. Dichloromethane/Silicone Oil MS 200, Arklone-P/Silicone Oil MS 200, Genklene-P/MS 200 Systems.

Again the fit to the activity coefficient data is good with a maximum deviation of about 3 %. $\chi_{12}T$-temperature plots for these systems are shown in Fig. 6.3.7. For the first two of the above systems, the experimental temperature range is too small to determine the exact nature of the relationship, but the comparison of these plots with the values of

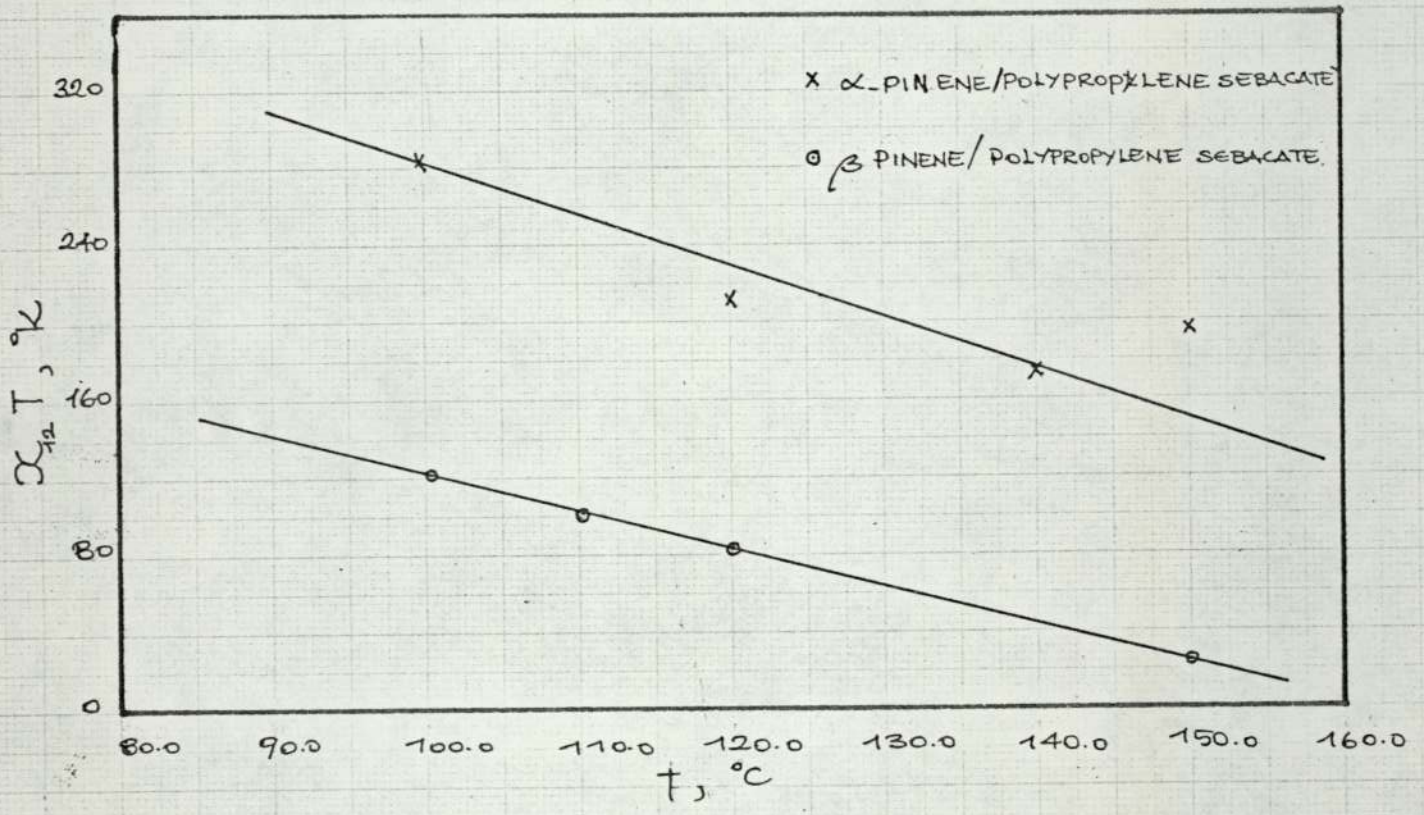

FIG.6.3.6 - TEMPERATURE DEPENDENCE OF THE INTERACTION PARAMETER

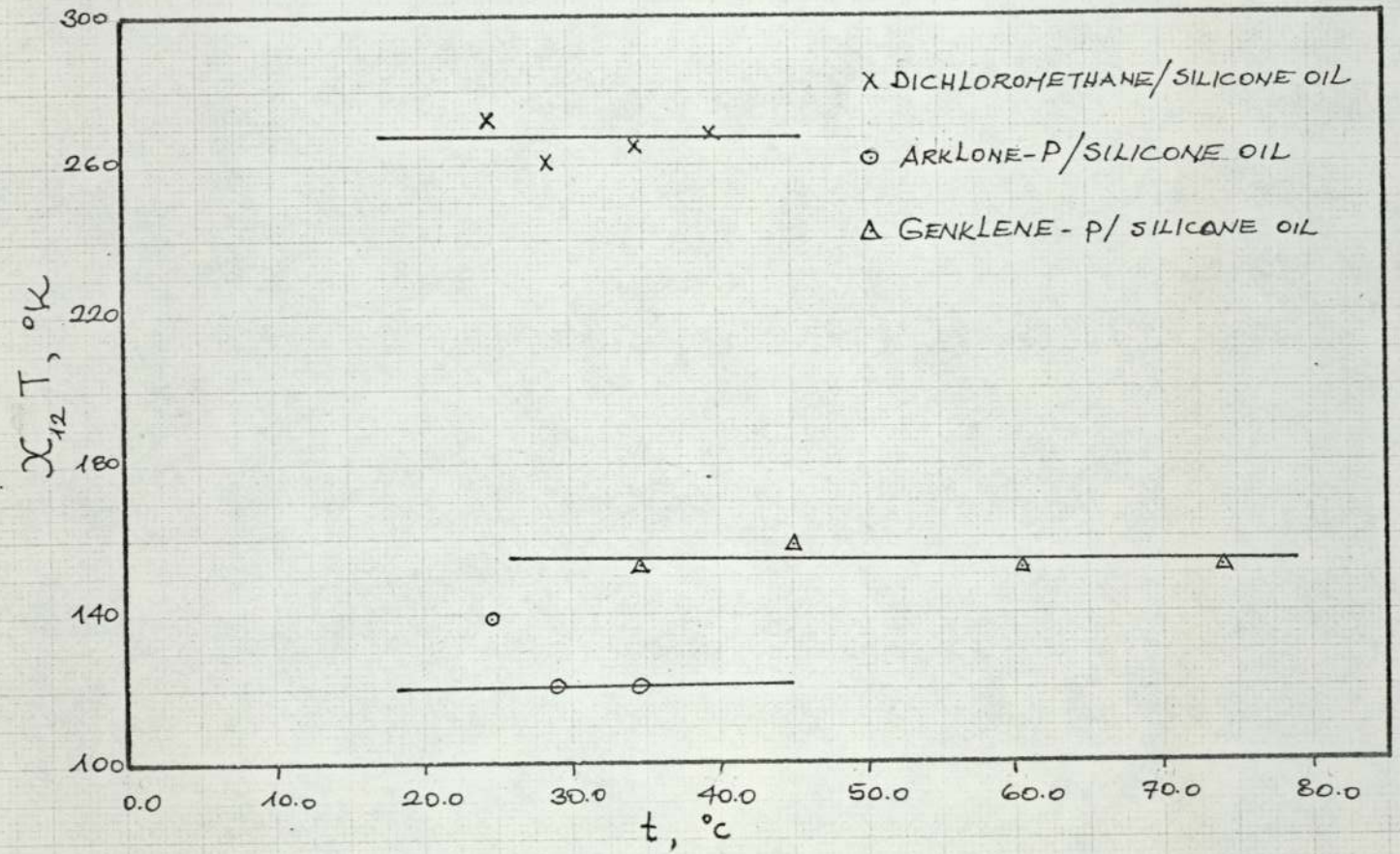

FIG. 6.3.7 - TEMPERATURE DEPENDENCE OF THE INTERACTION PARAMETER

$\chi_{\Delta s}$ in Table 6.3.8 indicates the first term on the right hand side of equation (6.3.14) cannot be ignored for these systems.

For the third system the data is well represented by a horizontal line to the temperature axis. This latter observation is in accordance with the very small value of $\chi_{\Delta s}$ found for Genklene-P (Table 6.3.8).

6.3.4 Correlation of the Data by Two-Parameter Flory-Huggins Equation.

In 1964 Everett and Munn (79) proposed that the parameter r should be regarded as temperature dependent on the basis that it is closely related to the number of configurations in the mixture, which can be expected to change with temperature. In analysing the hexane/hexadecane data of McGlashan and Morcom (131) they found that the values of both $\chi_{12}T$ and r $(=1/\rho)$ increased with temperature with the latter approaching to the value of the ratio of the molar volumes of pure liquid components near the boiling point of hexane. They also found the empirical relationship that the best fit values of χ_{12} and r are linearly related to one another.

In this work the two parameter Flory-Huggins equation was fitted to the data using the same computer program as in the previous section to find the best fit values of χ_{12} and r . The results are presented below. The activity coefficients calculated using these values are given in Appendix A.8. The fit is better than the one-parameter Flory-Huggins equation as would be expected.

1. α-Pinene/Polypropylene Sebacate, β-Pinene/Polypropylene Sebacate Systems.

The results on these systems, shown in Table 6.3.11, are inconclusive in determining the dependence of $r = (\frac{1}{\rho})$ and $\chi_{12}T$ on temperature, though there seems to be a general decrease in the values of both parameters with increasing temperature. This is in contrast to the findings of Everett and Munn. It should, however, be pointed out that the mixtures studied in this work involve molecules of very much widely different

Table 6.3.11. Best Fit Values of χ_{12} and ρ at Various Temperatures for the Systems α-Pinene/Polypropylene Sebacate and β-Pinene/Polypropylene Sebacate.

Solute	Temperature °C	ρ	χ_{12}	$\chi_{12}T$
α-Pinene	99.8	0.0321	1.106	412.3
	120.0	0.0276	1.156	454.3
	140.0	0.0442	0.593	244.9
	150.0	0.0373	0.774	327.4
β-Pinene	100.35	0.0174	1.351	504.4
	110.1	0.0378	0.599	229.5
	120.0	0.0303	0.756	297.1
	150.0	0.0580	0.0081	3.42

Table 6.3.12. Best Fit Values of χ_{12} and ρ at Various Temperatures for the Systems Dichloromethane/Silicone Oil MS 200, Arklone-P/Silicone Oil MS 200, Genklene-P/Silicone Oil MS 200.

Solute	Temperature °C	ρ	χ_{12}	$\chi_{12}T$
Dichloromethane	24.8	0.0136	0.5041	150.1
	29.1	0.00977	0.7650	231.1
	34.7	0.00906	0.8311	255.7
	39.8	0.0137	0.4302	137.1
Arklone-P	24.8	0.0107	0.8723	259.7
	29.1	0.0186	0.2730	82.5
	34.7	0.0195	0.2219	69.4
Genklene-P	34.7	0.00846	0.9389	288.9
	45.1	0.0102	0.7741	246.2
	60.5	0.0109	0.6823	227.6
	74.0	0.172	0.225	78.2

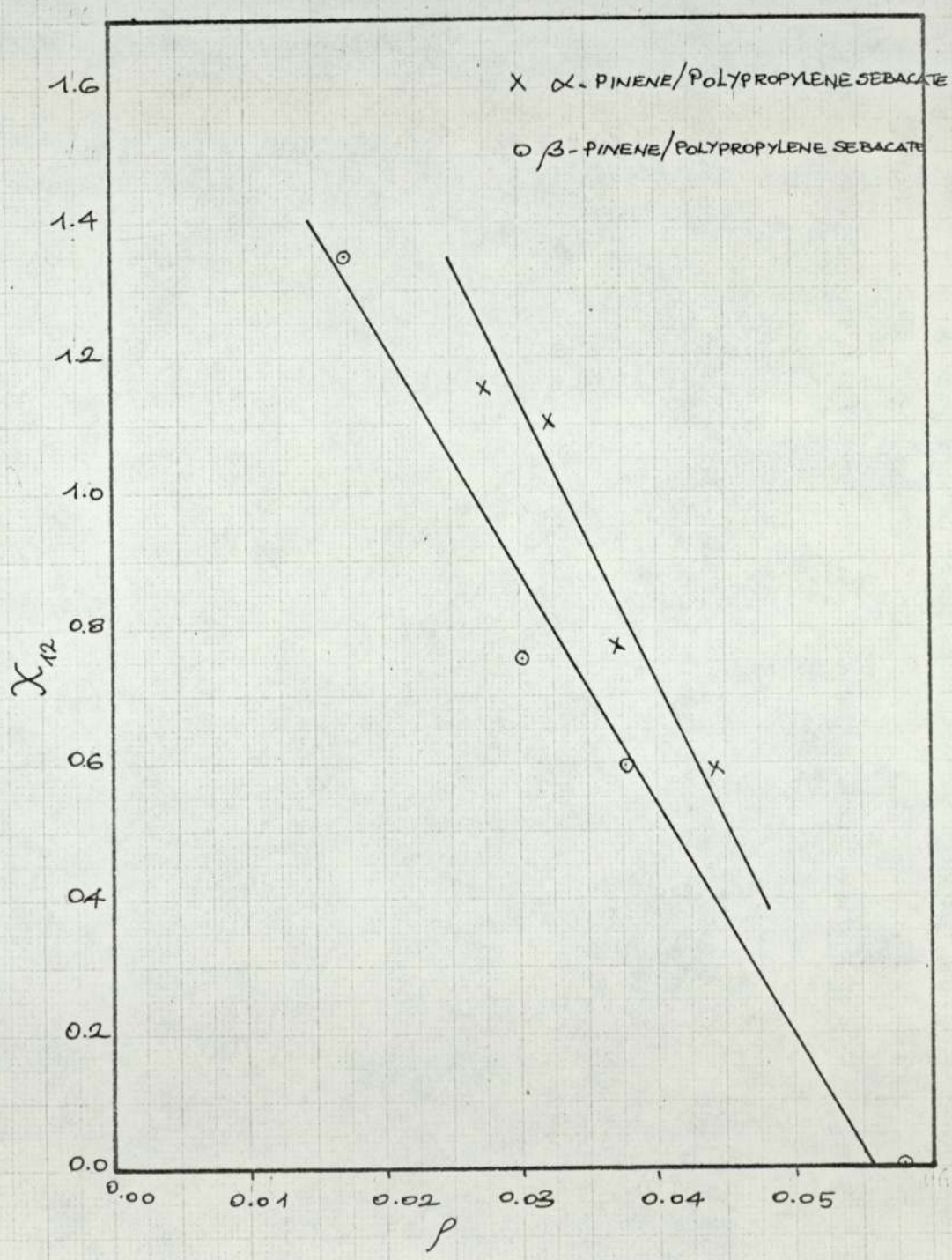

FIG. 6.3.8 - BEST FIT VALUES OF THE PARAMETERS OF THE FLORY-HUGGINS EQN.

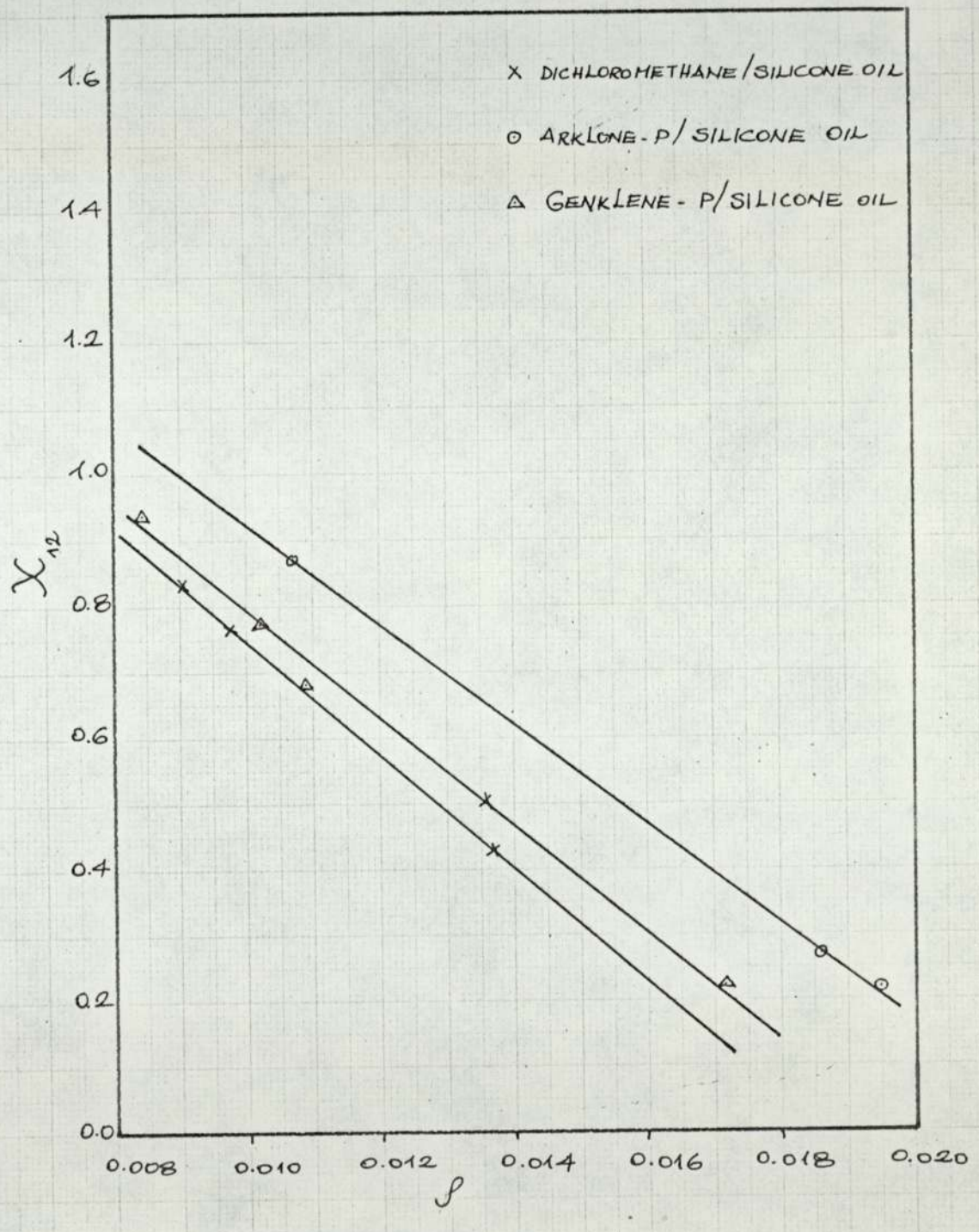

FIG 6.3.9- BEST FIT VALUES OF THE PARAMETERS OF THE FLORY-HUGGINS EQN.

molecular sizes and structures. On the other hand, Fig. 6.3.8 suggests a linear relationship between the best fit values of χ_{12} and ρ.

2. Dichloromethane/Silicone Oil MS 200, Arklone-P/Silicone Oil MS 200, Genklene-P/MSilicone Oil MS 200 Systems.

The results on these systems (Table 6.3.12) confirm the findings of the previous systems. Apart from the Dichloromethane/Silicone Oil MS 200 system, the decrease in the values of the parameter χ_{12} with increasing temperature are very pronounced. Again a linear relationship was found between the best fit values of the parameters.

An interesting feature of these systems is observed if the activity coefficient - mole fraction data over the whole temperature range for each system is plotted on the same graph (see Figs. 6.2.3 - 6.2.5). Apart from those at 24.8°C, they all fall on the same curve, even at 24.8°C the deviation is barely above the experimental precision. Therefore, it was decided to find the best fit values of χ_{12} and ρ for each system over the temperature range studied. These values are summarised below and the activity coefficients thus calculated are given in Appendix A.8. The deviation is somewhat large at infinite dilution condition with the fit improving up the concentration range.

Table 6.3.13. Best Fit Values of χ_{12} and ρ over the Whole Temperature Range.

Solute	ρ	χ_{12}
Dichloromethane	0.00810	0.9547
Arklone-P	0.01598	0.4376
Genklene-P	0.008537	0.9304

6.4 Heil Equation.

The binary Heil equation (equation 3.4.18) was fitted to the activity coefficient data of the halocarbons in Silicone Oil MS 200 in order to evaluate the two parameters. The fit was comparable to the two-parameter Flory-Huggins and slightly better than the one-parameter version of the same equation (see Appendix A.8). The parameter s was taken as unity for the halocarbons and 91 for the silicone Oil calculated from assuming $-(CH_3)si - O -$ to be the structural unit of the polymer. The constants thus evaluated are presented in the table below.

Table 6.4.1. The Parameters of the Heil Equation.

System	Temperature °C	$(g_{12}-g_{22})$	$(g_{21}-g_{11})$
Dichloromethane/ Silicone Oil MS 200	24.8	54.3	421.0
	29.1	142.2	187.2
	34.7	170.3	133.0
	39.8	-38.9	652.9
Arklone-P/ Silicone Oil MS 200	24.8	584.0	-1188.4
	29.1	19.9	163.5
	34.7	9.41	204.6
Genklene-P/ Silicone Oil MS 200	34.7	468.8	-874.9
	45.1	416.0	-770.6
	60.5	246.7	-422.7
	74.0	-71.9	577.0

If the parameter $(g_{ij}-g_{ii})$ is assumed to have the same physical significance as that in the Wilson equation then it should, theoretically, be independent of temperature (137-140). As Table 6.4.1 shows, however, no definite relationship can be observed with these systems. The reason for such erratic values can be understood by considering the plots in Figs. 6.4.1 and 6.4.2, which show the dependence of the error in the activity coefficients on the two parameters at x = 0.0 and x = 0.5 respectively.

The error, which is the parameter in the plots, is expressed both as an absolute value and as percentage. The true values of the activity coefficients are $\gamma_1 = 0.089241$ at $x = 0.0$ and $\gamma_1 = 0.16794$ at $x = 0.5$ as calculated from the Heil equation with $(g_{12}-g_{22}) = 9.0$ and $(g_{12}-g_{11}) = 205.0$. As seen, the error curves are a pair of parallel lines on either side of the point, representing the true values of the parameters, for each value of the error and getting closer to each other as the value of the error decreases. It is obvious from this that if the value of the error is made infinitesimally small the error curve would be represented by a single line passing through the "true" point. This, of course, means that if the parameters are evaluated by a least square fit of the data, as was done in this work, the values found will depend on the search technique employed as well as on the starting conditions, in other words, it is impossible to arrive at a unique pair. Two other important properties of the Heil equation can be deduced from these curves.

1. The slopes of the curves are near to -45° indicating that the activity coefficient is almost equally sensitive to both parameters.

2. A comparison of Figs. 6.4.1 and 6.4.2 shows that they are almost identical. This means that the sensitivity of the activity coefficient to the parameters is the same at the infinite dilution end and at the mid-range. In other words, if the parameters are determined from point values then the accuracy of the predicted values of activity coefficients at other points will be the same regardless of their position in the concentration range. This property is in contrast to those of the Wilson and NRTL equations which have similar theoretical backgrounds. In their case the error curvers are concentric loops larger at the mid-range than at the infinite dilution end making it possible to predict accurately (1%) the activity coefficients at finite concentrations from relatively inaccurate end values (10%). (141).

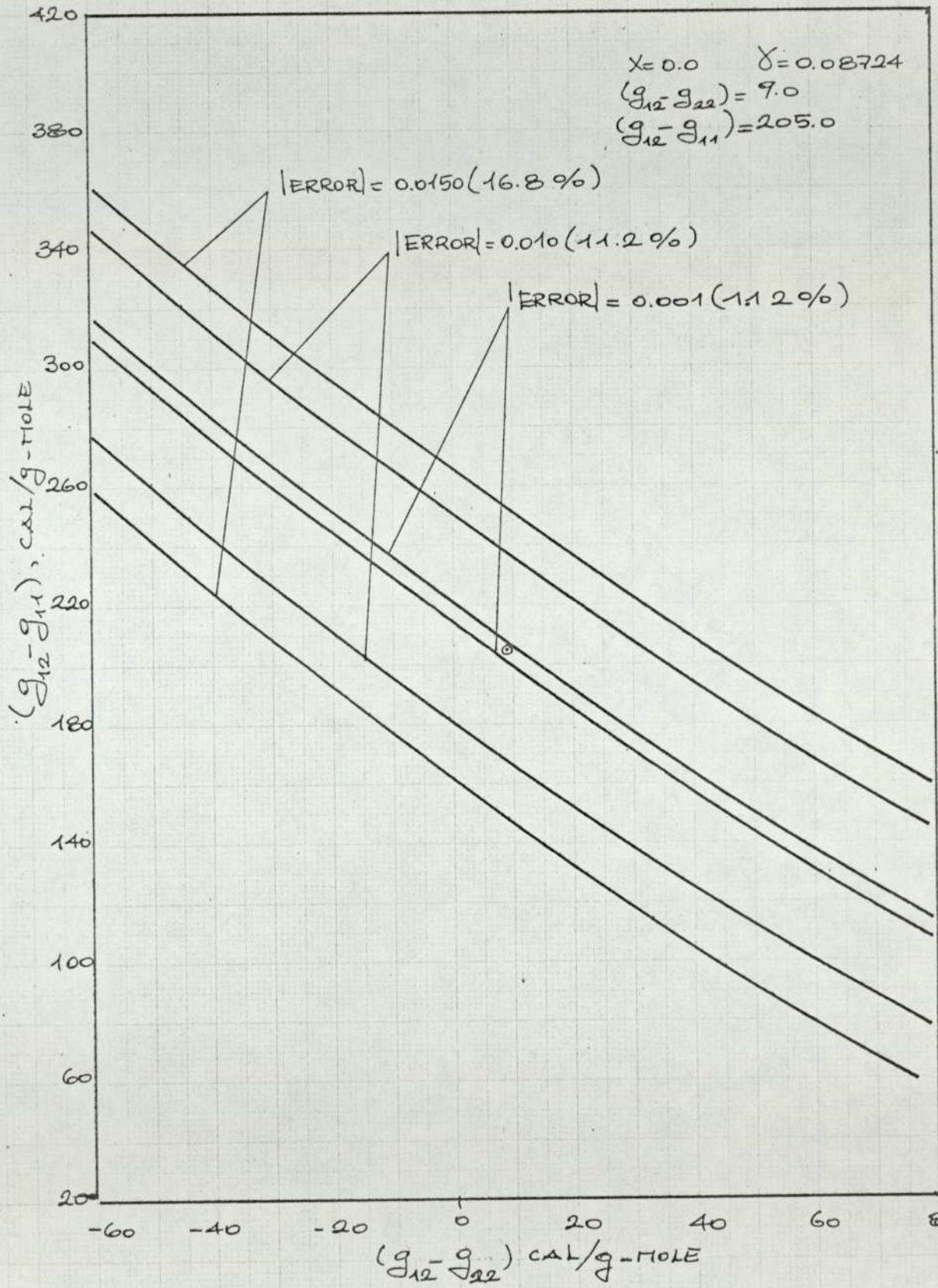

FIG. 6.4.1 - SENSITIVITY OF THE HEIL EQUATION TO ITS PARAMETERS

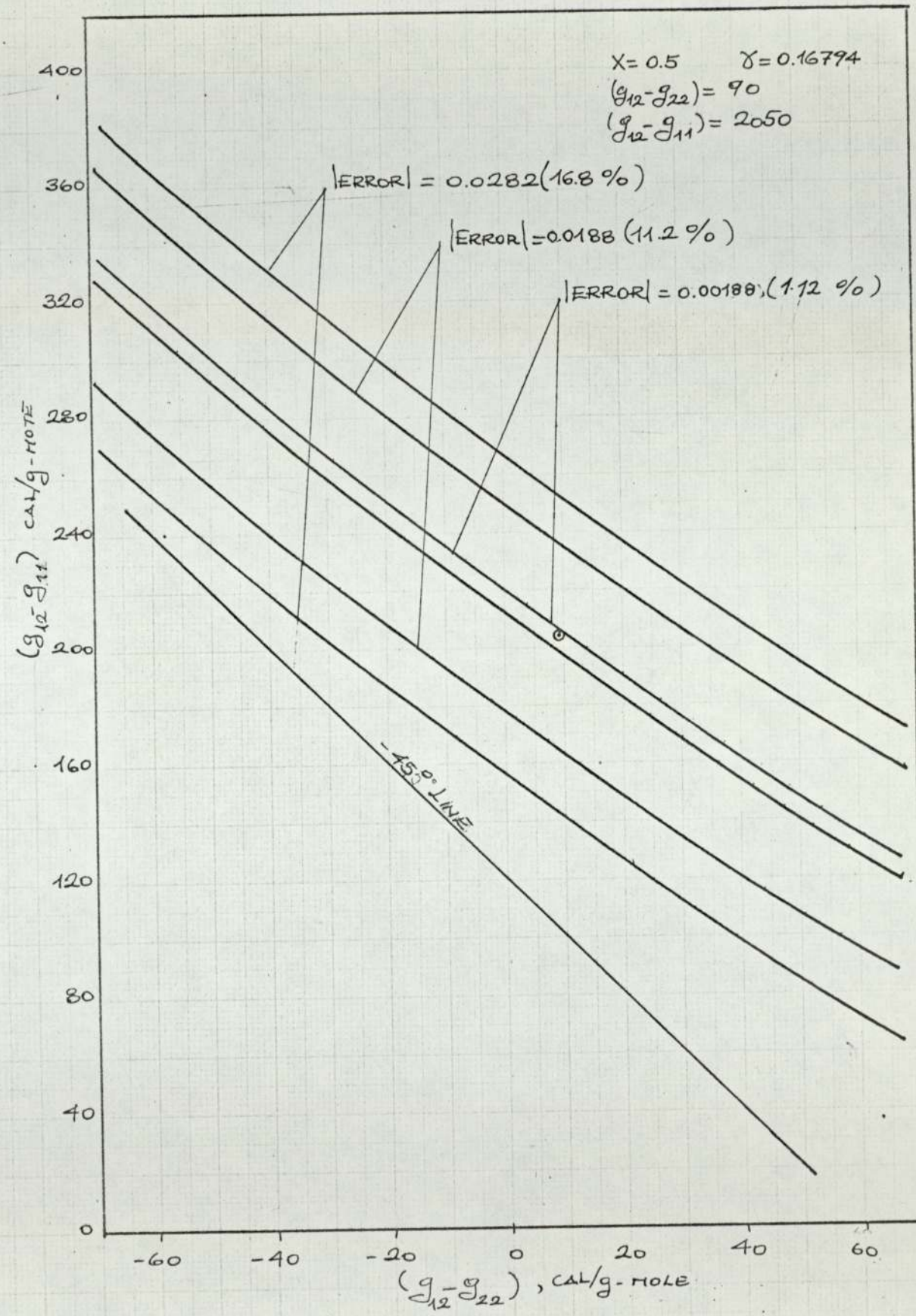

FIG 6.4.2 SENSITIVITY OF THE HEIL EQUATION TO ITS PARAMETERS

6.5 Calculation of the Excess Properties.

The excess partial molar enthalpy of mixing can be calculated from the dependence of the activity coefficient on temperature from equation (3.3.15), which at infinite dilution gives

$$\frac{d\ln \gamma_1^{\infty}}{d(1/T)} = \frac{\bar{h}_1^{E\infty}}{R} \qquad (6.5.1)$$

Another approach is by way of the temperature dependence of the specific retention volume V_G° which is defined by

$$V_G^{\circ} = \frac{V_N^{\circ}}{V_L \rho_L} \frac{273}{T} \qquad (6.5.2)$$

The activity coefficient is then given by

$$\ln \gamma_1^{\infty} = \ln \frac{273R}{M_2 P_1^{\circ} V_G^{\circ\infty}} + FC \qquad (6.5.3)$$

where FC is the fugacity correction term.

By differentiating both sides of equation (6.5.3) with respect to $\frac{1}{T}$ and by making use of the Clasius-Clapeyron equation (equation 6.3.12), it can be shown that

$$\frac{d\ln V_G^{\circ\infty}}{d(1/T)} = \frac{1}{R}(\Delta H_v - \bar{h}_1^{E\infty}) + \frac{d(FC)}{d(1/T)} = \frac{\bar{h}_1^{s\infty}}{R} + \frac{d(FC)}{d(1/T)} \qquad (6.5.4)$$

where $\bar{h}_1^{s\infty}$ is the molar heat of evaporation of the solute from solution at infinite dilution.

The two approaches are equivalent provided ΔH_v is evaluated at the temperature range studied rather than the value generally listed for the solute at its boiling point. In fact in this work only one value of ΔH_v was used to calculate the vapour pressures over the whole temperature range, so any error caused by this assumption is also inherent in the first approach. However, the second approach was preferred as the change in $V_G^{\circ\infty}$ with temperature is appreciably greater than in the activity

coefficient making the measurement of the slopes easier. The last term in equation (6.5.4) was ignored for all the five systems. Although the fugacity corrections were calculated for the halocarbons at some of the temperatures they contain B_{12} terms which could only be obtained from theoretical equations and, therefore, were not considered reliable enough for the present purpose. The $\ln V_G^{\circ\infty}$ versus 1/T data is presented in Table 6.5.1 and 6.5.2 and plotted on Figs. 6.5.1 and 6.5.2.

The values of $\bar{h}_1^{E\infty}$ and $\bar{h}_1^{s\infty}$ calculated from equation (6.5.4) and the values of ΔH_v listed in Tables 6.3.6 and 6.3.7 are presented in Table 6.5.3.

The excess partial molar entropy of mixing was calculated from equation (3.3.17)

$$RT\ln\gamma_1^{\infty} = \bar{h}_1^{E\infty} - T\bar{s}_1^{E\infty}$$

The athermal part of $\bar{s}_1^{E\infty}$ is given by the Flory-Huggins equation, i.e.

$$\ln\gamma_{a_1}^{\infty} = \ln\rho + (1-\rho) = -\frac{\bar{s}_{a_1}^{E\infty}}{R} \qquad (6.5.5)$$

and the thermal part is calculated from the balance. These results are shown in Tables 6.5.4 and 6.5.5 for the halocarbons and the pinenes respectively.

Table 6.5.1. $\ln V_G^{o}$ versus $^{1}/T$ for the Halocarbons in Silicone Oil MS 200 at Infinite Dilution.

$^{1}/Tx10^{3}$ K^{o-1}	$\ln V_G^{o\infty}$		
	Dichloromethane	Arklone-P	Genklene-P
3.3579	4.5545	4.7070	5.7583
3.3101	4.4459	4.5723	5.6877
3.2499	4.2248	4.3648	5.3869
3.1969	4.0376	4.1622	5.1705
3.1436	3.8854	4.0051	4.9824
2.9985	3.4184	3.5218	4.4901
2.8818	3.0431	3.1412	4.0385

Table 6.5.2. $\ln V_G^{o}$ versus $^{1}/T$ for the Pinenes in Polypropylene Sebacate at Infinite Dilution.

$^{1}/Tx10^{3}$ $^{o}K^{-1}$	$\ln V_G^{o\infty}$	
	α-Pinene	β-Pinene
2.6824	5.0181	-
2.6784	-	5.4935
2.6103	4.7185	5.1728
2.5445	4.4604	4.9038
2.4213	3.9407	4.3526
2.36406	3.6441	4.0645

Table 6.5.3. Excess Enthalpies of Mixing and Vaporisation.

	Dichloro-Methane/ Silicone Oil	Arklone-P/ Silicone Oil	Genklene-P/ Silicone Oil	α-Pinene/ PPS	β-Pinene/ PPS
$\bar{h}_i^{s}$ cal/g-mole	6359.0	6599.0	7240.5	8258.5	8906.5
$\bar{h}_i^{E}$ cal/g-mole	1216.5	511.5	311.8	1439.7	1129.9

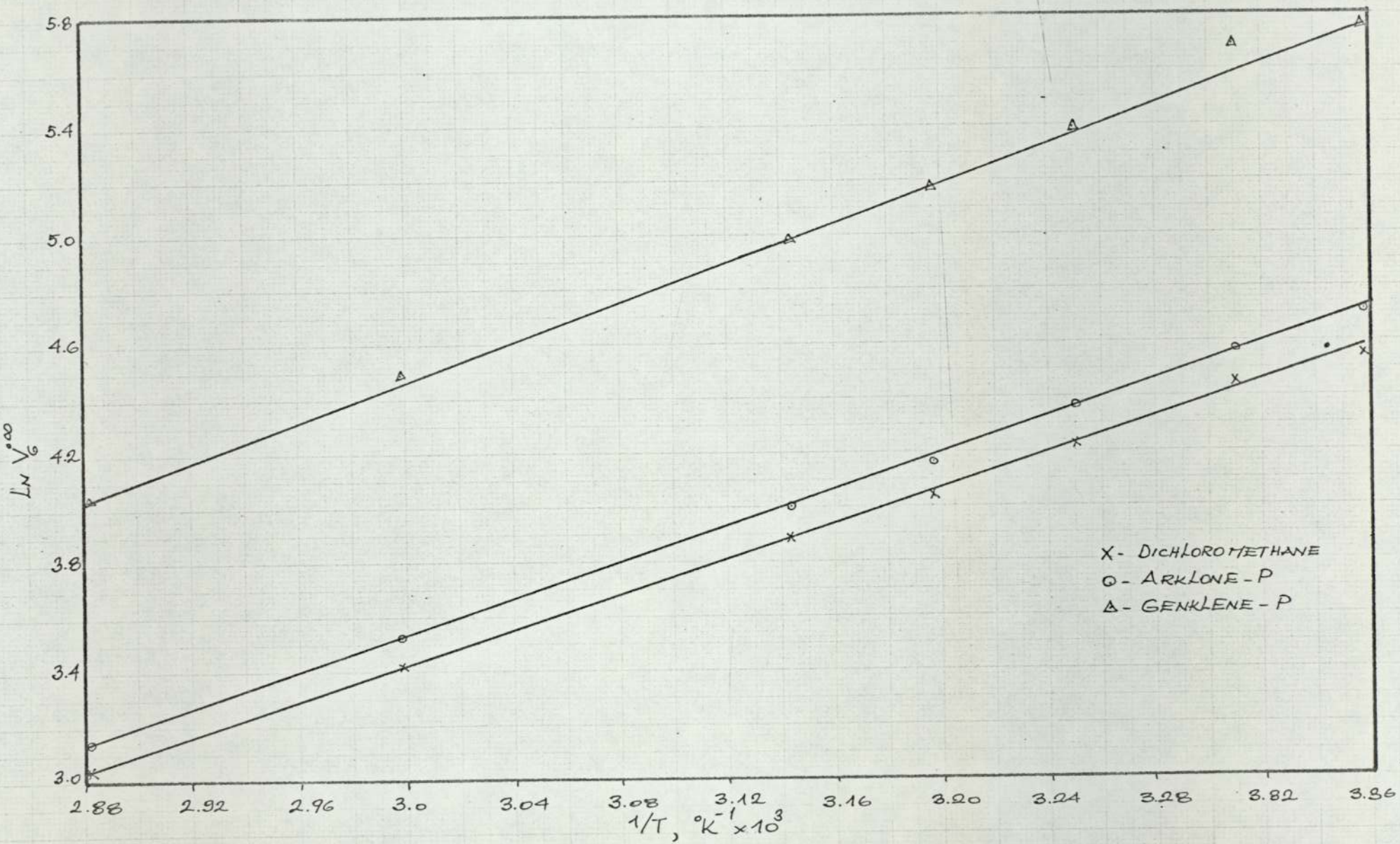

FIG. 6.5.1 TEMPERATURE DEPENDENCE OF THE SPECIFIC RETENTION VOLUME

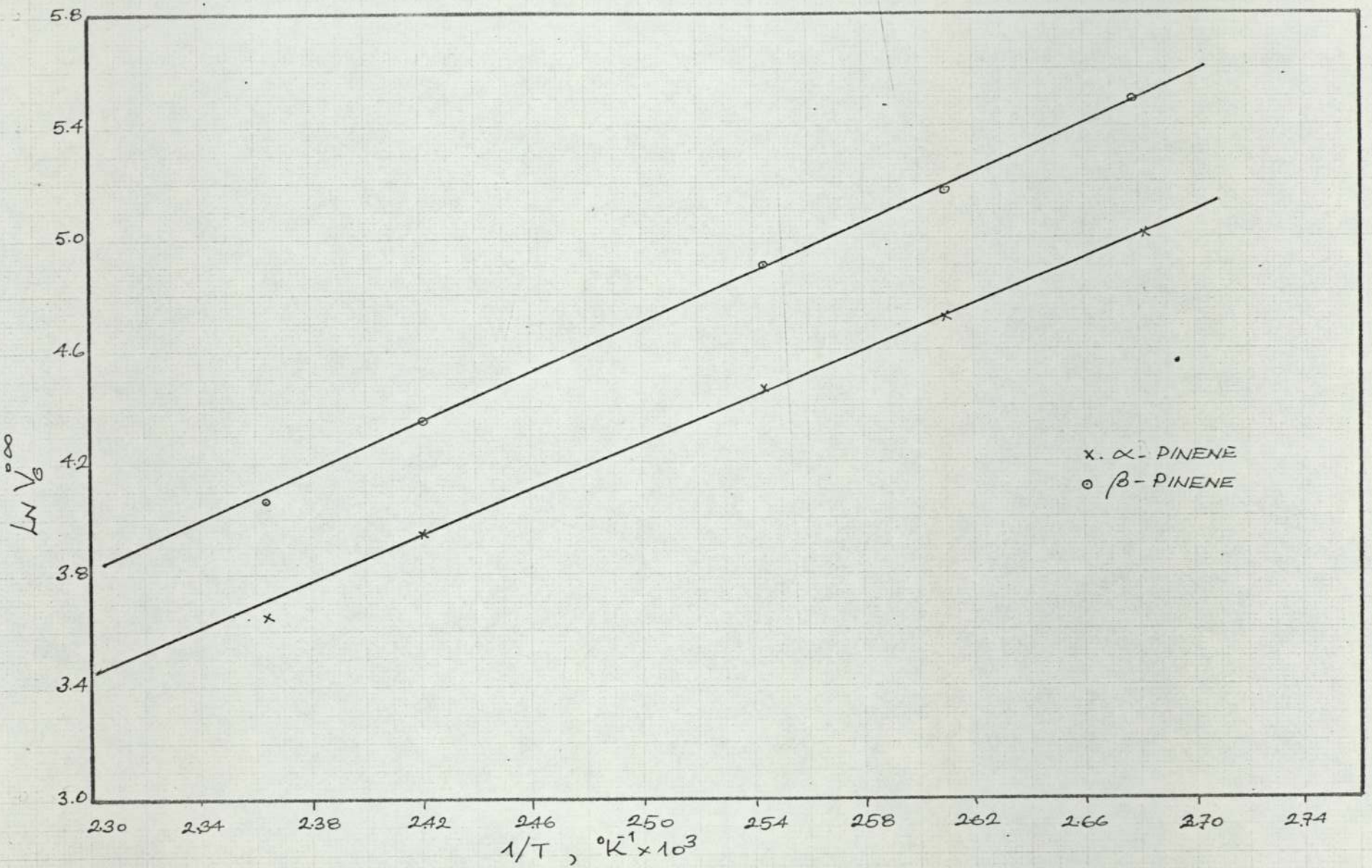

FIG. 6.5.2 - TEMPERATURE DEPENDENCE OF THE SPECIFIC RETENTION VOLUME

Table 6.5.4. Excess Entropies of Mixing of the Halocarbons in Silicone Oil MS 200.

Temperature °C	Dichloromethane		Arklone-P		Genklene-P	
	$-\bar{E}^{\infty}_{s_a}$ cal/ g-mole K	$-\bar{E}^{\infty}_{s_t}$ cal/ g-mole °K	$-\bar{E}^{\infty}_{s_a}$ cal/ g-mole °K	$-\bar{E}^{\infty}_{s_t}$ cal/ g-mole °K	$-\bar{E}^{\infty}_{s_a}$ cal/ g-mole °K	$-\bar{E}^{\infty}_{s_a}$ cal/ g-mole °K
24.8	7.439	2.188	6.228	0.850		
29.1	7.436	2.282	6.221	0.895		
34.7	7.438	2.228	6.221	0.873	6.563	0.080
39.8	7.442	2.180				
45.1					6.557	0.035
60.5					6.550	0.043
74.0					6.547	0.043

Table 6.5.5. Excess Entropies of Mixings of the Pinenes in Polypropylene Sebacate.

Temperature °C	α-Pinene		β-Pinene	
	$-\bar{E}^{\infty}_{s_a}$ cal/ g-mole °K	$-\bar{E}^{\infty}_{s_t}$ cal/ g-mole °K	$-\bar{E}^{\infty}_{s_a}$ cal/ g-mole °K	$-\bar{E}^{\infty}_{s_a}$ cal/ g-mole °K
99.8	3.924	2.701		
100.35			3.912	2.604
110.1			3.910	2.516
120.0	3.944	2.639	3.904	2.543
140.0	3.975	2.589		
150.0	3.993	2.514	3.887	2.511

7. CALCULATION OF TERNARY DATA.

7.1 Calculation of Partition Coefficients.

In the calculations of binary data from equation (3.1.7) the appearances of the term $(\partial q/\partial c)$ instead of the partition coefficient, K, and the term $(1-aJy_o)$ for the sorption effect arise from the fact that the molecules of the small sample are indistinguishable from the molecules of the plateau. If, however, a small sample of a different solute is injected on top of the plateau, the measured retention volume is that of the injected molecules and not of the pertubation caused by the injection. Therefore, the partition coefficient of the solute present at infinite dilution is now calculated from the James-Martin equation (3.1.1),

$$V_N^{o\infty} = J_3^2 V_N^{\infty} = J_3^2 (V_R^{\infty} - V_g) = K^{\infty} V_L$$

In contrast to equation (6.1.1) the partition coefficient in the above equation can be calculated from a single retention volume measurement.

The results are tabulated in Tables 7.1.1 to 7.1.8 and the plots of the gas concentration of the solute present at finite concentration (component 2) against the infinite dilution partition coefficient of the second solute (component 1) are shown in Figs. 7.1.1 to 7.1.8. The continuous lines are the best fit lines obtained by a least square analysis. Comparing these plots with the corresponding plots for the binary data, it is seen that the latter shows an apparent absence of scatter. This is an inevitable consequence of the integration process carried out in calculating the partition coefficients from the retention volume data (see equation 6.1.1). Therefore, the scatter shown on the plots in this section is a truer indication of the experimental precision of this work as a whole.

7.2 Calculation of Activity Coefficient from Retention Data.

The activity coefficient of a solute in a ternary mixture is given by equation (3.3.15). When the solute under consideration (component 1) is

Table 7.1.1. Infinite Dilution Partition Coefficient and Activity Coefficient of α-Pinene in presence of β-Pinene.

Temperature °C	$c_2 \times 10^4$ g/cm^3 at NTP	$J_2^3 V_{R1}^{\infty}$	K_1^{∞}	x_2	γ_1^{∞}	$\ln \gamma_1^{\infty}$
100.35	0.0	52.4	208.8	0.0	0.2437	-1.4118
	0.64	55.1	220.6	0.3441	0.2315	-1.463
	0.90	56.0	224.8	0.4282	0.2274	-1.481
	1.13	57.3	230.5	0.4879	0.2236	-1.498
	1.76	57.9	233.5	0.6059	0.2141	-1.541
	1.83	58.6	236.5	0.6161	0.2131	-1.546
	1.91	59.9	242.2	0.6272	0.2119	-1.552
	2.20	60.0	242.6	0.6631	0.2078	-1.571
	2.35	60.5	244.9	0.6794	0.2059	-1.580
110.1	0.0	40.8	157.9	0.0	0.2388	-1.432
	0.63	41.5	160.5	0.2743	0.2303	-1.468
	0.95	43.1	167.9	0.3668	0.2261	-1.487
	1.14	43.5	169.9	0.4124	0.2236	-1.497
	1.48	43.7	170.8	0.4811	0.2195	-1.516
	1.86	44.7	175.1	0.5427	0.2146	-1.539
	2.01	44.7	175.0	0.5637	0.2131	-1.546
	2.09	45.1	176.9	0.5742	0.2119	-1.551
	2.19	45.8	180.2	0.5868	0.2109	-1.556
120.0	0.0	33.2	124.7	0.0	0.2300	-1.469
	0.69	34.2	129.1	0.2407	0.2213	-1.508
	1.21	34.8	131.8	0.3616	0.2153	-1.536
	1.59	35.3	134.1	0.4293	0.2110	-1.556
	1.92	36.3	138.6	0.4795	0.2072	-1.594
	2.28	36.8	140.7	0.5254	0.2036	-1.592
	2.33	36.9	141.5	0.5313	0.2030	-1.595
150.0	0.0	19.7	58.1	0.0	0.2121	-1.550
	0.52	20.0	59.5	0.1006	0.2038	-1.592
	0.69	20.5	61.6	0.1301	0.2003	-1.608
	1.16	21.0	63.7	0.2045	0.1934	-1.643
	1.80	21.8	66.8	0.2911	0.1843	-1.691

Table 7.1.2. Infinite Dilution Partition Coefficient and Activity Coefficient of β-Pinene in presence of α-Pinene.

Temperature °C	$c_2 \times 10^4$ g/cm^3 at NTP	$J_3^2 V_{R1}^{\infty}$	K_1^{∞}	x_2	γ_1^{∞}	$\ln \gamma_1^{\infty}$
99.8	0.0	95.6	333.8	0.0	0.1789	-1.721
	0.78	98.4	343.1	0.2816	0.1736	-1.751
	0.92	98.0	341.6	0.3176	0.1726	-1.757
	1.51	100.8	352.0	0.4403	0.1689	-1.779
	1.61	100.5	350.8	0.4574	0.1682	-1.783
	1.91	103.8	363.0	0.5036	0.1664	-1.793
	2.77	106.6	373.4	0.6050	0.1613	-1.825
120.0	0.0	56.9	191.2	0.0	0.1670	-1.790
	0.625	58.4	196.8	0.1549	0.1637	-1.810
	1.06	58.6	197.7	0.2395	0.1614	-1.824
	1.325	59.5	200.8	0.2841	0.1601	-1.832
	1.51	58.5	197.1	0.3126	0.1592	-1.838
	1.575	59.3	200.1	0.3221	0.1589	-1.839
	2.06	59.3	200.4	0.3867	0.1565	-1.855
140.0	0.0	37.8	115.5	0.0	0.1535	-1.874
	0.40	39.6	121.9	0.0682	0.1504	-1.894
	0.71	39.6	121.9	0.1159	0.1481	-1.910
	0.95	39.6	121.9	0.1501	0.1463	-1.921
	1.20	40.1	123.9	0.1834	0.1446	-1.934
	1.71	40.6	125.5	0.2451	0.1411	-1.958
	1.76	40.8	126.4	0.2507	0.1408	-1.961
	2.60	42.0	130.9	0.3359	0.1354	-1.999
	4.18	43.9	137.8	0.4588	0.1264	-2.068
150.0	0.0	29.9	89.4	0.0	0.1513	-1.888
	0.70	30.9	90.3	0.0897	0.1507	-1.893
	0.912	31.1	91.1	0.1139	0.1505	-1.894
	1.24	30.7	89.8	0.1492	0.1503	-1.895
	1.95	30.5	90.4	0.2175	0.1497	-1.899
	2.46	30.5	89.6	0.2606	0.1492	-1.902

Table 7.1.3. Infinite Dilution Partition Coefficient and Activity Coefficient of Dichloromethane in presence of Arklone-P.

Temperature °C	$c_2 \times 10^4$ g/cm^3 at NTP	$J_3^2 V_{R1}^{\infty}$	K_1^{∞}	x_2	γ_1^{∞}	$\ln \gamma_1^{\infty}$
24.8	0.0	77.5	101.4	0.0	0.06084	-2.799
	0.6125	77.6	101.5	0.2200	0.06077	-2.800
	1.3375	78.1	102.1	0.3826	0.06041	-2.806
	1.700	78.9	103.4	0.4414	0.05970	-2.818
	2.750	79.9	104.8	0.5633	0.05892	-2.831
	3.6625	81.5	106.9	0.6338	0.05776	-2.851
29.1	0.0	70.9	91.5	0.0	0.05670	-2.869
	1.1625	69.8	89.9	0.3256	0.05776	-2.851
	1.950	70.3	90.6	0.4575	0.05735	-2.858
	2.8125	70.4	90.7	0.5466	0.05729	-2.859
	3.825	74.0	95.8	0.6256	0.05430	-2.913
	4.200	72.1	93.1	0.6489	0.05583	-2.885
34.7	0.0	59.2	74.6	0.0	0.05585	-2.885
	1.300	59.8	75.5	0.3090	0.05527	-2.892
	2.150	59.6	75.1	0.4286	0.05557	-2.901
	2.975	60.1	75.9	0.5126	0.05502	-2.901
	3.025	60.2	76.0	0.5169	0.05496	-2.901
	3.825	60.8	76.9	0.5781	0.05434	-2.905
	4.7125	60.5	76.3	0.6313	0.05472	-2.910

Table 7.1.4. Infinite Dilution Partition Coefficient and Activity Coefficient of Dichloromethane in presence of Genklene-P.

Temperature °C	$c_2 \times 10^4$ g/cm^3 at NTP	$J_3^2 V_{R1}^{\infty}$	K_1^{∞}	x_2	γ_1^{∞}	$\ln \gamma_1^{\infty}$
34.7	0.0	59.5	74.8	0.0	0.05568	-2.888
	0.900	60.6	76.3	0.5516	0.05470	-2.905
	1.950	63.3	80.0	0.7376	0.05214	-2.953
	2.675	65.9	83.8	0.7997	0.04986	-2.998
	3.100	65.6	83.3	0.8252	0.05017	-2.992
	3.750	67.3	85.7	0.	0.04876	-3.030
	4.250	68.5	87.4	0.8879	0.04785	-3.039
	4.500	69.2	88.2	0.	0.04738	-3.049
	5.440	71.5	91.5		0.04573	-3.084
45.1	0.0	44.7	53.7	0.0	0.05327	-2.932
	0.975	45.1	54.2	0.4750	0.05285	-2.940
	1.525	45.4	54.6	0.5902	0.05248	-2.947
	2.463	46.7	56.3	0.7045	0.05088	-2.978
	3.375	47.5	57.6	0.7713	0.04984	-2.999
	4.150	48.0	58.1	0.8093	0.04938	-3.008
60.5	0.0	31.2	34.7	0.0	0.04907	-3.014
	1.5125	32.1	35.9	0.4681	0.04753	-3.046
	2.1875	32.5	36.4	0.5632	0.04688	-3.060
	2.3375	32.1	35.9	0.5802	0.04747	-3.048
	3.175	32.6	36.6	0.6561	0.04662	-3.066
	4.025	32.4	36.3	0.7108	0.04713	-3.055
74.0	0.0	23.8	24.2	0.0	0.04663	-3.066
	0.9875	24.6	25.3	0.2778	0.04475	-3.106
	1.650	24.8	25.5	0.3941	0.04426	-3.118
	2.400	24.6	25.2	0.4896	0.04488	-3.104
	3.2125	24.8	25.6	0.5657	0.04434	-3.116
	4.500	25.3	26.2	0.6551	0.04330	-3.139

Table 7.1.5. Infinite Dilution Partition Coefficient and Activity Coefficient of Arklone-P in presence of Dichloromethane.

Temperature °C	$c_2 \times 10^4$ g/cm^3 at NTP	$J_3^2 V_{R1}^{\infty}$	K_1^{∞}	x_2	γ_1^{∞}	$\ln \gamma_1^{\infty}$
24.8	0.0	87.0	114.4	0.0	0.06944	-2.667
	1.150	91.3	120.4	0.5119	0.06596	-2.719
	1.8625	93.0	122.6	0.6366	0.06462	-2.739
	2.675	94.4	124.8	0.7224	0.06358	-2.755
	3.075	95.7	126.6	0.7525	0.06267	-2.769
	3.750	97.7	129.5	0.7933	0.06130	-2.792
	4.475	100.3	133.1	0.8238	0.05961	-2.820
29.1	0.0	79.1	102.8	0.0	0.06604	-2.717
	1.2375	81.7	106.3	0.5041	0.06382	-2.752
	1.8825	82.7	107.8	0.6125	0.06293	-2.766
	2.625	85.7	112.0	0.6925	0.06056	-2.804
	3.625	86.4	112.9	0.7622	0.06008	-2.812
	4.025	88.1	115.3	0.7827	0.05885	-2.833
	4.975	89.4	117.2	0.8207	0.05787	-2.849
34.7	0.0	65.7	83.5	0.0	0.06602	-2.709
	1.875	68.6	87.5	0.5593	0.06357	-2.756
	2.5125	69.7	88.9	0.6333	0.06249	-2.773
	3.050	69.9	89.3	0.6798	0.06224	-2.777
	3.975	72.1	92.4	0.7388	0.06018	-2.810
	4.845	72.2	92.5	0.7778	0.06011	-2.811
	5.35	73.8	94.7	0.7971	0.05866	-2.836
39.8	0.0	56.2	70.1	0.0	0.06699	-2.7031
	1.425	57.6	71.9	0.4435	0.06522	-2.730
	1.9375	58.3	73.0	0.5227	0.06428	-2.745
	2.1375	58.2	72.8	0.5481	0.06448	-2.741
	3.6375	60.9	76.6	0.6802	0.06125	-2.793
	4.525	61.4	77.3	0.7291	0.06064	-2.803
	5.000	61.9	78.0	0.7501	0.06010	-2.812

Table 7.1.6. Infinite Dilution Partition Coefficient and Activity Coefficient of Arklone-P in presence of Genklene-P.

Temperature °C	$c_2 \times 10^4$ g/cm^3 at NTP	$J_3^2 V_{R1}^{\infty}$	K_1^{∞}	x_2	γ_1^{∞}	$\ln \gamma_1^{\infty}$
34.7	0.0	66.5	84.6	0.0	0.06577	-2.722
	0.900	67.8	86.3	0.5516	0.06441	-2.742
	1.950	71.5	91.4	0.7376	0.06080	-2.800
	2.675	74.3	95.5	0.7997	0.05824	-2.843
	3.100	74.6	95.8	0.8252	0.05799	-2.847
	3.750	76.4	98.3	0.8547	0.05655	-2.873
	4.250	78.6	101.3	0.	0.06483	-2.904
	4.500	78.1	100.7	0.8795	0.05516	-2.897
	5.440	82.0	106.1	0.	0.05233	-2.950
45.1	0.0	49.8	60.7	0.0	0.06521	-2.730
	0.975	50.1	61.1	0.4750	0.06476	-2.737
	1.525	50.5	61.7	0.5902	0.06411	-2.747
	2.463	52.0	63.8	0.7045	0.06200	-2.780
	3.375	53.5	65.8	0.7713	0.06010	-2.812
	4.150	54.0	66.6	0.8093	0.05938	-2.824
60.5	0.0	34.1	38.6	0.0	0.06433	-2.744
	1.5125	35.1	40.0	0.4681	0.06204	-2.780
	2.1875	35.5	40.5	0.5632	0.06125	-2.793
	2.3375	35.6	40.7	0.5802	0.06099	-2.797
	3.175	36.3	41.6	0.6561	0.05963	-2.820
	4.025	36.3	41.6	0.7108	0.05960	-2.820
74.0	0.0	25.9	27.0	0.0	0.06358	-2.758
	0.9875	26.4	27.7	0.2778	0.06199	-2.779
	1.650	27.1	28.6	0.3941	0.06001	-2.793
	2.40	26.9	28.3	0.4896	0.06056	-2.808
	3.2125	27.1	28.7	0.5657	0.05975	-2.825
	4.50	27.9	29.7	0.6511	0.05779	-2.851

Table 7.1.7. Infinite Dilution Partition Coefficient and Activity Coefficient of Genklene-P in presence of Dichloromethane.

Temperature °C	$c_2 \times 10^4$ g/cm^3 at NTP	$J_3^2 V_{R1}^{\infty}$	K_1^{∞}	x_2	γ_1^{∞}	$\ln \gamma_1^{\infty}$
24.8	0.0	242.6	333.5	0.0	0.06131	-2.792
	1.150	258.2	355.5	0.5119	0.05750	-2.856
	1.8625	265.1	365.2	0.6366	0.05597	-2.883
	2.675	275.7	380.1	0.7224	0.05377	-2.923
	3.075	282.2	389.3	0.7525	0.05250	-2.947
	3.775	290.5	401.0	0.7933	0.05096	-2.977
	4.825	307.9	425.4	0.8375	0.04802	-3.036
29.1	0.0	214.6	293.0	0.0	0.05892	-2.832
	1.2375	225.8	308.5	0.5041	0.05595	-2.883
	1.885	231.9	317.1	0.6125	0.05443	-2.911
	2.975	241.9	331.1	0.7225	0.05211	-2.954
	4.025	249.0	341.1	0.7827	0.05058	-2.984
	4.975	267.0	366.3	0.8207	0.04710	-3.056
34.7	0.0	171.6	230.9	0.0	0.06031	-2.808
	1.875	184.4	248.7	0.5593	0.05597	-2.883
	2.5125	188.5	254.5	0.6333	0.05470	-2.906
	3.050	192.8	260.5	0.6798	0.05343	-2.929
	3.975	195.5	264.2	0.7388	0.05267	-2.944
	4.825	199.8	270.2	0.7778	0.05150	-2.966
	5.350	203.5	275.4	0.7971	0.05052	-2.985
39.8	0.0	144.2	192.3	0.0	0.06028	-2.809
	1.425	150.4	200.9	0.4435	0.05767	-2.853
	1.9375	149.3	199.5	0.5227	0.05808	-2.846
	2.1375	152.2	203.4	0.5481	0.05695	-2.865
	3.6375	159.3	213.3	0.6802	0.05430	-2.913
	4.525	163.5	219.1	0.7291	0.05284	-2.940
	5.00	166.3	223.1	0.7501	0.05190	-2.958

Table 7.1.8. Infinite Dilution Partition Coefficient and Activity Coefficient of Genklene-P in presence of Arklone-P.

Temperature °C	$c_2 \times 10^4$ g/cm^3 at NTP	$J_3^2 V_{R1}^{\infty}$	K_1^{∞}	x_2	γ_1^{∞}	$\ln \gamma_1^{\infty}$
24.8	0.0	241.9	332.9	0.0	0.06141	-2.790
	0.6750	246.1	339.9	0.2351	0.06015	-2.811
	1.3375	251.0	346.7	0.3826	0.05897	-2.831
	1.700	256.2	350.4	0.4414	0.05834	-2.841
	2.825	262.7	361.9	0.5710	0.05647	-2.874
	3.850	269.4	372.4	0.6450	0.05487	-2.903
29.1	0.0	214.7	293.3	0.0	0.05886	-2.832
	1.1825	217.6	297.3	0.3225	0.05806	-2.846
	1.950	221.2	302.3	0.4575	0.05708	-2.863
	2.875	225.3	308.1	0.5550	0.05601	-2.882
	3.800	230.7	315.7	0.6225	0.05466	-2.907
	4.250	232.5	318.2	0.6525	0.05422	-2.915
34.7	0.0	174.7	235.7	0.0	0.05909	-2.829
	1.300	180.9	243.1	0.3090	0.05729	-2.860
	2.150	183.5	247.9	0.4286	0.05617	-2.879
	2.975	189.0	252.5	0.5126	0.05512	-2.898
	3.025	186.6	252.8	0.5169	0.05506	-2.899
	3.825	189.0	257.4	0.5781	0.05409	-2.917

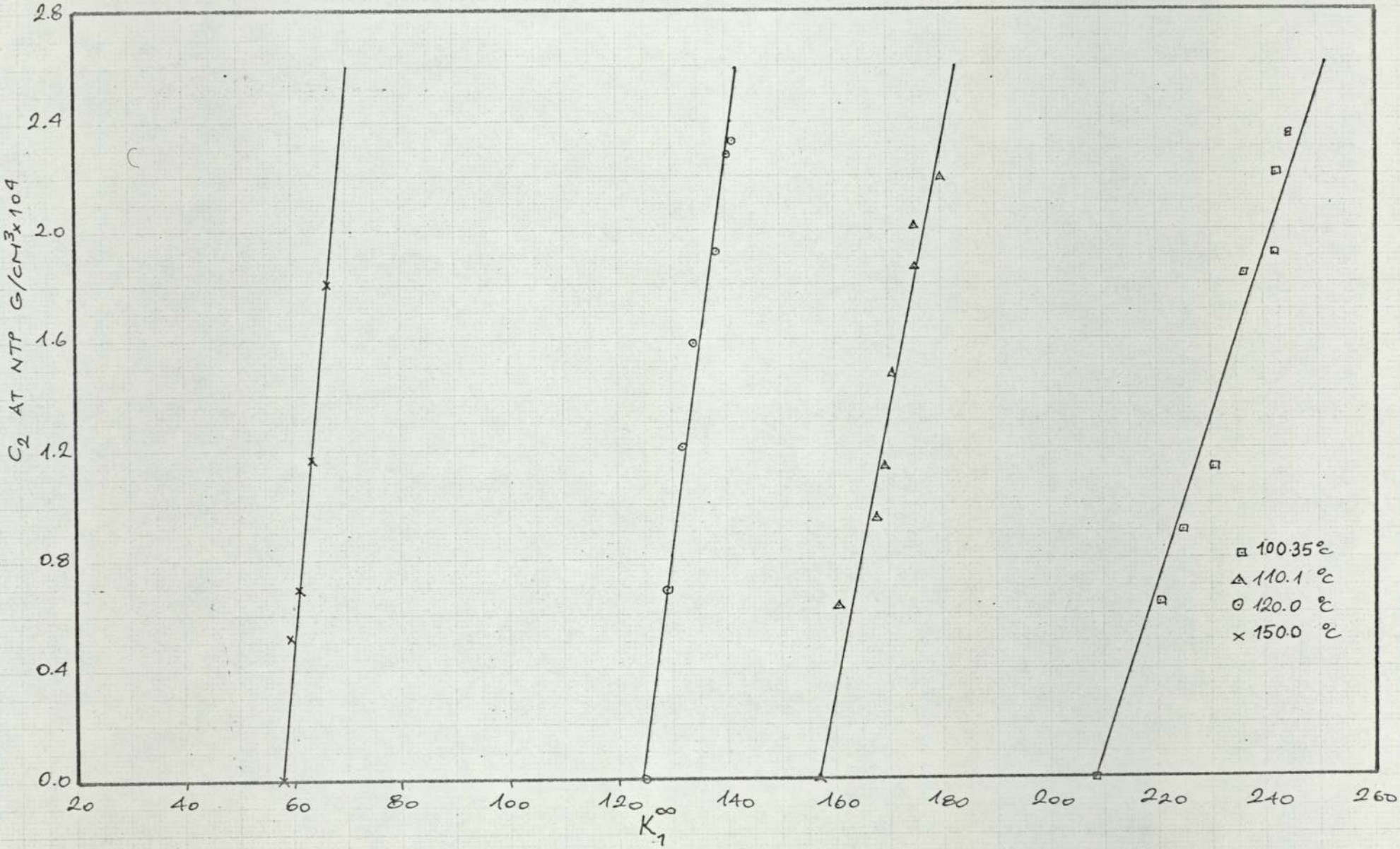

FIG. 7.1.1 - INFINITE DILUTION PARTITION COEFFICIENT OF α-PINENE IN PRESENCE OF β-PINENE

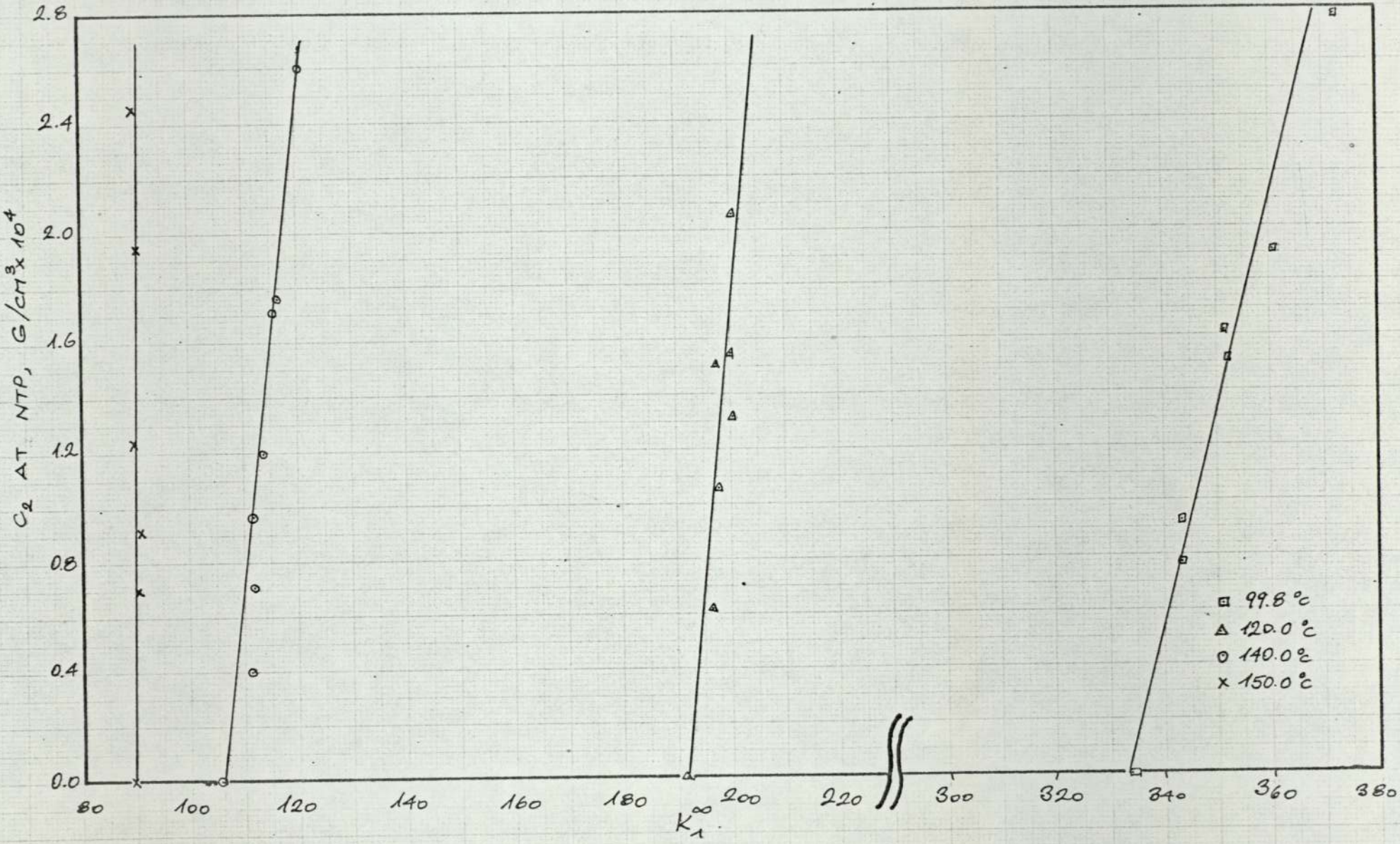

FIG. 7.1.2 - INFINITE DILUTION PARTITION COEFFICIENT of β-PINENE IN PRESENCE OF α-PINENE

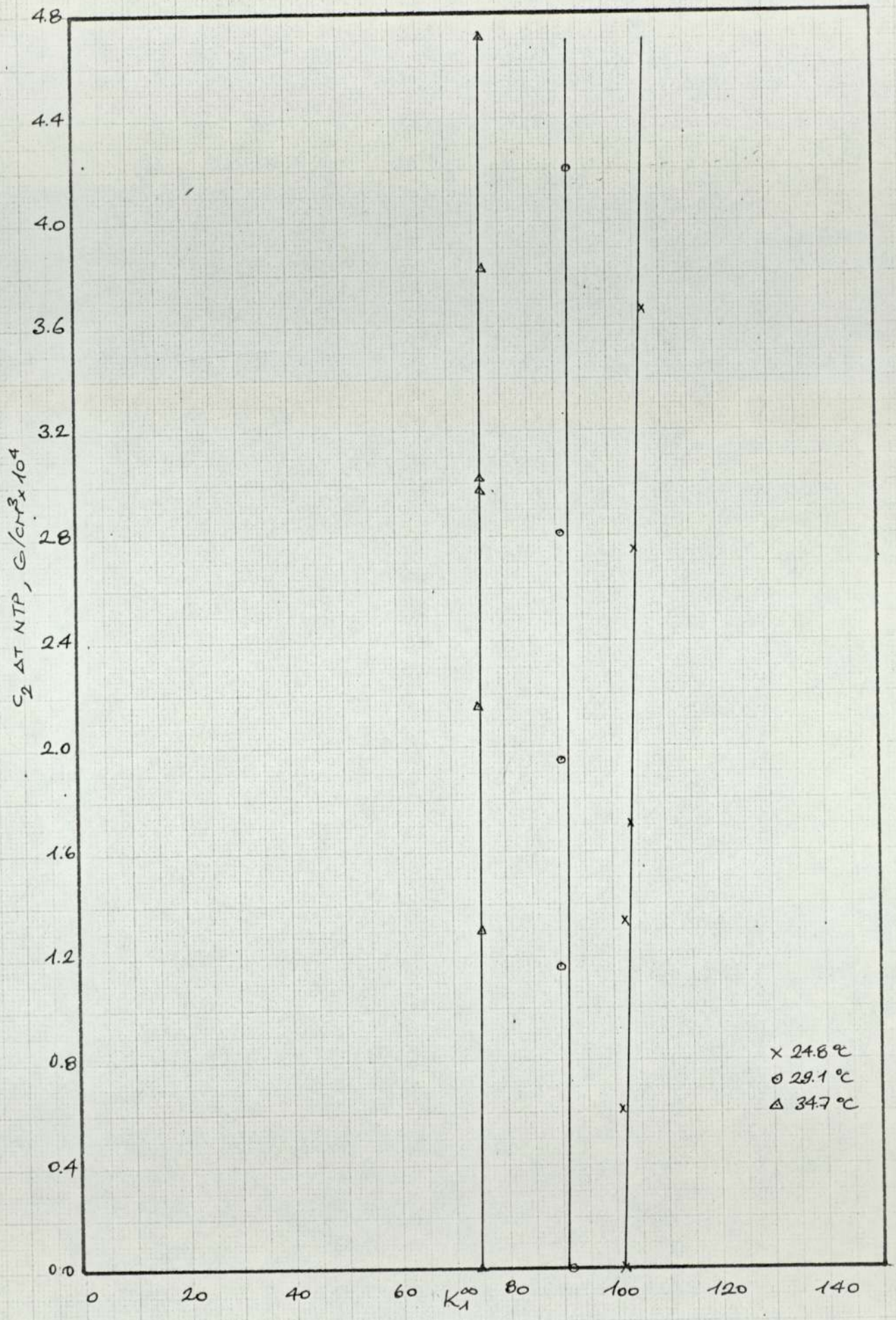

FIG. 7.1.3 INFINITE DILUTION PARTITION COEFFICIENT OF DICHLOROMETHANE IN PRESENCE OF ARKLONE-P

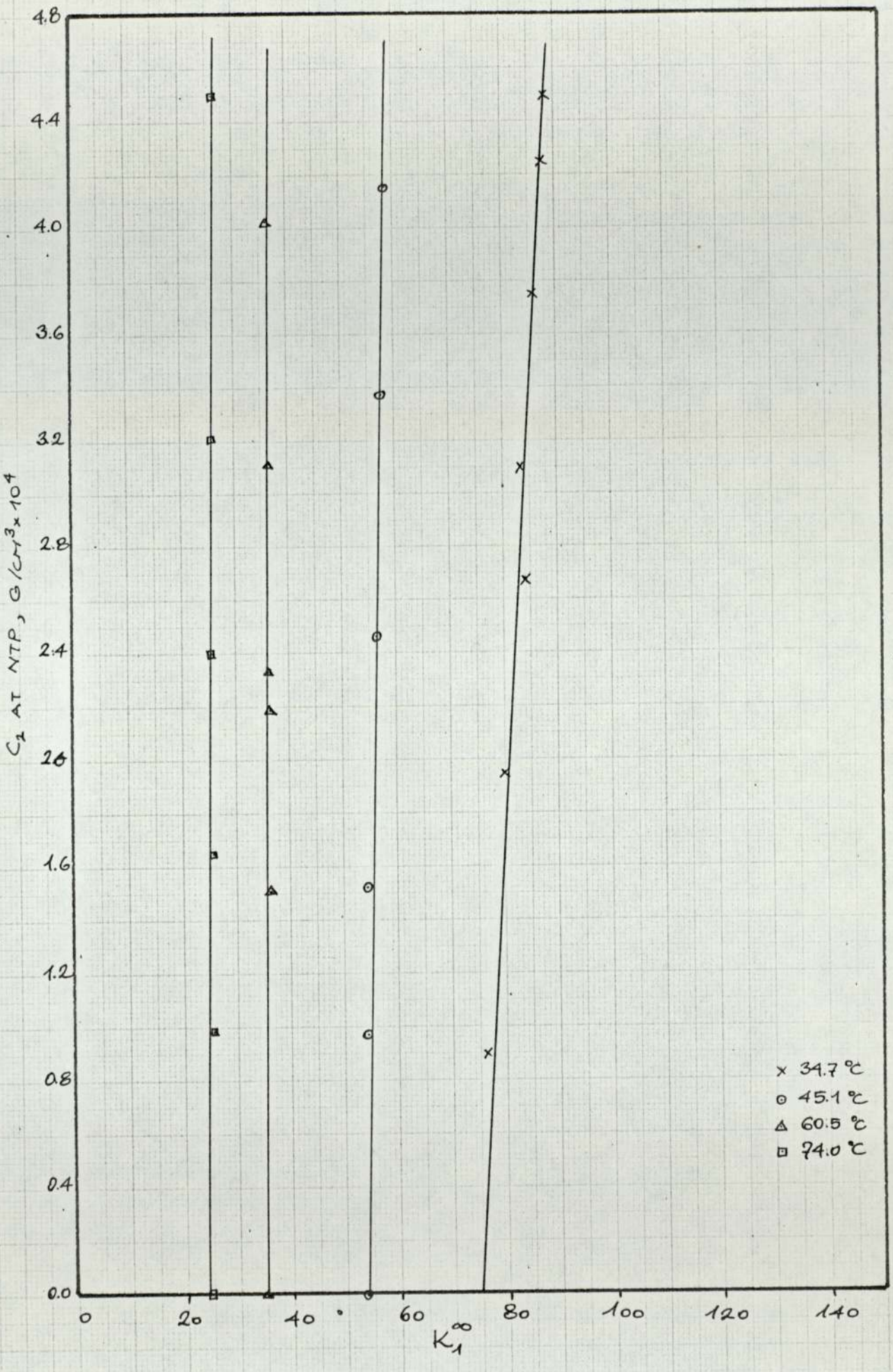

FIG. 7.1.4 . INFINITE DILUTION PARTITION COEFFICIENT OF DICHLOROMETHANE IN PRESENCE OF GENKLENE - P

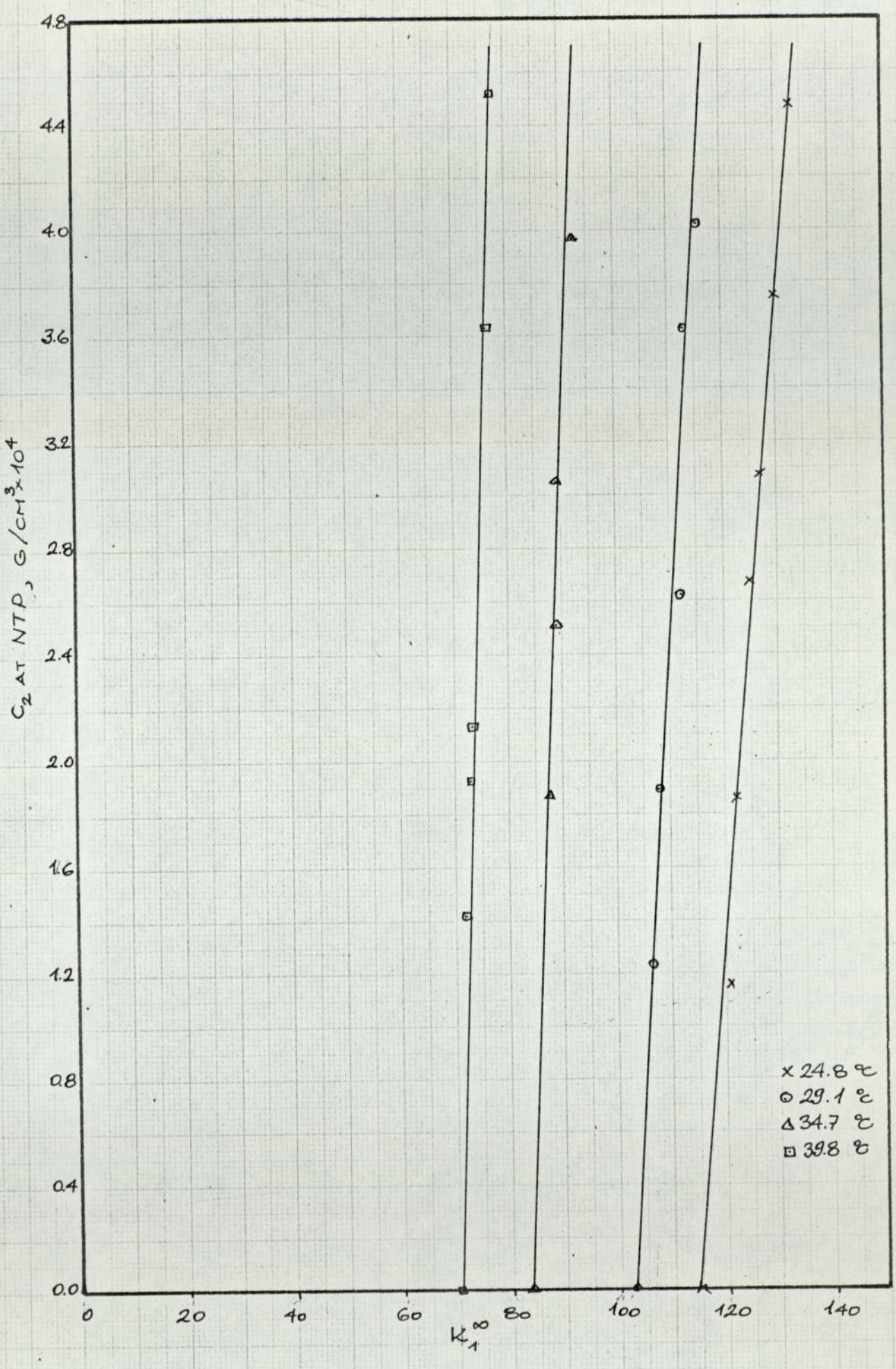

FIG. 7.1.5 - INFINITE DILUTION PARTITION COEFFICIENT OF ARKLONE-P IN PRESENCE OF DICHLOREMETHANE

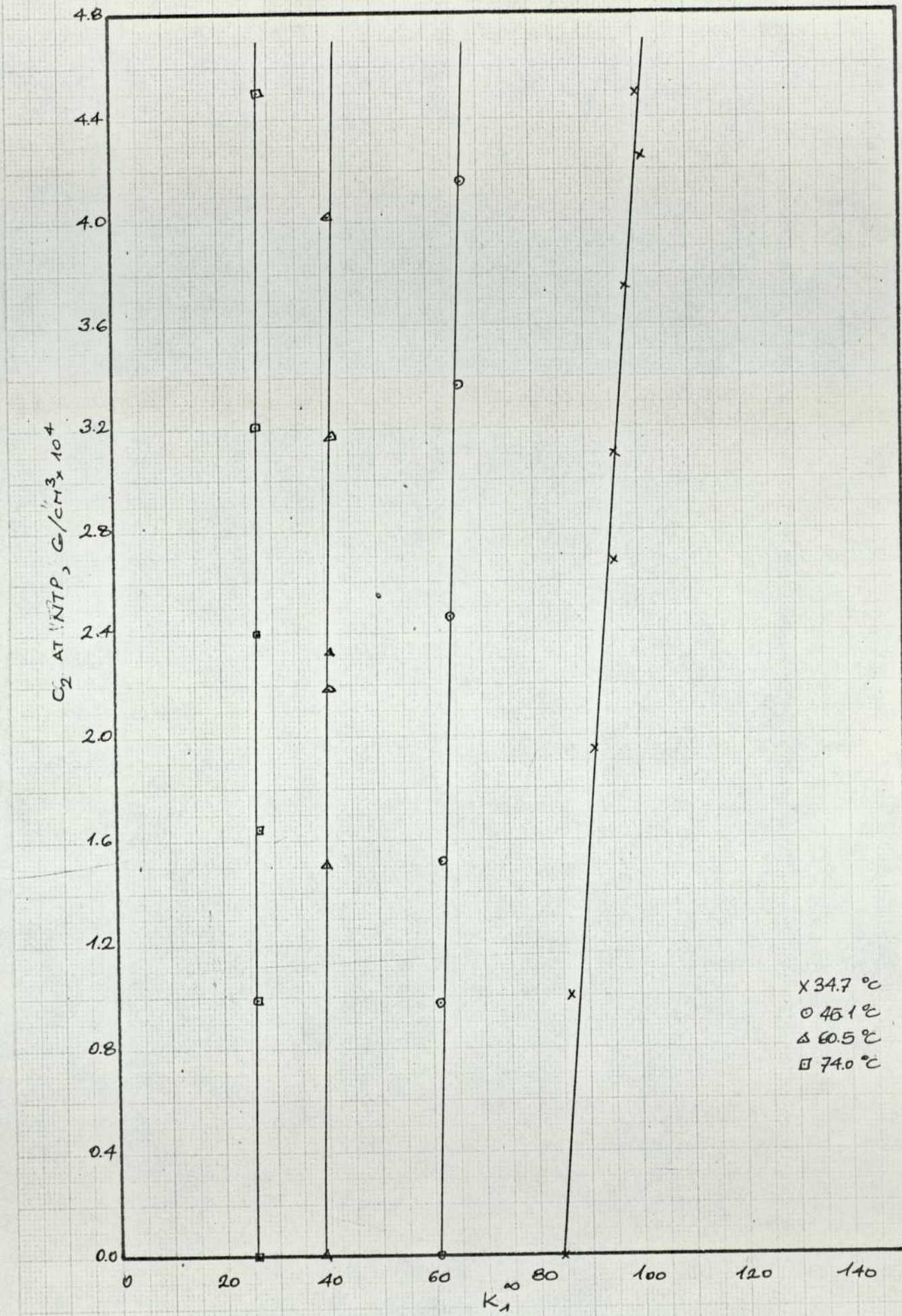

FIG. 7.1.6 INFINITE DILUTION PARTITION COEFFICIENT OF ARKLONE-P IN PRESENCE OF BENKLENE-P

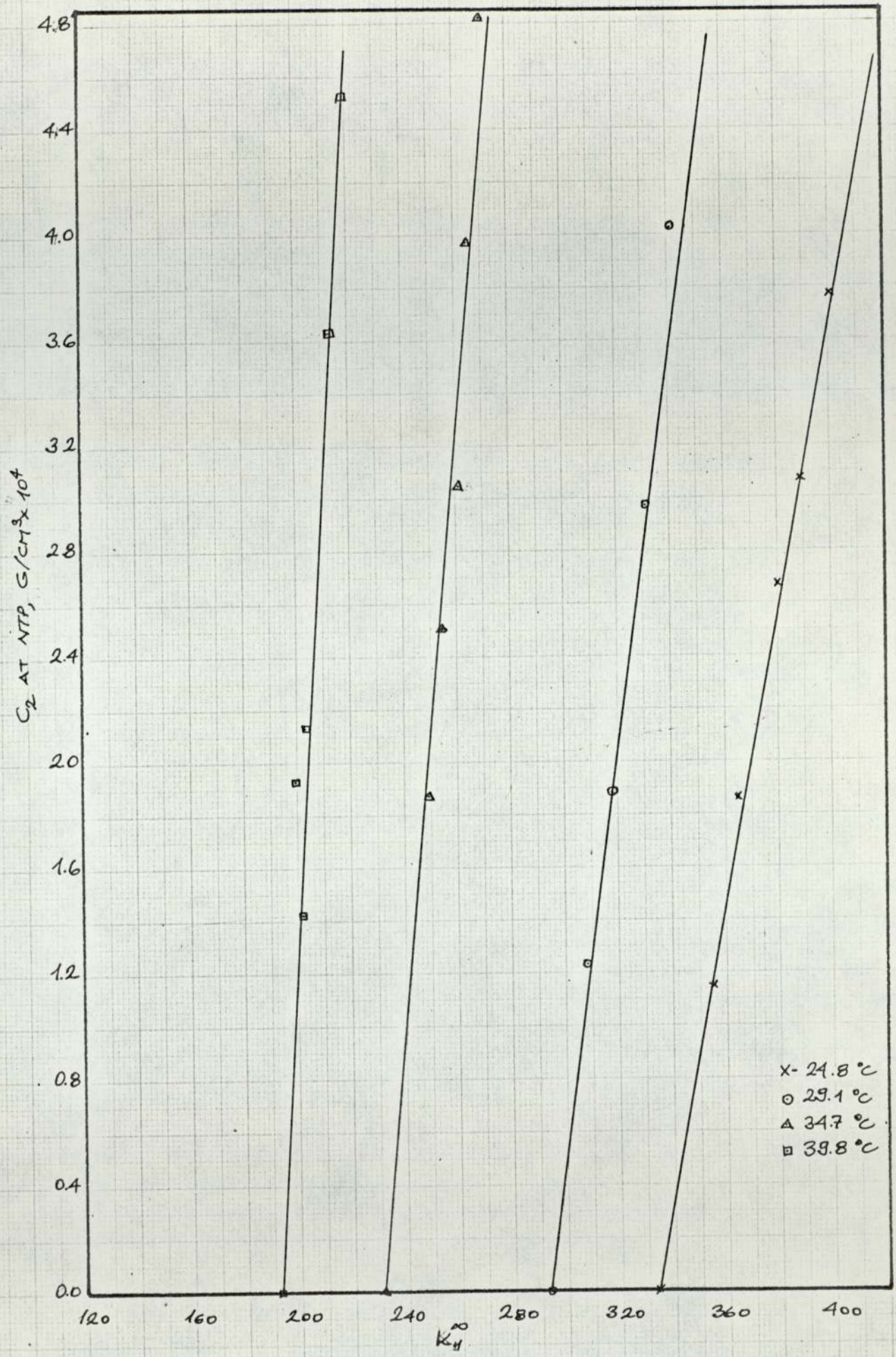

FIG. 7.1.7 – INFINITE DILUTION PARTITION COEFFICIENT of BENKLENE-P IN PRESENCE of DICHLOROMETHANE

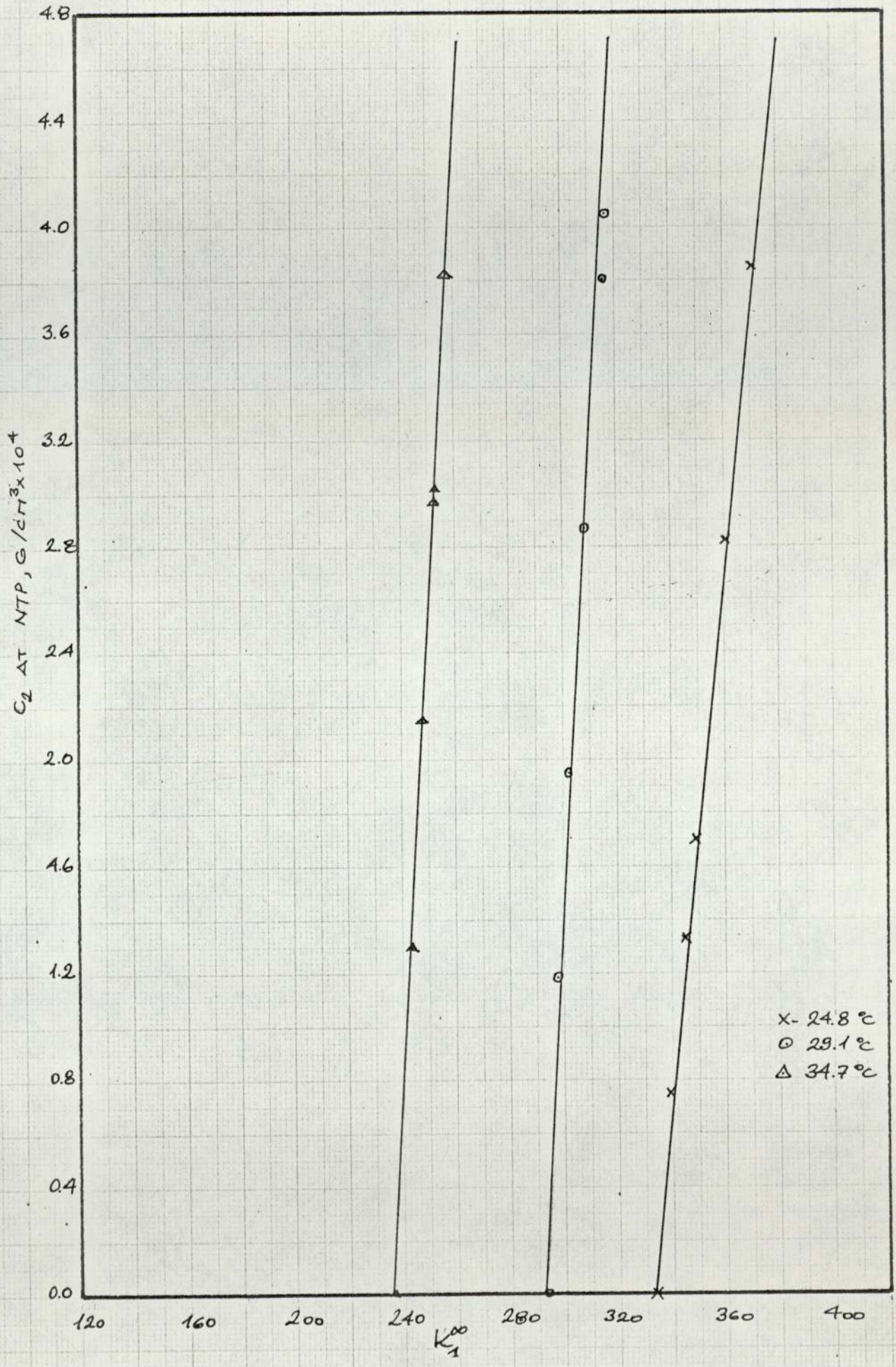

FIG. 7.1.8 INFINITE DILUTION PARTITION COEFFICIENT OF GENKLENE - P : IN PRESENCE OF ARKLONE - P

present at infinite dilution condition, $y_1 \rightarrow o$, the substitutions of equations (3.3.9) and (3.3.13) into equation (3.3.15) give

$$\ln \gamma_1^{\infty}(o) = \ln \frac{RTn}{P_1^{o} K_1^{\infty} V_L} + \frac{P_o J_4^{3}}{RT}\left[2y_{o2}J_4^{3}B_{12} + 2(1-y_{o2}J_4^{3})B_{13} - \bar{V}_1^{\infty}\right] - \frac{P_1^{o}}{RT}(B_{11} V_1^{o}) \qquad (7.2.1)$$

The subscript 2 refers to the solute at finite concentration and 3 to the carrier gas (nitrogen).

The non-logarithmic terms in the above equation are corrections for the non-ideality of the vapour mixture. Preliminary calculations showed that the contributions of these correction terms is less than 0.5% which is well within the experimental precision. Also taking into account the uncertainty in the value of P_1^{o} for the reasons explained below, it was decided to ignore these correction terms for the halocarbons also and calculate the activity coefficient from the logarithmic term only.

Equation (6.2.3) used to calculate the vapour pressures is only valid up to the normal boiling point temperature of a particular solute. Therefore, the calculated activity coefficients in cases where the temperature is above the boiling point temperature of the solute under consideration must be highly suspect. Fortunately this applies to only some activity coefficients of dichloromethane and Arklone-P in the presence of Genklene-P. The results are tabulated in Tables 7.1.1 to 7.1.8 and plotted on Figs. 7.2.1 to 7.2.8.

7.3 Application of the Flory-Huggins Equation.

For a component at infinite dilution, the ternary Flory-Huggins equation (equation 3.4.19) assumes the following form in terms of mole fractions,

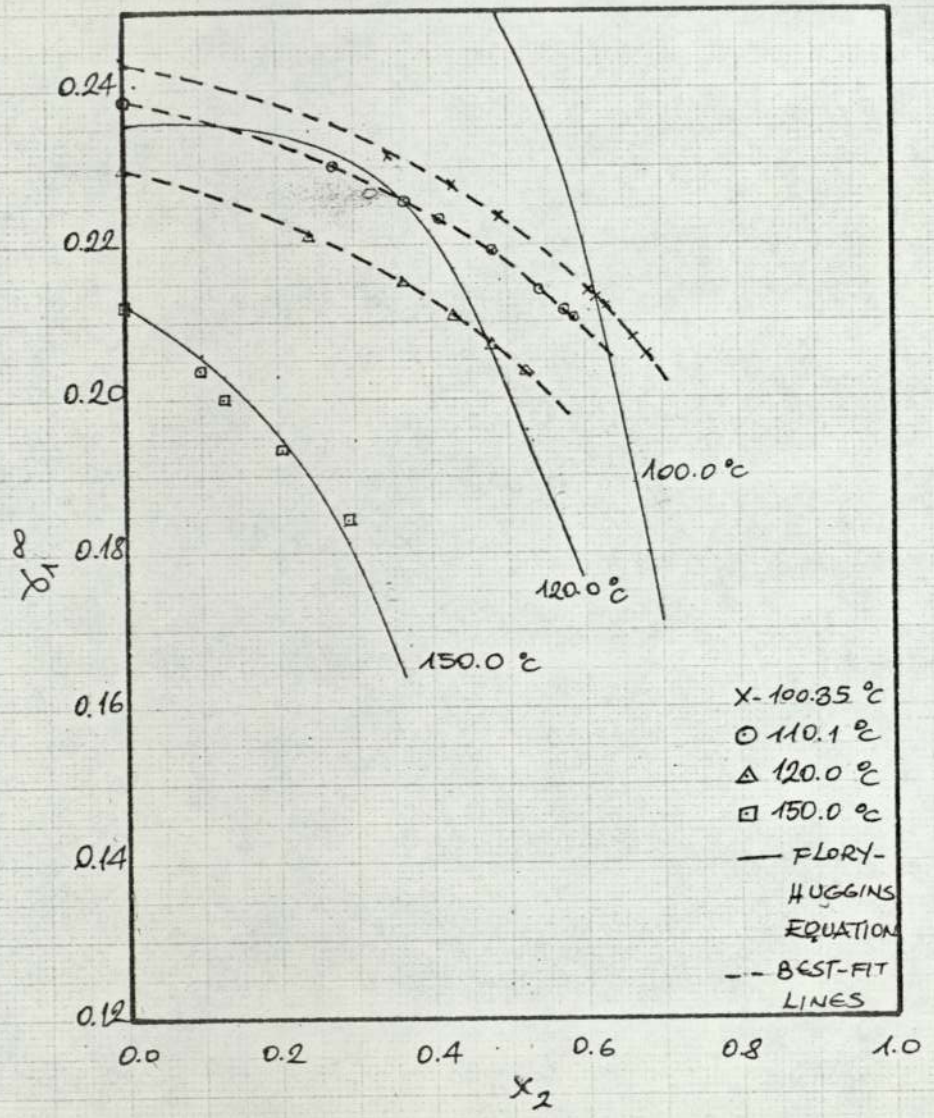

FIG.7.2.1. INFINITE DILUTION ACTIVITY COEFFICIENT OF α-PINENE IN PRESENCE OF β-PINENE

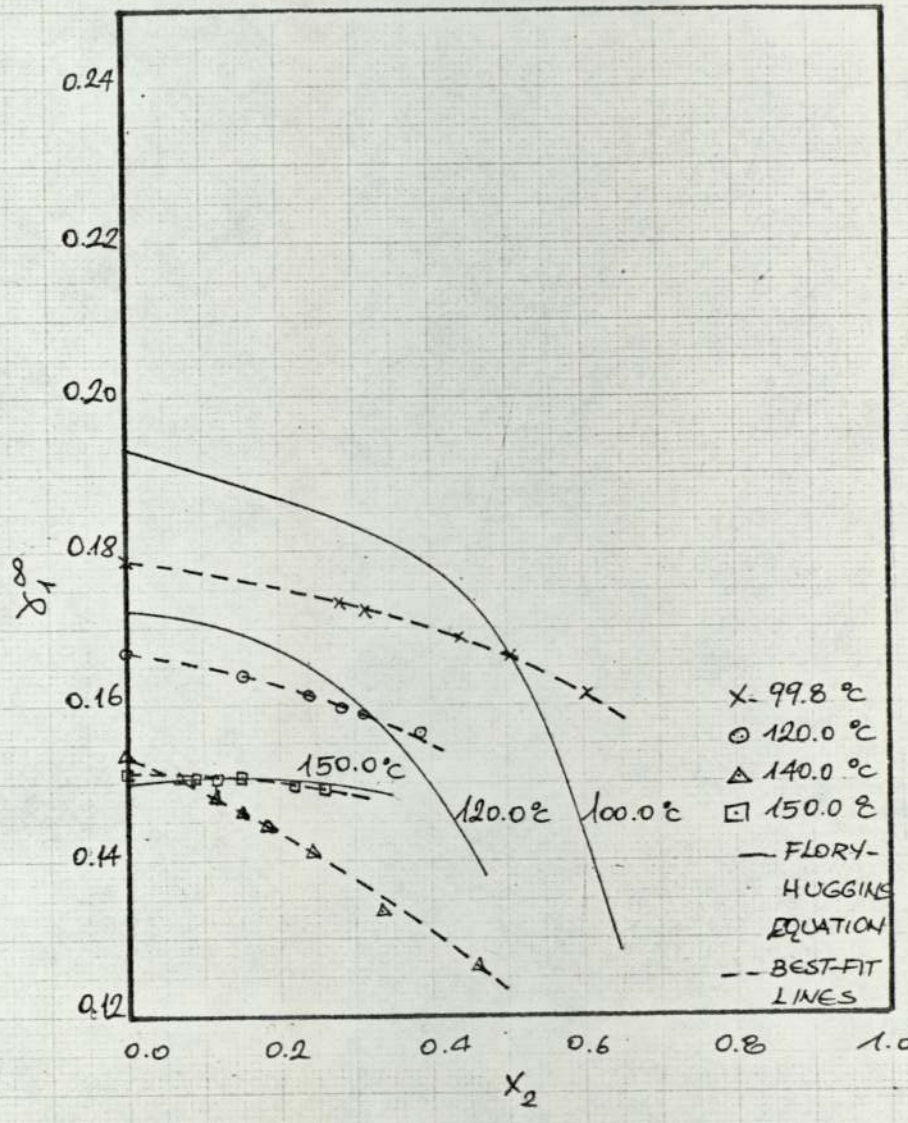

FIG.7.2.2 INFINITE DILUTION ACTIVITY COEFFICIENT OF β-PINENE IN PRESENCE OF α-PINENE

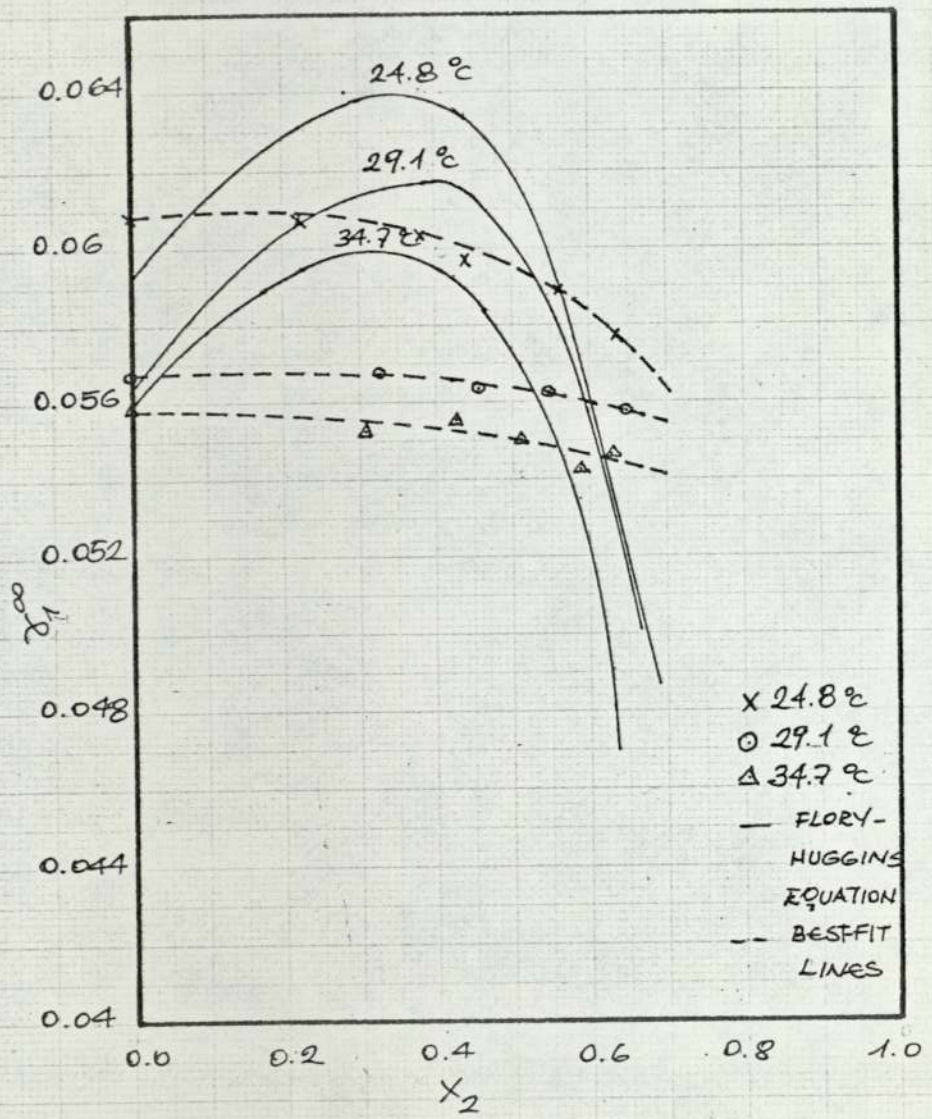

FIG. 7.2.3 INFINITE DILUTION ACTIVITY COEFFICIENT OF DICHLOROMETHANE IN PRESENCE OF ARKLONE-P

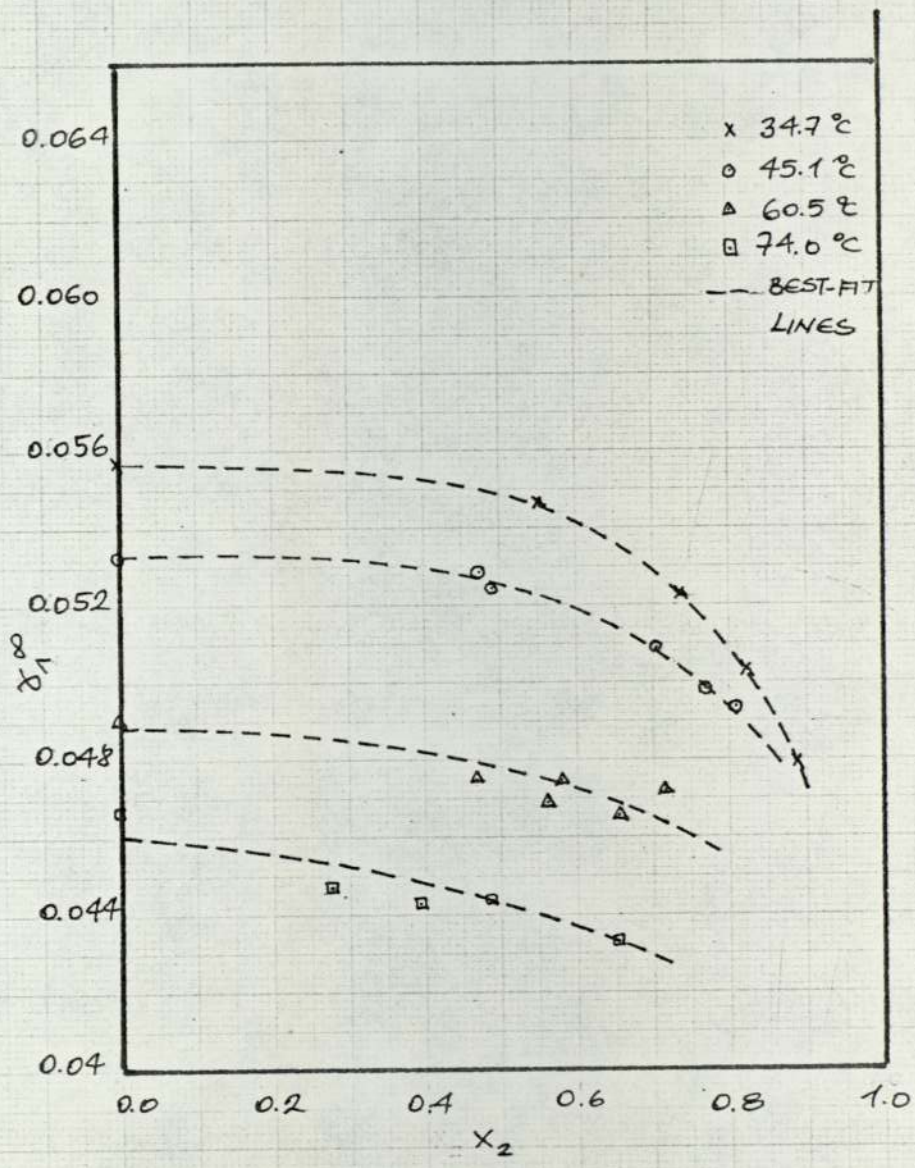

FIG. 7.2.4. INFINITE DILUTION ACTIVITY COEFFICIENT OF DICHLOROMETHANE IN PRESENCE OF GENKLENE-P

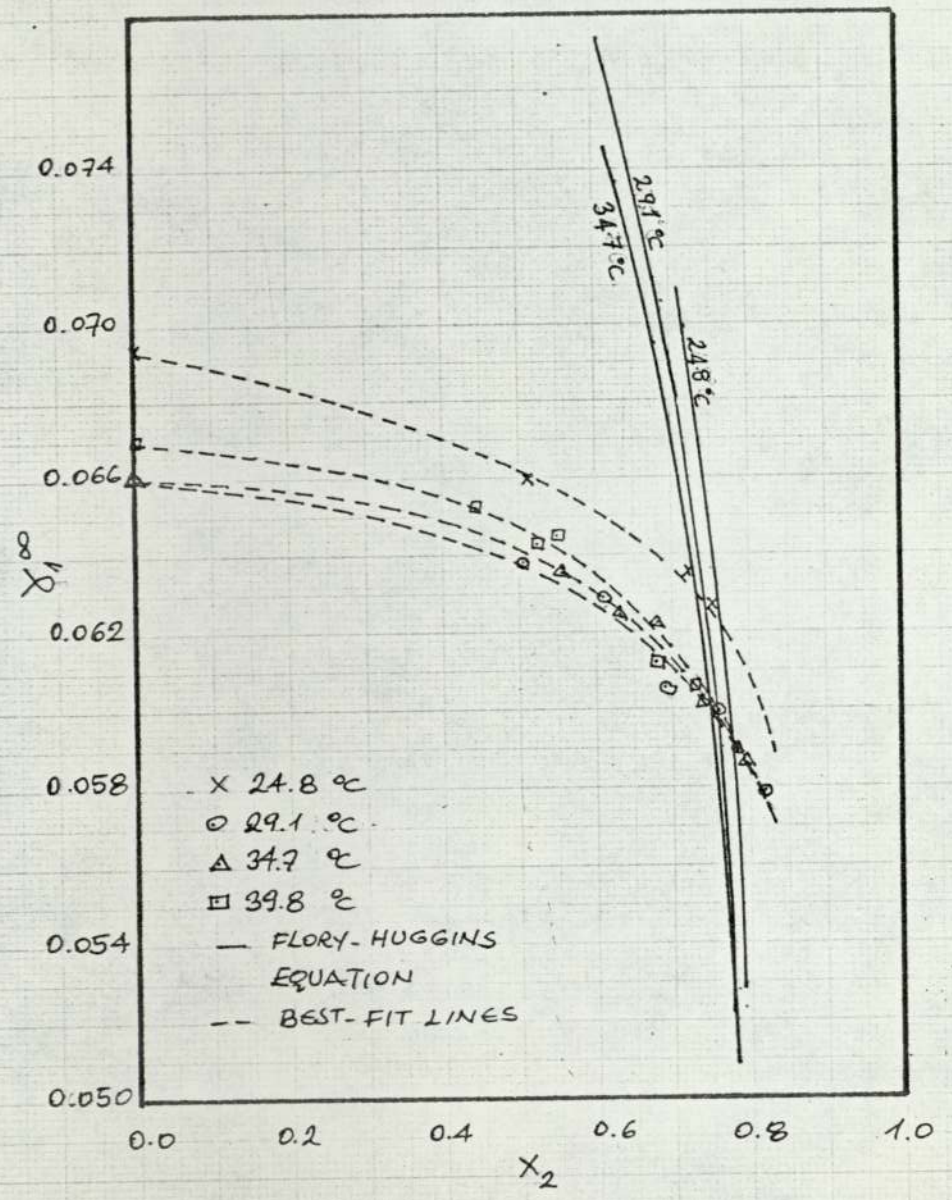

FIG. 7.2.5 INFINITE DILUTION ACTIVITY COEFFICIENT OF ARKLONE-P IN PRESENCE OF DICHLOROMETHANE

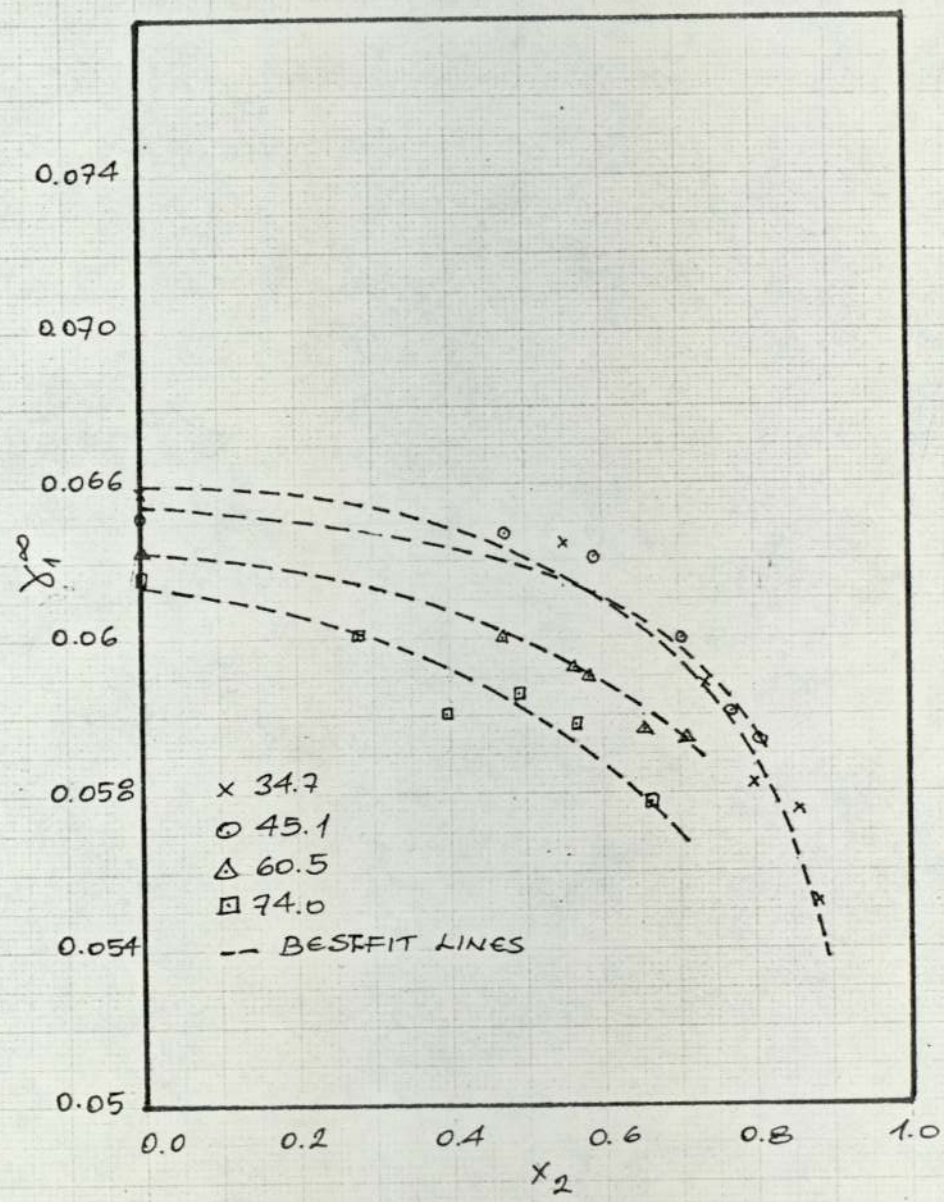

FIG. 7.2.6. INFINITE DILUTION ACTIVITY COEFFICIENT OF ARKLONE-P IN PRESENCE OF GENKLENE-P

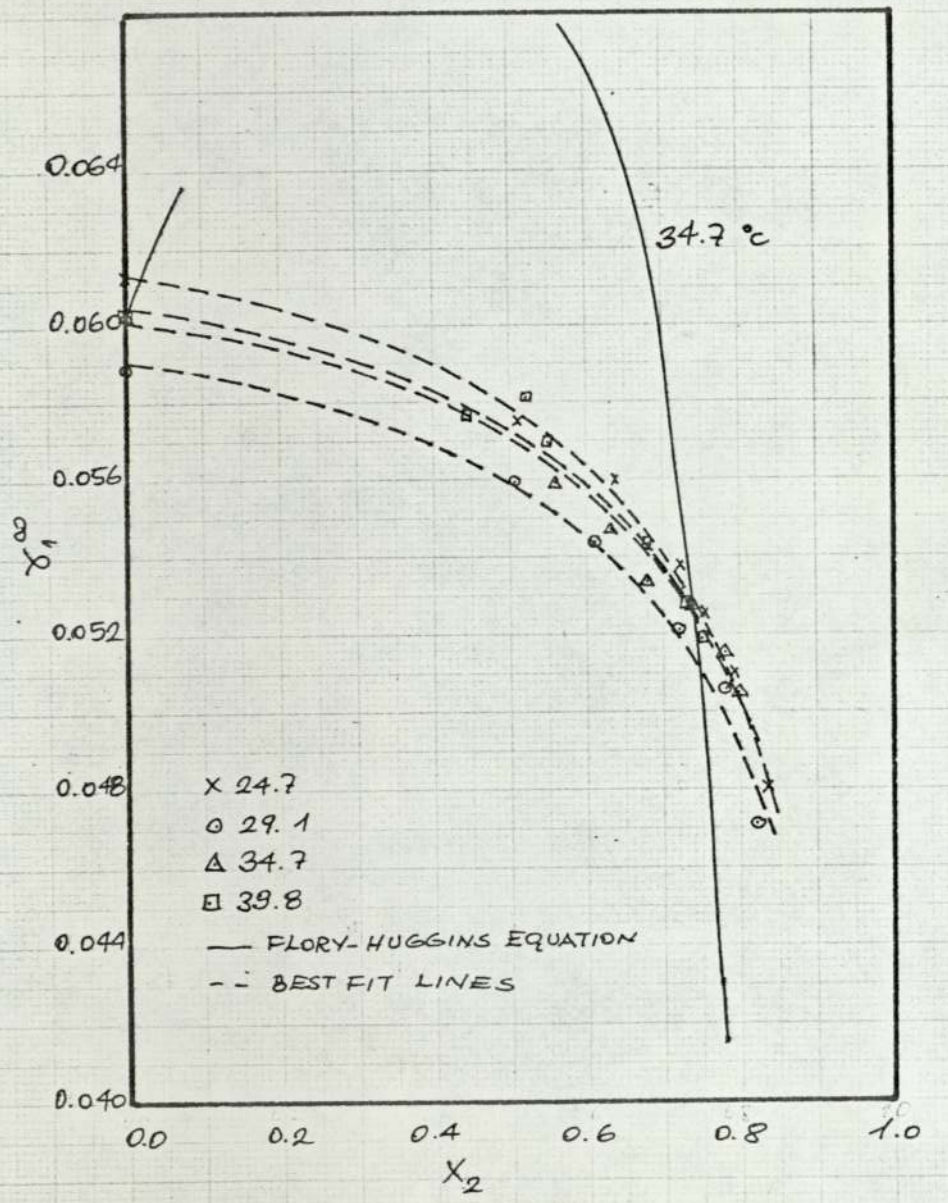

FIG. 7.2.7 INFINITE DILUTION ACTIVITY COEFFICIENT OF GENKLENE-P IN PRESENCE OF DICHLOROMETHANE

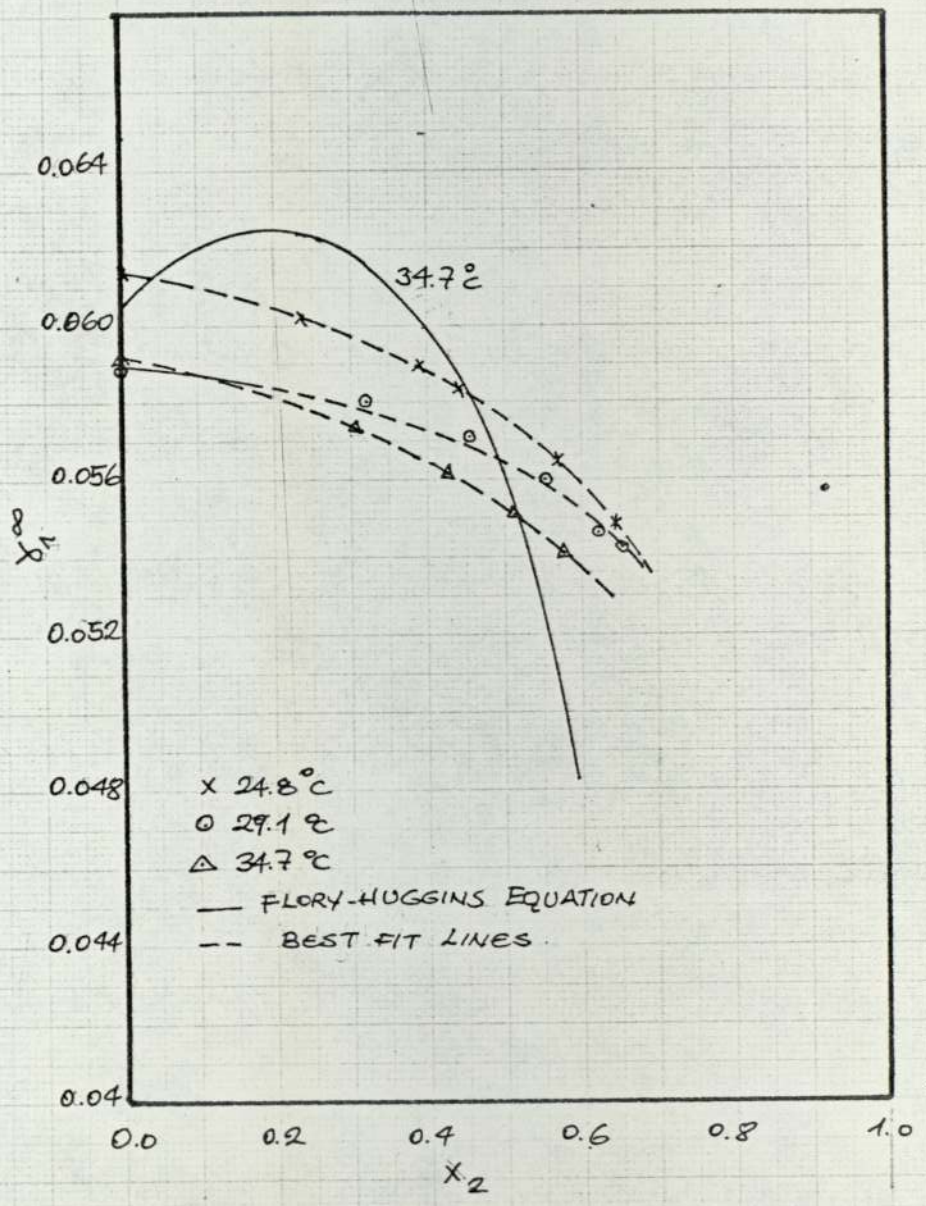

FIG. 7.2.8 - INFINITE DILUTION PARTITION COEFFICIENT OF GENKLENE-P IN PRESENCE OF ARKLONE-P

$$\gamma_1^{\infty} = \frac{\rho_1}{\rho_1 x_2 + x_3} \exp\left[1 - \frac{\rho_1}{\rho_2 x_2 + x_3} - \frac{\chi_{23}\rho_1 x_3 x_2}{(\rho_2 x_2 + x_3)^2} + \frac{\chi_{12}\rho_1 x_2 + \chi_{13} x_3}{(\rho_2 x_2 + x_3)}\right] \quad (7.3.1)$$

Here 2 refers to the component present at finite concentration and 3 to the polymer stationary phase. The parameter χ_{ij} is the interaction parameter of the i-j pair as obtained from binary data. In this work χ_{13} and χ_{23} were obtained from the activity coefficient of a single solute in the stationary phase as explained in the previous chapter. The measurement of the solute-solute interaction parameter χ_{12}, however, was beyond the scope of this work and no data could be found in the literature, making it impossible to check directly the applicability of the above equation to the systems studied. A different and indirect approach was, therefore, employed that involved the estimation of χ_{12} from the ternary activity coefficient data. For this purpose equation (7.3.1) was fitted to the experimental data using the same computer program as in the case of the binary data. It should be pointed out that not all the data could be utilised but only those at the temperatures where both χ_{13} and χ_{23} were available. The calculated values of χ_{12} are tabulated below and the activity coefficients thus calculated are given in Appendix A.9, and are also shown as continuous lines on Figs. 7.2.1 to 7.2.8.

The values of the binary parameters used in the calculations were those calculated from the single-parameter Flory-Huggins equation. For the halocarbons the parameters from the two-parameter Flory-Huggins were also tried but the results were not significantly different from those in Table 7.3.1.

As seen all the results are negative. This is in contradiction with what one would expect from equation (6.3.10) relating the solubility parameters to the interaction parameter. According to this equation χ_{12} should be very small and positive for all the systems studied. Equation (6.3.10) is based on the theory of regular solutions which can only predict

Table 7.3.1. Solute-Solute Interaction Parameter.

Component 1	Component 2	Temperature °C	χ_{12}
α-Pinene	β-Pinene	100	-11.8
		120.0	-13.9
		150.0	-21.5
β-Pinene	α-Pinene	100	-13.6
		120.0	-16.0
		150.0	-14.0
Dichloromethane	Arklone-P	24.8	-69.9
		29.1	-67.0
		34.7	-72.0
Arklone-P	Dichloromethane	24.8	-28.1
		29.1	-27.9
		34.7	-28.7
Dichloromethane	Genklene-P	34.7	-43.8
Genklene-P	Dichloromethane	34.7	-36.8
Arklone-P	Genklene-P	34.7	-23.2
Genklene-P	Arklone-P	34.7	-53.9

positive deviations from Raoult's law (i.e. positive heat of mixing) and is generally applicable to non-polar systems only. In many polar systems negative values of χ_{12} have been observed (61). Although some polar interactions in the halocarbon mixtures might be expected, the structures of the pinenes suggest only very slight polarity. In view of this and the very large negative values found the applicability of equation (7.3.1), which was derived for inert solvents, must be questioned. This observation is also augmented by the poor fits obtained with average deviations of up to 25% in some cases. In fact for the halocarbon systems it predicts very prominent maxima while the experimental data is one of a gradual decrease of the activity coefficient with increase in the liquid mole fraction of the second component.

8. DISCUSSION.

8.1 Measurement of the Retention Volumes and Calculation of the Partition Coefficients.

The finite concentration partition coefficients of five solutes in two stationary phases were calculated from the retention volumes of small samples injected into a chromatographic column which had been equilibriated with a mixture of nitrogen carrier gas and solute prior to the injection. With binary systems the solute in the sample was the same as that in the carrier mixture in which case the partition coefficients were calculated from equation (3.1.7). These systems were α- and β-pinene isomers in polypropylene sebacate and three halocarbons, dichloromethane, Arklone-P and Genklene-P, in Silicone Oil MS 200 (a polydimethyl siloxane). By using a different solute in the sample a ternary system was created where two components, the stationary phase and the solute of the carrier mixture, were present at finite concentration. Since the molecules of the sample were now distinguishable from the solute molecules of the carrier, the partition coefficients were calculated from the simpler equation (3.1.1). As the sample concentration was assumed to be negligible compared with the concentration of the plateau set up, the partition coefficients measured in the ternary system were the infinite dilution values. The upper limit of sample size where this assumption holds were determined by observing the change in the retention volume with increase in sample size.

No effect of the carrier flow rates on the retention volume could be detected. This was expected as the retention volume measurements were carried out on peak maxima and, therefore, the results were free from the kinetic effects such as diffusion or slow mass transfer. The mean column pressures were only slightly above atmospheric and thus well within the theoretical limits of both the equations (3.1.1) and (3.1.7). The only assumption not taken into account in these equations is the possible

presence of solid surface and liquid surface adsorption. However, an investigation of the effect of sample size on elution volumes and peak shapes indicated that these processes did not make any significant contribution to the bulk liquid partition coefficient. Indeed, with very high stationary phase loadings and high solubilities involved it was unlikely that they would do so.

8.2 Calculation of the Activity Coefficients.

The activity coefficients were based on mole fractions in which case the molecular weight of the polymer stationary phase is included in the calculations. Since this is many times larger than the molecular weight of the solute, the calculated activity coefficients have extremely small numerical values indicating strong negative deviations from Raoult's law. Obviously, this is an ambiguous and, from the purely thermodynamic point of view, an unsatisfactory way of determining the ideality of liquid mixtures. The use of volume or weight fractions would give far more meaningful results. However, the choice was based on the consideration of the utilisation of the data in evaluating the performance of large scale chromatographs where the use of mole fractions is an established practice.

The gas phase fugacity corrections were applied only in the case of the binary data for the halocarbons for which the second virial coefficient data was available. In all cases the contribution of the correction to the activity coefficient was 1% or less. As this was less than the estimated accuracy of the experimental technique it was ignored with the ternary data.

8.3 Accuracy and Limitations of the Technique.

The accuracy of the retention volume results are determined by the precision with which the carrier flow rate and the retention times could be measured. The measurement of the carrier flow rate was made difficult by the design of the FID detectors which were not gas-tight. The two methods

used, one with ∝-pinene runs that involved the direct measurement from the column end and the other which depended on the pressure drop across the column, are considered equally accurate to 1-2%, though the former greatly lengthened the duration of the runs. The accuracy of retention time measurements, on the other hand, depended very much on the level of concentration. The reproducibility of repeated injections at infinite dilution was well within 1%, but at higher concentration the peaks became broader and flat topped making it very difficult to locate the peak maximum and the reproducibility was reduced to 3-4% at the upper ends of the concentration ranges. This phenomenon, coupled with the need to keep the sample size small, places a severe limitation on the concentration ranges that can be investigated with this technique.

Another practical difficulty experienced was condensation and absorption on the septum, both of which were particularly accute at high gas concentrations. The former was eliminated by heating the septum holder at the expense of reducing the septum life, but the latter was never completely eliminated as the various materials tested were found to swell considerably in all the five solutes. Keeping solute concentration of the carrier mixture constant also presented a problem. The saturator system used with ∝-pinene was better in this respect but somewhat limited the maximum attainable concentration, and also caused fractionation. On the other hand, the constancy of the concentration obtained from the capillary pump system, that was used with other solvents, was found to be very sensitive to the design and the temperature of the vaporisation section requiring lengthy and tedious adjustments to get the right combination.

In the calculation of the activity coefficient from the retention volume measurements two other parameters are involved, apart from the stationary phase molecular weight which needs to be quoted with such activity coefficient data. One of them is the gas phase concentration.

With the present apparatus it was impossible to check independently its accuracy. Although it was infeasible to separate the fluctuation in the gas phase concentration from the reproducibility of the gas sampling valve,an overall reproducibility of about 2% obtained throughout this work can be regarded as a good indication of the accuracy of these measurements. The other parameter involved is the vapour pressure of the solute. Although such data was available for all the five solutes, the source was not known to enable an estimate of their accuracy to be made, but the discrepancy found between the values of the heat of vaporisation quoted in Ref. 122 and the values obtained from the vapour pressure data of Ref. 113 gives some idea of the uncertainty involved (Table 6.2.1). The difference is the largest for Genklene-P, 460.4 cal/g-mole. Although the effect of such a discrepancy on the vapour pressure and consequently on the activity coefficient is small, about 1% at 45.1°C, it renders the heats of mixing calculated from equation (6.5.4), 311.8 cal/g-mole for Genklene-P, highly unreliable.

8.4 Application of the Thermodynamic Equations.

The aim of any thermodynamic equation is to enable the vapour-liquid equilibrium data to be calculated either from other, more readily available, physical properties or from the data at some other conditions. Of the two equations, the Flory-Huggins and the Heil, applied to the present systems the former looked more promising, particularly from the GLC point of view.

The finite concentration runs in this work took, on average, two to four hours depending on the concentration which is comparable to the conventional still methods. Therefore, the real advantage of GLC lies in the infinite dilution measurements where the runs could indeed be conducted very rapidly. Therefore, the choice of a thermodynamic equation must be based on its ability to predict the activity coefficient at other

concentrations from its infinite dilution value. However, when one of the compounds is non-volatile as is usual in GLC, only the activity coefficient of the solute can be measured. Therefore, a one parameter equation would be far more useful than a multi-parameter one. Both the two parameter Flory-Huggins and the Heil (applied to the halocarbons only) described the data equally well, but the one parameter version of the former was only slightly less accurate. Although, interaction parameter χ_{12}, of the Flory-Huggins equation is concentration dependent, more so in the pinene/polypropylene sebacate systems than the halocarbon/Silicone Oil systems, a value of χ_{12} calculated from an infinite dilution measurement would give a reasonable description of the data, particularly for the latter system. Of course, a value obtained at mid concentration range would give even more accurate results.

The attempt to estimate the parameters in both equations from other physical properties was unsuccessful. In the case of the Flory-Huggins equation it seems that there is a large entropic contribution to χ_{12}. In any case it is doubtful whether even the enthalpic contribution to χ_{12} can be described adequately in terms of the regular solution theory which does not take into account any specific interactions between the unlike molecules that may be present in the mixture. With the Heil equation no physical significance could be attached to the two parameters. In fact, it was shown that a unique pair could not be obtained by a least square fit of the data. More meaningful results can be obtained by evaluating the parameters over small concentration ranges, but at present it can only be regarded as an empirical equation that fits the data.

The application of the ternary Flory-Huggins equation was not successful. The fit was poor and the values of the solute-solute interaction parameter obtained by a least square fit of the data were unreasonable.

The sensitivity of the equation to this parameter must be investigated before anything definite can be established about its true value, but in any case it should really be evaluated from the binary mixtures of the solutes.

9. CONCLUSIONS AND RECOMMENDATIONS FOR FUTURE WORK.

9.1 Conclusions.

A commercial chromatograph was successfully modified to measure the partition coefficients at finite concentrations by the technique of "Elution on a Plateau". With all the five solutes they were found to increase in the presence of both themselves and the other solutes as was suspected from the operation of the large scale chromatographs using the same systems. In each case the increase was linear with the gas phase concentration to the solute.

The binary activity coefficient data obtained from the corresponding partition coefficient data were correlated by the one-parameter Flory-Huggins, two parameter Flory-Huggins and the Heil equations. For the last two equations the fit to the data was equally well with the root mean square deviations of the calculated values from the experimental values ranging from 0.0001 to 0.0070 (0.08% and 3.0% at infinite dilution) for the pinene - PPS systems and 0.00006 to 0.002 (0.2% and 4.0% at infinite dilution) for the halocarbon - silicone oil systems. With the first equation the fit was slightly worse, but it is recommended for chromatographic work by virtue of its having only one parameter which can be determined from a single measurement at infinite dilution. This preference is also influenced by the fact that the accuracy of the measurements deteriorates at high concentrations while the reverse is true for the conventional still techniques. No adequate physical interpretation could be given to the parameters of the above equations. This was particularly true for the two parameters of the Heil equation where it was; shown that it is impossible to arrive at a unique pair of values.

The attempt to correlate the ternary data by the ternary Flory-Huggins equation was unsuccessful. The fit was poor and the calculated values of the solute-solute interaction parameters were unreasonable.

Although the EP technique is, apart from the use of isotopes, intrinsicly the most accurate chromatographic technique, because of the

loss of accuracy at high concentrations, it is felt that GLC should be regarded as complementary to the still rather than a replacement.

9.2 Recommendations for Future Work.

It would be interesting to compare the ternary data obtained in this work with the data predicted solely from binary data. The solute-solute data could be obtained either chromatographically or from the conventional equilibrium still.

The prediction of polymer solution behaviour is already very difficult without the added complication of a considerable molecular weight distribution encountered in this work. More insight could be gained into the applicability of various solution theories if narrow cut polymers were employed.

PART 2

CONTINUOUS COUNTER-CURRENT CHROMATOGRAPHY

10. LITERATURE SURVEY

The powerful separating ability of analytical GLC has encouraged considerable effort in extending this technique to preparative and production scale separations through the use of larger columns. Various schemes have been proposed and tried with the aim of improving the efficiency of these large scale columns. The classification of these schemes proposed here is based on the mode of feed introduction depending on whether it is 1) Batch, 2) Continuous. The earlier work largely concentrated on the batch schemes which are a direct scale-up of analytical columns where a sample of feed mixtures is introduced at one end of the column and the separated components are individually collected from the other end. With the continuous systems, on the other hand, the feed is introduced continuously while the stationary phase is moved relative to the gas phase either continuously or in discreet steps.

In this chapter a brief review of the theoretical background to both schemes is given, accompanied by more recent examples of each.

10.1 Batch Systems.

Most of the effort on batch systems has been directed at finding out the reasons for the relative inefficiency of the large columns when compared with the analytical columns. Such a direct comparison is, however, somewhat misleading as the main emphasis is no longer on just the purity of the products but on the throughput that can be accomplished with a given limit on the impurity level. The most commonly accepted criteria for the efficiency of different scale chromatographic separations are given as

1. Analytical GLC (up to 0.5 cm diameter columns). The accepted criterion here is "Height Equivalent of a Theoretical Plate (h)", which directly determines the degree of separation between two chromatographic peaks.

2. Preparative scale GLC (up to 30 cm diameter columns). In this case the criterion is the throughput of a component per unit time (Q_r).

3. Production scale GLC. The above definition cannot be satisfactory for commercial systems as the throughput can be increased almost indefinitely by increasing the length of the column and thus also increasing the cost. The proposed definition of efficiency is, therefore, the throughput rate divided by the total processing cost per unit time (Q_r/C_t) or (Q_r/h) if the plate height can be assumed to be directly proportional to the total cost.

As will be seen later, each definition contains the one above it as a parameter to be optimised, so in investigating the effect of various operational and geometric variables it is logical to start with the plate height (h).

10.1.1 Height Equivalent of a Theoretical Plate (h).

A big step forward in the field of interpretation of peak dispersion in chromatography was made in 1956 by Van Deemter et al (142) and by Klingberg and Sjenitzer (143). Their work led to the well known 'Van Deemter' equation

$$h = A + B/\bar{u} + C_s\bar{u} + C_m\bar{u} \qquad (10.1.1)$$

The first term accounts for the band broadening due to eddy diffusion. The second term is the contribution of axial molecular diffusion and the third and last terms are related to the mass transfer resistances in the stationary and gas phases. The constants in the above equation are, in fact, functions of other variables such as column diameter (d_c), particle diameter (d_p), $\bar{u}$, the partition coefficient of the component (K), diffusion coefficients in the gas phase and the stationary phase (D_g and D_s respectively), the stationary phase thickness etc. Considering the number

of variables involved and the uncertainties in their measurement, perhaps it is not surprising that numerous experimental and theoretical studies have led to many equations. In a recent study by Bethea and Bentsen (144) nine different models were compared using an eight component nitroparaffin system. A statistical analysis of the results showed that two of the models, 1) Gidding's power series in terms of Peclet number (145,146), and 2) Bethea and Adams' modification (147) of the Van Deemter equation, were superior.

It is known that (148) axial mixing in chromatographic columns under normal conditions is inadequate in compensating for the axial variations in concentration caused by flow irregularities. Various treatments (149-151) have produced one additional term to equation (10.1.1) of the form

$$h_{prep} = \frac{Cd_c^2\bar{u}}{D_g} \qquad (10.1.2)$$

According to this equation, the plate height in large columns should increase with the square of the column diameter. However, this is not necessarily true as C itself may be dependent on the ratio of particle diameter to column diameter (152). As a result the exact relationship between the plate height is still a debatable matter, but it is obvious that enhancing the radial mixing by baffle systems (153) or reducing the path of radial diffusion using an annular column (154) should help to minimise the effects of flow maldistribution. Since non-uniform density distribution is known to be a major contributor to the plate height, care should be taken in packing the columns. Albrecht and Verzele (155), who investigated various packing techniques, recommend a shake-turn-pressure procedure.

On the basis of what already has been said it is obvious that it is impossible at this point in time to ascertain the exact functional

dependence of the plate height on the various parameters. However, certain qualitative conclusions can be drawn.

1. The plate height - velocity profile is of the classical Van Deemter type, but the optimum velocity range is greater than analytical columns (156,157).

2. The stationary phase loading should be as small as possible to reduce the mass transfer resistance in that phase.

3. Particle diameter should be as small as possible with the pressure drop being the limiting factor.

4. The effect of column diameter is, as indicated earlier, uncertain, with different packing techniques employed by different workers is thought to be the main cause of the discrepancies. However, it can be safely said that the plate height will increase with increasing diameter.

It should also be pointed out that the above expressions for plate height exclude the contributions from a non-plug sample injection. For best results Albrecht and Verzele (156) recommend an injection system composed of a long narrow tube placed before the column.

10.1.2 Preparative Column Efficiency (Q_r).

Since the throughput rate is the main concern here it is obvious that various conflicting influences need to be optimised. With the necessary addition of extra variables (feed volume, feed concentration, the number of injections per unit time, the point of cut on the eluting band etc.), the problem becomes very complex and no complete treatment has yet been given. One expression for the simplified case of a double cut on repeated injections of a mixture containing two equimolar components is given by de Clerk (152)

$$Q_{r1} = \left[\frac{\sqrt{2\pi}\, C_i \epsilon \pi d_c^2 u_i}{96R}\right] \left[1 - \frac{16(1+k_1)^2 R^2 h}{k_1(\alpha-1)L}\right]^{\frac{1}{2}} \left[1 + \text{erf}\sqrt{2R}\right] \quad (10.1.3)$$

where C_i is the inlet concentration

ϵ is the voidage fraction in the column

u_i is the inlet gas velocity

k_1 is the capacity ratio of component 1

L is the column length

α is the relative volatility of the components

R is the resolution defined as $\Delta x/4\sigma$, where Δx is the distance between the peak maxima and σ is total peak variance of the least retarded component at the outlet.

The most surprising conclusion that can be drawn from this equation and others similar to it (158) is that the plate height has little or no effect on the throughput. This is due to the fact that for a given resolution any improvement on the throughput by an increased number of injections per unit time through increased efficiency is almost exactly compensated by a reduction in the feed volume that can be injected.

The velocity $\bar{u}$ appears both explicitly in the first term and implicitly through h. Since the latter has a small overall influence it is obvious that higher values of $\bar{u}$ are required than for analytical columns. While Conder (159) recommends the highest possible velocity, the calculations of Pretorious and de Clerk (160) and of Hupe (161) indicate an optimum. Other parameters like the column diameter, stationary phase loading and inlet volume are also present both explicitly and implicitly (through h), and as such it is difficult to predict accurately their relationship to the throughput. In general, however, it is expected that the throughput will increase with increasing diameter (161) and perhaps reach an optimum at very high values (152). The stationary phase, although it does not have a critical influence, is also

likely to have an optimum. The numerical calculations of Conder (159) indicate an optimum feed volume which is far larger than for analytical columns.

10.1.3 Production Scale Chromatography Efficiency (Q_r/C_t).

To derive the functional dependence of this efficiency on the parameters discussed above, the total cost must also be expressed in terms of the same parameters. The cost data for production scale chromatography is yet very scarce and the two treatments found in the literature (159,161) both rely on the experimental data of Ryan and co-workers for an α/β -pinene separation on a 4 in. column (162,163). Since the column length is closely related to the overall cost it is now a parameter to be optimised. However, the inlet feed band width, resolution and the column length are all dependent on each other, given two the third is automatically fixed. The usual design philosophy is to adopt the first two parameters as independent and the column length as a dependent variable. The efficiency is maximised with regards to the other parameters and then the length required is evaluated. When this is done, Conder (159) found that the variation of Q_r/C_t was very much like that of Q_r on its own. He also found an optimum temperature at about the boiling point of the solute both for Q_r and Q_r/C_t. This finding is also confirmed by the experimental results of Craven (157) with the same system on a similar column.

It should be noted that all the treatments reviewed above are based on the assumption of a linear partition isotherm. Conder (19) attempts to take into account non-linearity by a correction factor which needs to be evaluated for each system from the experimental data.

10.1.4 Recent Work on Preparative and Production Scale Batch Chromatography.

Ryan (164) reported a design study for a GC plant capable

of separating 50 million Kg/yr of a p-xylene - m-xylene mixture with 99% pure products. The design was based on two 14 ft dia., 14 ft long columns operating with alternate feed injection and on a packing that had a separation factor of 1.3 for the isomers. The total capital cost was estimated to be $1,530,000 and the operating cost was 1.2 ¢ per kilogram of product.

Carel et al (165) described an apparatus capable of holding up to 16 ft of 12 in. columns. No efficiency data has been reported, but its separating power has been compared with smaller diameter columns on the basis of the maximum single-injection sample volume which gave base line separation between a pair of n-hexane and n-heptane peaks. An almost linear relationship was found between the cross sectional area and the maximum sample size.

10.2 Continuous Systems.

As mentioned earlier, the word 'continuous' as used here refers to the introduction of the feed and the collection of the products. Although there have been many different approaches towards achieving this continuity, the most comprehensively evaluated scheme is the one where the liquid phase moves in a counter-current fashion to the gas phase. In its most straightforward form, it involves a vertical column in which the gas flows upwards and the coated support moves downwards under its own gravity (166-169). The feed is continuously led somewhere near the middle of the column. The least retarted components move preferentially in the gas phase to the top-off take while the most retarted components are carried down with the liquid phase and are stripped off it in a separate section of the column, either by heat or an increased gas flow rate or a combination of both (Fig. 10.2.1). This scheme is usually termed as "moving bed chromatography".

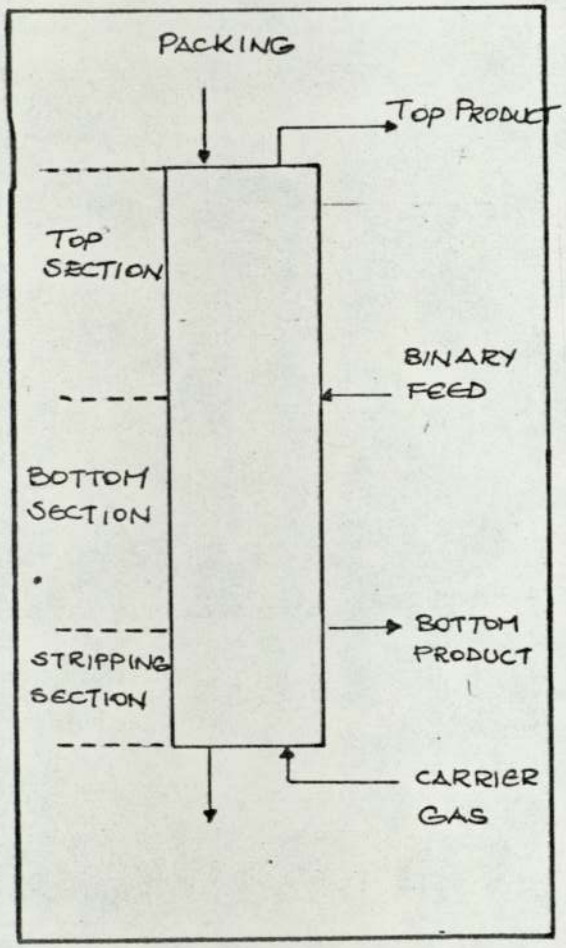

FIG.10.2.1- MOVING BED CHROMATOGRAPHY FOR BINARY SEPARATION

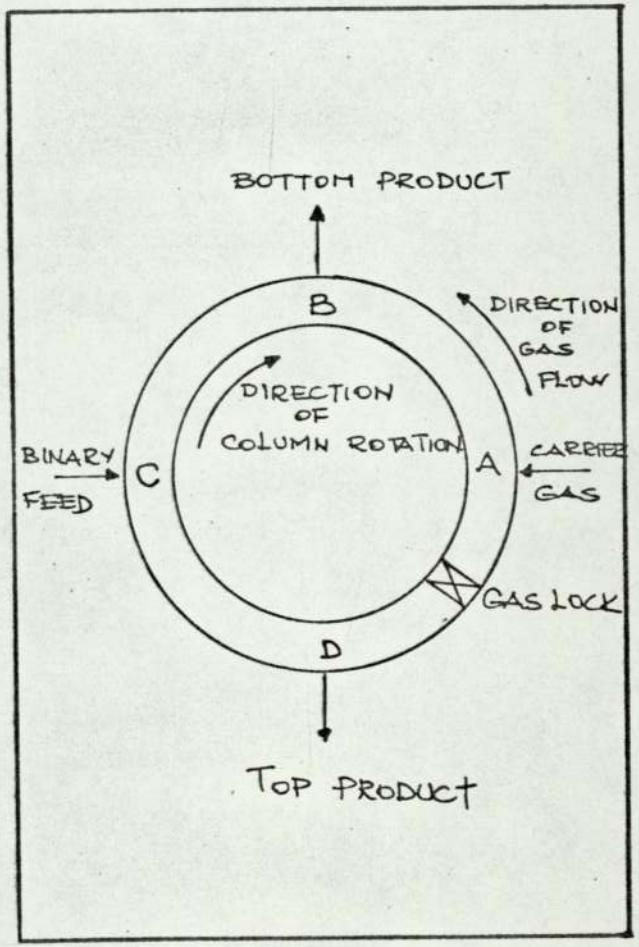

FIG. 10.2.2_ ROTATING CHROMATOGRAPHY FOR BINARY SEPARATION

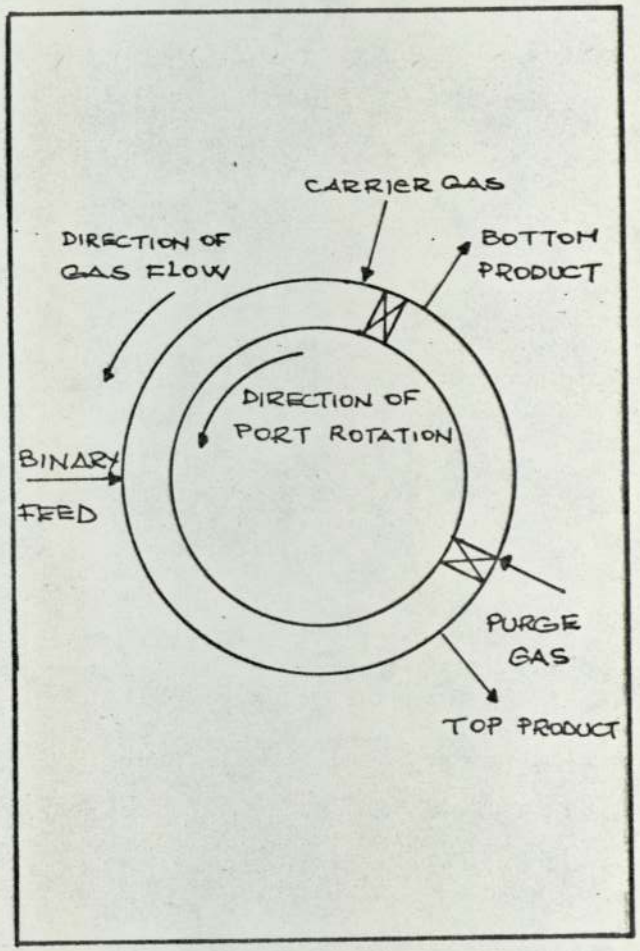

FIG.10.2.3. SQUENTIEL CHROTTATOGRAPHY FOR BINARY SEPARATION

The more sophisticated chromatographs of Barker and co-workers (170, 171), including the device used in this work, are an extension of the above idea whereby the two ends of the column are joined to form a closed loop. The packing is now held stationary in the column which is rotated in the opposite direction to the gas flow. The principle of operation is shown in Fig. 10.2.2. The gas is introduced through the port marked 'A' and the feed through 'C". As in the moving bed chromatograph, the ratio of gas to liquid flow rate is so adjusted that the component having the strongest affinity for the liquid phase tend to move with the column, and it is then stripped off the liquid phase in the section AB. The less soluble component, on the other hand, continues its progress in the direction of the gas flow and is taken off from the port marked D. A gas lock between the gas inlet and top product port ensures that the gas flow is unidirectional. This scheme overcomes the problem of solid support attrition experienced in the moving bed chromatographs and also facilitates the use of longer columns in a confined space by forming a cylindrical nest of tubes connected alternately at top and bottom as in the present device.

The problem of sealing between the stationary ports and the moving column encountered in practice with the 'Rotating Chromatographs' is avoided in a recent device developed by Barker and Deeble (172). In this device, described in more detail later in this section, the counter-current movement of liquid and gas phase phases is achieved by the rotation of the ports instead of the column.

In all the circular chromatographs an element of discontinuity is introduced into their operations as the packing is exposed to the gas phase in discreet volumes. Barker and Deeble (172) recognising this step-wise operation have called their machine a "Sequential Chromatograph".

Amongst all the different continuous chromatographic systems the

moving bed chromatography is, by virtue of its very continuous nature and its close analogy with other counter-current separation processes, most readily open to theoretical treatment. The various theories in this field are briefly reviewed below while a plate model developed for the circular chromatographs is discussed in detail in Appendix A.10.

10.2.1 Theory of Moving Bed Chromatography.

10.2.1.1 Condition for Separation

If a binary solute mixture of A and B is introduced into a counter-current chromatographic column, the condition for separation can be shown to be (167)

$$K_A < G/L < K_B \qquad (10.2.1)$$

where K_A and K_B are the partition coefficients of less strongly and more strongly absorbed components respectively.

G and L are the volumetric flow rates of the gas and the liquid phases.

If the partition coefficients change with concentration the effect of this will be to shift the whole operating range according to the equation (166)

$$K_A + \beta_A < G/L < K_B + \beta_B \qquad (10.2.2)$$

The effect of a finite column length, i.e. a finite number of theoretical plates is to narrow the operating range

$$K_A + \beta_A + \delta_A < G/L < K_B + \beta_B - \delta_B \qquad (10.2.3)$$

In order to vaporise the component B in the stripping section the necessary condition is

$$K'_B < G_s/L \qquad (10.2.4)$$

where K'_B is the partition coefficient of B in the stripping section and

G_s is the total gas flow rate in the same section.

10.2.1.2 HETP Model.

Using the analogy between liquid-liquid extraction process and moving bed chromatography, Tiley and co-workers (166) derived an expression for the number of equivalent theoretical plates required to separate an equimolar binary mixture, based on the assumptions of equal product purity and a central feed point. Removing these restrictions, Huntington (173) arrived at a more general equation

$$\log \frac{\phi_{max}}{\phi_{min}} = \log \frac{K_B}{K_A} + \frac{2}{N} \left[\log \left(1 - \frac{a}{W_A} \right) + \log \left(\frac{b}{W_B} \right) \right] \qquad (10.2.5)$$

where ϕ_{max}, ϕ_{min} = Operating G/L in the separating section which are the maximum and minimum values to allow products of the required purity to be achieved.

N is the total number of theoretical plates

a and b are the product collection rates of components A and B at the top of the column

W_A, W_B are the feed rates of the components

This equation was used both by Huntington (173) and Al-Madfai (174) to evaluate the overall efficiency of their circular chromatographs whenever the operating conditions permitted its application with reasonable accuracy.

The major weakness of the above treatment is the assumption of a constant partition coefficient throughout the column which is hardly ever true in practice. Tiley (175), recognising this fact, developed a plate to plate calculation using a digital computer, based on eliminating mismatch in liquid composition at the feed stage. The results were also compared with the available short cut methods (176) which were often taken as the starting point for the more rigorous analysis. The calculations showed that the limiting value of feed to solvent ratio was

dependent on temperature and that there existed an optimum operating temperature which was explained by the dependence of the stripping factors (G/KL) on temperature. An approximate agreement was obtained between these calculations and the experimental results obtained on a 1.3 m x 25 mm column for the separation of a binary volatile mixture on dinonyl pthalate (177).

Another interesting feature of the computer calculations was the prediction of a possible pinch point in the column as a result of changing partition coefficient with concentration. This, in fact, was experimentally observed by Huntington (173) in the separation of a benzene-cyclohexane mixture in a moving bed chromatograph.

10.2.1.3 HTU Model.

The theoretical plate model assumes that the separation process is split into many small compartments, but in fact the chromatographic column is a continuous packed column. It is, therefore, more realistic to express the efficiency in terms of HTU (Height of a Transfer Unit) as originally suggested by Chilton and Colburn (178). The total column length is then given by

$$Z = H_{OG} \; N_{OG} \qquad (10.2.6)$$

where H_{OG} is the height of an overall gas transfer unit (HTU) = $G/K_G a$

and $K_G a$ is the overall gas phase mass transfer coefficient

N_{OG} is the number of overall gas transfer units = $\int_{y_2}^{y_1} dy/(y-y_e)$

and y_e is the gas concentration in equilibrium with the liquid concentration x.

For linear equilibrium and operating lines N_{OG} can be shown to be equal to

$$N_{OG} = \frac{y_1 - y_2}{(y-y_e)_1 - (y-y_e)_2} \ln \frac{(y-y_e)_1}{(y-y_e)_2} \qquad (10.2.7)$$

Starting from the same basic principles as in equation (10.2.6) and together with appropriate boundary conditions, it is possible to derive an equation relating the solute concentration to the distance along the column. For this equation to be used a value for the HTU must be assumed or evaluated from the physical parameters of the materials. In Appendix A.11 a similar approach is described where longitudinal diffusion in the gas phase is also taken into account.

10.2.2 New Continuous Chromatographic Devices.

Sequential Chromatograph.

In 1973 Barker and Deeble reported a new design for a preparative scale chromatograph (172). The principle of operation can be understood with reference to Fig. 10.2.3. It is very similar to the earlier rotating chromatographs except that instead of rotating the column counter-current to the gas flow, all the inlet and outlet ports are sequenced round in the same direction as the gas flow. Another difference is the isolation of the stripping section from the rest of the column. It consists of twelve fixed 7.6 cm diameter 61 cm long copper columns linked alternately at top and bottom. The inlet and outlet operations as well as the transfer between the columns are controlled by solenoid valves connected to an electronic timing unit. This sequences each individual port function by one tube so that the tube which was in the stripping section in the previous time interval now becomes the first tube in the top section, and the tube which was at the end of the bottom section is isolated to be purged. The experimental work was done on the Arklone-P/Genklene-P system with Silicone Oil MS 200 as the liquid phase. With an equivolume mixture as feed stock, purities in excess of 99.8% were achieved for both products,

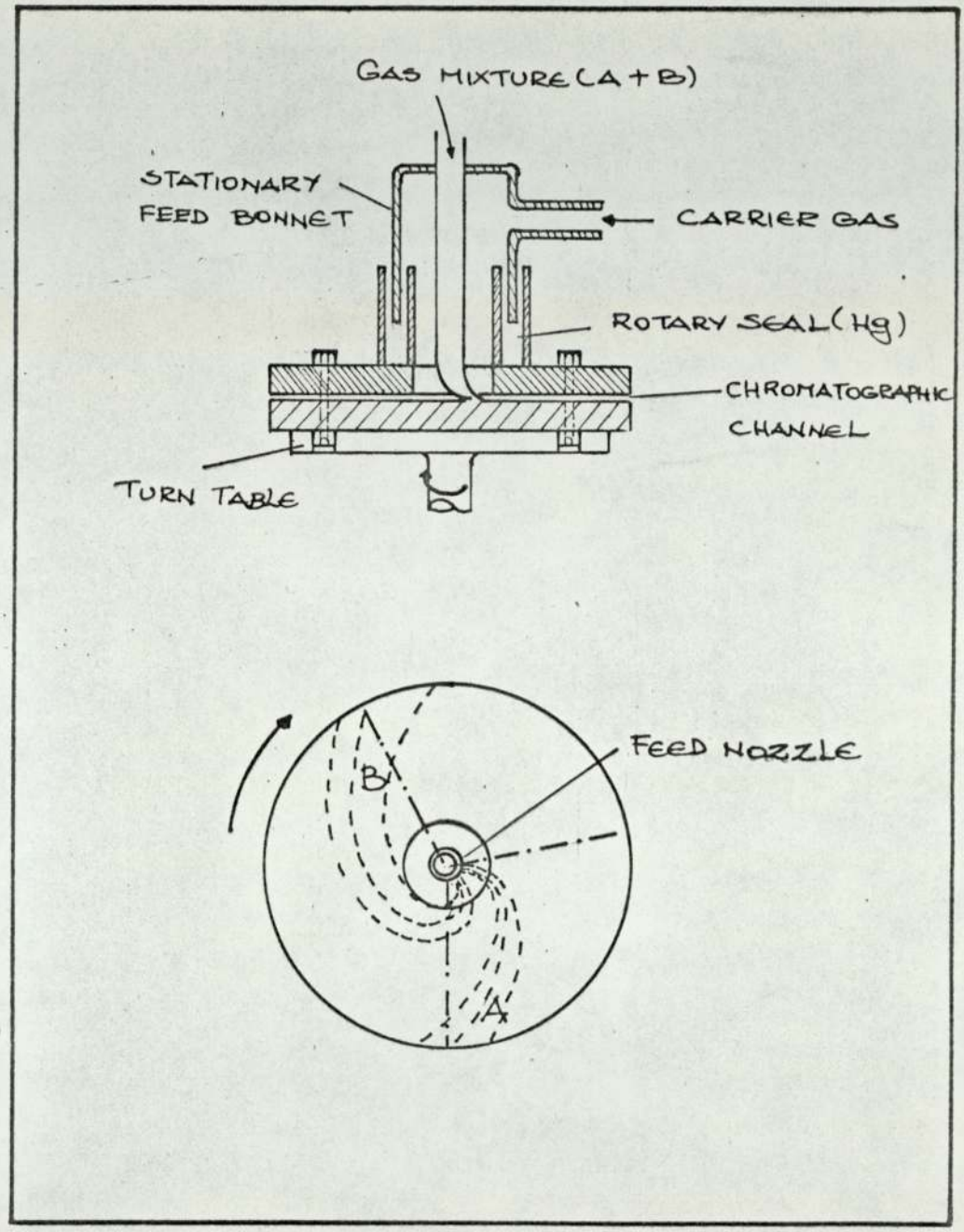

FIG. 10.2.4 – DISC CHROMATOGRAPH

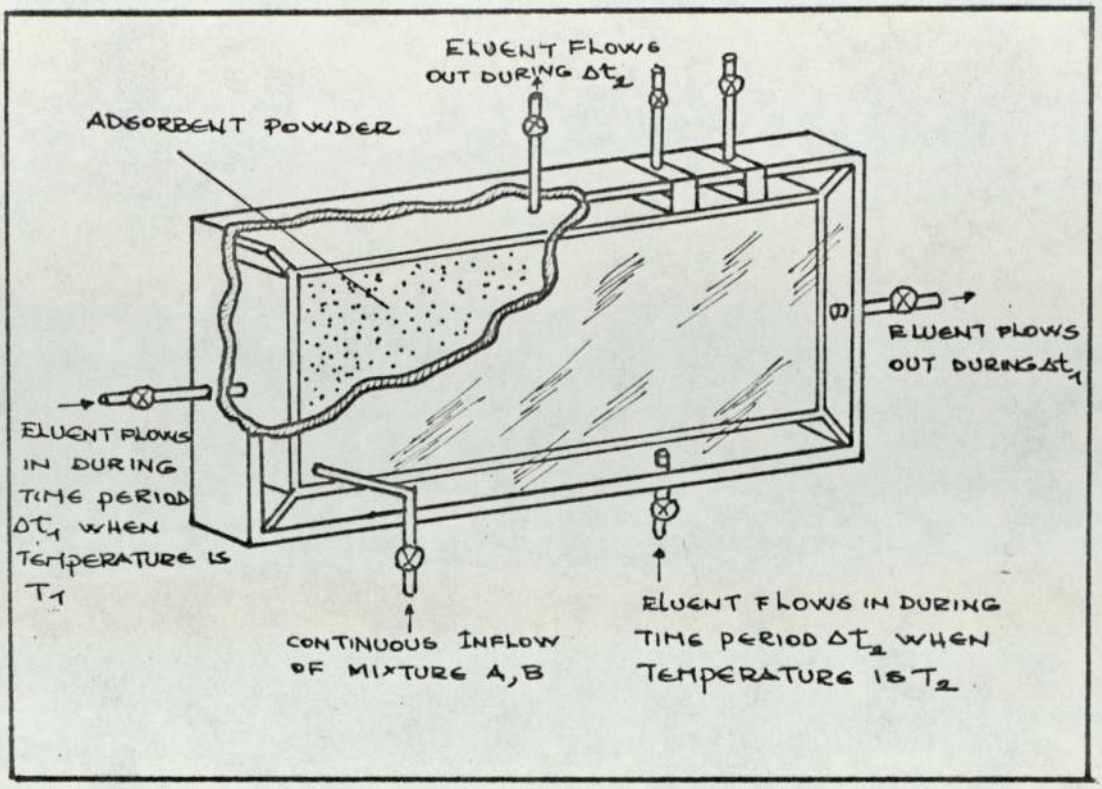

FIG. 10.2.5 SCHEMATIC DRAWING OF SLAB CHROMATOGRAPH

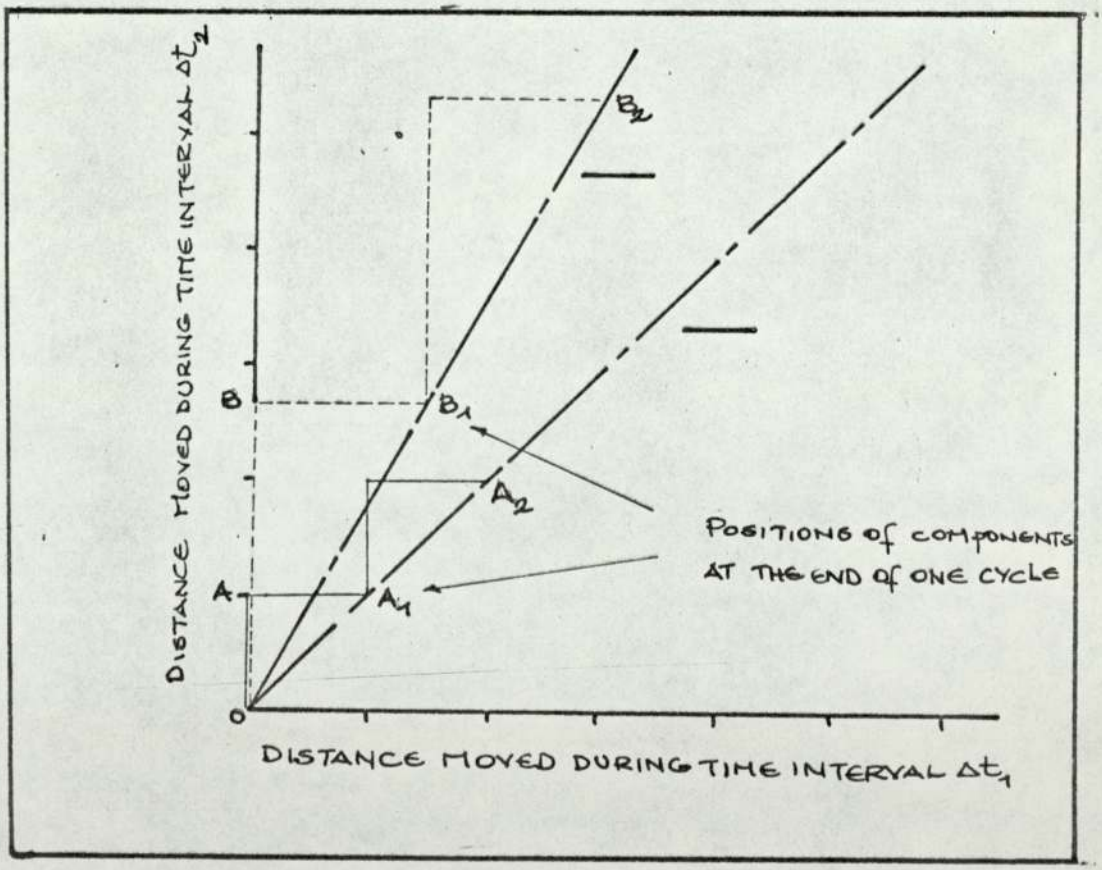

FIG. 10.2.6 PRINCIPLE OF SEPARATION OF SLAB CHROMATOGRAPH

up to a feed rate of 700 cm^3/h (179). The column efficiency was evaluated in terms of H.E.T.P., which was found to increase from an average value of 10.7 mm at a feed rate of 300 cm^3/h to 14.3 mm at 600 cm^3/hr. At a constant G/L ratio, the concentration profiles of both components were found to move towards the bottom exit. This observation is consistent with the equilibrium studies conducted in this work which found that the partition coefficients of these solutes increased with concentration.

Disc Chromatograph. (180)

A chromatographic channel is formed between two parallel flat glass discs held apart by small plastic spacers (Fig. 10.2.4). The facing surfaces of the glass discs are thinly covered by a non-volatile liquid phase. The carrier gas and the gaseous feed mixture are introduced through an orifice at the centre. Each component of the feed is pushed towards the periphery of the discs at a rate that depends on its solubility in the liquid phase. Since the discs are rotated slowly while the feed nozzle remains stationary, each component reaches the exit at an angle proportional to its rate of travel.

Slab Chromatograph. (181)

A Schematic drawing of the chromatograph is shown in Fig. 10.2.5. The technique relies on the change of the separation factor (K_i/K_j) of the components with temperature. The feed mixture is continuously introduced into one corner of a rectangular slab containing adsorbent powder. The carrier gas is alternately changed at right angles simultaneously with a change in temperature of the whole system. Since the ratio of the rates of travel of the components is different at different temperatures the feed mixture is eventually separated into individual component streams as depicted in Fig. 10.2.6. No experimental work has yet been reported but the need to change the temperature of the

whole system instantaneously looks like being a major weakness of the technique that would become progressively difficult to overcome with increasing size.

11. THE DESIGN AND OPERATION OF THE ROTATING CHROMATOGRAPH.

The rotating chromatograph used in this work was designed and built by Barker in conjunction with The Universal Fisher Engineering Co. Ltd., Crawley (182). The constructional details of the chromatographic unit are discussed elsewhere (174). In this chapter a brief description of the chromatographic column and the auxillary equipment is given, together with the principle of operation.

11.1 General Operating Principles.

The rotating GLC unit is illustrated in Plates 11.1, 11.2 and 11.3. It consisted of a 34 ft long column made of 44 tubes. As shown in Fig.11.1.1,the tubes were vertically mounted between two annular rings and connected alternatively at top and bottom to give a continuous carrier gas flow. The column had gas lock valves between the ports (I) and (IV), thus making the gas flow in a unidirectional manner. A pre-heated carrier gas (nitrogen)entered the column at port (I) and travelled countercurrently to the direction of rotation of the column. The feed mixture, pumped by a positive displacement D.C.L. micropump, entered the column at port (III). The less strongly absorbed components moved towards the top off-take port (IV) and the more strongly absorbed components travelled in the direction of the column rotation and were stripped off the packing in the section between the ports (II) and (I), usually by an excess carrier gas rate. The bottom products were then taken off from port (II).

11.2 Main Features of the Column.

11.2.1 Column Tubes.

The column consisted of 44 tubes, 2.54 cm (1 in) id., 2.86 cm ($1\frac{1}{8}$ in) od., 21.6 cm ($8\frac{1}{2}$ in) long, made of stainless steel. Each tube was welded to a flange at its bottom end and sealed against another flange at the

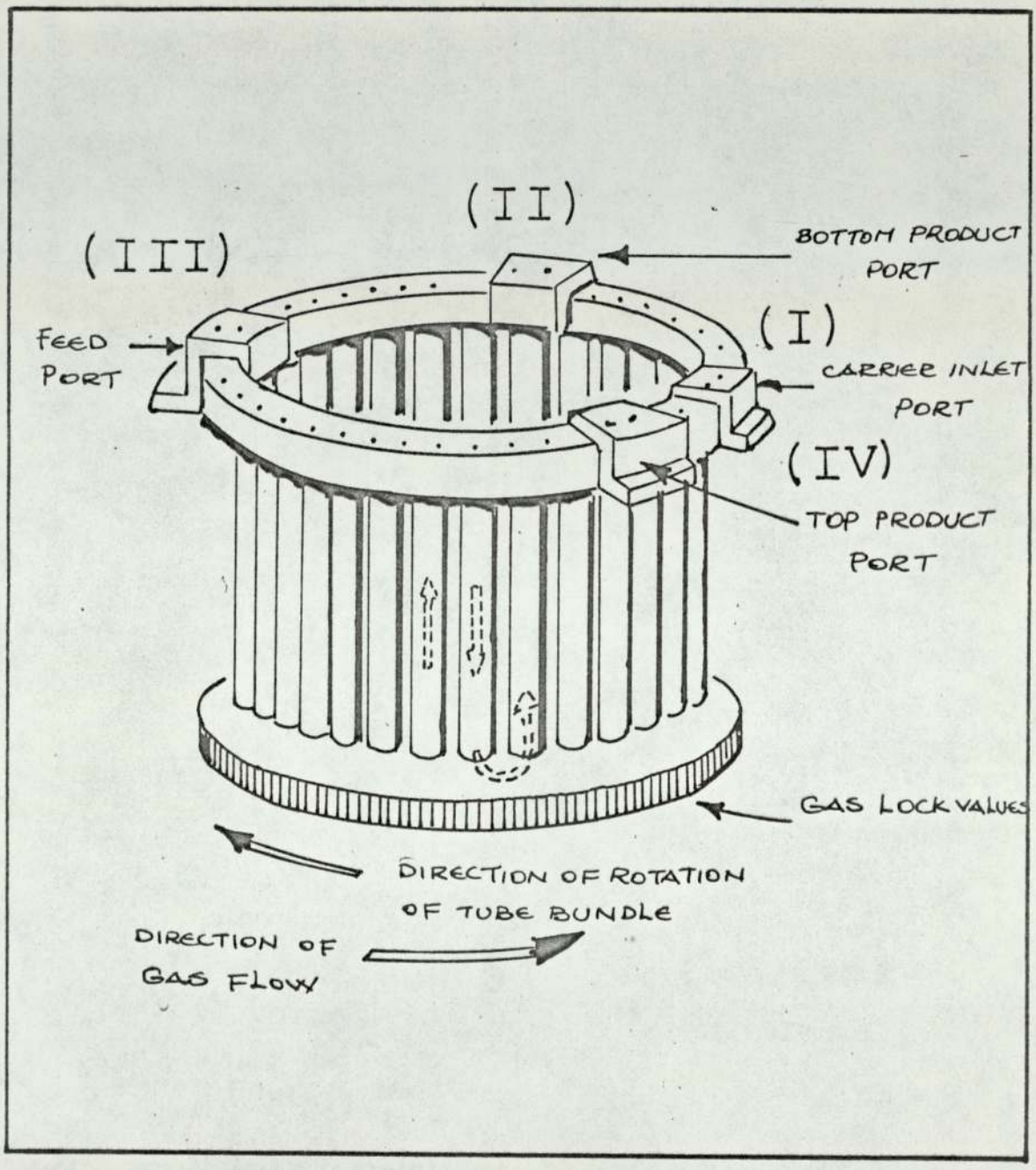

FIG. 11.1.1. SCHEMATIC OF ROTATING CHROMATOGRAPH.

Plate 11-1 - Details of the Rotating Chromatograph

I - Carrier Inlet Port
II - Bottom Product Port
III - Feed Port
IV - Top Product Port
FP - Feed Passages
FV - Feed Valves
GLV - Position of Gas Lock Cam
GP - Gas Passages
GV - Gas Valves
M - Top Ring
N - Bottom Ring
S - Cappilary Sample Lines.

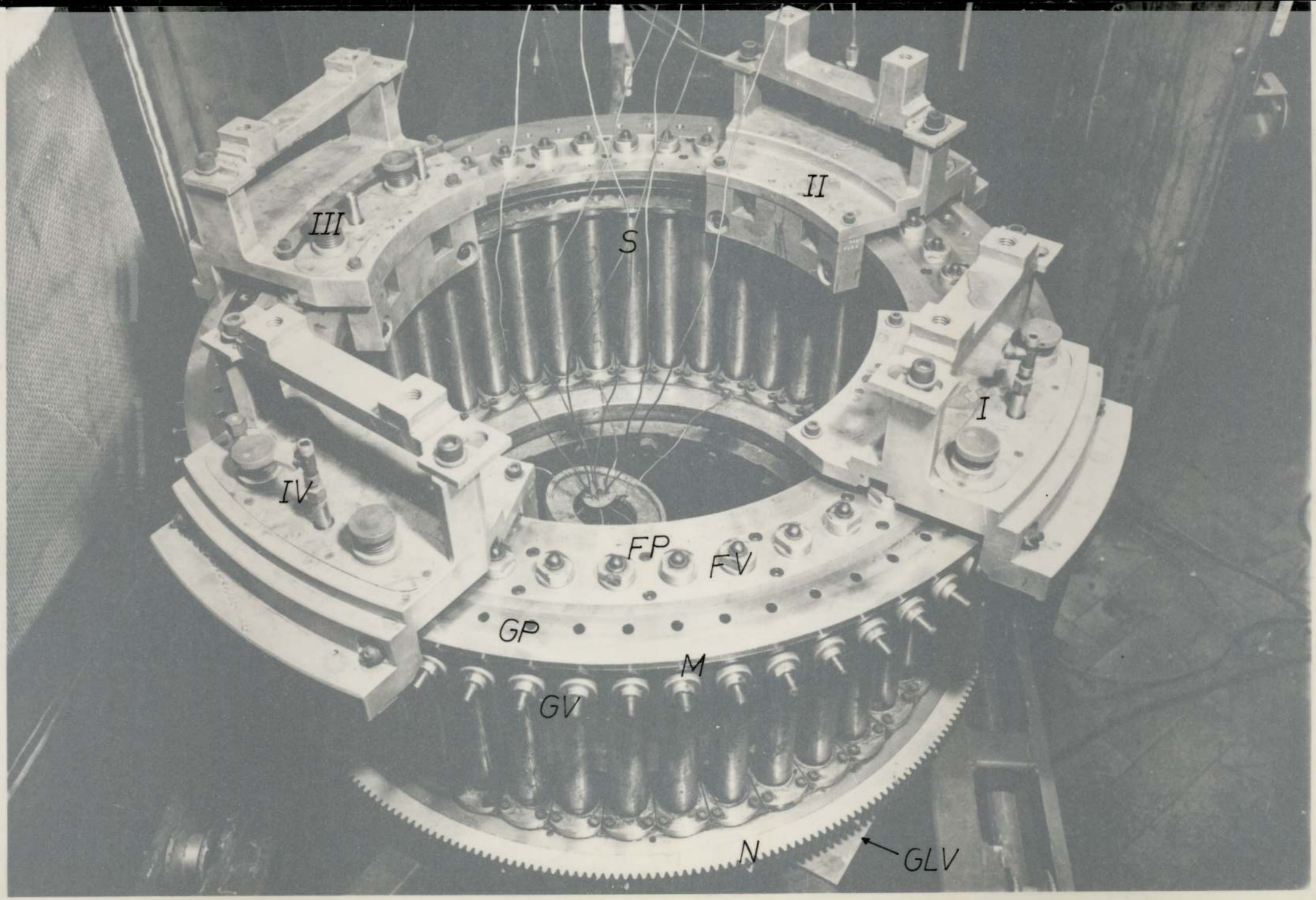
III
II
S
I
IV
FP
FV
GP
M
GV
N
GLV

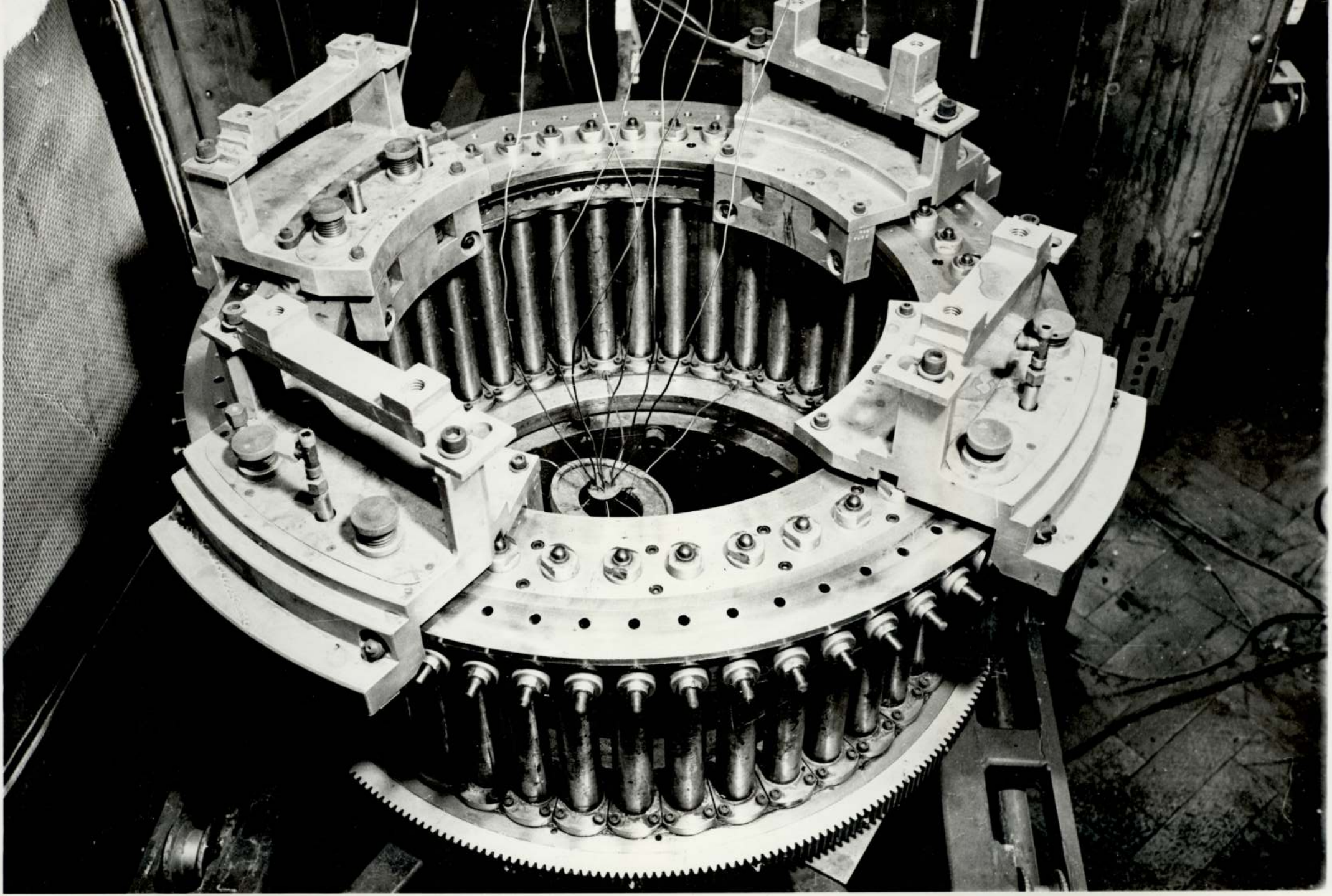

top end by means of a teflon or viton O ring. The flanges were sealed to the rings by a pair of specially shaped high temperature gaskets. Stainless steel gauze was mounted on both sides of the tubes so as to hold firm the 20.6 cm ($8\frac{1}{4}$ in) high packing in each tube.

11.2.2 Top Ring.

The top annular ring was made up of two main parts; a stationary part to which the tubes were connected and a movable part that provided access to the tubes for the packing operation. The stationary part provided 22 tube junctions which were sealed from one another by a gasket placed between the two parts of the top ring. For each junction there were three gas passages drilled through the stationary ring and two feed passages drilled through the movable part of the ring. Each passage was controlled by a press to open type of valve. The sealing was achieved by a pair of viton 'O' rings mounted on each valve.

11.2.3 Bottom Ring.

The bottom ring provided the necessary connections of the tubes and housed the gas locks which were accomplished by press to close valves, each having two 'O' rings and operated by a camming mechanism. Again the sealing between each tube junction was achieved by an annular gasket placed between the bottom ring and another ring, made up of 11 segments and screwed on to the bottom ring.

11.2.4 Ports.

The column had four ports; carrier gas inlet, bottom off-take, feed inlet and top off-take. All ports were stationary and fixed to the top of the oven that housed the chromatograph. The sealing between each port and the corresponding passages in the top ring relied on a specially machined graphlon 'O'ring. These curved 'O' rings were held in similar shaped shoes under each port and covered at least 4 feed or gas passages

Plate II-2 - General View of the Rotating Chromatographic Unit

CP - Control Panel
DS - Drive Shaft
F - Feed Reservoir and Burette
FP - Feed Pump
RS - Rotating Chromatograph
SL - Sample Lines to the Analytical Unit
TI - Temperature Indicator
TC - Thermocouple Compensating Wires
TS - Multi-Pole Thermocouple Switch.

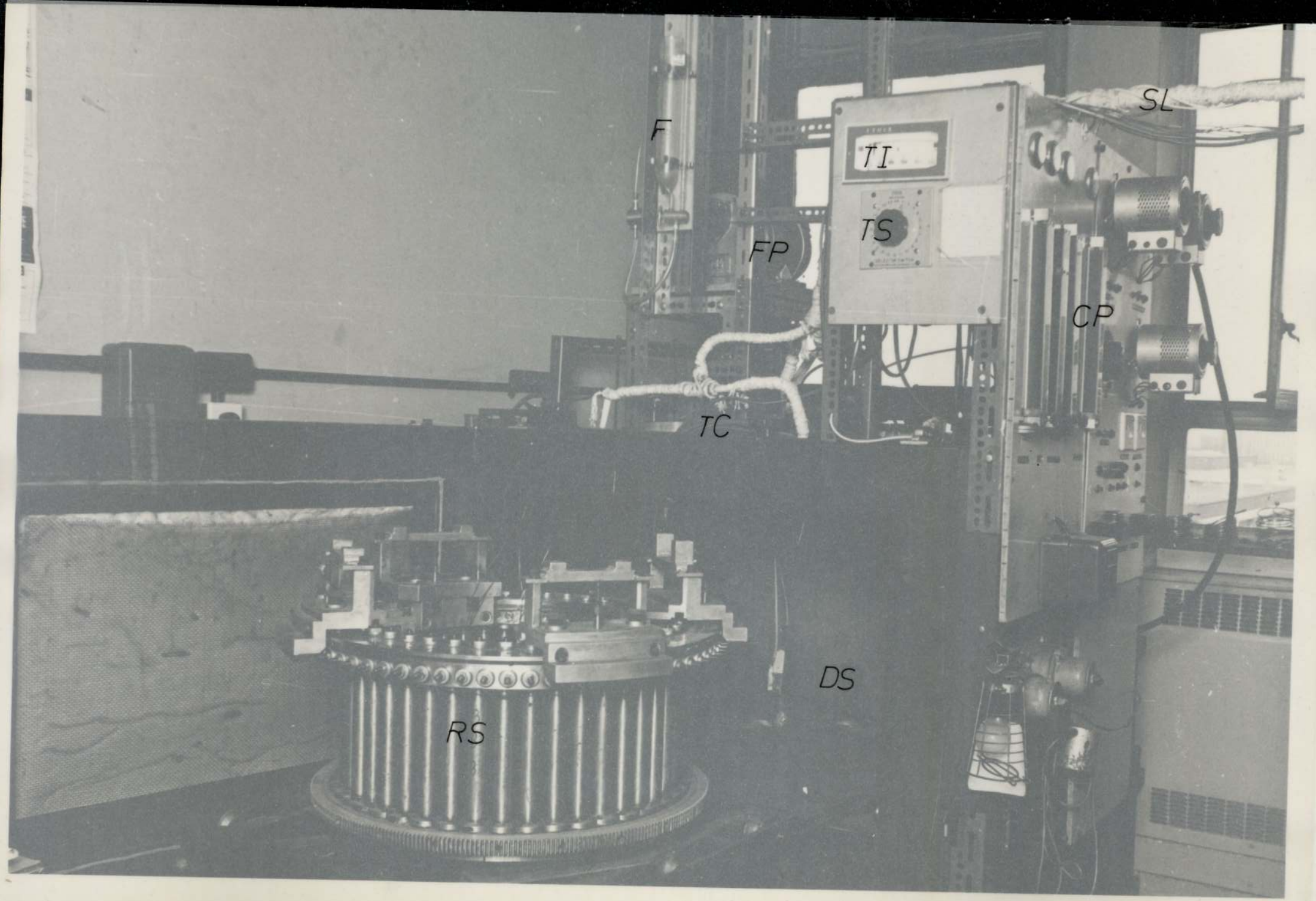
F
TI
SL
TS
FP
CP
TC
DS
RS

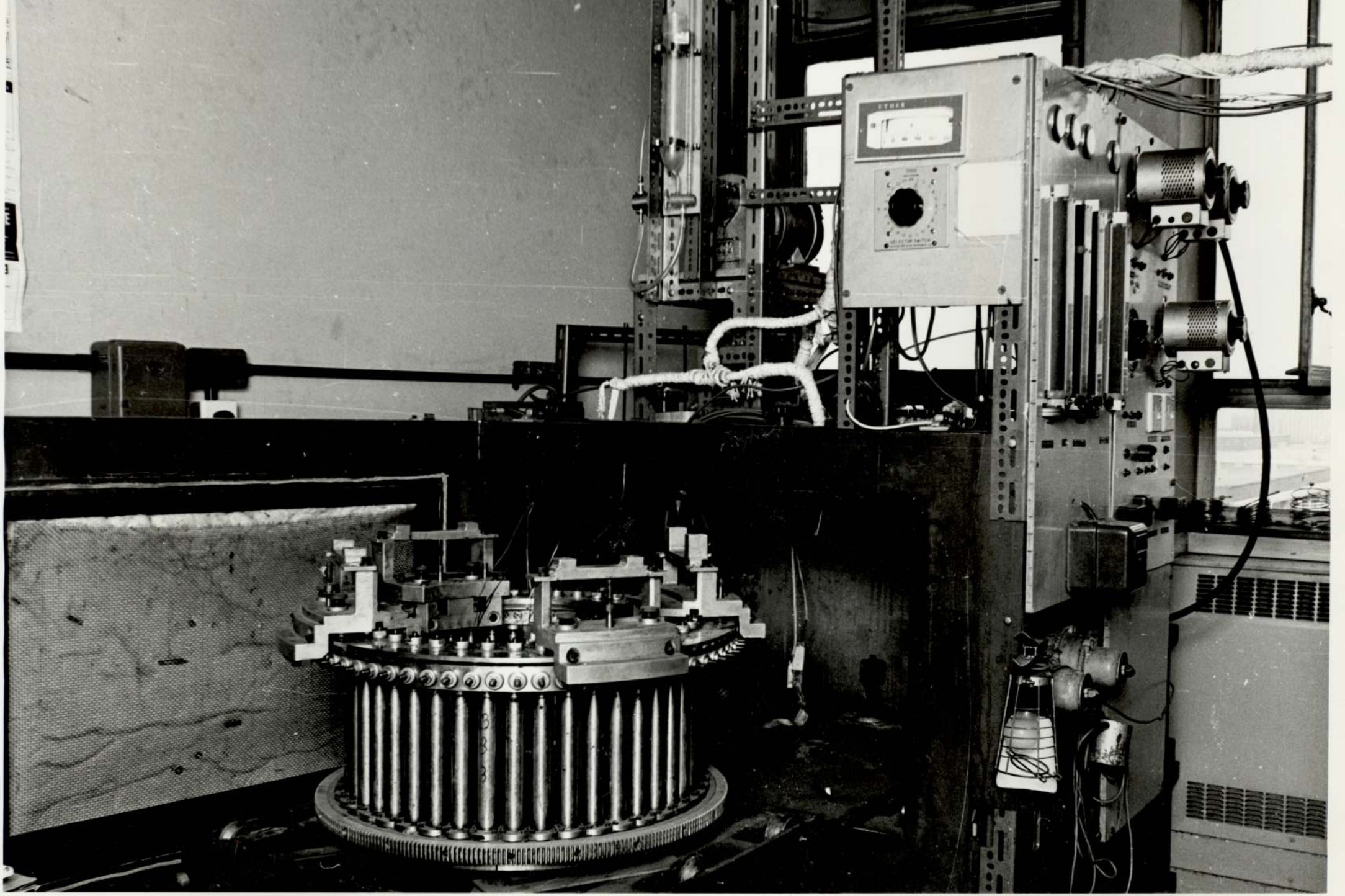

Plate 11-3 - Control Panel

EF - Extracting Fan

F1, F2, F3, F4 - Carrier Inlet, Bottom Off-take, Purge and Top Off-take Rotameters.

FP - Feed Pump Switch

MS - Drive Motor Switch

N - Purge Needle Valve.

P1, P2, P3, P4 - Carrier Inlet, Bottom Off-take, Purges, Top Off-take Pressure Gauges

R1, R2 - Off-take Flow Regulators

S1, S2 - Oven Heater Switches

V1, V2, V3 - Feed Line, Purge Line, Off-take Line Heater, Switches and Variacs

V4 - Carrier Gas Preheater Switch and Variac.

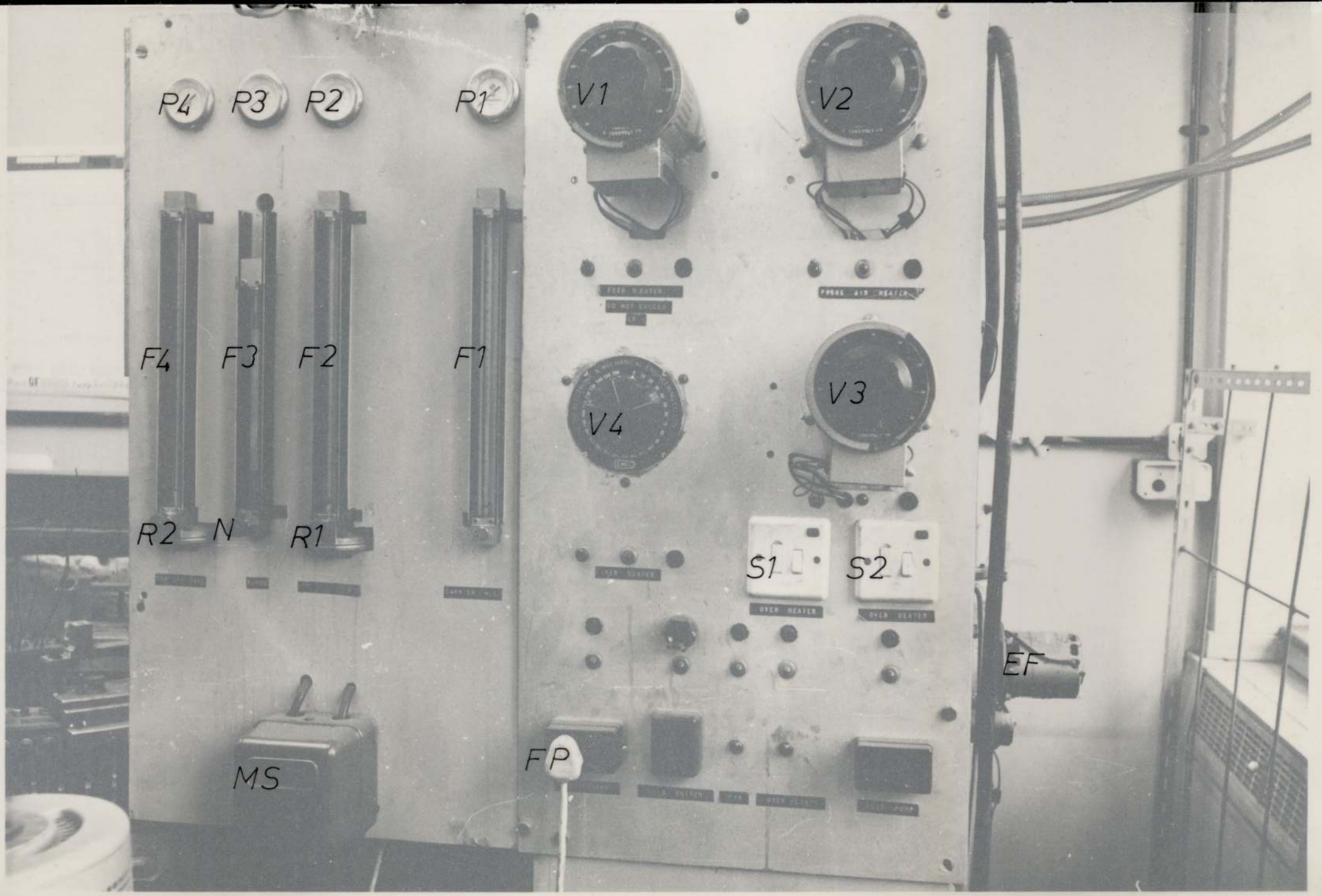
P4
P3
P2
P1
V1
V2
F4
F3
F2
F1
V4
V3
R2
N
R1
S1
S2
EF
MS
FP

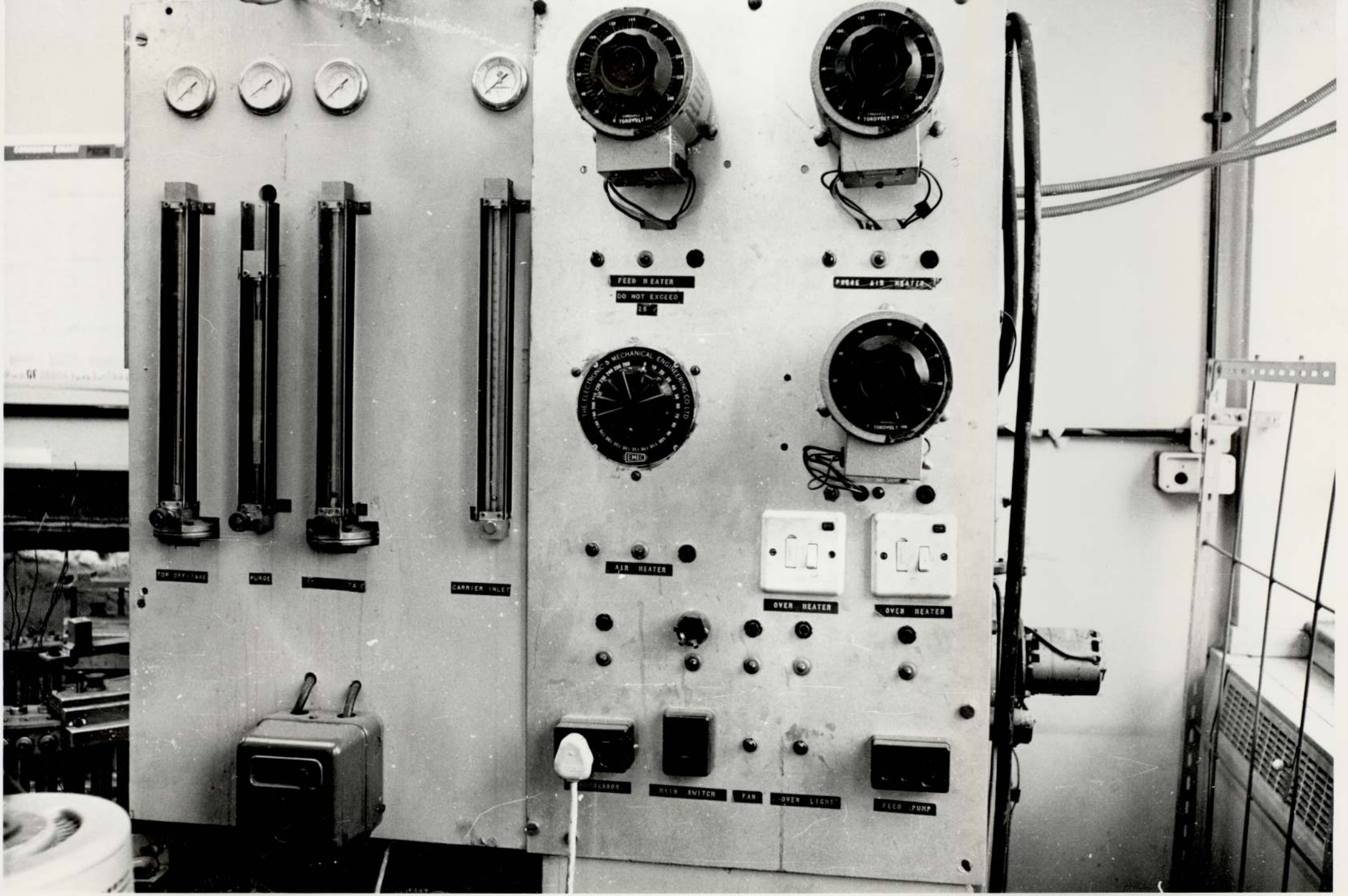
FEED HEATER
DO NOT EXCEED
PURGE AIR HEATER
AIR HEATER
OVEN HEATER
OVEN HEATER
MAIN SWITCH
FAN
OVEN LIGHT
FEED PUMP
CARRIER INLET
PURGE

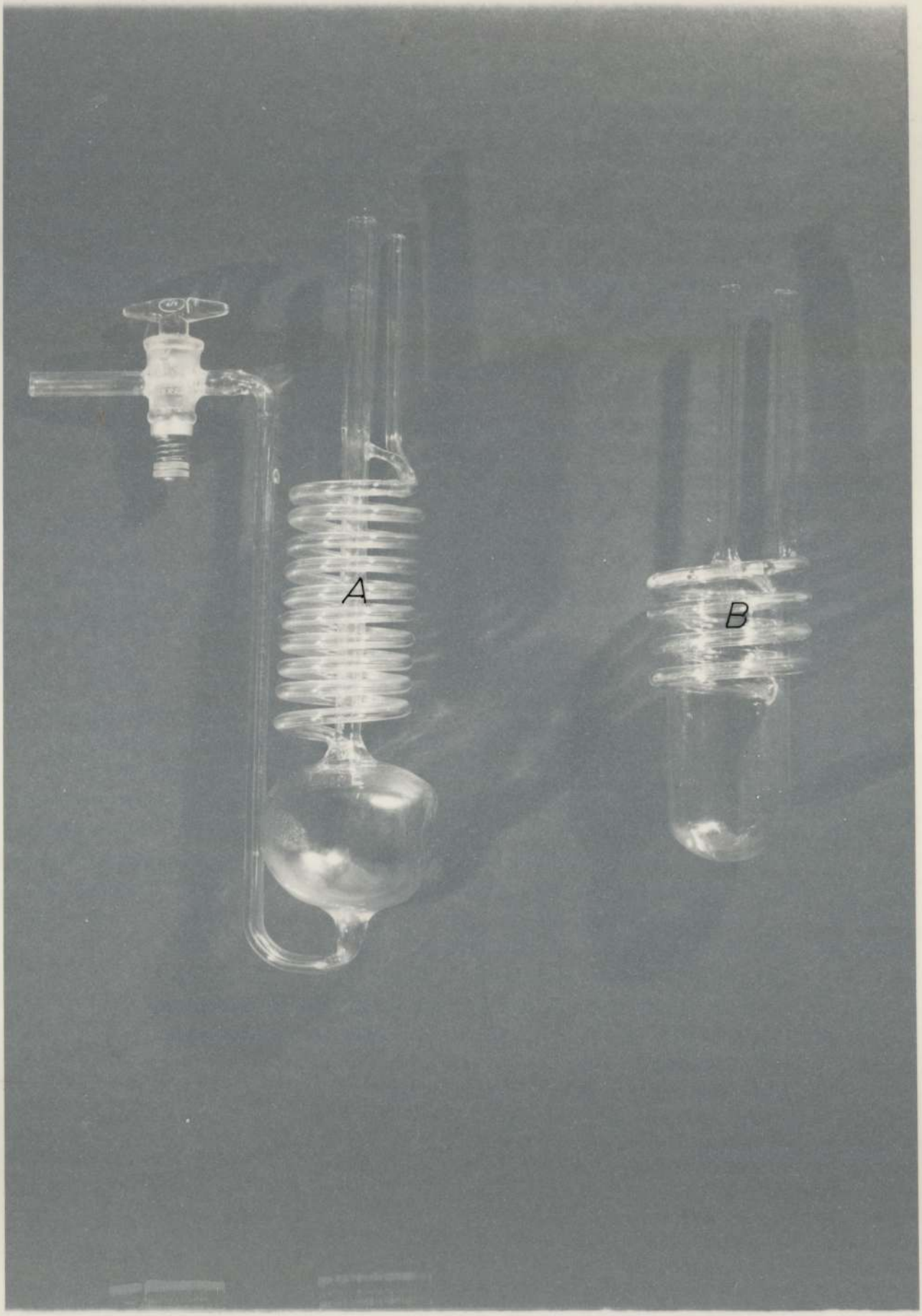

Plate 11·4 – Traps

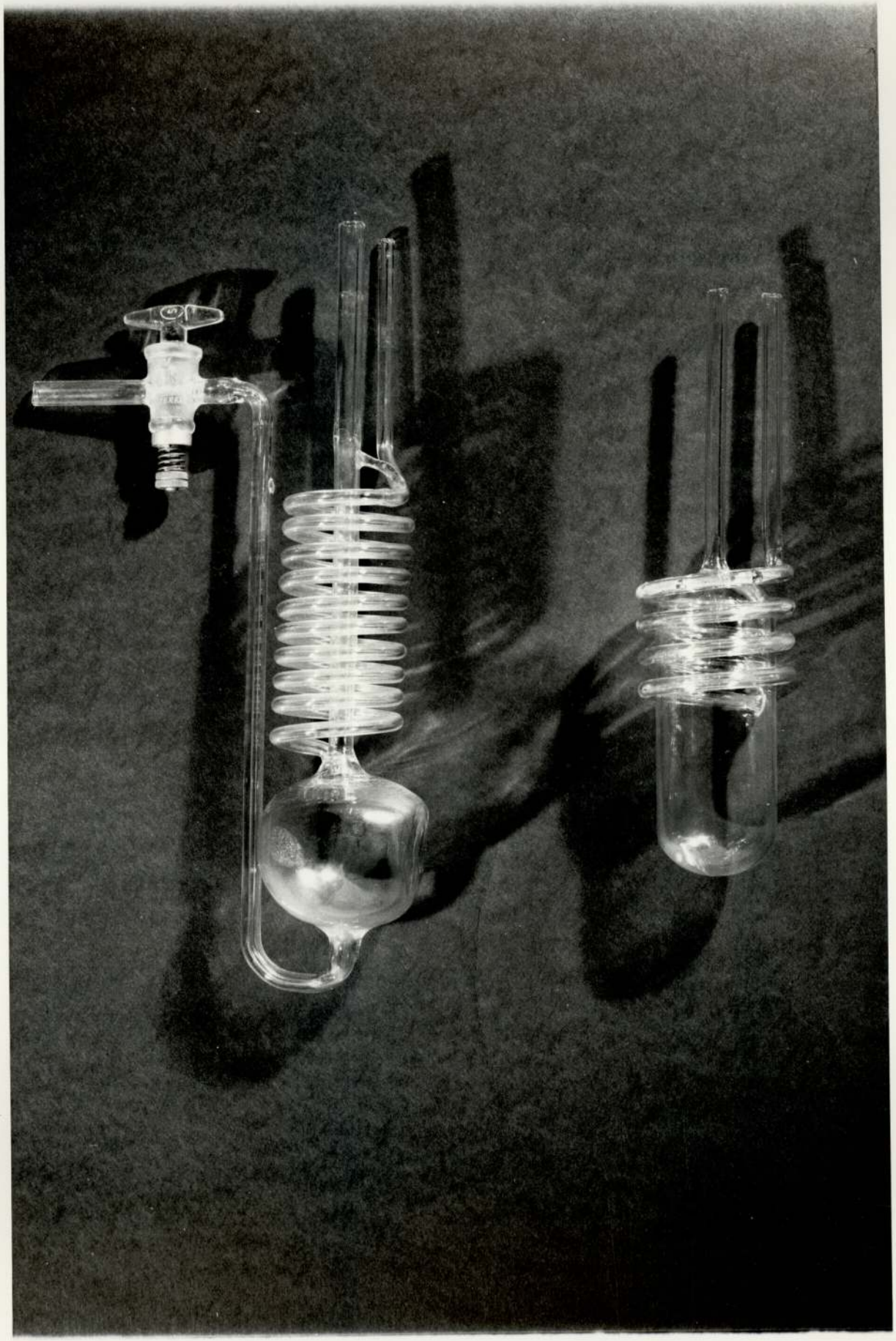

at any time. Each port also carried a cam which pushed open the valves as they came under it.

11.3 Auxiliary Equipment

11.3.1 Gas Flow Measurement and Control.

The carrier gas, supplied from a high pressure nitrogen cylinder, passed through a rotameter, a preheater and entered the column at port (I). A part of the gas was taken off from port (II) and the rest continued to be taken off from port (IV). Each off-take line passed through a pair of traps for product removal and the flow rates were measured by rotameters placed at the outlet. A facility existed for the diversion of a small part of the inlet gas supply through a rotameter and into the feed port (III) to help to push the feed in.

In the original equipment the flow rates were adjusted by diaphragm type valves placed on each flow line. Mainly because of the ever present leakages in the column these valves proved to be very inadequate in controlling the flowrates, and reading the flow rates from the rotameters to any degree of accuracy was an impossibility. On the off-take lines these valves were replaced by self-acting Brooks flow regulators of the type that controlled the downstream mass flow rate for varying upstream pressure (R2 and R4 on Plate 11.3). Integral with each regulator and placed at the inlet side of it there was a needle valve for precise adjustment. The inlet pressure was set from the cylinder head and the purge rate was adjusted by a needle valve. This arrangement kept the rotameter floats very steady, but it also meant that any change in the leakage rate registered as pressure fluctuations in the chromatograph as observed on the pressure gauges placed on the off-take lines before the flow regulator.

11.3.2 Temperatute Control and Measurement.

The oven was heated by two 3 KW heating elements. Each heater had its

own thermostat and control unit. A blower was also provided to circulate air out of the oven so as to prevent the build up of any explosive mixture. All the solute carrying lines were heated by heating tapes controlled by variacs.

The temperatures were measured at five points just above the ports (carrier inlet, bottom off-take, feed and purge inlet, top off-take) by iron-constantan, bonded junction type thermocouples, obtained from Pyrotenax. The outputs from the thermocouples passed through a multi-point, double pole switch and were normally read directly on an electronic temperature indicator having an electronically compensated cold junction.

11.3.3 Sampling System.

The chromatograph was equipped with 6 capillary tubes each connected to the bottom end of a tube for sampling round the chromatograph. The other end of each capillary could be connected by a plastic sleeving to a 0.476 cm (3/16 in.) o.d. stainless steel tube which extended to the analytical chromatograph. Two other similar sampling lines were permanently connected to each of the off-take lines before the traps. Each sampling line had a toggle valve placed just before all three joined the solute carrying line of the apparatus used for the equilibrium studies (see Figs. 4.1 and 4.2).

Two glass traps of the types shown in Plate 11.4 were connected in series for product collection. Frequent liquid samples could be drawn from the first trap (type A in Plate 11.4) for analysis and weighing. The traps were held in dewar flasks and cooled by ice. Provided the first trap was adequately supplied with ice no condensation could be observed in the second trap.

11.4 Operational Difficulties.

The main problem with the apparatus was the leakage, particularly

between stationary graphlon rings and the rotating top ring surface. Firstly, it was found that the seal was particularly sensitive to the spring pressure applied to the graphlon shoes. The greater this pressure the better was the seal, but this invariably gave rise to grooves being produced on the graphlon surface by the feed and gas holes and thus led to a gradual worsening of the seal with use. The top ring surface was ground to a 20μm smoothness, but its flatness could never be checked because of its size. The graphlon rings were made as flat as possible by grinding them with a fine grinding paste on a glass plate, but uneven shine obtained on their contacting surfaces indicated that some parts were never touching the ring surface even after months of grinding in.

Another source of leakage was the valves. Although the manufacturer's specification for the viton 'O'rings is higher than the temperatures employed in this work (115 - 130^{o}C), in the presence of pinene vapours the rings became brittle and stopped being effective after some use. The gas valves could be taken out and the rings replaced without having to take the top ring off and thus avoiding the breaking of the gasket. With the feed valves, however, this was not possible and if one failed the corresponding passage was blocked.

The gas valves were also prone to sticking. This was caused by the cams hitting their long stems and bending them. With a few of the valves the stems were worn so much that they failed to open at all.

In summary, the operation of the chromatograph was very unreliable. Even though the gas leakage rate might be very small at the start of a run, it would invariably get worse during the course of the run, and a valve failure would force it to be completely abandoned. The high temperatures employed in this work are thought to be the main cause of

the problems. Al-Madfai, who used the same apparatus but with non-degrading materials at lower temperatures, obtained reasonably good operation for two periods lasting four months.

12. EXPERIMENTAL WORK.

12.1 Experimental Procedure.

Before starting any run the column was tested for leaks at the column operating pressure. As explained previously the apparatus was never free of leakage. With the three runs that were conducted with any degree of success, the leakage rate was about 5% as measured at the start of a run. The oven was usually left on overnight before the start of a run, but it was found to be impossible to reach a steady temperature. Instead it cycled with a large amplitude (about 7-10^{o}C). However, because of the appreciable mass of the column, the temperature fluctuation in the gas streams were a lot smaller, $\pm$ 2-3^{o}C about the mean. The extracting fan was almost directly behind the bottom port where it caused some cooling. This problem was, to some extent, alleviated by keeping the temperature of the inlet carrier gas at a high temperature than the mean column temperature.

When the conditions became as steady as possible, the column was rotated at the required speed and the feed mixture was pumped in. The pumped feed rate was measured from a burette and it was checked against the volume of products collected in the traps. The efficiency of the traps was estimated to be better than 95% by sampling the streams after the traps.

The gas flow rates were set at the required values and were subsequently checked at frequent intervals together with the pressures. The off-take flow rates were usually very steady, and any change in the leakage rate registered as fluctuations in the pressure readings as well as in the inlet carrier rate.

The concentrations and compositions of the product streams were continuously monitored, one at a time, by bleeding a small amount of product stream to the gas sampling valve. The flow rate of these streams

and of the streams from the sampling points on the column were adjusted to give a time lag of about 10 seconds. The temperature of the analytical column was 120°C at which it was possible to analyse a sample every three minutes.

The position of a sampling point on the column was calculated from the time that had elapsed since it was at a known position and from the speed of rotation. Usually only about six samples per hour were analysed in this way. In the time between two injections the line was purged by an excess pure nitrogen stream.

The liquid samples from the traps were collected in marked sample bottles. These were usually analysed at the end of the run using the second channel of the analytical unit.

12.2 Purification of the Feed Mixture.

In an early period of the experimental work it was observed that the top few centimeters of the packing in the tubes had become brown coloured. The cause and the nature of this brown deposit could not be determined, but it was also observed during the batch distillation of commercial turpentine that the fraction in the still would gradually become darkened and viscous. Since this fraction contained a large percentage of the unidentified heavy components of the turpentine mixture, it was decided to cut out these fractions in the hope of lessening the problem, but whatever the contribution of the heavy components was towards this phenomenon, the fact that some slight colouring was also observed with the packings of the analytical columns seems to suggest that the pinenes themselves degrade to form some non-volatile compounds under the influence of high temperatures.

The starting α and β pinene mixtures were the same as those used in the equilibrium studies. The distillation was also carried out on the same column. The two relatively purified mixtures were then mixed to give a

feed mixture with the following composition by weight:

α-Pinene, 62.9%; β-Pinene, 34.0%; Camphene, 2.3%; heavy components, 0.7%; light components, 0.1%.

12.3 Experimental Runs.

Numerous runs were conducted over a period of about 18 months. A large proportion of these runs were abandoned after a few hours because of a mechanical failure. Some of the earlier runs, where the operating conditions were reasonably steady over 10 hours or more, indicated that the separation process was not reaching a steady state. However, at this stage the gas sampling valve was not yet installed, and some doubt remained as to whether the concentration fluctuations observed, particularly in the bottom off-take, was due to unstable operation or to inaccurate gas sampling by a syringe.

Only after the installation of the gas sampling valve was it possible to carry out a systematic investigation of the nature of the fluctuations. These manifested themselves as changes in 1) the gas phase concentration and composition at a particular point in the column, 2) the amount of product collected in the traps over a given time, 3) the composition of products in the traps. Only three runs could be conducted for this purpose, where the operating conditions were reasonably steady over periods of time (14-24 hours) that were considered long enough to reach equilibrium. The third run, where the addition of the automatic injection capability released more time for other measurements, was particularly complete in exposing the unsteady state operation of the apparatus.

In all the three runs documented below, the following operating conditions were identical:

Speed of rotation = 1.0 rev/h, Liquid rate = 348.5 g/h

Length of top section = 272 cm (13 tubes)

Length of bottom section = 252 cm (12 tubes)

Length of stripping section = 293 cm (14 tubes)

It should be pointed out, however, that as the ports cover 3 or 4 valves at a time, the above figures are subject to an error of one tube length.

Run 1.

The operating conditions are summarised below. Where it has been impossible to compute a mean value, the maximum and the minimum recorded values are given.

Table 12.3.1. Operating Conditions

Mean Column Temp = 120°C ; Pumped Feed Rate = 32.1 cm^3/h				
Flow Rates at NTP L/h		Mean Pressure in the Separating Section KN/m^2	G/L at Mean Column Conditions	
			Top Section	Bottom Section
Carrier inlet	531.0-513.5	178.6	154.9-149.8	136.9-131.4
Purge +	6.6			
Bottom Off-Take	453.0-446.5			
Top Off-Take	56.4-52.3			
% Leakage	5.9-1.8			

The run lasted 18 hours. The top product concentration was monitored in the last hour of the run. The variation as measured in terms of the total peak area was 24.5% about the mean. The bottom product was sampled every four minutes over the 17th hour. The fluctuations were very rapid and the measured concentrations bore no relation to each other.

There were also some variations in the trap collection rates. About 37% of the incoming feed was lost. These measurements are given below:

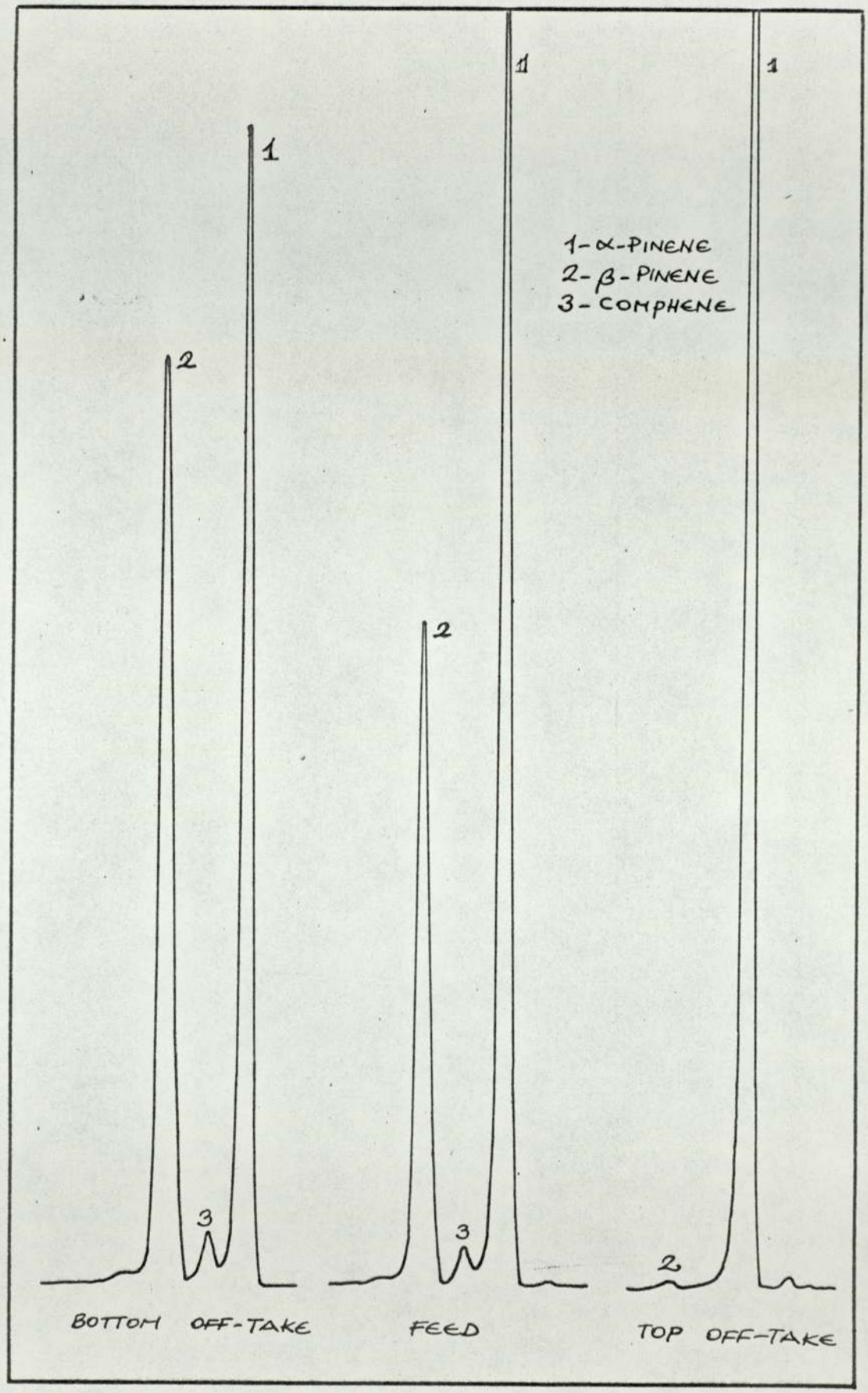

FIG. 12.3.1 - SEPARATION OF PINENE ISOMERS, RUN 1

Table 12.3.2. Trap Collection Rates.

Time of collection h	Collection Rates cm^3/h Top	Bottom	Total
17th	4.55	15.0	19.65
18th	4.30	16.2	20.50

There was a considerable variation in the composition of the bottom product throughout the run, but this was not very noticeable in the top product by virtue of it being nearly pure. The analysis recorded in Fig. 12.3.1 is of the products collected over the last five hours of the run. These values together with the feed composition are given in the table below.

Table 12.3.3. Feed and Product Compositions.

	Composition, % by weight				
	Lights	α-Pinene	Camphene	β-Pinene	Heavies
Feed	0.1	62.9	2.3	34.0	0.7
Top Product	0.8	98.8	-	0.4	-
Bottom Product	-	50.4	3.3	45.4	0.9

Run 2.

The operating conditions for the run are given below:

Table 12.3.4. Operating Conditions.

Mean Column Temperature = 117.5°C Pumped Feed Rate = 28.8 cm^3/h				
Flow Rates at NTP L/h		Mean Pressure in the Separating Section KN/m^2	G/L at Mean Column Conditions Top Section	Bottom Section
Carrier Inlet	537.0-525.0	196.5	180.1-168.6	164.9-157.7
Purge	4.5			
Bottom Off-Take	440.0			
Top Off-Take	66.0-64.1			
% Leakage	4.7-7.3			

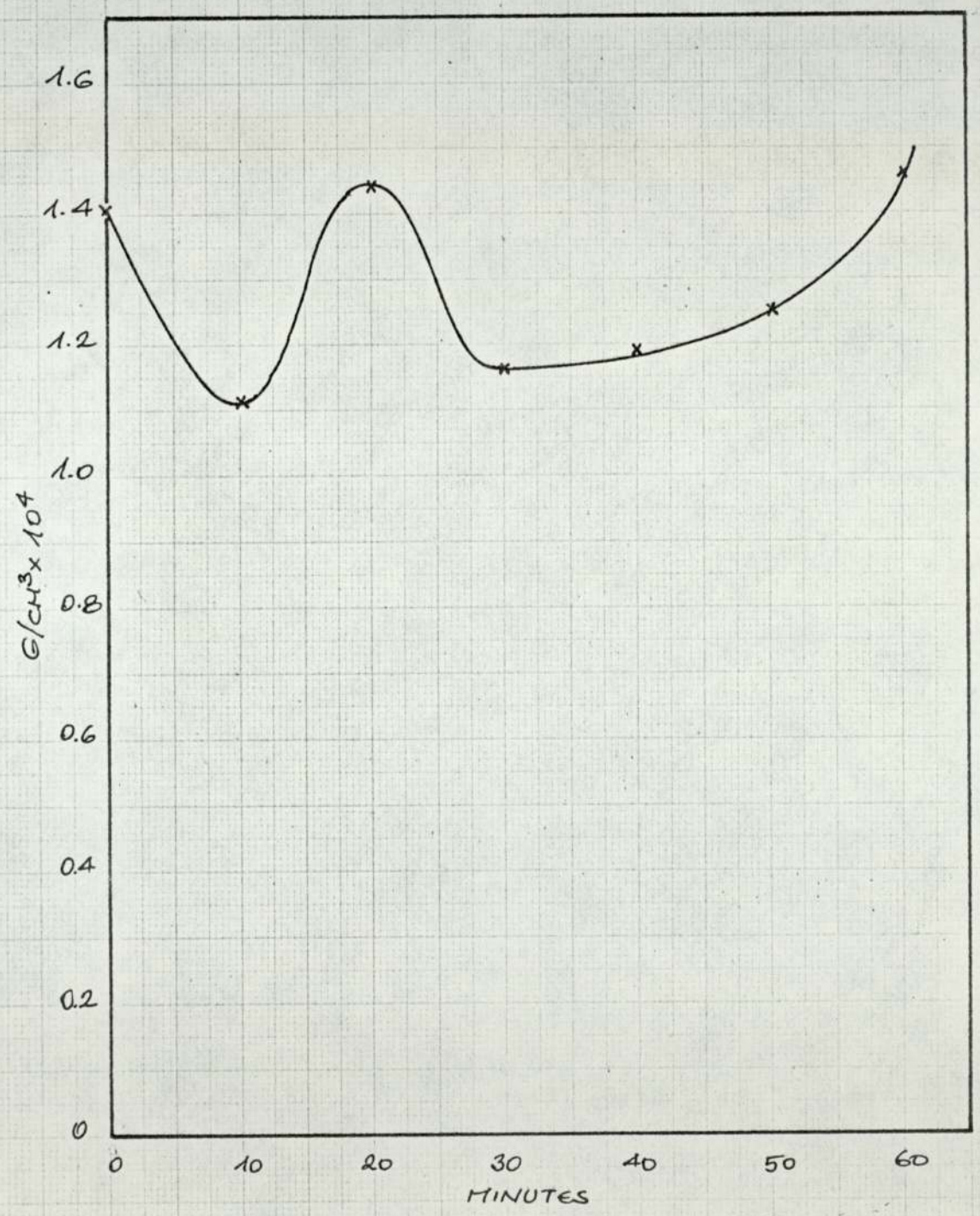

FIG. 12.3.2- VARIATION OF α-PINENE CONCENTRATION IN TOP PRODUCT WITH TIME, RUN 2

The concentration of the bottom stream was again very random. The variation of concentration in the top off-take was about the same as in the previous run. Fig. 12.3.2 shows the variation of the gas phase concentration of α-pinene (about 99% of the total top product) in the top off-take with time. The samples were taken every 10 minutes over the 8th hour of the run.

The compositions of the products were monitored by analysing liquid samples from the traps, collected over 1 hour for 7 consecutive hours, starting 7 hours after the beginning of the run. Table 12.3.5 shows the collection rates as well as the approximate compositions. As in the previous run, the changes in the top product purity were barely detectable, undoubtedly because of its high purity. The bottom product, which had all the components of the feed in appreciable quantities, showed considerable fluctuations in its composition.

Run 3.

The feed mixture used in this run was different from the other two runs. One of the aims of this run was to obtain pure β-pinene for the equilibrium studies. For this purpose, the bottom products collected in the previous runs were distilled once to cut out the heavy components, and the resultant mixture was used as the feed with the following composition:

α-Pinene: 13.6%; Camphene: 1.6%; β-Pinene: 84.8%.

The run lasted for approximately 24 hours. The operating conditions are given in Table 12.3.6.

Table 12.3.5. Variation of Product Purities with Time.

Time of Collection, h	Collection Rate cm^3/h			% of Bottom Product	Composition of Top Product %			Composition of Bottom Product %		
	Top	Bottom	Total		α-Pinene	Camphene	β-Pinene	α-Pinene	Camphene	β-Pinene
8th	7.8	6.3	14.1	44.7	99.0	-	0.5	3.6	3.7	92.7
9th	8.0	6.0	14.0	42.8	"		"	4.8	5.6	89.6
10th	7.3	9.1	16.4	55.5	"		"	13.8	7.8	78.4
11th	5.1	11.5	16.6	69.3	"		"	40.2	4.2	55.6
12th	5.0	8.3	13.3	62.4	"		"	32.2	4.9	62.6
14th	5.8	7.6	13.4	56.7	"		"	19.7	5.3	75.0
15th	7.1	8.3	15.4	53.9	"		"	23.9	5.5	70.6

Table 12.3.6. Operating Conditions.

Mean Column Temp = 115.0°C		Pumped Feed Rate = 342 cm^3/h		
Flow Rates at NTP L/h		Mean Pressure in the Separating Section KN/m^2	G/L at Mean Column Conditions	
			Top Section	Bottom Section
Carrier in	345.0-370.0	101.4	216.9-211.8	209.0-214.5
Purge	0.9			
Bottom Off-Take	216.0-222.0			
Top Off-Take	82.2-84.1			
% Leakage	12.0-19.0			

The top off-take was monitored for three hours, five hours after the start of the run by taking gas samples at approximately 3 minute intervals. Fig. 12.3.3 shows the results as peak area, and percentage peak area of α-pinene. These plots confirm the findings of the earlier runs in that the changes in the compositions of the products, although considerable, are not as big as the fluctuations in the vapour phase concentrations. The solute vapour concentration of the bottom product was also steadier than in the previous runs. In Fig. 12.3.4 the peak area and percentage peak area of β-pinene are plotted against time.

The concentration profile along the column was also followed for three cycles in the later stages of the run. The result is shown in Fig. 12.3.5 as the peak areas of the pinenes, while the composition as expressed in percentage peak area is shown in Fig. 12.3.6.

The product collection rates and their compositions are given in the table below. These results also reflect the comparative steadiness of this run.

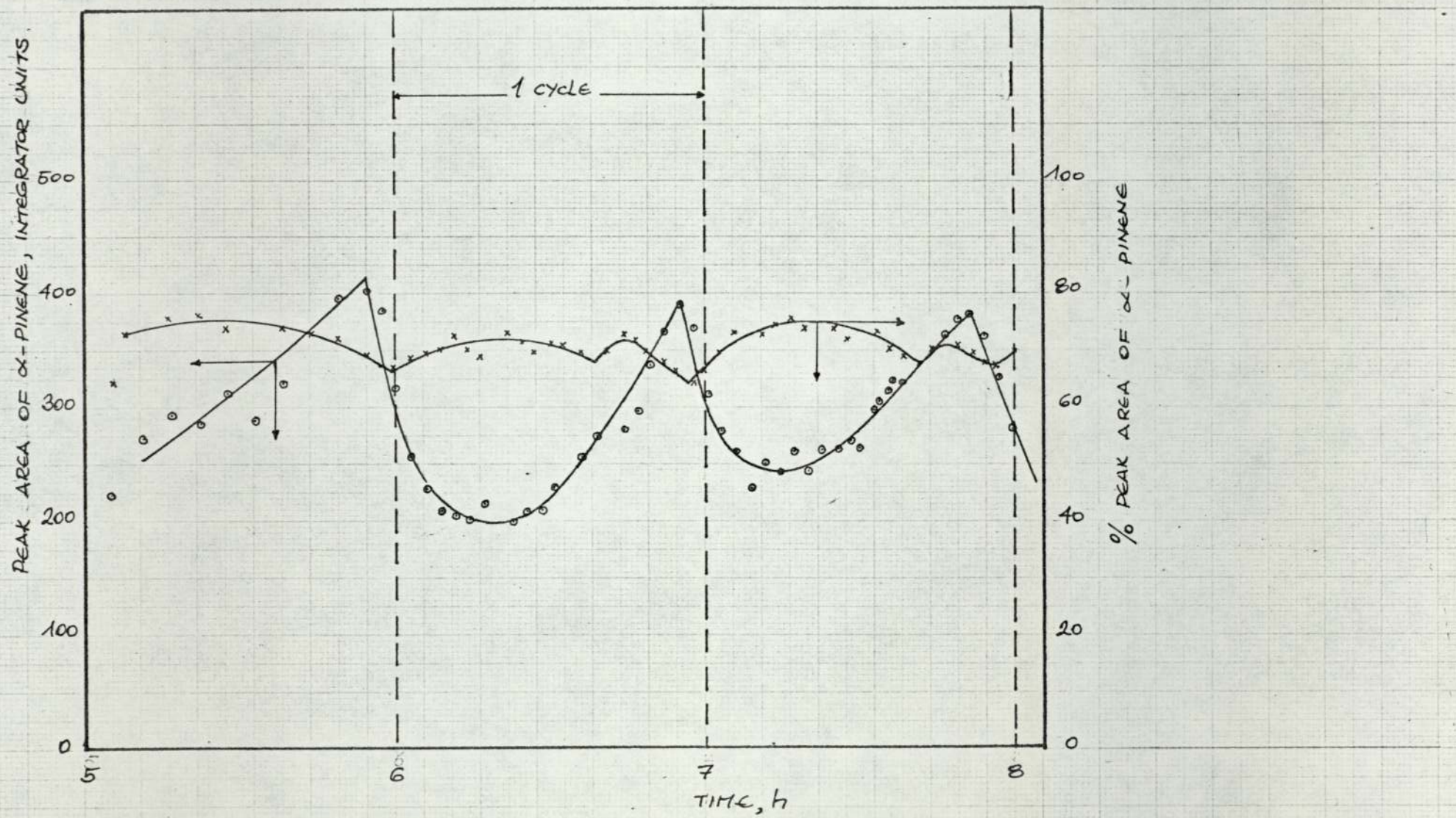

FIG. 12.3.3 – VARIATION OF TOP PRODUCT VAPOUR PHASE CONCENTRATION AND COMPOSITION, RUN 3

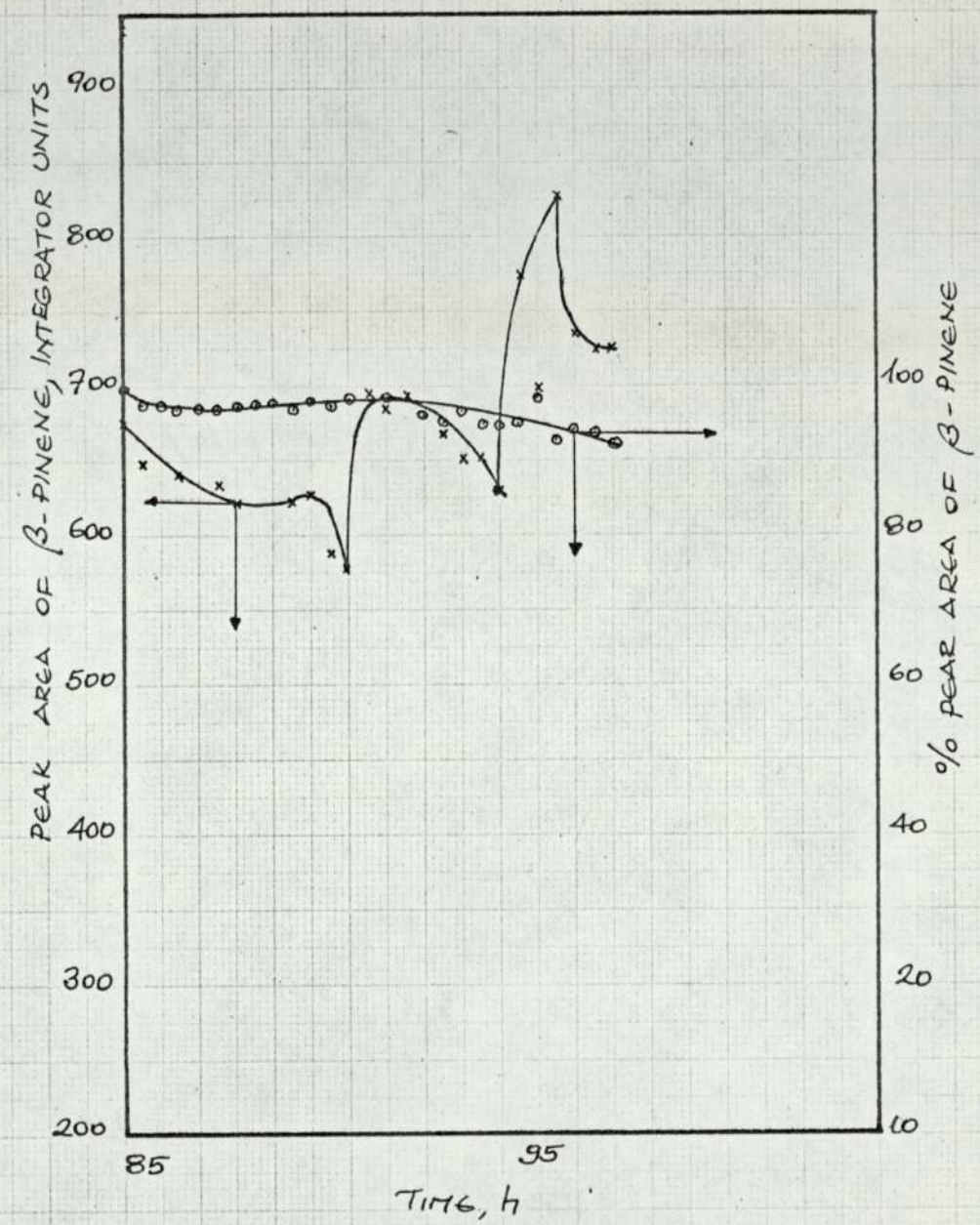

FIG 12.34 - VARIATION OF BOTTOM PRODUCT VAPOUR PHASE CONCENTRATION AND COMPOSITION WITH TIME, RUN 3

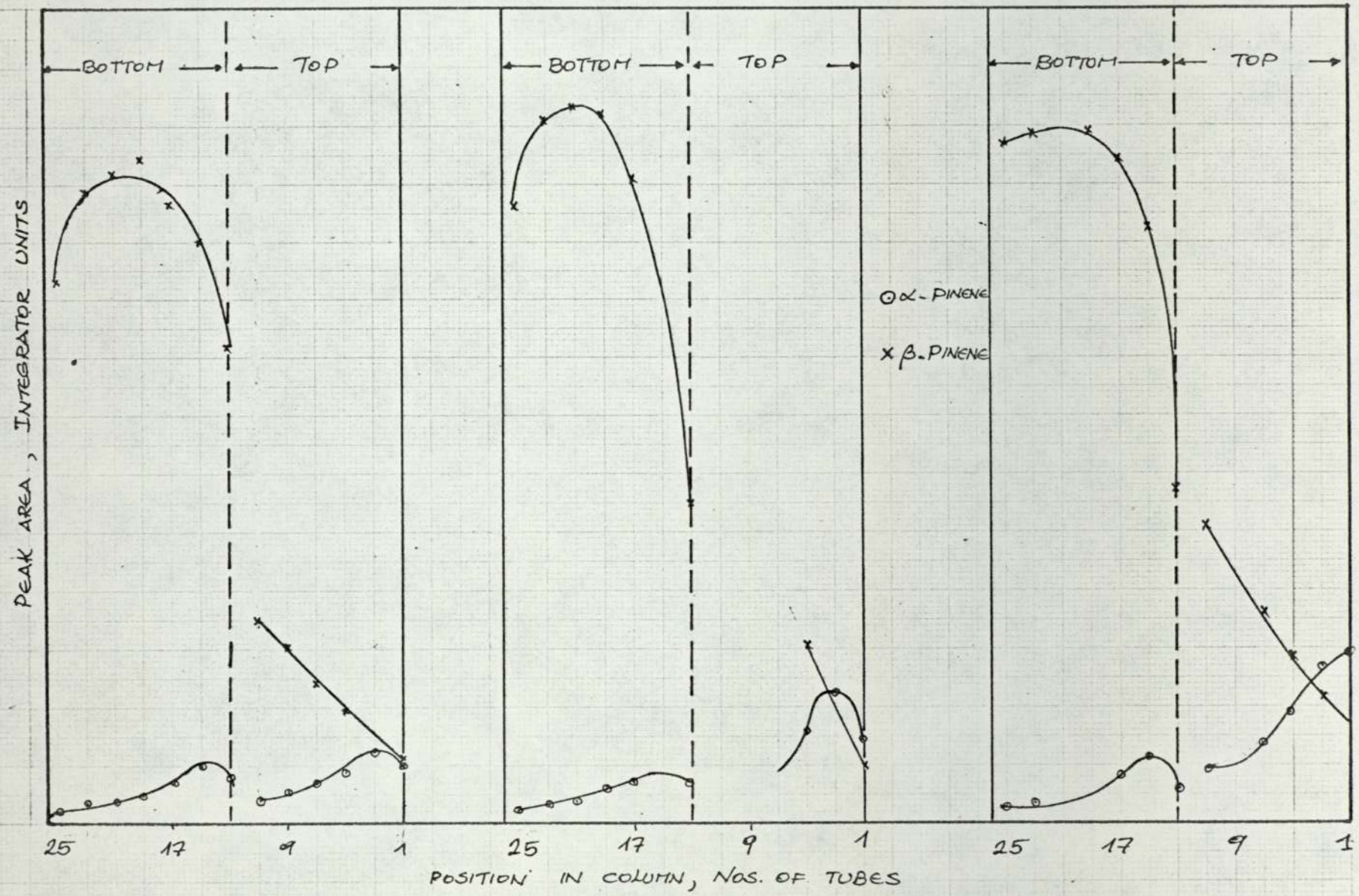

FIG. 12.3.5- VAPOUR PHASE CONCENTRATION PROFILE IN THREE CONSECUTIVE CYCLES, RUN 3

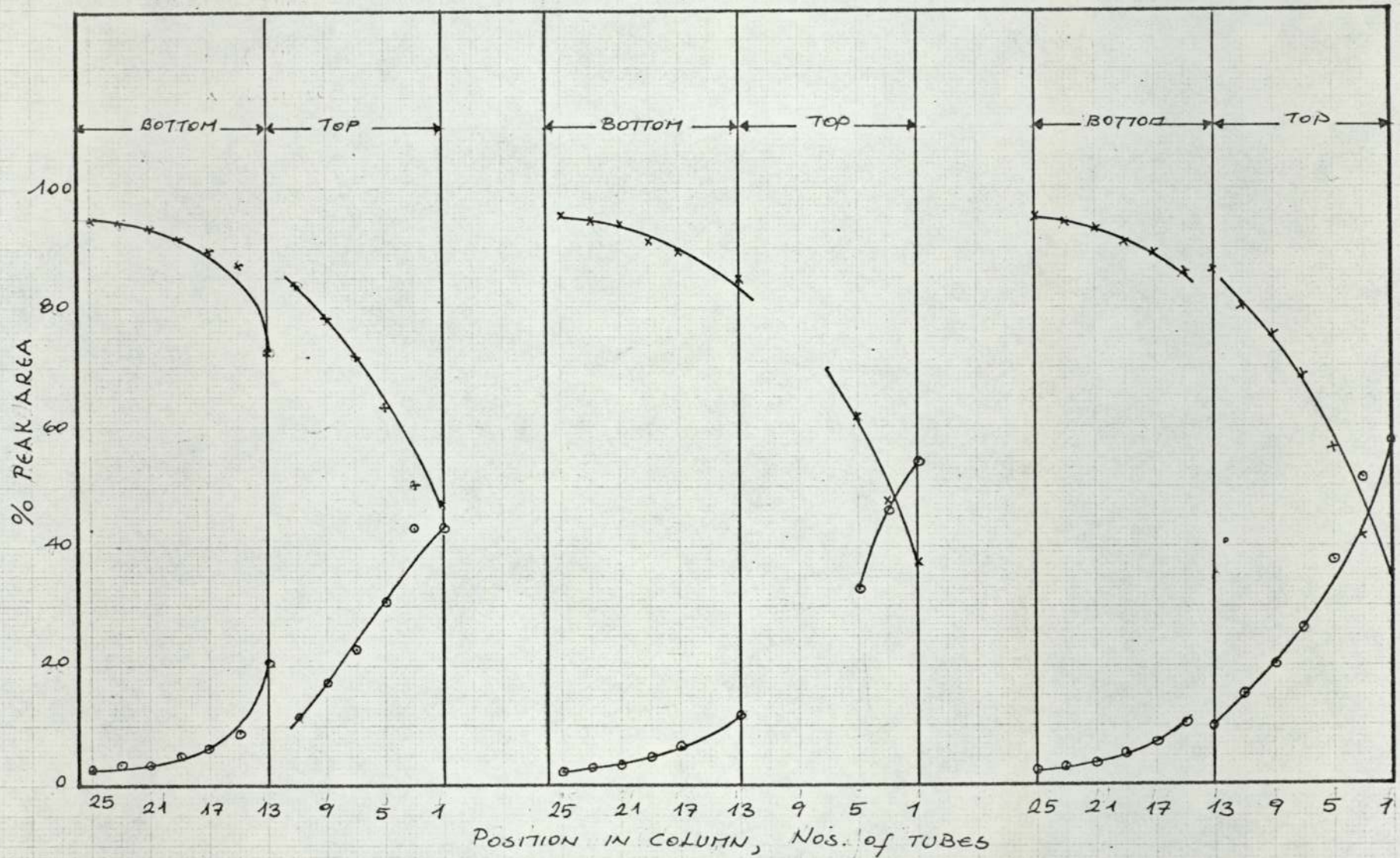

12-3-6 VAPOUR PHASE COMPOSITION PROFILE IN THREE CONSECUTIVE CYCLES, RUN 3

Table 12.3.7. Variation of Product Purities with Time.

Time of Collection h	Collection Rates cm^3/h			Top Product Composition %			Bottom Product Composition %		
	Top	Bottom	Total	α-Pinene	Camphene	β-Pinene	α-Pinene	Camphene	β-Pinene
10th	4.4	17.0	21.4	87.9	4.9	7.2	-	1.0	99.0
11th	3.85	20.0	23.85	87.7	5.0	7.3	-	1.0	99.0
12th	3.50	18.5	22.0	87.2	5.3	7.5	-	1.1	98.9
13th	3.9	17.5	21.4	85.9	5.4	8.7	-	0.9	99.1
14th	3.7	17.5	21.2	86.9	4.8	8.3	-	1.0	99.0
15th	4.0	-	-	88.4	4.5	7.1	-	0.8	99.2
16th	3.45	16.0	19.45	89.4	4.5	6.1	-	1.0	99.0

12.4 Discussion.

In discussing the operation of the rotating chromatograph, a distinction must be made between the liquid samples from the traps, that are a mean of one hour of operation, and the gas samples that give point values in the time domain.

The fact that the trap collection rates as well as the product purities varied from one cycle to the next was proof of changing stripping factors (G/LK) with time. Since the column rotation rate was constant throughout each run, only the gas rate (G) and the partition coefficient (K) could cause the fluctuations. As pointed out earlier, the fluctuations in G were very much a random affair, completely at the mercy of the mechanical seals functioning properly. As such there was no guarantee that the gas rates in one cycle would be duplicated in the following cycles.

There were two reasons for the changes in the value of K. The first one was the temperature fluctuations which followed a sinusoidal pattern with a frequency of about 2 cycles/h and am amplitude of $2^{o}C$. It is difficult to visualise the effect of such a fluctuation, but since the pattern was stable over the whole run it may not have had an overall effect on the results. The second reason, which may have had a bigger part to play, concerned the irregular feed rate. As seen from the Tables 12.3.2, 12.3.5 and 12.3.7, the total collection rate varied during the runs, so that 35-50% of the pumped feed volume was lost. The reason for this was undoubtedly the leakage from the feed port. One could actually see the liquid bubbling from the sides of the graphlon ring. As the partition coefficient of the pinenes are concentration dependent, a changing feed rate at a constant gas rate would be expected to alter the values of K throughout the column.

The spurious results of the gas samples, particularly from the bottom off-take, have a more interesting origin which the computer simulation

discussed in Appendix A.10 greatly helped to explain. It concerns the sequential operation of the apparatus which can be understood with reference to Figs. 12.4.2 and 12.4.1. They show the expected concentration levels in the top and the bottom off-takes with time.

As explained in Appendix A.10, the movement of the column past the product ports can be represented as a sequential advance of two tubes in a time $\theta = \frac{2t}{44}$. Within the time θ the column operates as a batch process. In the top off-take, at the end of θ two fresh beds are introduced into the gas stream, the concentration profile is then represented by a break through curve. Since there are two off-take points, the concentration level never comes down to the baseline. In the bottom off-take, the process is a reverse of this with the difference that the profiles are likely to be slimmer because of a higher gas flow rate in the stripping section. With enough gas flow rate the concentration level may even come down to zero before the next pair of beds are introduced.

The result of all these variations is that, unless the sample is taken at a particular point in time within each θ, the concentrations as well as the composition of the products will be different. The variations will be particularly severe in the bottom off-take where the concentration may change from a very high value down to zero. In support of this analysis, it can be seen that in Run 3, where the stripping rate was smaller than the other two runs, the bottom off-take concentrations were relatively steadier. With θ = 2.73 minutes in the present work, the time spacing between the samples needed to be accurate to within a few seconds. This sort of accuracy was impossible to achieve, partly because of the uncertainty in the timing of the valve operations as well as the inevitable time lag in the sample lines. The latter could not be controlled with a precision because of the practical difficulty of regulating the flow rate of a solute carrying stream. For the same

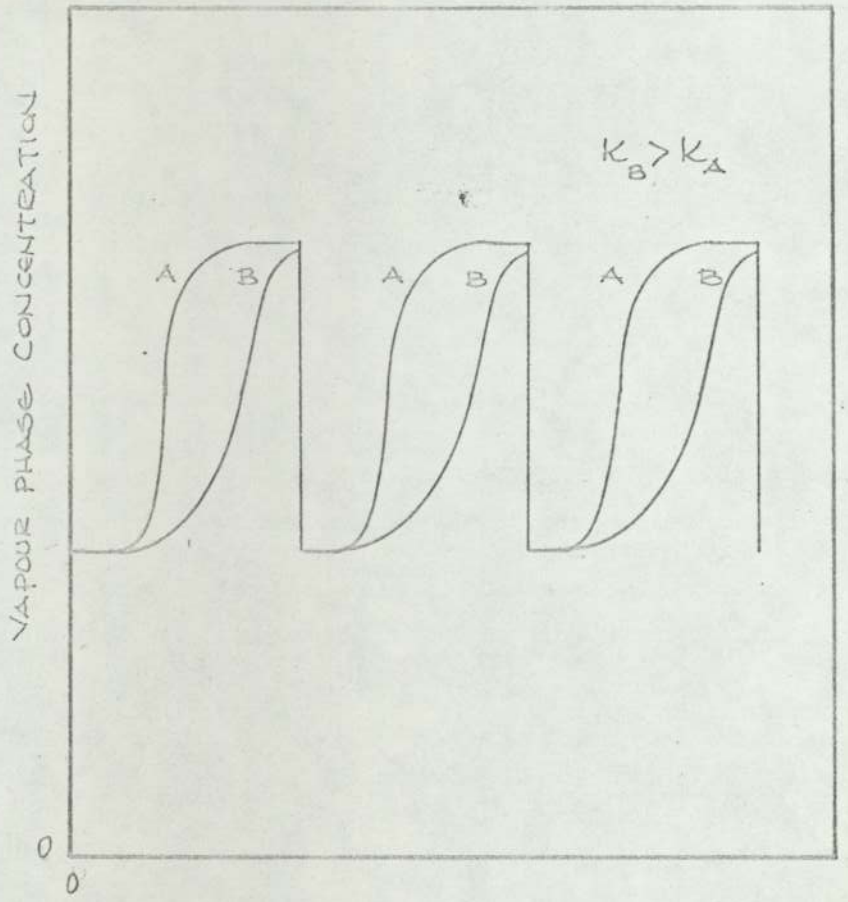

FIG. 12.4.1- TOP PRODUCT CONCENTRATION PROFILE

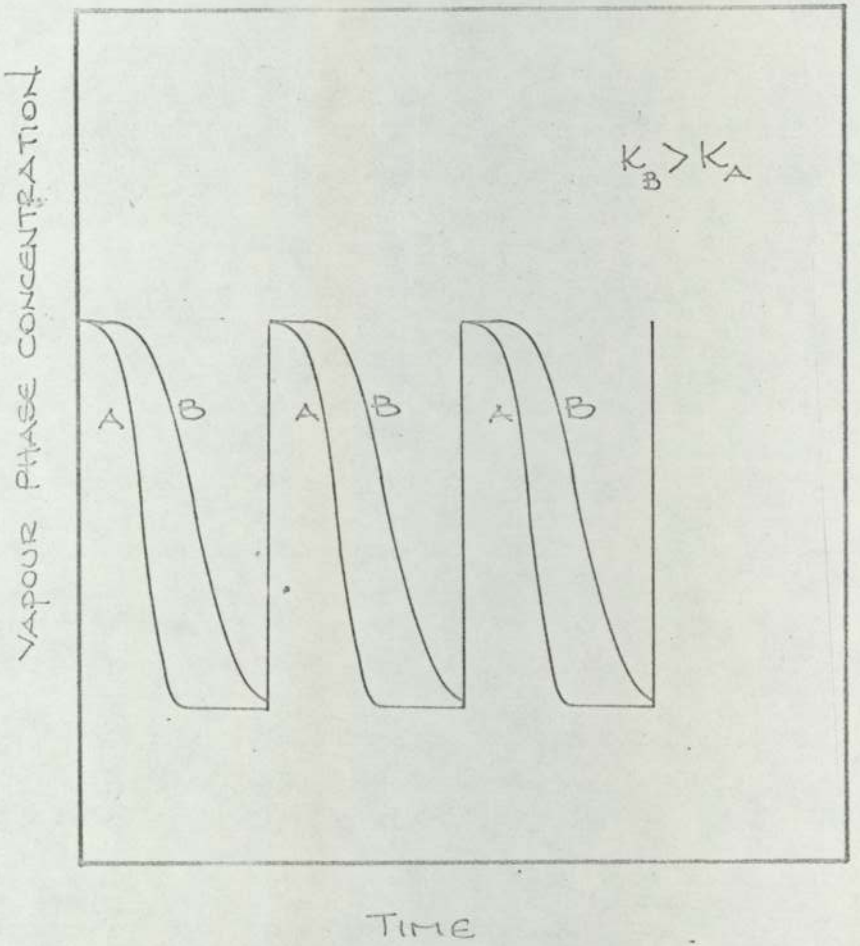

FIG. 12.4.2- BOTTOM PRODUCT CONCENTRATION PROFILE

reason the above theory could not be verified experimentally in the present work, but working with low boiling mixtures of Arklone-P and Genklene-P, Deeble (179) was able to monitor continuously the product streams and show that the theory was, in fact, correct.

The computer programme also offered a means of evaluating efficiency in terms of the'chromatographic plate' concept. This could be done by varying the number of plates in the programme until the experimental and predicted concentration profiles matched, but unfortunately the programme in the present state is very time consuming. Another approach would be an experimental one of measuring the peak width of a batch sample. Either approach is complicated by non-linearity, and the known difference between the batch plate and continuous plate concepts further clouds the issue. In any case, reliable and precise experimental data is needed before any of these approaches can be exploited.

13. CONCLUSION.

The limited amount of runs carried out with a pinene mixture showed that high purities could be achieved with a separation factor of about 1.6. No efficiency data could, however, be evaluated. The reason was twofold. The first one was the problem of leakage which could not be overcome without a major redesign and which prevented the stable operation of the chromatograph. The other, although it posed considerable practical difficulties, was more of a fundamental in nature. It arose from the transient behaviour of the system and as such the normal chemical engineering concepts of efficiency could not be applied. A computer programme developed to simulate the process did offer some hope of applying 'the chromatographic plate concept'. However, this could not be achieved in the present work because of a lack of reliable data as well as the excessive computer time required.

APPENDIX A.1.

Definition of the Terms in Equation 3.1.7.

$$j = J_3^{\,2}\left[1 + \frac{y_o^{\,2} p_o B_{22}(J_3^{\,2}-1)}{RT}\right] \qquad (A.1.1)$$

$$J_3^{\,2} = \frac{3}{2}\left[\frac{(p_i/p_o)^2-1}{(p_i/p_o)^3-1}\right] \qquad (A.1.2)$$

$$a = \frac{b_2^{\,1}}{b_3^{\,2}}\left[1 + \frac{2y_o p_o B_{22}(1-y_o J_2^{\,1})}{RT}\right] \qquad (A.1.3)$$

$$b_n^{\,m} = 1 + k(1-J_n^{\,m} y_o) \qquad (A.1.4)$$

APPENDIX A.2.

Carrier Flow Rate Calibration for Detector 'A'.

Table A.2.1. Carrier Flow Rate versus Pressure Drop Across Column 2.A at different Temperatures.

Temperature °C	Flow Rate at NTP, cm^3/min	Pressure Drop mm CCl_4
100	8.05	202.0
	9.37	234.0
	9.66	242.5
	9.45	253.0
	9.90	247.5
	10.88	271.0
	11.67	290.5
	12.19	304.5
	13.92	348.5
	14.37	357.5
	15.78	392.0
110	8.34	222.0
	8.52	227.5
	8.98	238.5
	9.40	249.0
	10.04	268.5
	10.73	284.5
	11.06	296.0
	11.90	312.5
	12.38	329.0
	12.91	345.0
	13.31	355.0
	13.97	362.5
	14.58	388.0
	15.65	415.5
	16.69	441.0

Continued ...

Table A.2.1. Continued.

120	8.18	223.5
	9.13	250.0
	9.94	271.0
	10.35	282.5
	11.16	304.5
	13.30	355.0
	13.67	370.5
	14.25	384.0
	14.75	399.0
	15.99	431.5
	16.56	446.5
150	8.05	245.0
	8.96	274.5
	9.84	305.0
	10.55	319.5
	11.43	347.0
	11.82	357.5
	11.93	361.0
	12.85	390.5
	13.94	421.0
	14.59	439.5
	14.93	452.0

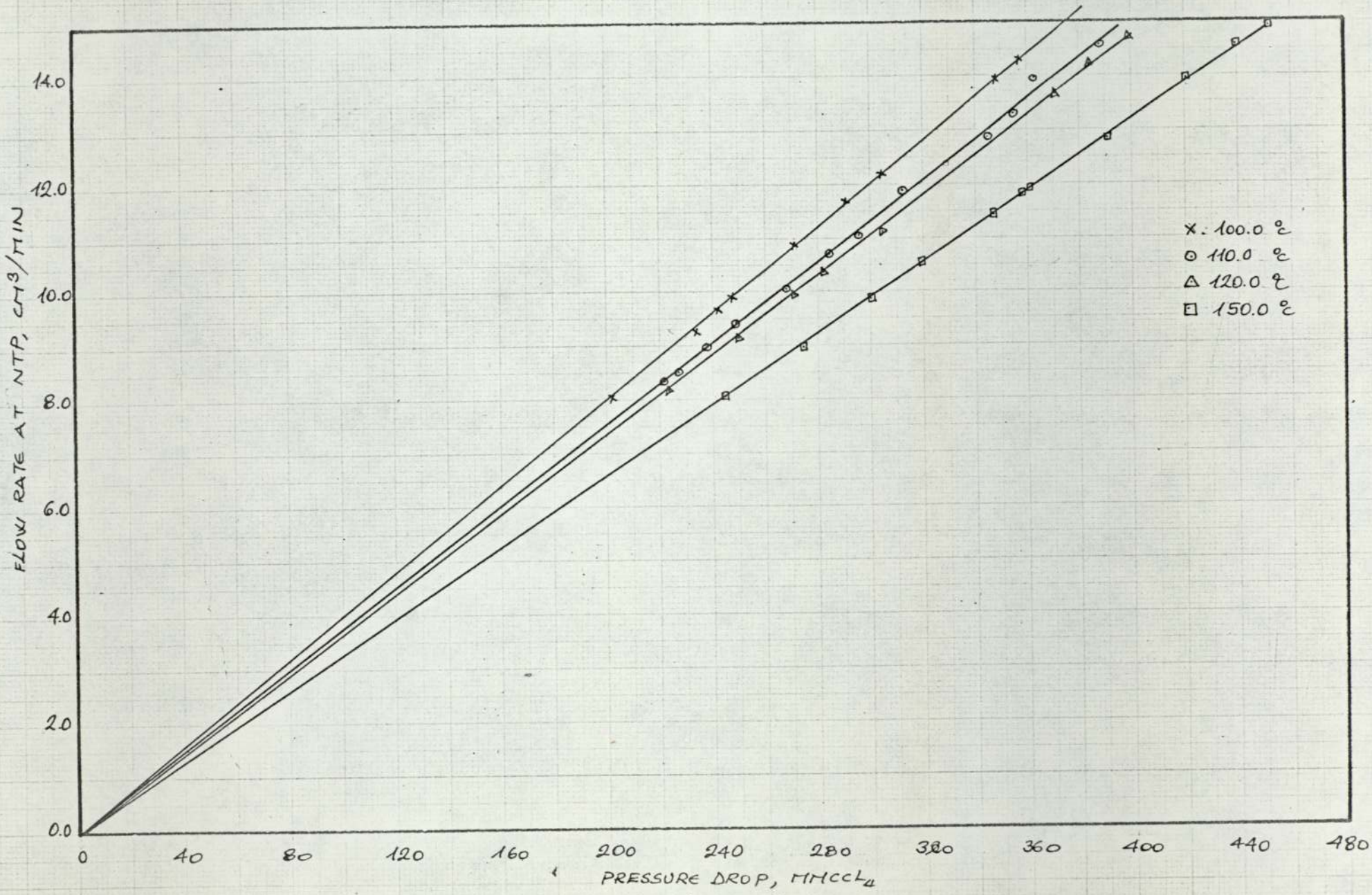

FIG. A.2.1. CARRIER FLOW RATE CALIBRATION of COLUMN 2-A

Table A.2.2. Carrier Flow Rate versus Pressure Drop Across Column 3.A. at Different Temperatures.

Temperature °C	Flow Rate at NTP, cm^3/min	Pressure Drop mm CCl_4
24.8	29.99	752.5
	30.91	774.5
	31.55	788.5
	33.39	833.5
	34.88	872.0
	35.42	882.5
	35.78	892.5
	36.60	912.0
	37.26	927.5
	38.11	945.0
	38.49	956.0
	38.75	958.0
29.0	23.58	607.5
	23.96	609.0
	26.06	658.5
	26.94	677.5
	27.75	701.0
	28.91	727.5
	30.19	758.5
	30.39	764.0
	30.50	767.0
	31.51	789.5
	32.24	807.5
	32.55	814.0
	33.06	831.5
	34.15	854.5
	35.65	888.0
	36.70	917.5
	38.87	968.5
34.7	14.54	392.5
	14.49	392.5
	18.92	507.5
	18.87	507.5

Continued ...

Table A.2.2. Continued.

	21.69	580.0
	21.73	581.5
	25.65	684.5
	25.66	685.5
	27.35	727.5
	27.42	730.5
	30.37	806.0
	30.63	813.0
39.8	11.92	335.5
	13.22	371.5
	15.72	439.0
	17.88	497.0
	20.38	564.5
	23.39	647.5
	27.53	755.5
	29.78	817.0
	30.89	847.0
	31.18	852.0
	31.82	867.5
	31.88	869.5
45.2	13.33	386.0
	13.36	387.0
	16.58	474.4
	16.60	476.5
	19.07	548.0
	20.81	598.0
	23.12	662.5
	26.59	756.0
	29.87	847.0
	29.98	849.0
60.5	11.28	351.5
	13.13	406.5
	13.13	408.5
	16.78	519.0
	16.82	520.0

Continued ...

Table A.2.2. Continued.

	18.95	581.0
	18.88	581.0
	21.08	648.0
	21.13	648.0
	23.18	710.5
	23.25	712.0
	27.38	834.5
	27.53	840.5
	27.74	846.5
74.0	9.32	313.5
	10.23	344.5
	10.75	361.5
	13.38	447.0
	14.46	489.5
	14.71	492.0
	16.45	547.0
	19.40	640.5
	23.05	756.0
	25.03	819.0
	25.15	822.0
	25.25	826.0

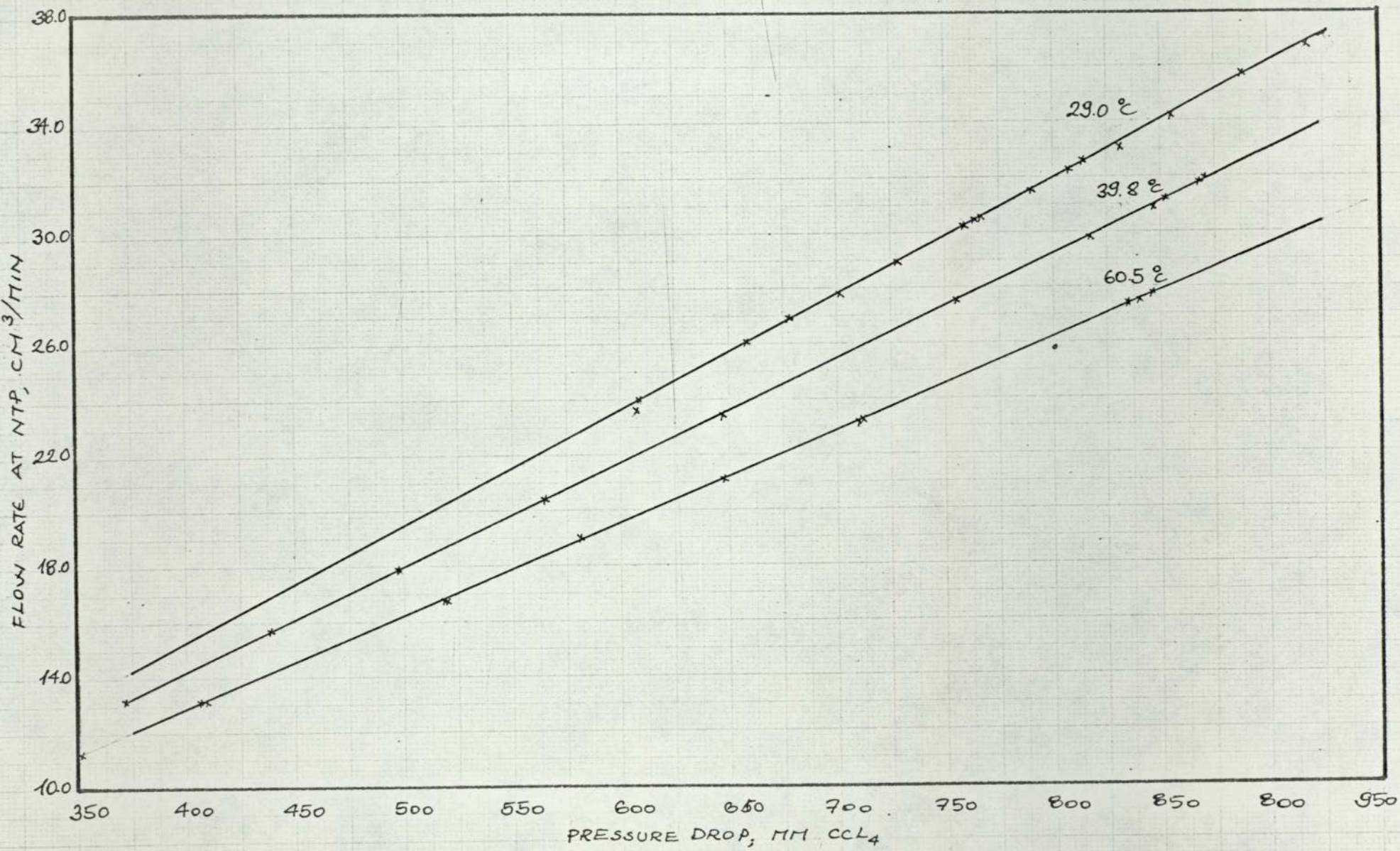

FIG A.2.2. CARRIER FLOW RATE CALIBRATION OF COLUMN 3-A

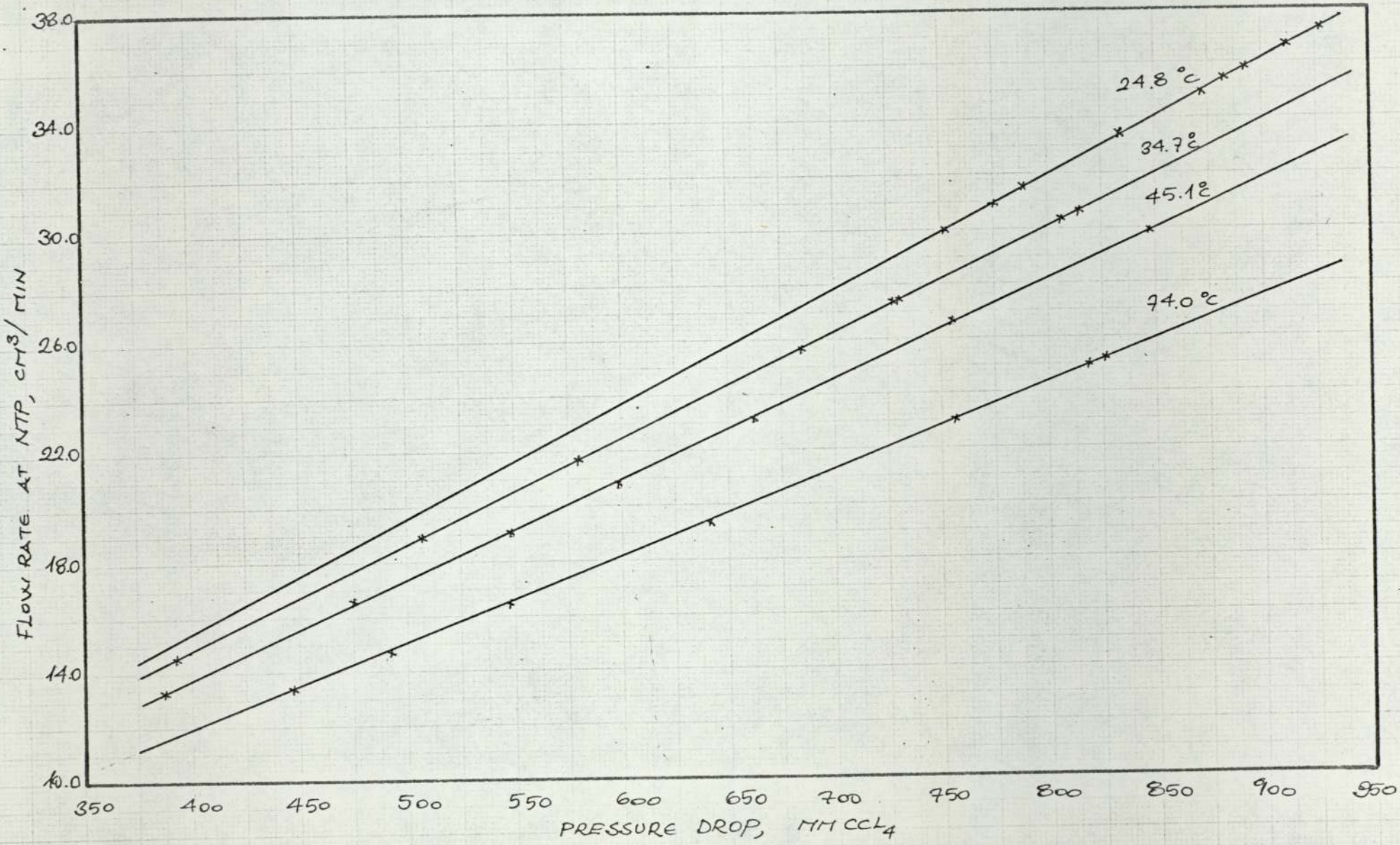

FIG. A.2.2 CARRIER FLOW RATE CALIBRATION OF COLUMN 3-A

APPENDIX A.3.

Densities.

Table A.3.1. Density of the Manometer Fluid.

t °C	18.0	21.0	24.0	26.0
ρ g/cm^3	1.5805	1.5750	1.5693	1.5635

Table A.3.2. Densities of the Halocarbons.

Dichloromethane		Arklone-P		Genklene-P	
t °C	ρ g/cm^3	t °C	ρ g/cm^3	t °C	ρ g/cm^3
22.0	1.3197	22.0	1.5719	22.0	1.3344
27.0	1.30855	27.0	1.5554	35.0	1.3126
32.0	1.3020	32.0	1.5453	60.0	1.2753

Table A.3.3. Densities of the Pinenes.

α-Pinene		β-Pinene	
t °C	ρ g/cm^3	t °C	ρ g/cm^3
27.0	0.85142	22.0	0.68816
60.0	0.82304	35.0	0.85702
80.0	0.81145	80.0	0.81964

Table A.3.4. Density of Polypropylene Sebacate.

t °C	20.0	100.0	110.0	120.0	130.0	140.0	150.0
ρ g/cm^3	1.0635	1.0108	1.0048	0.9975	0.9899	0.9830	0.9778

Table A.3.5. Density of Silicone Oil MS 200.

t °C	30.0	40.0	50.0	60.0	70.0	80.0
ρ g/cm^3	0.9590	0.9505	0.9416	0.9334	0.9247	0.9162

APPENDIX A.4

The Gas Phase Viscosities of Pure Solutes and Mixtures.

1. Dichloromethane/Arklone-P/Genklene-P.

The vapour viscosities of these compounds were calculated from the Bromley-Wilke equation(112),

$$\mu = \frac{33.3(M\,T_c)^{\frac{1}{2}}}{V_c^{2/3}}\; f(1.33\,T_r) \qquad (A.4.1)$$

where $$f(1.33\,T_r) = 1.058\,T_r^{0.645} - \frac{0.261}{(1.9\,T_r)^{0.9\log(1.9\,T_r)}} \qquad (A.4.2)$$

M is the molecular weight

T_c is the critical temperature in ^{o}K

V_c is the critical volume in $cm^3/g\text{-mole}$

T_r is the reduced temperature, T/T_c

μ is the viscosity in micropoise

The critical constants of these compounds are listed in Appendix A.7.

The expected accuracy of equation (A.4.1) is 3%(113a). This was checked by calculating the viscosity of a structurally similar compound, namely chloroform, for which experimental data is available. The results are presented in Table A.4.1.

Table A.4.1. Viscosity of Chloroform Vapour versus Temperature.

Temperature ^{o}C	Experimental Viscosity, cp	Calculated Viscosity, cp	% Error
25.0	0.01017	0.01012	0.50
50.0	0.01100	0.01096	0.32
75.0	0.01182	0.01184	0.16

The experimental critical data used in the above calculation was obtained from Reference(189). Although some of the critical data for the three halocarbons used in this work had to be calculated from other physical data, in view of the agreement shown in Table A.4.1, the calculated viscosities for these three compounds are expected to be accurate to at least 1.0%. These are tabulated in Table A.4.2.

Table A.4.2. Vapour Viscosities of Dichloromethane, Arklone-P, Genklene-P versus Temperature.

Temperature °C	Calculated Viscosities, cp		
	DCM	A-P	G-P
24.8	0.010064	0.010888	
29.1	0.010210	0.01105	
34.7	0.010410	0.011261	
39.8	0.10587	-	0.009763
45.1	-	-	0.010104
60.5	-	-	0.010609
74.0	-	-	0.011052

2. β-Pinene.

In the absence of any experimental critical data, and in view of its more complex structure which makes it difficult to calculate such data, the simpler but somewhat less accurate Arnold's Equation (111) was used to calculate the vapour phase viscosity of β-pinene,

$$\mu = \frac{27.0 \; M^{\frac{1}{2}} \; T^{3/2}}{V_b^{2/3}(T + 1.47 \; T_b)} \qquad (A.4.3)$$

where T_b is the boiling point, °K

V_b is the molar volume at the boiling point, cm^3/g-mole.

The expected accuracy of equation (A.4.3) is 5-6%(113a).This was again checked with cyclohexane which forms the basic structural unit of the pinenes. The results are given in Table A.4.3.

Table A.4.3. Vapour Viscosity of Cyclohexane versus Temperature.

Temperature °C	Experimental Viscosity, cp	Calculated Viscosity, cp	% Error
50.0	0.00770	0.007134	-7.3
100.0	0.00878	0.008356	-4.8
150.0	0.00986	0.009557	-3.1

V_b for β-pinene was calculated from the experimental density data, (Appendix A.3), extrapolated to its boiling point. Since a similar procedure was employed for cylcohexane, an error of the same order of magnitude as in Table A.4.3 is expected in the calculated viscosity values of β-pinene vapour. These are tabulated in Table A.4.4.

Table A.4.4. Vapour Viscosity of β-Pinene.

Temperature °C	Calculated Viscosity cp
100.0	0.007122
110.0	0.007339
120.0	0.007553
140.0	0.008194

3. Nitrogen.

The viscosity of nitrogen is widely available in the literature(113b,190). However, equation (A.4.1) was found to describe the experimental data with an average error of 3.0%. Since most of the calculations were performed on a digital computer it was expedient to use equation (A.4.1) to calculate

the viscosities of both nitrogen and the three halocarbon compounds.

Table A.4.5. Viscosity of Nitrogen versus Temperature.

Temperature ^{o}C	Calculated Viscosity cp
24.8	0.017083
29.1	0.017269
34.7	0.017510
39.8	0.017727
45.1	0.017952
60.5	0.018594
74.0	0.019146
100.0	0.020180
110.0	0.020414
120.0	0.020777
150.0	0.022080

4. Nitrogen-Solute Vapour Mixtures.

The viscosities of low pressure gas mixtures can be calculated either from equation (A.4.4),(113a)

$$\mu(y) = \frac{\sum y_i \mu_i (M_i)^{\frac{1}{2}}}{\sum y_i (M_i)^{\frac{1}{2}}} \qquad (A.4.4)$$

or from the somewhat more accurate but more complicated Wilke equation(191)

$$\mu(y) = \frac{\mu_1}{1 + \frac{(y_2/y_1)\left[1 + (\mu_1/\mu_2)^{\frac{1}{2}}(M_2/M_1)^{\frac{1}{4}}\right]^2}{(4/\sqrt{2})\left[1 + (M_1/M_2)\right]^{\frac{1}{2}}}} + \frac{\mu_2}{1 + \frac{(y_1/y_2)\left[1 + (\mu_2/\mu_1)^{\frac{1}{2}}(M_1/M_2)^{\frac{1}{4}}\right]^2}{(4/\sqrt{2})\left[1 + (M_2/M_1)\right]^{\frac{1}{2}}}} \qquad (A.4.5)$$

With the present mixtures it was found that equations (A.4.4) and (A.4.5) gave almost identical results. Therefore, the simpler equation (A.4.4) was used. This equation is well tested with hydrocarbon mixtures and industrial multicomponent mixtures and was found to represent the data uniformly within about 2% (113a).

APPENDIX A.5.

Molecular Weight Determination of Polypropylene Sebacate.

A.5.1 Definitions of Polymer Molecular Weights.

A sample of high molecular compound whether natural or synthetic always consists of a mixture of molecules of different molecular weights depending on the conditions of isolation, purification or synthesis.

The following three average molecular weights proposed by Lansing and Kraemer(192)are the most commonly used parameters in the characterisation of polymers.

1. Number average molecular weight (M_n) defined by

$$\bar{M}_n = \frac{\sum M_x N_x}{\sum N_x} \qquad (A.5.1)$$

where N_x is the number of molecules having the molecular weight of M_x.

2. Weight average molecular weight ($\bar{M}_w$) defined by

$$\bar{M}_w = \frac{\sum M_x^2 N_x}{\sum M_x N_x} \qquad (A.5.2)$$

3. Z-average molecular weight ($\bar{M}_z$) defined by

$$\bar{M}_z = \frac{\sum M_x^3 N_x}{\sum M_x N_x} \qquad (A.5.3)$$

A fourth molecular weight is the viscosity average molecular weight defined as

$$\bar{M}_v = \left[\frac{\sum C_i M_i^a}{\sum C_i} \right]^{1/a} \qquad (A.5.4)$$

where C_i is a constant corresponding to the molecular weight M_i, and a is the exponent in the Mark-Houwink equation.

In practice different methods of determination are used to calculate the above molecular weights.

For a monodisperse product all average values are equal , but for a polymer

$$\bar{M}_z > \bar{M}_w > \bar{M}_v > \bar{M}_n$$

In this work the viscosity average molecular weight was determined by the method of intrinsic viscosity.

A.5.2 Calculation of the Viscosity Average Molecular Weight of Polypropylene Sebacate.

Staudinger was the first to notice the dependence of the viscosity of dilute polymer solutions on their molecular weight and attempted to express it quantitatively(193) by

$$[\mu] = KM \qquad (A.5.5)$$

where K is a constant.

The intrinsic viscosity $[\mu]$ is defined according to the relationships;

$$\mu_{rel} = \frac{\text{dynamic viscosity of solution}}{\text{dynamic viscosity of solvent}}$$

$$\mu_{sp} = \mu_{rel} - 1$$

and $$[\mu] = \left[\mu_{sp}/c \right]_{c \to o}$$

where c is the concentration of the polymer in solution.

Extensive studies by later workers particularly Mark(193),Houwink(194) and by Batzer(195)showed that the most general equation (known as Mark-Houwink equation) expressing the dependence of the intrinsic viscosity on the molecular weight is

$$[\mu] = KM^a \qquad (A.5.6)$$

where a is another constant which is somewhat dependent on the molecular weight.

In this work the intrinsic viscosities of polypropylene sebacate in two solvents, benzene and chloroform, were calculated from the viscosity measurements carried out in this department using an Ostwald viscometer at 20°C. The results are shown in Tables A.5.1 and A.5.2 and plotted in Figs. A.5.1 and A.5.2.

From Fig. A.5.1 for the Benzene - PPS solution $[\mu] = 0.1025$ $100cm^3/g$

and from Fig. A.5.2 for the Chloroform - PPS solution $[\mu] = 0.14299$ $100cm^3/g$

In the absence of any data on this polymer Mark-Houwink constants used in equation (A.5.6) were those for Poly(hexamethylene Sebacate)(196-198).

For Benzene $K = 6.22 \times 10^{-4}$ $a = 0.69$ at 20°C

For Chloroform $K = 7.25 \times 10^{-4}$ $a = 0.70$ at 20°C

The substitution of these values in equation (A.5.6) yielded the following values of $\bar{M}_v$

In Benzene $\bar{M}_v = 1633$

In Chloroform $\bar{M}_v = 1900$

The value of $\bar{M}_v$ from benzene measurement agrees very well with the value of $M_n = 1620$ obtained by the "Rubber and Plastics Research Association" (RAPRA) from GPC measurements based on a Polystyrene calibration. That the viscosity average molecular wt measured in this work should agree with the number average molecular wt of GPC measurements is not surprising in view of the fact that the above constants were obtained from an osmotic method which measures M_n (196-198).

A point of interest is the ratios of the molecular wts measured by RAPRA

$$\bar{M}_n : \bar{M}_w : \bar{M}_z = 1 : 1.95 : 3.07$$

These are very near to those predicted by Flory(199), $\bar{M}_n : M_w : \bar{M}_z = 1:2:3$, for the product of a polycondensation reaction that has gone to completion.

Table A.5.1. Viscosity of Benzene-PPS Solution versus Concentration of PPS.

Concentration g/100 cm^3	μ_{rel}	μ_{sp}/c 100 cm^3/g
0.5197	1.05329	0.1025
1.0343	1.09438	0.09125
1.5667	1.16588	0.10655
2.1007	1.21546	0.1025

Table A.5.2. Viscosity of Chloroform-PPS Solution versus Concentration of PPS.

Concentration g/100 cm^3	μ_{rel}	μ_{sp}/c 100 cm^3/g
0.5582	1.07901	0.14154
1.0266	1.15378	0.14979
1.5470	1.21395	0.13830
2.0280	1.28866	0.14230

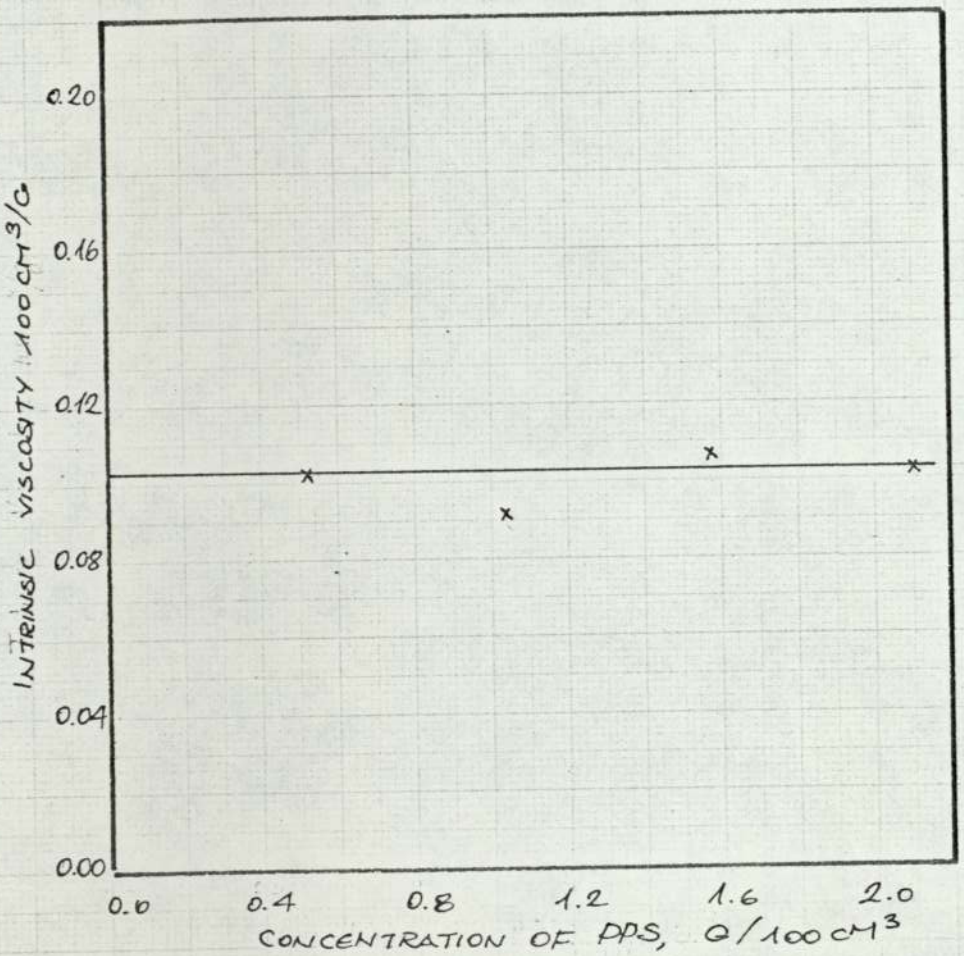

FIG: A.5.1 - INTRINSIC VISCOSITY OF BENZENE - PPS SOLUTION

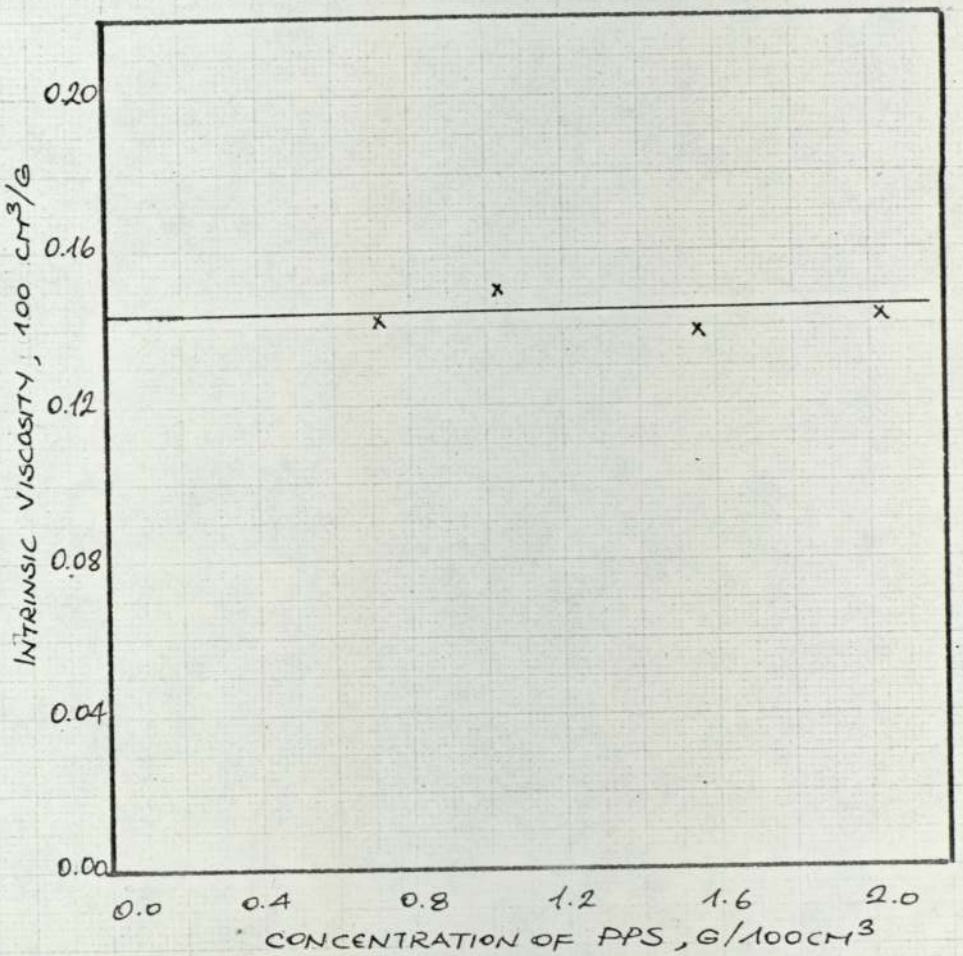

FIG. A.5.2. INTRINSIC VISCOSITY OF CHLOROFORM - PPS SOLUTION

APPENDIX A.6.

Calculations of the Second Virial Coefficients.

A.6.1 Pure Vapours.

Nitrogen

Dymond and Smith(123) compiled the data on the second virial coefficient of nitrogen obtained by different sets of workers and found them in good agreement. In this work their smoothed data was compared with the results obtained from the following equations

1. The Adlard equation (116)

$$B = 50.46 - \frac{1344.5}{0.08206T} - \frac{4.2 \times 10^7}{T^3} \qquad (A.6.1)$$

2. The three parameter Pitzer equation (127)

$$\frac{BP_c}{RT_c} = B_o^*(T_r) + w\, B_1^*(T_r) \qquad (A.6.2)$$

where w, the accentric factor is defined as

$$w \equiv - \log P^o/P_c \Big|_{T_r=0.7} - 1.0 = 0.040 \text{ for nitrogen(200)}$$

The reduced virial coefficient functions, B_o^* and B_1^*, are expressed as follows

$$B_o^* = 0.1445 - \frac{0.330}{T_r} - \frac{0.1385}{T_r^2} - \frac{0.0121}{T_r^3} \qquad (A.6.3)$$

$$B_1^* = 0.073 + \frac{0.46}{T_r} - \frac{0.50}{T_r^2} - \frac{0.097}{T_r^3} - \frac{0.0073}{T_r^8} \qquad (A.6.4)$$

Calculations showed that there was very little to choose between the two equations with the Adlard equation lying below the experimental data at low temperatures and above at higher temperatures, while the Pitzer equation behaving in the opposite manner. However, both equations represented the data within the experimental precision quoted by Dymond and Smith. The Pitzer equation was employed in this work to calculate the

second virial coefficients of nitrogen at various temperatures.

Halocarbons (Dichloromethane, Arklone-P, Genklene-P).

The data compiled by Dymond and Smith(123) on these halocarbons were assessed to be correct within 10% or 15 cm^3/mole. The following equations were used to correlate the data.

1. The McGlashen-Potter equation (97)

$$\frac{B}{V_c} = 0.430 - \frac{0.886}{T_r} - \frac{0.694}{T_r^2} - 0.0375\,(n-1)\left(\frac{1}{T_r}\right)^{4.5} \qquad (A.6.5)$$

This equation was originally developed for alkanes where n denotes the number of carbon atoms in the chain. For other compounds n may be calculated from the vapour pressure data, but Dantzler and Knobler (201), who used this equation with normal perfluorocarbons, found that the best fit was obtained with the actual value of n. They also found that while the fit was reasonable, the temperature dependence was incorrect. The calculated values were too positive at low temperatures and too negative at high temperatures. These findings were confirmed by the calculations carried out on Dichloromethane and the fit could not be improved by changing the value of n as expected from the form of the equation.

2. The Pitzer equation.

Using the values of w calculated from the vapour pressure data this equation gave values that were not negative enough.

3. The O'Connel Prausnitz equation (for polar fluids) (202)

$$\frac{P_c B}{RT_c} = B_o^*(T_r) + w_H\, B_1^*(T_r) + f_\mu\,(\mu_r, T_r) + \eta\, f_a(T_r) \qquad (A.6.6)$$

where w_H is the accentric factor of the polar molecule's homomorph (a non-polar molecular of about the same size and shape)

η is an empirical constant - a measure of the tendency to form dimers

$$\mu_r = \frac{10^5 \mu^2 P_c}{T_c^2}$$ where P_c is in atm. and T_c in ^oK

μ is the dipole moment in debyes

$$f(\mu_r, T_r) = -5.23722 + 5.665807(\ln\mu_r) - 2.133816(\ln\mu_r)^2 + 0.2525373(\ln\mu_r)^3 + \frac{1}{T_r}\left[5.76977 - 6.181427(\ln\mu_r) + 2.283270(\ln\mu_r)^2 - 0.264907(\ln\mu_r)^3\right] \quad \text{(A.6.7)}$$

$$f_a(T_r) = \exp\left[6.6(0.7 - T_r)\right] \quad \text{(A.6.8)}$$

This equation was employed to calculate the second virial coefficients of Dichloromethane and Arklone-P with the following values for the parameters taken from the author's paper:

Arklone-P	$w_H = 0.240$	$\mu = 1.40$	$\eta = 0.0$
Dichloromethane	$w_H = 0.152$	$\mu = 1.54$	$\eta = 0.320$

The results were too far off the experimental data. In fact all the calculated second virial coefficients were positive.

Another approach employed was to fit the equation to the experimental data to obtain the best fit values of the parameters w_H and η. With all the three halocarbons the best fit value of w_H was greater than unity and η negative. Even then the fit was not good. The change of B with temperature was too steep indicating an incorrect temperature dependence of the equation.

4. The Halm-Stiel equation. (125)

This equation like the previous one is an extension of the Pitzer equation to polar molecules,

$$\frac{BP_o}{RT_c} = B_o^*(T_r) + w\,B_1^*(T_r) + X^*B_2^*(T_r) + X^{*2}B_3^*(T_r) + w^6B_4^*(T_r) + wX^*B_5^* \quad (A.6.9)$$

where X^* is a constant characteristic of the polarity and is calculated from

$$X^* = \log P^o/P_c\Big|_{T_r=0.6} + 1.552 + 1.7w \quad (A.6.10)$$

The reduced coefficients, B_2^*, B_3^*, B_4^* and B_5^* are presented in a tabulated form by the authors. These values were correlated by 5th order polynomials in $(1/T_r)$ by a least square analysis. The constants of the polynomials are given below.

Table A.6.1.

Reduced Coefficient	C_0	C_1	C_2	C_3	C_4	C_5
B_2^*	-13756.0	50630.0	-73345.0	52097.0	-18061.0	2426.6
B_3^*	187440.0	-726730.0	1118700.0	-853560.0	322360.0	-48144.0
B_4^*	-11278.0	44513.0	-69908.0	54581.0	-21165.0	3256.0
B_5^*	23612.0	-86045.0	123030.0	-85851.0	29033.0	-3766.5

The calculations on Arklone-P and Genklene-P with the parameters calculated from the vapour pressure data showed that while the calculated values did not match the data, the temperature dependence was correct. Therefore, the parameters were recalculated by a least square analysis of the experimental data. These values together with those obtained from the vapour pressure data are shown below and the calculated second virial coefficients using the best fit values of the parameters are shown as continuous lines in Fig. A.6.1.

Table A.6.1.

	From Vapour Pressure Data		Best Fit Values	
	X*	w	X*	w
Dichloromethane	-	-	0.005925	-0.095735
Arklone-P	0.00592	0.25512	-0.002338	0.09116
Genklene-P	-0.004585	0.14552	-0.004382	0.12601

A.6.2 Vapour Mixtures.

The cross second virial coefficients of the vapour mixtures were also calculated through the Halm-Stiel equation using the following mixing rules

$$w_{12} = \frac{w_1 + w_2}{2} \tag{A.6.11}$$

$$X^*_{12} = \frac{X^*_1 + X^*_2}{2} \tag{A.6.12}$$

$$T_{c12} = \frac{\left[T_{c1}\, T_{c2}\, U^*(w_1, X^*_1)\, U^*(w_2, X^*_2)\right]^{\frac{1}{2}}}{U^{o}(w_{12}, X^*_{12})} \tag{A.6.13}$$

$$P_{c12} = T_{c12} \left[\frac{2\,\sigma^*(w_{12}, X^*_{12})}{\sigma^*(w_1, X^*_1)\left(\frac{T_{c1}}{P_{c1}}\right)^{\frac{1}{3}} + \sigma^*(w_2, X^*_2)\left(\frac{T_{c2}}{P_{c2}}\right)^{\frac{1}{3}}} \right]^3 \tag{A.6.14}$$

$$U^*(w, X^*) = 1.0 + 2.84w - 73.7\, X^* \tag{A.6.15}$$

$$\sigma^*(w, X^*) = 2.39 + 4.25w - 12.7w^2 - 71.4\, X^* \tag{A.6.16}$$

When nitrogen is one of the components its value for the parameter X* was taken as zero as it is a non-polar gas.

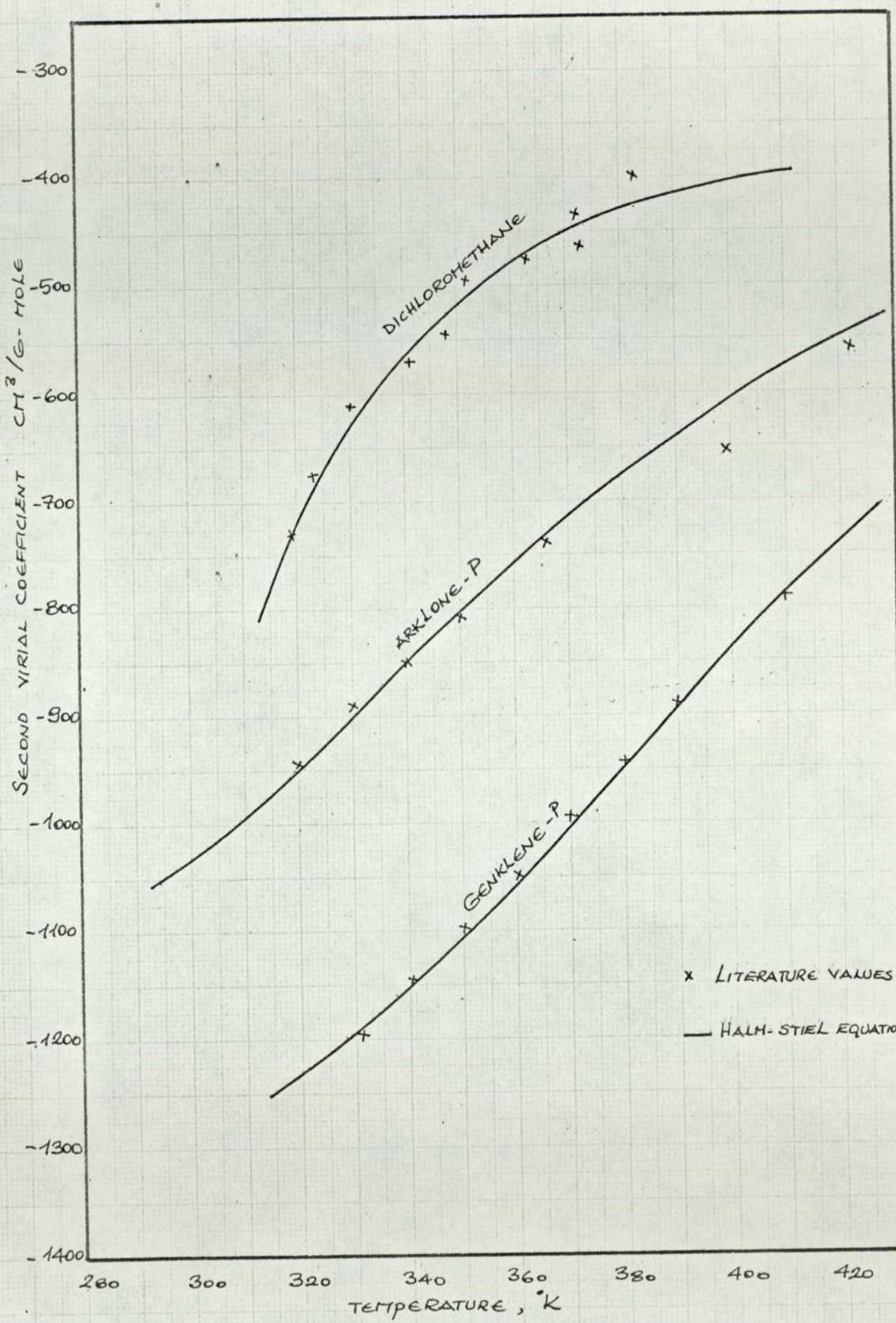

FIG. A.6.1 SECOND VIRIAL COEFFICIENT OF HALOCARBONS

APPENDIX A.7.

Calculations of the Critical Constants.

Experimental data on the critical constants of substances are rare in the literature, and with continual creation of many new compounds this situation is likely to remain. To overcome this problem numerous correlating equations have been developed to calculate them from other physical parameters. Unfortunately some of these equations require input parameters that are more difficult to find than the critical constants themselves. Thus, in the case of the pinenes these difficulties were found to be insurmountable and the attempt to calculate their critical constants was abandoned.

Some of the critical constants of the halocarbons used in this work were available in the literature. Those that were not available were calculated from equations whose reliabilities were checked by comparing their results for structurally similar compounds with the experimental data. These equations are briefly reviewed here and their results are summarised in Table A.7.1.

A.7.1 Critical Temperature T_c.

1. The Eduljee Method. (113c)

The critical temperatures of organic compounds are estimated by summing the additive contributions of Eduljee. The sum of the contributions denoted by $\sum\Delta T$ is then substituted into

$$T_c = \frac{T_b}{\sum\Delta T/100} \qquad (A.7.1)$$

where T_c and the boiling point temperature, T_b, is in ^{o}R

$\Delta T_C = -55.32$ $\Delta T_H = 28.52$ $\Delta T_{Cl} = 29.89$

$\Delta T_F = 29.75$

2. The Meissner and Redding Correlation. (203)

For substances containing halogens or sulphur and boiling above 235°K

$$T_c = 1.41\ T_b + 66\text{-}11\ F \qquad (A.7.2)$$

where T_c and T_b are in °K

F is the number of fluorine atoms in the molecule.

Table A.7.1 shows that the accuracy of these two equations are comparable and both seem to fit the experimental data better as the number of chlorine atoms is increased. Therefore, a value of 282°C for the critical temperature of Genklene-P may be expected to be accurate within 2%.

A.7.2 Critical Pressure P_c.

1. The Eduljee Method. (113c)

Critical pressure may be estimated by summing up the additive contributions of Eduljee

$$P_c = \frac{10^4 M}{(\Sigma \Delta P)^2} \qquad (A.7.3)$$

where P_c is in atm. absolute

$\Delta P_C = -9.35$ $\Delta P_H = 16.20$ $\Delta P_{Cl} = 4.80$ $\Delta P_F = 39.9$

2. The Meissner Method. (203)

$$P_c = 60.3\ T_c/(1.5\ |P| + 9 - 4.34\ [R_D])^{1.226} \qquad (A.7.4)$$

where P_c is in atm. and T_c in °K

$|P|$ is the Parochor contribution

$[R_D]$ is the molar refraction contribution

$\Delta P_C = 9.2$ $\Delta P_H = 15.4$ $\Delta P_{Cl} = 55$ $\Delta P_F = 25.5$

$[R_D]_C = 2.418$ $[R_D]_H = 1.100$ $[R_D]_{Cl} = 5.967$ $[R_D]_F = 1.1$

On the whole equation (A.7.3) seems to be more accurate than equation (A.7.4) with average accuracies of 2.5% and 5% respectively. The value calculated for Genklene-P from both equations, however, agree within 1%. Therefore, a value of P_c = 44 atm. is expected to be accurate to 3-4%.

A.7.3 Critical Volume V_c.

1. The Benson Correlation. (113c)

$$V_c = V_b\ (0.422 \log P_c + 1.981) \qquad (A.7.5)$$

where V_c and molar liquid volume at T_b, V_b are in cm^3/mole, P_c is in atm. V_b is estimated by summation of the additive contributions

$$V_b = \Sigma \Delta V_b \qquad (A.7.6)$$

$\Delta V_{bC} = 14.8$ $\Delta V_{bH} = 3.7$ $\Delta V_{bCl} = 21.6$ $\Delta V_{bF} = 8.7$

2. The Meissner and Redding Correlations. (203)

$$V_c = (0.377 \sum |P| + 11.0)^{1.25} \qquad (A.7.7)$$

where $|P|$ is the Parochor contribution.

Equation (A.7.5) seems to represent the experimental data better as the number of chlorine atoms increases while the reverse is true for equation (A.7.7), but for Dichloromethane they give almost identical results, and the average of these two values, 195 cm^3/mole, was taken to be the true value. Based on the same reasoning, the value for Genklene-P was taken to be 282 cm^3/mole as calculated from equation (A.7.5).

Table A.7.1. Critical Properties of Halocarbons.

	CRITICAL TEMPERATURE °C			CRITICAL PRESSURE Atm.			CRITICAL VOLUME cm^3/mole			Molecular Weight	Exp. Boiling Point °C	V_b cm^3/mole from Eqn A.7.6
	Exp.	Eqn A.7.1	Eqn A.7.2	Exp.	Eqn A.7.3	Eqn A.7.4	Exp.	A.7.5	A.7.7			
CH_3Cl	141.3			65.9			143.0	130.5	141.3			47.5
Dichloromethane	236.2	236.5	235.0	60.4	60.0	59.9	-	195.5	194.5	84.94	40.7	
$CHCl_3$	263.4			54.0			240.0	226.0	248.3			83.3
CCl_4	283.2			45.0			276.0	271.0	304.8			101.2
C_2H_5Cl	187.2	193.5	195.0	52.0	53.0	60.6	-	188.5	194.2	64.52	12.3	69.7
$1,1C_2H_4Cl_2$	250.0	264.5	258.5	50.0	49.0	53.3	-	236.3	244.9	98.97	57.4	87.6
$1,2C_2H_4Cl_1$	288.0	296.0	294.0	53.0	50.1	55.3	220.0	237.3	249.2	98.97	82.4	87.6
Genklene-P	-	281.0	282.5	-	44.3	43.8	-	282.2	302.1	133.92	74.1	105.5
Arklone-P	214.1	210.0	206.0	33.7	32.85	31.9	325.0			187.39	47.6	

APPENDIX A.8.

The Comparison of the Flory-Huggins and Heil Equations.

Table A.8.1. ∝-Pinene/Polypropylene Sebacate System.

Temperature	x_1	γ_1	
		Single-parameter Flory-Huggins	Two-parameter Flory-Huggins
99.8	0.0	0.2631	0.2551
	0.2815	0.3426	0.3372
	0.3176	0.3563	0.3517
	0.4403	0.4124	0.4115
	0.4574	0.4216	0.4214
	0.5036	0.4486	0.4509
	0.6050	0.5212	0.5319
RMSD		0.0127	0.00697
120.0	0.0	0.2353	0.2316
	0.1549	0.2704	0.2682
	0.2395	0.2943	0.2935
	0.2841	0.3087	0.3089
	0.3126	0.3187	0.3195
	0.3867	0.3477	0.3510
	0.3221	0.3221	0.3233
RMSD		0.0031	0.000978
140.0	0.0	0.2086	0.2080
	0.0682	0.2215	0.2210
	0.1159	0.2315	0.2310
	0.1501	0.2392	0.2389
	0.1824	0.2470	0.2468
	0.2451	0.2636	0.2636
	0.2507	0.2652	0.2652
	0.3360	0.2921	0.2925
	0.4588	0.3419	0.3432
RMSD		0.0006	0.000359

Continued ...

Table A.8.1. Continued.

150.0	0.0	0.2127	0.2120
	0.0897	0.2302	0.2299
	0.1139	0.2355	0.2353
	0.1492	0.2436	0.2436
	0.2175	0.2609	0.2614
	0.2606	0.2732	0.2740
RMSD			0.000159

Table A.8.2. β-Pinene/Polypropylene Sebacate

Temperature	x_1	γ_1	
		Single-parameter Flory-Huggins	Two-parameter Flory-Huggins
100.35	0.0	0.1936	0.1794
	0.3441	0.2746	0.2622
	0.4282	0.3059	0.2955
	0.4879	0.3326	0.3247
	0.6059	0.4018	0.4032
	0.6161	0.4091	0.4118
	0.6272	0.4174	0.4215
	0.6631	0.4465	0.4565
	0.6794	0.4610	0.4743
RMSD		0.0129	0.00337
110.1	0.0	0.1824	0.1800
	0.2743	0.2391	0.2371
	0.3668	0.2670	0.2655
	0.4124	0.2833	0.2822
	0.4810	0.3119	0.3156
	0.4864	0.3144	0.3141
	0.5427	0.3430	0.3436
	0.5637	0.3550	0.3560
	0.5742	0.3613	0.3626
	0.5868	0.3692	0.3708
RMSD		0.0055	0.00411
120.0	0.0	0.1726	0.1698
	0.2407	0.2183	0.2164
	0.3616	0.2518	0.2509
	0.4293	0.2754	0.2755
	0.4795	0.2960	0.2969
	0.5254	0.3176	0.3198
	0.5313	0.3206	0.3229
RMSD		0.0044	0.00267

Continued ...

150.0	0.0	0.1501	0.1501
	0.1006	0.1648	0.1648
	0.1301	0.1697	0.1697
	0.2045	0.1833	0.1833
	0.2912	0.2023	0.2022
RMSD		0.0023	0.00229

Table A.8.3. Dichloromethane/Silicone Oil MS 200.

Temperature °C	x_1	χ_1			
		Single-parameter Flory-Huggins	Two-parameter Flory-Huggins	*Two-parameter Flory-Huggins	Heil
24.8	0.0	0.05924	0.06056	0.05675	0.06066
	0.5119	0.1172	0.1189	0.1125	0.1191
	0.6366	0.1538	0.1554	0.1479	0.1555
	0.7227	0.1960	0.1969	0.1886	0.1970
	0.7525	0.2168	0.2172	0.2088	0.2173
	0.7933	0.2531	0.2525	0.2442	0.2526
	0.8238	0.2893	0.2872	0.2795	0.2873
RMSD		0.0016	0.00043		0.00047
29.1	0.0	0.05625	0.05653	0.05675	0.05653
	0.5040	0.1098	0.1101	0.1108	0.1011
	0.6125	0.1379	0.1383	0.1394	0.1383
	0.6925	0.1702	0.1704	0.1721	0.1704
	0.7622	0.2137	0.2137	0.2163	0.2137
	0.7827	0.2310	0.2308	0.2339	0.2308
	0.8207	0.2717	0.2712	0.2754	0.2713
RMSD		0.0004	0.00031		0.00031
34.7	0.0	0.05595	0.05603	0.05675	0.05603
	0.5592	0.1219	0.1219	0.1237	0.1220
	0.6333	0.1443	0.1444	0.1446	0.1444
	0.6798	0.1633	0.1633	0.1659	0.1634
	0.7388	0.1958	0.1958	0.1991	0.1958
	0.7778	0.2255	0.2255	0.2294	0.2254
	0.7971	0.2437	0.2436	0.2481	0.2436
RMSD		0.0002	0.0002		0.0002

Continued ...

Table A.8.3. Continued.

39.8	0.0	0.05565	0.05643	0.05675	0.05712
	0.4435	0.09747	0.09833	0.09946	0.09908
	0.5226	0.1125	0.1133	0.1149	0.1140
	0.6802	0.1626	0.1628	0.1661	0.1629
	0.7291	0.1887	0.1882	0.1928	0.1879
	0.7501	0.2026	0.2018	0.2070	0.2011
RMSD		0.002	0.0020	0.0046	0.0019

* Over the whole temperature range.

Table A.8.4. Arklone-P/Silicone Oil MS 200.

Temperature °C	x_1	γ_1			
		Single-parameter Flory-Huggins	Two-parameter Flory-Huggins	*Two-parameter Flory-Huggins	Heil
24.8	0.0	0.06939	0.06884	0.06624	0.06851
	0.2200	0.08778	0.08727	0.08384	0.08695
	0.3826	0.1092	0.1088	0.1043	0.1085
	0.4414	0.1197	0.1194	0.1144	0.1193
	0.5633	0.1496	0.1498	0.1432	0.1499
	0.6338	0.1749	0.1757	0.1675	0.1761
RMSD		0.0018	0.0013		0.0010
29.1	0.0	0.06517	0.06531	0.06624	0.06531
	0.3256	0.09455	0.09468	0.09609	0.09469
	0.5446	0.1357	0.1357	0.1378	0.1357
	0.6256	0.1616	0.1616	0.1642	0.1616
	0.6489	0.1711	0.1709	0.1738	0.1709
RMSD		0.0002	0.00016		0.00016
34.7	0.0	0.06473	0.06487	0.06624	0.06489
	0.3090	0.0918	0.09193	0.09393	0.09195
	0.4286	0.1095	0.1096	0.1121	0.1096
	0.5126	0.1267	0.1267	0.1296	0.1267
	0.5169	0.1277	0.1278	0.1307	0.1278
	0.5781	0.1444	0.1443	0.1477	0.1443
	0.6313	0.1628	0.1626	0.1665	0.1626
RMSD		0.0001	0.00006	0.0039	0.00006

* Over the whole temperature range.

Table A.8.5. Genklene-P/Silicone Oil MS 200.

Temperature °C	x_1	γ_1			
		Single-parameter Flory-Huggins	Two-parameter Flory-Huggins	*Two-parameter Flory-Huggins	Heil
34.7	0.0	0.06047	0.05832	0.05833	0.05764
	0.5516	0.1283	0.1250	0.1250	0.1239
	0.7376	0.2063	0.2032	0.2032	0.2021
	0.7997	0.2586	0.2567	0.2566	0.2560
	0.8252	0.2886	0.2877	0.2876	0.2874
	0.8547	0.3331	0.3344	0.3343	0.3348
	0.8795	0.3825	0.3870	0.3867	0.3886
RMSD		0.0037	0.0012		0.00079
45.1	0.0	0.06053	0.05973	0.05833	0.05902
	0.4750	0.1111	0.1102	0.1079	0.1092
	0.5902	0.1394	0.1385	0.1359	0.1376
	0.7054	0.1868	0.1863	0.1833	0.1859
	0.7713	0.2319	0.2322	0.2291	0.2325
	0.8093	0.2693	0.2705	0.2675	0.2717
RMSD		0.0016	0.0008		0.00023
60.5	0.0	0.0584	0.05801	0.05833	0.05790
	0.4681	0.1060	0.1056	0.1066	0.1056
	0.5632	0.1270	0.1268	0.1281	0.1268
	0.5802	0.1317	0.1315	0.1329	0.1315
	0.6561	0.1575	0.1576	0.1595	0.1577
	0.7108	0.1835	0.1838	0.1864	0.1841
RMSD		0.0004	0.0002		0.00008
74.0	0.0	0.05749	0.05764	0.05833	0.05806
	0.2778	0.07841	0.07855	0.07976	0.07892
	0.3941	0.09249	0.09260	0.09425	0.9289
	0.4896	0.1085	0.1086	0.1108	0.1087
	0.5657	0.1258	0.1258	0.1288	0.1257
	0.6551	0.1533	0.1531	0.1574	0.1525
RMSD		0.0005	0.0004	0.0021	0.00007

* Over the whole temperature range.

APPENDIX A.9

Calculated Activity Coefficients from the Ternary Flory-Huggins Equation.

Table A.9.1.

α-Pinene/β-Pinene/PPS

Temperature °C	x_2	γ_1^∞
100	0.0	0.2631
	0.3441	0.2673
	0.4282	0.2594
	0.4879	0.2497
	0.6059	0.2155
	0.6161	0.2114
	0.6272	0.2066
	0.6631	0.1892
	0.6795	0.1803
RMSD		0.022
120.0	0.0	0.2353
	0.2407	0.2350
	0.3616	0.2263
	0.4293	0.2170
	0.4794	0.2073
	0.5254	0.1960
	0.5313	0.1944
RMSD		0.0085
150	0.0	0.2127
	0.1006	0.2058
	0.1301	0.2031
	0.2045	0.1948
	0.2911	0.1816
RMSD		0.0021

β-Pinene/α-Pinene/PPS

Temperature °C	x_2	γ_1^∞
100	0.0	0.1936
	0.2816	0.1914
	0.3176	0.1893
	0.4403	0.1765
	0.4574	0.1739
	0.5036	0.1655
	0.6050	0.1389
RMSD		0.014
120.0	0.0	0.1726
	0.1549	0.1696
	0.2395	0.1654
	0.2841	0.1621
	0.3126	0.1595
	0.3221	0.1586
	0.3867	0.1509
RMSD		0.0041
150.0	0.0	0.1501
	0.08966	0.1509
	0.1139	0.1510
	0.1492	0.1508
	0.2175	0.1498
	0.2606	0.1486
RMSD		0.00064

Table A.9.2.

DCM/Arklone-P/Silicone Oil

Temperature °C	x_2	γ_1^∞
24.8	0.0	0.05924
	0.2200	0.06314
	0.3826	0.06408
	0.4414	0.06346
	0.5633	0.05906
	0.6338	0.05342
RMSD		0.0033
29.1	0.0	0.05625
	0.3256	0.06162
	0.4575	0.06130
	0.5466	0.05878
	0.6256	0.05375
	0.6489	0.05156
RMSD		0.0036
34.7	0.0	0.05595
	0.3090	0.05995
	0.4286	0.05929
	0.5126	0.05701
	0.5169	0.05683
	0.5781	0.05352
	0.6313	0.04913
RMSD		0.0033

Arklone-P/DCM/Silicone Oil

Temperature °C	x_2	γ_1^∞
24.8	0.0	0.06939
	0.5119	0.08446
	0.6366	0.08046
	0.7224	0.06990
	0.7525	0.06363
	0.7933	0.05231
	0.8238	0.04157
RMSD		0.012
29.1	0.0	0.06517
	0.5041	0.07958
	0.6125	0.07740
	0.6925	0.07060
	0.7622	0.05808
	0.7827	0.05278
	0.8207	0.04071
RMSD		0.011
34.7	0.0	0.06473
	0.5593	0.07722
	0.6333	0.07384
	0.6798	0.06951
	0.7388	0.06029
	0.7778	0.05117
	0.7971	0.04563
RMSD		0.0094

Table A.9.2. Continued.

DCM/Genklene-P/Silicone Oil

Temperature °C	x_2	γ_1^∞
34.7	0.0	0.05595
	0.5516	0.07479
	0.7376	0.06782
	0.7997	0.05628
	0.8252	0.04900
	0.8547	0.03844
	0.8879	0.02421
RMSD		0.015

Genklene-P/DCM/Silicone Oil

Temperature °C	x_2	γ_1^∞
34.7	0.0	0.06047
	0.5593	0.06933
	0.6333	0.06538
	0.6798	0.06080
	0.7388	0.05162
	0.7778	0.04294
	0.7971	0.03781
		0.0095

Arklone-P/Genklene-P/Silicone Oil

Temperature °C	x_2	γ_1^∞
34.7	0.0	0.06473
	0.5516	0.08656
	0.7376	0.07856
	0.7997	0.06523
	0.8252	0.05683
	0.8547	0.04462
	0.8795	0.03252
RMSD		0.016

Genklene-P/Arklone-P/Silicone Oil

Temperature °C	x_2	γ_1^∞
34.7	0.0	0.06047
	0.3090	0.06183
	0.4286	0.05926
	0.5126	0.05524
	0.5169	0.05497
	0.5781	0.05021
		0.0028

APPENDIX A.10

Plate Model

The model discussed here is basically an attempt at simulating the later versions of the rotating chromatographs developed by Barker (170, 172) As explained earlier, in these chromatographs the stationary phase is exposed to the solute carrying gas stream in finite volumes. Therefore, the basic process is very similar to what is usually termed as "frontal elution chromatography". The overall behaviour of the chromatograph is then described by imposing a switching mechanism on the basic process that simulates the relative movements of the gas and stationary phases as well as the various port functions. Below, the basic equation is derived, and later is explained a program developed for the present apparatus.

A.10.1 The Theory.

In accordance with all the plate models, the chromatographic column is taken to be a series of ideal mixing stages, each of which is called a theoretical plate. Referring to Fig.A.10.1 , a mass balance is taken over the n^{th} plate in the column

$$G\, y_{n-1} = G\, y_n + V_G \frac{dy_n}{dt} + V_L \frac{dx_n}{dt} \qquad \text{(A.10.1)}$$

where V_G and V_L are the volumes of gas and liquid phase occupying the plate

y and x are gas and liquid concentrations of the solute

and G is the volumetric gas flow rate.

Noting that the partition coefficient is defined as $K_n = \frac{x_n}{y_n}$, a rearrangement of A.10.1 gives

$$G\, y_{n-1} = G\, y_n + v_n \frac{dy_n}{dt} \qquad \text{(A.10.2)}$$

where v_n is the total plate volume ($= V_G + K_n V_L$).

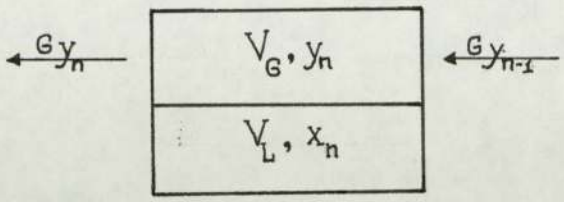

Fig- A-10-1 Mass Balance Over n^{th} Plate

If the time increment (Δt) over which the above equation is integrated is small then y_{n-1} may be taken as being constant. In this case taking Laplace transforms of both sides and rearranging it

$$\bar{y}_n = \frac{y_{n-1}}{s\left(1+\frac{V_n}{G}s\right)} + \frac{V_n}{G\left(1+\frac{V_n}{G}s\right)} y_n(0) \qquad (A.10.3)$$

where $y_n(0)$ is the value of y_n at the beginning of the time increment. Now taking inverse Laplace transform,

$$y_n = y_{n-1}\left(1-e^{-\frac{G}{V_n}\Delta t}\right) + y_n(o)e^{\frac{-G}{V_n}\Delta t} \qquad (A.10.4)$$

y_n in the above equation is the gas phase concentration at the end of the time increment (Δt) and the first term on the right hand side is the contribution to it from the inlet concentration (this may be the output from the previous plate and/or an external feed) and the second term is the contribution of the concentration which was present in the plate at the beginning of the time interval.

A.10.2 The Sequencing Mechanism.

For modelling purposes the chromatograph is visualised as an infinite series of beds linearly connected to form a column of infinite length. The number of beds involved in the chromatographic process at any time is marked by the carrier inlet point at one end and the top off-take point

at the other. The countercurrent movement is then simulated by sequencing the beds past the stationary ports. In the actual apparatus it is difficult to determine exactly the point in time when a valve opens or closes. For the purpose of these models the switching mechanisms depicted in Figs. A.10.2 and A.10.3 were assumed to prevail.

For the off-take ports the cams were assumed to cover four valves at any time, and for the feed inlet port, three valves. Since the tubes are connected alternately at top and bottom, the gas flow in one bed is in the opposite direction to the gas flows in the beds on either side of it. For the following program, the gas was assumed to flow in an upward direction in even numbered beds and in the downward direction in the odd numbered beds. If a 'switching interval' is defined as the time during which a bed stays in the same position in space, then the feed inlet and off-take functions are from the same points over two switching intervals. The switching mechanism for the carrier inlet is not critical and so it was allowed to sequence every switching interval.

A.10.3 The Lay-out of the Programme.

Referring to Fig. A.10.4, five different sections are identified in the chromatographic column:-

The stripping section (Section 1) - In equation (A.10.4), y_{n-1} is the output from the previous plate, except for the first plate where it is zero. The total gas flow rate is $(G+G_b)$, where G is the top off-take flow rate and G_b is the bottom off-take flow rate.

Section 2 - The basic equation is the same as in the above section except that the gas flow rate is now $G + G_b/2$. Here it was arbitrarily assumed that the bottom product was taken off at equal rates from the two off-take points.

Section 3 - Equation (A.10.4) is again applicable to this section except

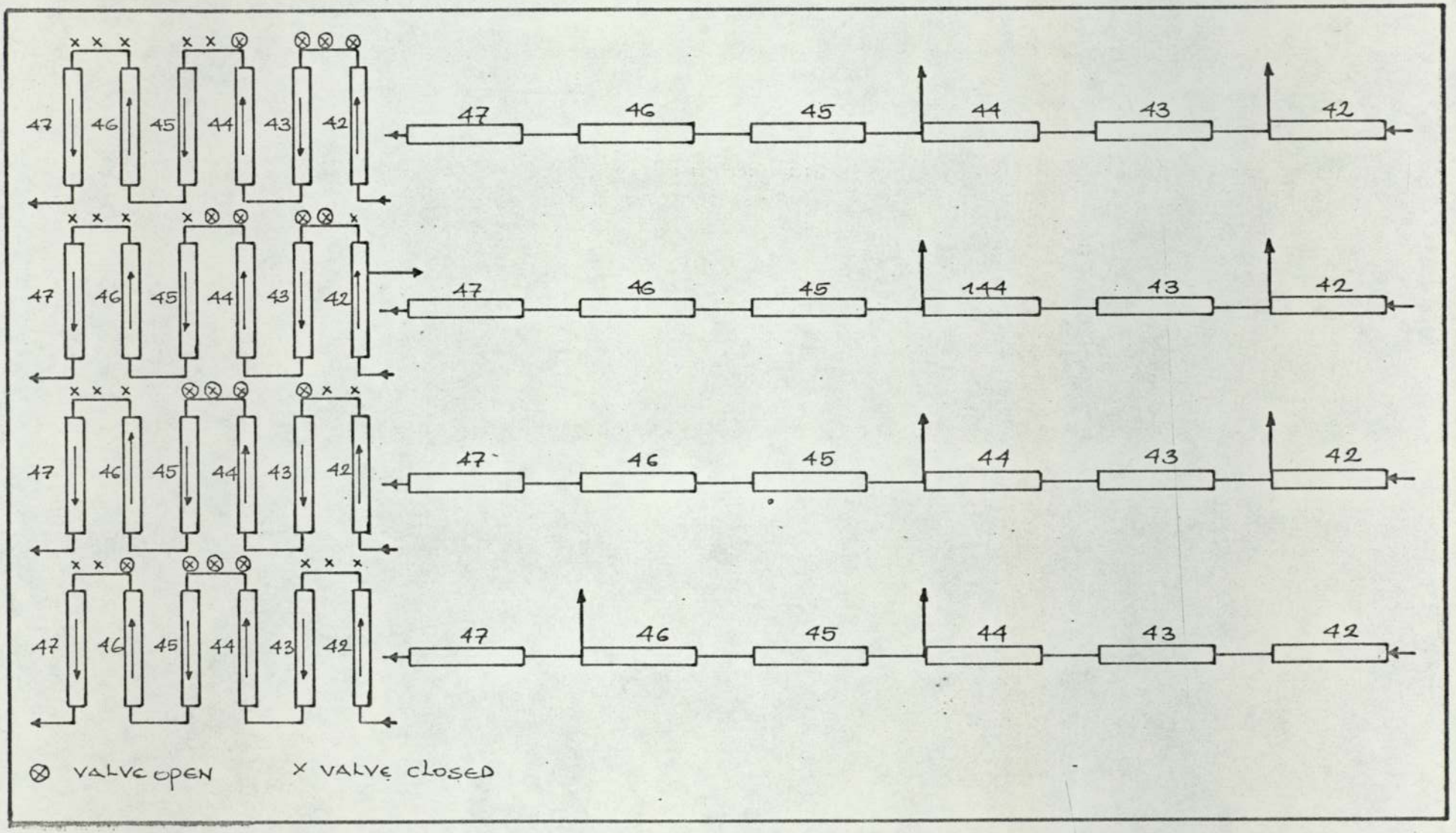

FIG. A.10.2. SWITCHING MECHANISM FOR OFF-TAKES.

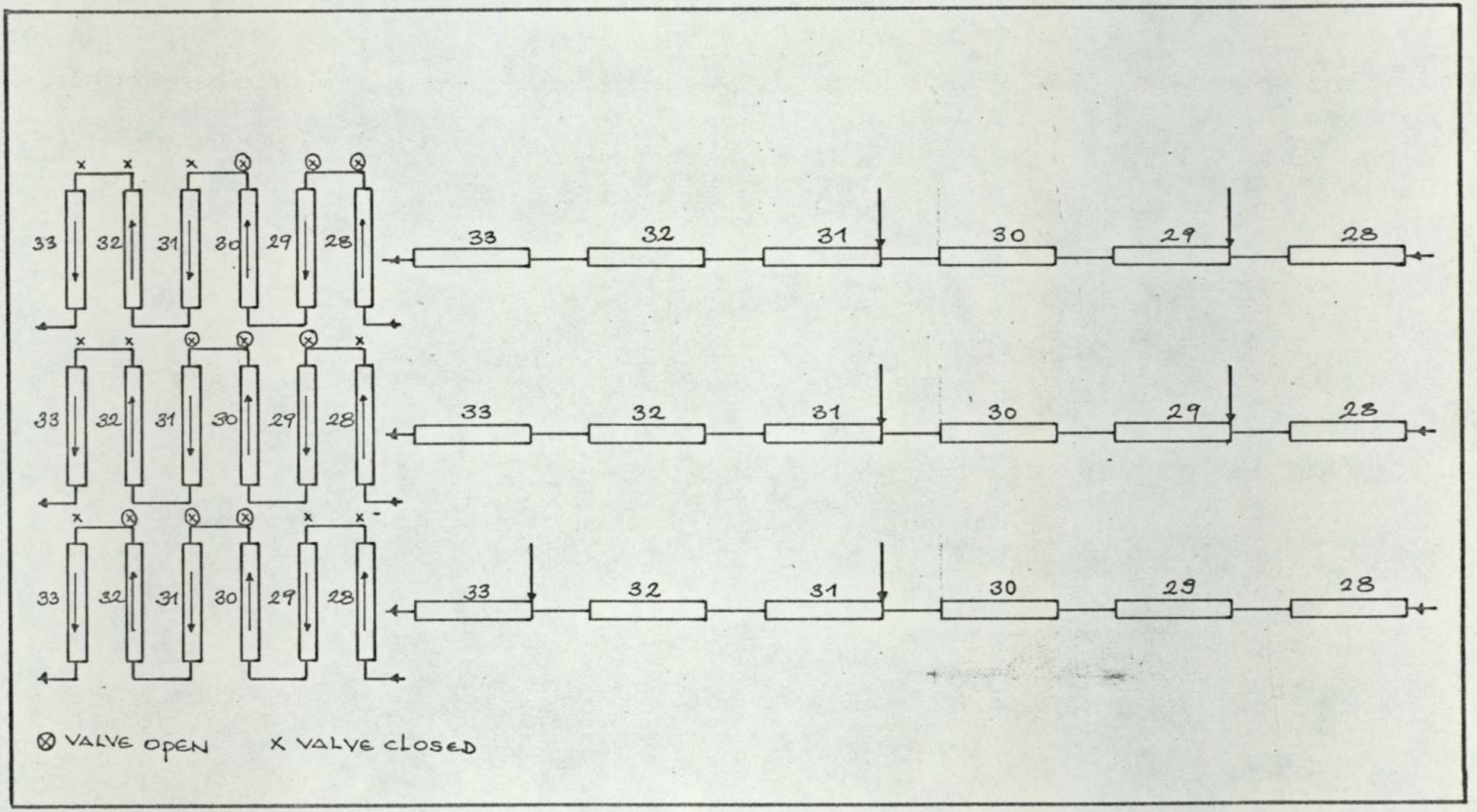

FIG. A.10.3 - SWITCHING MECHANISM FOR FEED INLET

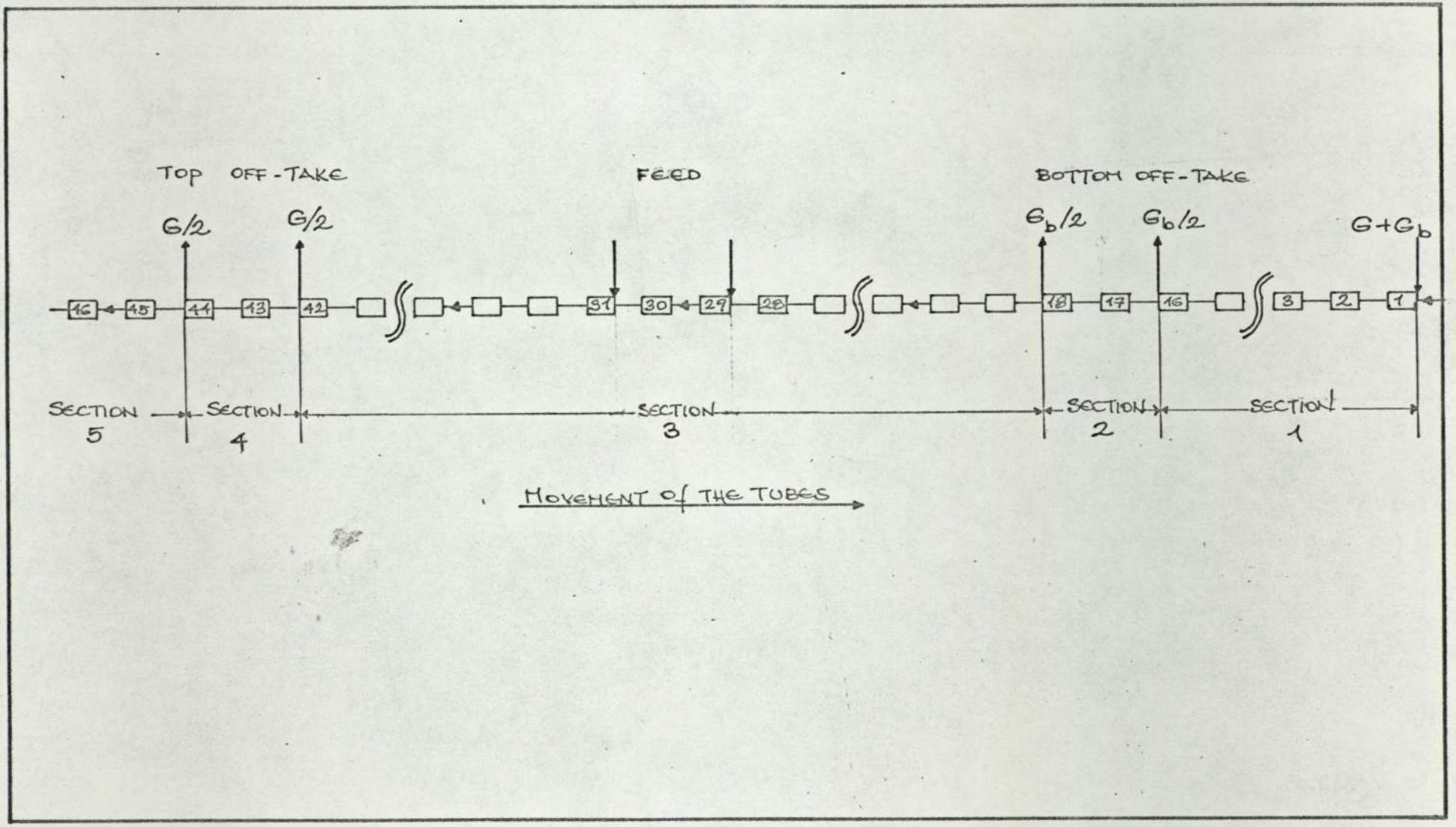

FIG. A.10.4 – POSITIONS OF THE SECTIONS IN THE ROTATING CHROMATOGRAPH.

for the first plates of the two feed beds. In the latter instances, y_{n-1} is replaced by $(y_{n-1} + f_n)$ where f_n is the external feed concentration.

Section 4 - This section is very similar to section 2, but the gas flow rate is now G/2.

Section 5 - In this section the concentration is zero throughout, and no calculation is performed.

As mentioned earlier, equation (A.10.4) is applicable only for very small time increments. Therefore, in the actual running of the program each time interval was divided into an appropriate number of equal 'time increments'. At each time increment the computer calculates the concentration at each plate from equation (A.10.4) starting from the first plate of interest. Tests are performed to locate the position of each plate in the chromatograph for the appropriate form of equation (A.10.4). This operation is performed for every consecutive time increment until the end of a time interval at which point the port functions are sequenced. A simplified flow chart of the programme and the programme itself in Fortran IV are given in the following pages.

A.10.4 Application of the Programme.

The model developed here, although very simple, is very flexible. It can easily be made to incorporate a non-linear partition isotherm, or the column pressure drop. However, the major drawback, which prevented the comparison with the available experimental data, is the enormous amount of computer time required. For example, it was attempted to simulate one of the runs carried out by Al-Madfai (174) with hexane isomers on the present apparatus. The component chosen was n-hexane with a stripping factor (G/LK) of 0.685 and a total number of plates of 176. The computer time required on an ICL 1900 for 59 switching intervals equivalent to 4750 seconds of real time was 2000 seconds and the solute was still accumulating

in the column. This example was carried out with a time increment (Δt) of 2.5 seconds, but preliminary runs showed that under these conditions Δt needs to be reduced to about 1 second for accurate computation. This would then make the ratio of computer time to real time roughly unity. Since it is known that in the actual experiments the time required to reach a steady state operation is several hours, the use of this programme would be impracticable in most cases.

An initial aim in developing this model was to find out whether the fluctuations observed in the off-take concentrations and compositions, even after several hours of operation, was an intrinsic property of the apparatus. However, computer runs carried out with arbitrary input values chosen to give a large numerical value for the stripping factor, did in fact show that a sort of a steady state operation should be achieved whereby the column concentration profiles are repeated from one switching interval to another and from one cycle to another.

FLOW DIAGRAM FOR PLATE MODEL

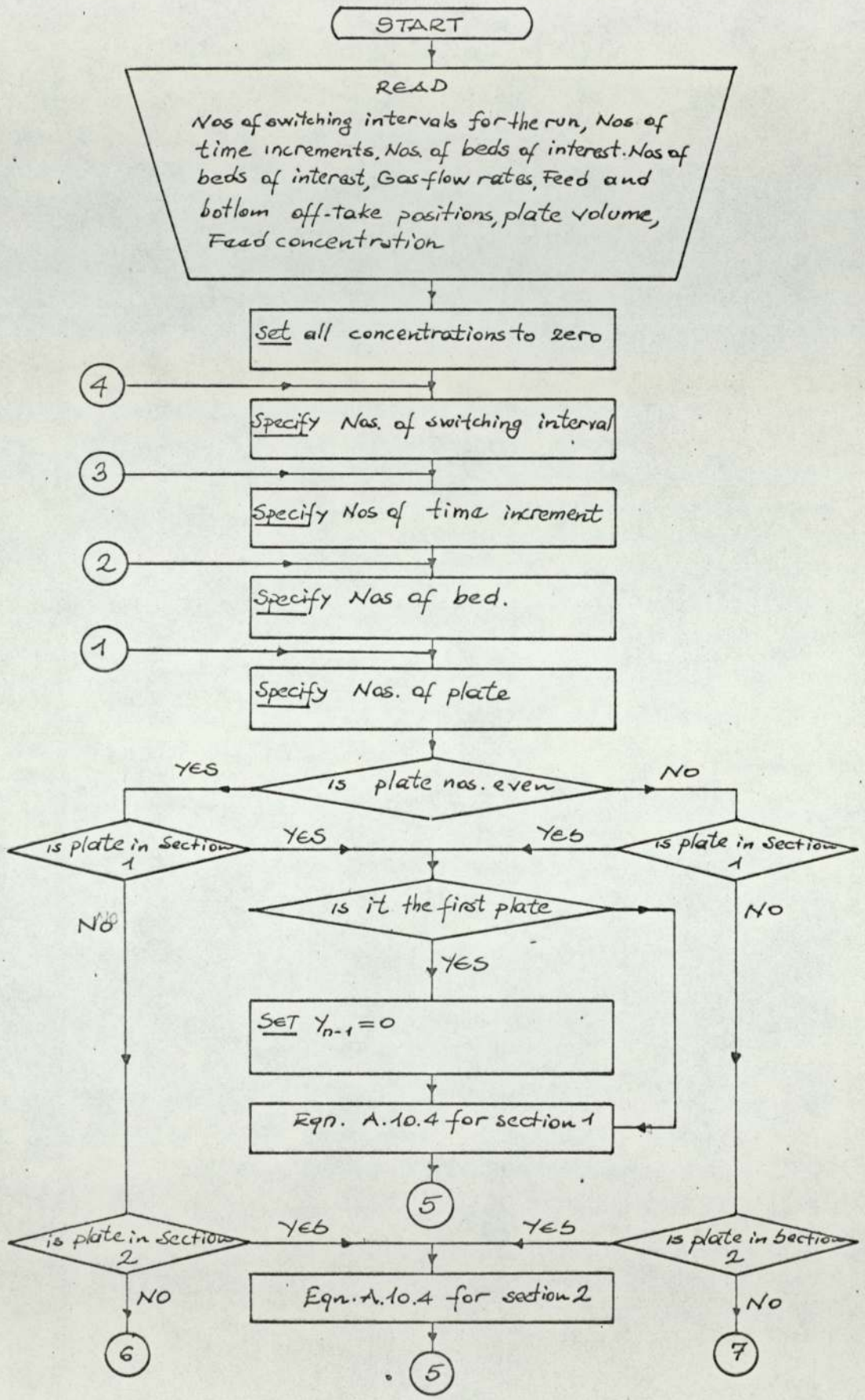

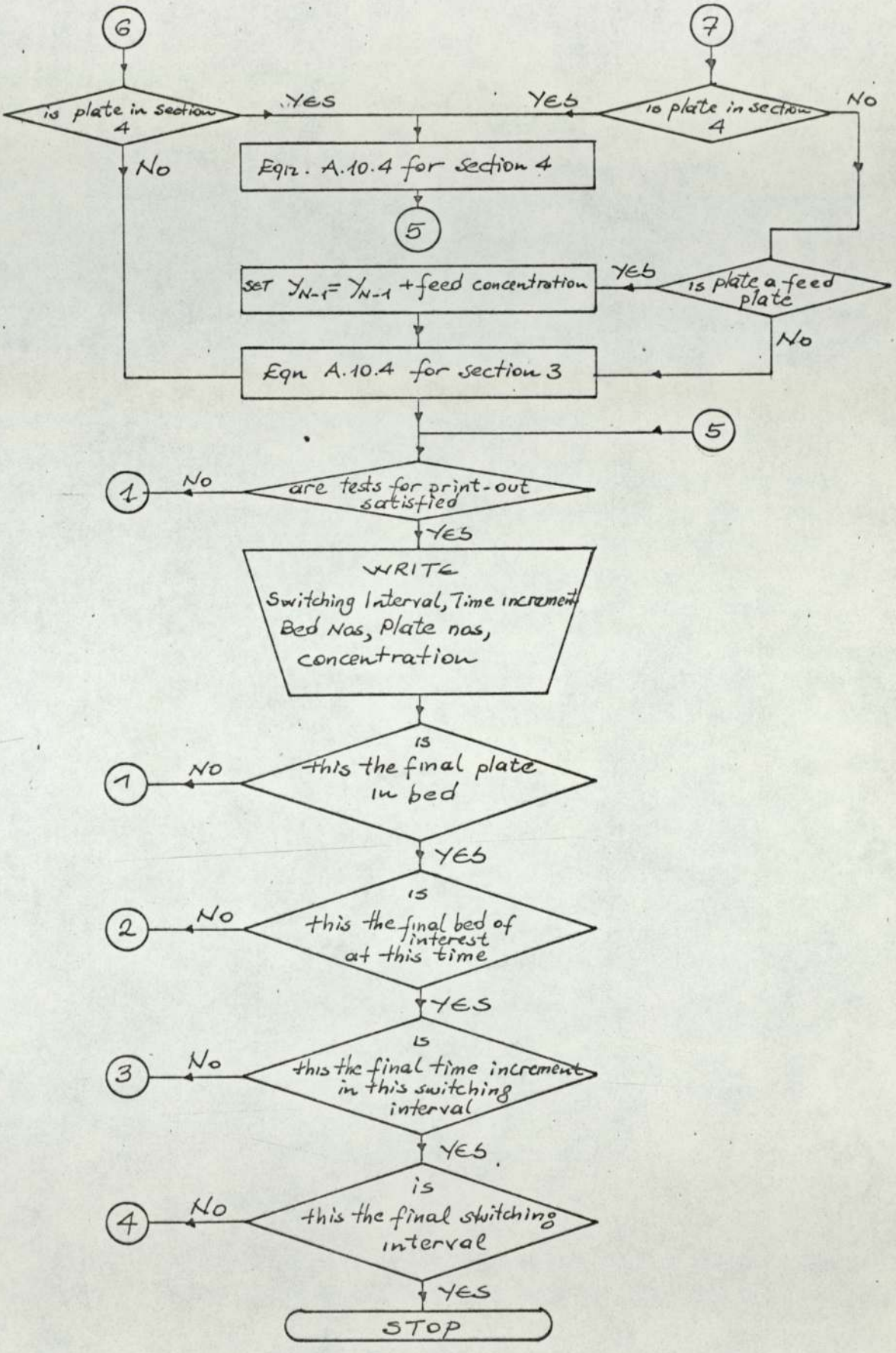
6
7
is plate in section 4
YES
YES
is plate in section 4
NO
NO
Eqn. A.10.4 for section 4
5
SET $y_{N-1} = y_{N-1}$ + feed concentration
YES
is plate a feed plate
NO
Eqn A.10.4 for section 3
5
1
NO
are tests for print-out satisfied
YES
WRITE
Switching Interval, Time increment
Bed Nos, Plate nos,
concentration
1
NO
is this the final plate in bed
YES
2
NO
is this the final bed of interest at this time
YES
3
NO
is this the final time increment in this switching interval
YES
4
NO
is this the final switching interval
YES
STOP

```
      MASTER
C=====================================================================
C        -44 TUBES-/SUHAM/ HEXANE ISOMERS/ RUN 9.6
C=====================================================================
      DIMENSION C(3000)
      INTEGER BT1,BT2,F1,F2,TKK,TNN,L,LC,R,LPC,LTC,GBTP1,GBTP2,GFP1,GFP2
C F=CARRIER FLOW RATE
C FS=STRIPPING FLOW RATE
C V=EFFECTIVE PLATE VOLUME
C DT=TIME INCREMENT IN MINUTES
C CON=FEED CONCENTRATION
CBT1,BT2 ARE POSITIONS OF BOTTOM PORT,MUST BE EVEN NUMBERS
CF1,F2 ARE POSITIONS OF FEED PORT,MUST BE ODD NUMBERS
C NO=NO. OF PLATES/BED
C R=NO. OF BEDS/CYCLE
C LPC=NO. OF PLATES/PRINT
C LTC=NO. OF TIME INCREMENTS/PRINT
C NT=NO. OF TIME INCREMENTS /SWITCHING TIME
C NS=TOTAL NO. OF SWITCHING TIMES
      READ(1,11)F,FS,V,DT,CON,BT1,BT2,F1,F2,NO,R,LPC,LTC,NT,NS
 11   FORMAT(5F0.0,10I0)
      WRITE(2,85)F,FS,V,DT,CON
 85   FORMAT(1H0,2HF=,F15.8,5X,3HFS=,E15.8,5X,2HV=,E15.8,5X,3HDT=,E15.8,
     $5X,4HCON=,E15.8)
      WRITE(2,95)BT1,BT2,F1,F2,NO,R,LPC,LTC,NT,NS


 95   FORMAT(1H0,4HBT1=,I2,5X,4HBT2=,I2,5X,3HF1=,I2,5X,3HF2=,I2,5X,3HNO=
     9,I2,5X,2HR=,I2,5X,4HLPC=,I2,5X,4HLTC=,I2,5X,3HNT=,I2,5X,3HNS=,I3)
      WRITE(2,92)
 92   FORMAT(1H0,1X,2HK=,6X,3HKK=,6X,2HN=,6X,3HNN=,10X,6HC(NN)=)
      DO 5 NN=1,1100
      C(NN)=0.0
 5    CONTINUE
      AS1=1.0-EXP(-((FS+F)/V)*DT)
      BS1=1.0-AS1
      AS2=1.0-EXP(-((FS/2.0+F)/V)*DT)
      BS2=1.0-AS2
      A3=1.0-EXP(-(F/V)*DT)
      B3=1.0-A3
      A4=1.0-EXP(-((F/2.0)/V)*DT)
      B4=1.0-A4
CSIMULATION TIME IS 8 HOURS
CEACH SIMILATION TIME IS DIVIDED INTO NT EQUAL TIME INCREMENTS
CPLATES BEFORE FIRST FEED PLATE
      M1=(F1-1)*NO
      M2=R*NO
C     TIME COUNTER
      TKK=1
      DO 1 K=1,NS
C GENERAL BOTTOM PLATES
      GBTP1=(BT1-3+2*((K+1)/2))*NO+1
      GBTP2=GBTP1+2*NO
C GENERAL FEED PLATES
      GFP1=(F1-3+2*((K+1)/2))*NO+1
      GFP2=GFP1+2*NO
      WRITE(2,16)GBTP1,GBTP2,GFP1,GFP2
 16   FORMAT(1H0,73X,6HGBTP1=,I4,2X,6HGBTP2=,I4,2X,5HGFP1=,I4,2X,5HGFP2=
     $ 3,I4)
      J=NT*(K-1)+1
```

```
      M=NT*K
      DO 2 KK=J,M
      I=K+R-1
C     PLATE COUNTER
      TNN=(NO/LPC)*(K-1)+1
      DO 3 N=K,I
      L=NO*(N-1)+1
      LC=N*NO
      DO 4 NN=L,LC
CTEST FOR BEDS UPTO F1
      IF(NN.LT.M1) GO TO 40
      N1=N-R
CTEST FOR EVEN NUMBER BEDS
      N2=2*(N/2)
      IF(N.EQ.N2) GO TO 10
CTESTS ON ODD  NUMBER BEDS
C                              IN SECTION 1
      N3=N-(BT1-1)
      IF((K.GT.N3).AND.(K.LE.N)) GO TO 15
C                              IN SECTION 2
      N4=N-(BT2-1)
      IF((K.GT.N4).AND.(K.LE.N3)) GO TO 20
C                              IN SECTION 4
      N5=N-R+1
      N6=N-R+3
      IF((K.GT.N5).AND.(K.LE.N6)) GO TO 25
C                              IN SECTION 3 FOR FEED PLATES AND TIMES
      N7=(N-1)*NO+1
      N8=N-F1
      N9=N-F1+2


      N10=N-F2
      N11=N-F2+2
      IF((NN.EQ.N7).AND.(((K.GT.N8).AND.(K.LE.N9)).OR.((K.GT.N10).AND.(K
     1.LE.N11)))) GO TO 30
      IF(N.EQ.I) GO TO 4
      GO TO 35
CTESTS ON EVEN NUMBER BEDS
C                              IN SECTION 1
      N12=N-BT1
 10   IF((K.GT.N12).AND.(K.LE.N)) GO TO 15
C                              IN SECTION 2
      N13=N-BT2
      IF((K.GT.N13).AND.(K.LE.N12)) GO TO 20
C                              IN SECTION 4
      N14=N-R+2
      IF((K.GT.N1).AND.(K.LE.N14)) GO TO 25
CREMAINING BEDS ARE IN SECTION 3
      GO TO 35
 15   IF((NN.EQ.N7).AND.(N.EQ.K)) C(NN-1)=0
      C(NN)=AS1*C(NN-1)+BS1*(C(NN))
      GO TO 40
 20   C(NN)=AS2*C(NN-1)+BS2*C(NN)
      GO TO 40
 25   C(NN)=A4*C(NN-1)+B4*C(NN)
      GO TO 40
 30   C(NN)=A3*(C(NN-1)+CON)+B3*C(NN)
      GO TO 40
 35   C(NN)=A3*C(NN-1)+B3*C(NN)
 40   IF((NN.EQ.(LPC*TNN)).AND.(KK.EQ.(LTC*TKK))) GO TO 45
      GO TO 50
 45    WRITE(2,55) K,KK,N,NN,C(NN)
```

```
 55   FORMAT(1X,I3,5X,I4,5X,I4,5X,I4,5X,E16.7)
 50   IF(NN.EQ.(LPC*TNN)) TNN=TNN+1
 4    CONTINUE
 3    CONTINUE
      IF(KK.EQ.(LTC*TKK)) GO TO 65
      GO TO 2
 65   TKK=TKK+1
       WRITE(2,90)
 90   FORMAT(1H0)
 2    CONTINUE
       WRITE(2,75)
 75   FORMAT(10X,18HSWITCHING INTERVAL)
 1    CONTINUE
      STOP
      END
```

APPENDIX A.11

Rate Model with Longitudinal Diffusion in Gas Phase.

A.11.1 The Theory.

It is generally accepted that a rate model is more useful than a plate model in providing insight into the various physical processes taking place in a chemical engineering operation. It was shown with the plate model that although the continuous chromatograph exhibits a transient behaviour within a switching period, an overall steady state should be achieved in the sense that the concentration profile in one cycle should be repeated in the following cycles. For this reason and also for the fact that the mathematics are greatly simplified, the present model is based on a steady state operation. It was hoped to extend this model, eventually, to take into account the non-linear isotherm effects, but in its present state it is restricted to a constant partition coefficient.

The following additional assumptions were made in deriving the equation:-

1. The interphase mass transfer can be described in terms of the 'two-film theory' and that the resistance to mass transfer lies in the gas phase. This is consistent with the findings of Lloyd(168) and Huntington (173).
2. There is no diffusion in the liquid phase. This assumption is likely to hold in view of the fact that the liquid phase is coated on individual particles which may have only point contacts with each other.
3. Eddy diffusion can be expressed in terms of Fick's second law. The justification for the use of Fick's law is that its solution is indentical with the solution of a more complex equation derived from statistical considerations of turbulence (204).
4. The concentration of the solute in both phases is small enough to assume constant flow rate throughout the column.
5. The pressure drop is ignored.

The following notation is used:-

L = Volumetric flow rate of liquid phase cm^3/h

G = Volumetric flow rate of gas cm^3/h

x = Concentration of solute in liquid phase g/cm^3

y = Concentration of solute in gas phase g/cm^3

K = Partition coefficient ($= {}^{x}/y^*$)

y^* = Fictitious gas phase concentration in equilibrium with x.

N_D = Flux of solute due to axial diffusion ($=Ea_c \frac{dy}{dz}$) gm/h

E = Total diffusivity in gas phase (molecular diffusivity + eddy diffusivity) cm^2/h

a_c = Column cross sectional area occupied by gas cm^2

K_{OG} = Overall mass transfer coefficient based on gas film

a = Mass transfer area per unit length of column cm^2/cm

l = Length of column, cm

Referring to Fig. A.11.1, a mass balance over a differential element δ_z gives:

For the gas phase

$$Ea_c \frac{d^2y}{dz} + G \frac{dy}{dz} = K_{OG}\, a\, (y-y^*) \qquad \text{(A.11.1)}$$

$$LK \frac{dy^*}{dz} = K_{OG}\, a\, (y-y^*) \qquad \text{(A.11.2)}$$

Defining the following the dimensionless quantities,

α' = G/LK Stripping factor

Pe = Gl/a_cE Peclet number

N_T = $K_{OG}aL/G$ Total number of transfer units

Γ = y/y_{inlet} Gas phase concentration

where $y_{inlet} = F/G$, F is the feed rate in g/h

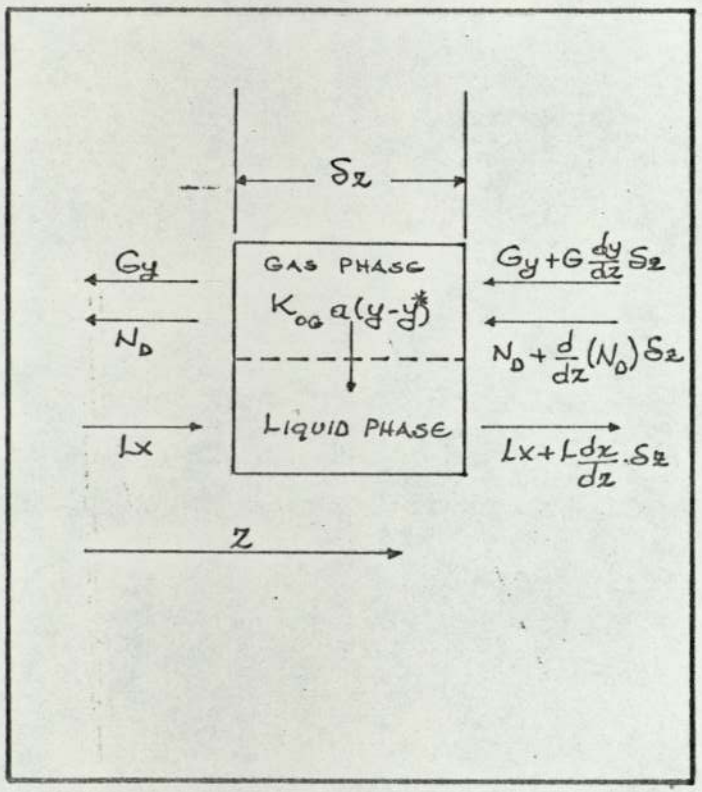

FIG.A.11.1- DIFFERENTIAL MASS BALANCE

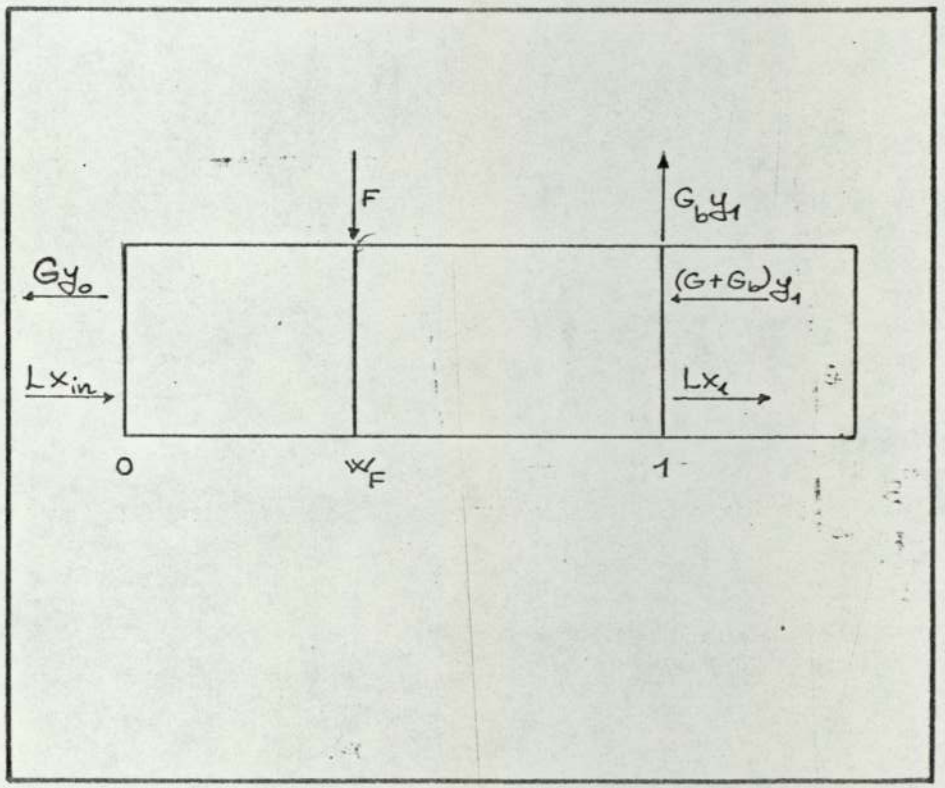

FIG.A.11.2. OVERALL MASS BALANCE

$\varphi = y^*/\alpha' y_{inlet}$ Liquid phase concentration

$w = z/l$ Distance from liquid inlet

Equation (A.11.1) becomes

$$D^2\Gamma + Pe\, D\Gamma = N_t Pe(\Gamma - \alpha'\varphi) \qquad (A.11.3)$$

and from equation (A.11.2)

$$D\varphi = N_t(\Gamma - \alpha'\varphi) \qquad (A.11.4)$$

where D is the differential operator.

Since α' is constant, equations (A.11.3) and (A.11.4) can be solved analytically to give

$$\Gamma = A + Be^{\lambda_1 w} + Ce^{\lambda_2 w} \qquad (A.11.5)$$

$$\varphi = \frac{A}{\alpha'} + \frac{N_t}{(\lambda_1 + \alpha' N_t)} Be^{\lambda_1 w} + \frac{N_t}{(\lambda_2 + \alpha' N_t)} Ce^{\lambda_2 w} \qquad (A.11.6)$$

where λ_1 and λ_2 are the roots of the auxillary equation,

$$D^2 + (Pe + \alpha' N_t)D - N_t Pe(1 - \alpha') = 0 \qquad (A.11.7)$$

Since there is a discontinuity at the feed point, there are two pairs of equations of the type (A.11.5) and (A.11.6); one for the top section and the other for the bottom section with two different sets of constants.

Boundary Conditions.

In deriving the boundary conditions the following assumptions were made:-

1. Uniform temperature exists in the separating section.
2. Inlet solvent is free of solute, i.e. the stripping process is complete.
3. In doing mass balances around the boundary sections, the interface mass transfer is assumed to be negligibly small (205-208).
4. Peclet numbers throughout the separating and stripping sections are assumed to be the same.

The overall mass balance is indicated in Fig. A.11.2. In the following equations the subscripts 0,F,1 refer to the top-off take, feed and bottom off-take points respectively.

Top Off-Take (w=o).

Since no mass transfer takes place outside the columns, there is no discontinuity in the concentration levels at this point. Also assuming that there is no eddy diffusion outside the column, a mass balance over the gas phase gives

$$\left.\frac{d\Gamma_T}{dw}\right)_o = 0 \qquad \text{(A.11.8)}$$

and over the liquid phase

$$\varphi_T\Big)_{in} = \varphi_T\Big)_o = 0 \qquad \text{(A.11.9)}$$

Feed Inlet ($w=w_F$).

From mass balance over the gas phase,

$$\Gamma_T\Big)_F + \frac{1}{Pe}\left.\frac{d\Gamma_T}{dw}\right)_F = \Gamma_B\Big)_F - \frac{1}{Pe}\left.\frac{d\Gamma_B}{dw}\right)_F + R \qquad \text{(A.11.10)}$$

where R is the fraction of feed in vapour phase

over the liquid phase

$$(1-R) + \varphi_T\Big)_F = \varphi_B\Big)_F \qquad \text{(A.11.11)}$$

Bottom Off-Take (w=1).

Assuming a continuity in the concentration level at this point, a mass balance over the whole column yields

$$G\,\Gamma_T\Big)_o + G_b\,\Gamma_B\Big)_1 = G \qquad \text{(A.11.12)}$$

where G_b is the gas flow rate in the bottom off-take.

and from a mass balance over the stripping section,

$$\varphi_B \Big)_1 = \left(1 + \frac{G_b}{G}\right) \Gamma_B \Big)_1 \qquad \text{(A.11.13)}$$

We now have six equations and six arbitrary constants to be determined. Equations (A.11.8) to (A.11.13) were solved simultaneously using a library subroutine on an ICL 1900 computer. The flow chart and the programme are given at the end of this Appendix. The computer language used was Fortran IV.

A similar programme was written for the case where plug flow conditions are assumed to prevail in the column, i.e. $Pe \rightarrow \infty$ The equivalents of equations (A.11.5) and (A.11.6) are now,

$$\Gamma = A + B\, e^{\lambda w} \qquad \text{(A.11.14)}$$

$$\varphi = \frac{A}{\alpha'} + B\, e^{\lambda w} \qquad \text{(A.11.15)}$$

and the number of boundary conditions are reduced to four. This programme is also presented at the end of this section.

A.11.2 Comparison with Experimental Work.

In view of the lack of reliable data from the present work, the computer calculations were checked against the work of Huntington (173) on his moving bed chromatograph with the system Cyclohexane/Benzene Polyoxyethyelene 400 diricionoleate

Liquid loading = 25.18% w/w, Column length = 152.4 cm (60 in)

Column temperature = 24.3°C, K_{CH} = 255 K_B = 675

G = 63900 cm^3/h G_b = 94500 cm^3/h L = 117.2 cm^3/h

F_{CH} = 5.85 g/h F_B = 6.60 g/h

The height of a transfer unit for cyclohexane was measured to be 9.23 cm (3.63 in) from the concentration profile in the top 22.6 cm (9 in) of

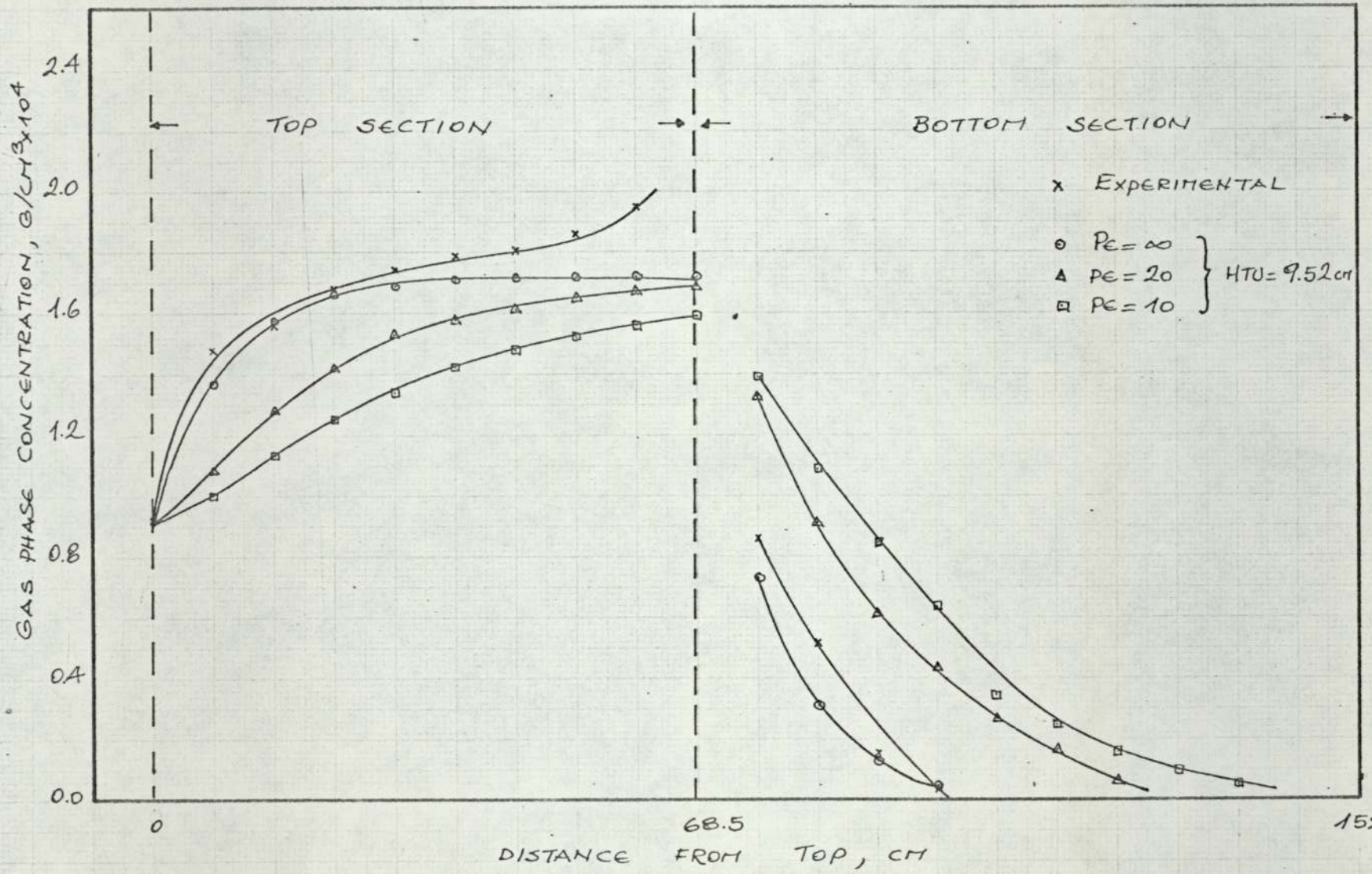

FIG. A.11.3. CONCENTRATION PROFILE OF CYCLOHEXANE

the column. This gives a total number of transfer units of 16.5 for the separating section of the column. The Reynold's number based on particle diameter $\left(\frac{ud_p\rho}{\mu}\right)$ was calculated to be 3.96 and the corresponding Peclet number $(Pe)_{d_p} = \left(\frac{ud_p}{E}\right)$ for cyclohexane was estimated from Hiby's equation (209) to be 3.43. This value of $(Pe)_{d_p}$ seems a little high in the light of various theoretical and experimental work(204,210) which suggests that it reaches a maximum of 2 for gases at very low Reynold's numbers.

Taking $(Pe)_{d_p} = 3.43$, the column length based Peclet number (Pe) was then calculated to be 5080. However, at Pe greater than 20, the subroutine of the programme broke down and, therefore, in Fig. A.11.3, the experimental profile for cyclohexane is compared for Pe = 10 and 20 together with the plug flow condition ($Pe \rightarrow \infty$). The feed was assumed to be in liquid state as reported by Huntington. As observed from this graph, the best agreement with the experimental profile is obtained with the plug flow calculation. Since the profile moves towards the experimental curve as the Peclet number increases, at the estimated value of Pe = 5080, the calculated profile can be expected to be very near the plug flow curve. This would then suggest that the effect of axial mixing on the separating efficiency is negligible. The failure of the programme at relatively low Peclet numbers is, undoubtedly, a reflection of this physical reality. Furthermore, calculations also showed that the effect of axial mixing is to increase the value of overall HTU away from the feed point. This prediction is completely contradicted by the experimental observations of most workers (168,173).

A.11.3 Computer Programme for Rate Model with Diffusion.

In setting up the programme, equations (A.11.8) to (A.11.13) were combined with equations (A.11.5) and (A.11.6) to form a set of linear simultaneous equations in six arbitrary constants(three for the top section

and three for the bottom section). Since the library subroutine used a matrix inversion method, the equations were arranged to form a matrix, with the left hand sides containing the arbitrary constants.

The inputs to the programme were:

G as (G) and liquid (L) flow rates, bottom off-take flow rate (G_b), feed rate (F), partition coefficient (KEQ), total number of transfer units (NTU), Peclet number (Pe), feed point position (WF) and fraction of vapour in feed (R).

With these values the programme calculated y(Y) and y*(YEQ) at specified intervals (W) along the column for twenty combinations of various values of PE, NTU, R.

FLOW DIAGRAM FOR HTU MODEL

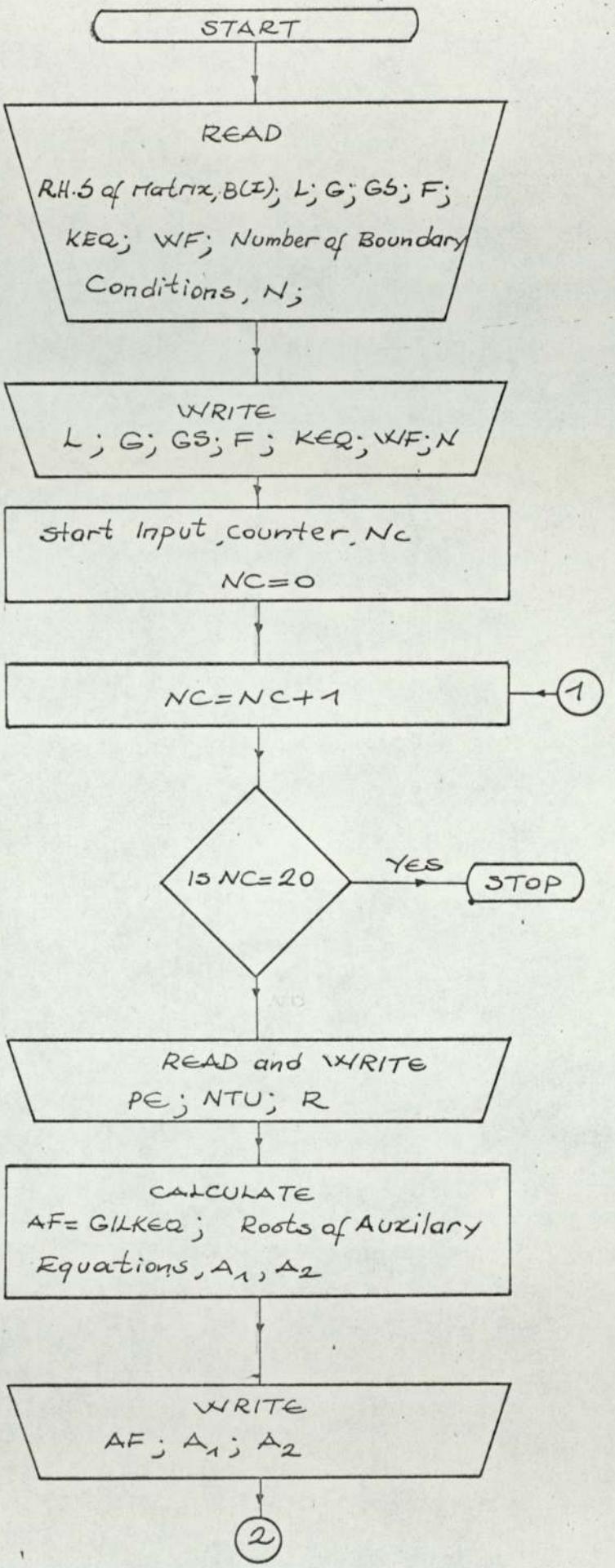

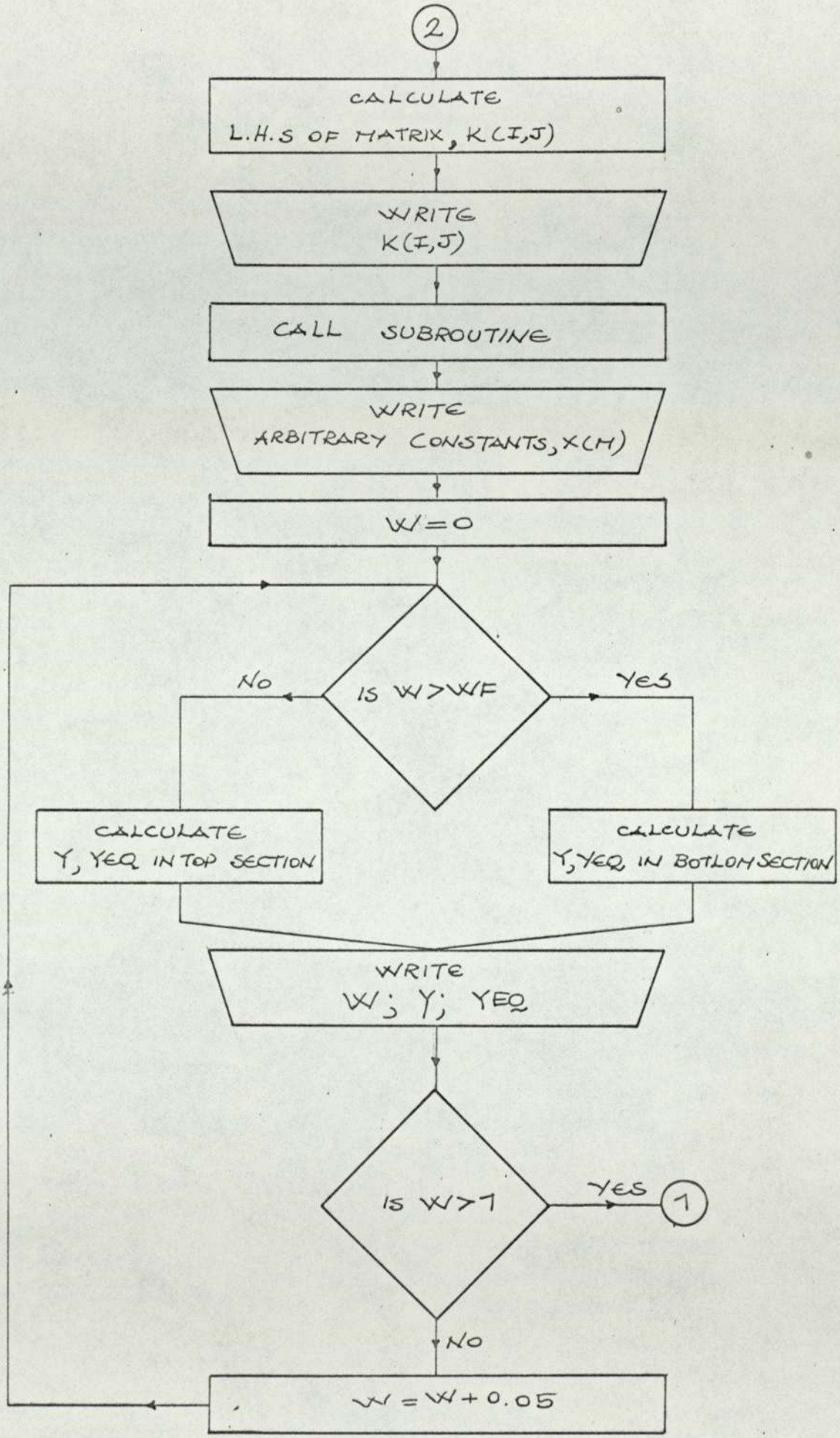
2
CALCULATE
L.H.S OF MATRIX, K(I,J)
WRITE
K(I,J)
CALL SUBROUTINE
WRITE
ARBITRARY CONSTANTS, X(M)
W=0
IS W>WF
No
YES
CALCULATE
Y, YEQ IN TOP SECTION
CALCULATE
Y, YEQ IN BOTLOM SECTION
WRITE
W; Y; YEQ
IS W>1
YES
1
No
W = W + 0.05

```
      MASTER
      DIMENSION A(400),B(20),X(20),K(20,20),AA(400),BB(20),REINT(20)
      INTEGER IN,NA,NB,ID,IT
      REAL L,NTU,KEQ,LE,K
C                    DATA BASED ON  CH/B RUN 12  FOR CH
C  L=SOLVENT RATE
C  G=TOP OFF-TAKE RATE
C  GS=BOTTOM OFF-TAKE RATE
C  F=FEED RATE
C  PE=PECLET NUMBER  (G*LE)/(AG*E)
C  KEQ=PARTITION COEFFIENT
C  NTU=NO OF TRANSFERUNITS IN SEPATION SECTION  (KOG*A*L)/G
C  E=DIFFUSIVITY
C  AG=VOIDAGE FRACTION
C  W=DIMENSIONLESS LENGTH
C  WF=POSITION OF FEED POINT
C  LE=LENGTH OF SEPERATION SECTION
C  N=NO OF BOUNDARY CONDITIONS
      READ(10,10)L,G,GS,F,KEQ,WF,N
   10 FORMAT(6F0.0,I0)
      WRITE(20,11)L,G,GS,F
   11 FORMAT(1H0,2HL=,E16.8,5X,2HG=,E16.8,5X,3HGS=,E16.8,5X,2HF=,E16.8)
      WRITE(20,12)KEQ,WF
   12 FORMAT(1H0,4HKEQ=,F8.3,5X,3HWF=,F8.3)
      WRITE(20,13)LE,N
   13 FORMAT(1H0,3HLE=,F8.3,5X,2HN=,I2)
   60 READ(10,21)PE,NTU,R
   21 FORMAT(3F0.0)
      IF(PE.EQ.0.0) GO TO 61
      WRITE(20,22)PE,NTU,R
   22 FORMAT(1H0,20X,3HPE=,F8.3,10X,4HNTU=,F8.3,10X,2HR=,F8.3)
C  AF=ABSORPTION FACTOR
      AF=(G/L)/KEQ
C  R1,R2=ROOTES OF AUXILARY EQUATION
      A1=-(PE+AF*NTU)
      A2=SQRT((PE-AF*NTU)**2+4.0*NTU*PE)
      R1=(A1+A2)/2.0
      R2=(A1-A2)/2.0
      WRITE(20,65)AF
   65 FORMAT(1H0,23HABSORPTION FACTOR (AF)=,F9.5)
      WRITE(20,70)R1,R2
   70 FORMAT(1H0,22HROOTS OF AUXILARY EQN.,5X,3HR1=,E16.8,5X,3HR2=,E16.
     5)
      B(1)=0.0
      B(2)=1.0
      B(3)=R-1.0
      B(4)=R
      B(5)=0.0
      B(6)=0.0
      K(1,1)=-(1.0/AF-1.0-GS/G)
      K(1,2)=-(NTU/(R1+AF*NTU)-1.0-GS/G)*EXP(R1)
      K(1,3)=-(NTU/(R2+AF*NTU)-1.0-GS/G)*EXP(R2)
      K(1,4)=0.0
      K(1,5)=0.0
      K(1,6)=0.0
      K(2,1)=GS/G
      K(2,2)=(GS/G)*EXP(R1)
      K(2,3)=(GS/G)*EXP(R2)
      K(2,4)=1.0
      K(2,5)=1.0
      K(2,6)=1.0
      K(3,1)=-(1.0/AF)
      K(3,2)=-(NTU*EXP(R1*WF)/(R1+AF*NTU))
      K(3,3)=-(NTU*EXP(R2*WF)/(R2+AF*NTU))
```

```
      K(3,4)=-K(3,1)
      K(3,5)=-K(3,2)
      K(3,6)=-K(3,3)
      K(4,1)=-1.0
      K(4,2)=-(1.0-R1/PE)*EXP(R1*WF)
      K(4,3)=-(1.0-R2/PE)*EXP(R2*WF)
      K(4,4)=1.0
      K(4,5)=(1.0+R1/PE)*EXP(R1*WF)
      K(4,6)=(1.0+R2/PE)*EXP(R2*WF)
      K(5,1)=0.0
      K(5,2)=0.0
      K(5,3)=0.0
      K(5,4)=1.0/AF
      K(5,5)=NTU/(R1+NTU*AF)
      K(5,6)=NTU/(R2+NTU*AF)
      K(6,1)=0.0
      K(6,2)=0.0
      K(6,3)=0.0
      K(6,4)=0.0
      K(6,5)=-R1
      K(6,6)=-R2
      WRITE(20,72)
   72 FORMAT(1H0,50X,13HK(I,J) MATRIX)
      WRITE(20,71) ((K(I,J),J=1,6),I=1,6)
   71 FORMAT(1H0,6(5X,E16.8))
      IN=1
      NA=N*N
      NB=N
      DO 15 I=1,N
      DO 15 J=1,N
   15 A(I+N*(J-1))=K(I,J)
C SUBROUTINE FOR SOLVING  SIMULTANEOUS LINEAR EQUATIONS
      CALL F4ACSL(A,B,N,NA,NB,IN,X,D,ID,IT,AA,BB,REINT)
      WRITE(20,16)
   16 FORMAT(1H0,19HARBITRARY CONSTANTS)
      DO 25 M=1,N
   25 WRITE(20,20)X(M)
   20 FORMAT(1X,5HX(M)=,E16.8)
      WRITE(20,30)IT
   30 FORMAT(1H0,21HNUMBER OF ITERATIONS=,I5)
      W=0.0
      T1=NTU/(R1+NTU*AF)
      T2=NTU/(R2+NTU*AF)
      WRITE(20,55)
   55 FORMAT(1H0,10X,16HGAS PHASE CONC.=,5X,20H(LIQ. PHASE CONC.)/K)
   35 IF(W.GT.WF)GO TO 40
C  TOP SECTION CONCENTRATIONS
      Y=(X(4)+X(5)*EXP(R1*W)+X(6)*EXP(R2*W))*(F/G)
      YEQ=(X(4)/AF+T1*X(5)*EXP(R1*W)+T2*X(6)*EXP(R2*W))*(F/G)*AF
      GO TO 45
C     BOTTOM SECTION CONCENTRATIONS
   40 Y=(X(1)+X(2)*EXP(R1*W)+X(3)*EXP(R2*W))*(F/G)
      YEQ=(X(1)/AF+T1*X(2)*EXP(R1*W)+T2*X(3)*EXP(R2*W))*(F/G)*AF
   45 WRITE(20,50)W,Y,YEQ
   50 FORMAT(1X,F5.3,5X,E16.8,5X,E16.8)
      IF(W.GT.1.0) GO TO 60
      W=W+0.05
      GO TO 35
   61 STOP
      END
```

```
      MASTER
      DIMENSION A(400),B(20),X(20),K(20,20),AA(400),BB(20),REINT(20)
      REAL L,NTU,KEQ,LE,K
C                    DIFFUSION FREE HTU MODEL
C                    DATA BASED ON  CH/B RUN 12  FOR CH
C  L=SOLVENT RATE
C  G=TOP OFF-TAKE RATE
C  GS=BOTTOM OFF-TAKE RATE
C  F=FEED RATE
C  KEQ=PARTITION COEFFIENT
C  NTU=NO OF TRANSFERUNITS IN SEPATION SECTION  (KOG*A*L)/G
C  W=DIMENSIONLESS LENGTH
C  WF=POSITION OF FEED POINT
C  R=FRACTION OF VAPOUR IN FEED
C  N=NO OF BOUNDARY CONDITIONS
      READ(10,81)L,G,GS,WF,N
 81   FORMAT(4F0.0,I0)
      WRITE(20,11)L,G,GS
 11   FORMAT(1H0,2HL=,F16.8,5X,2HG=,E16.8,5X,3HGS=,E16.8)
      WRITE(20,95)WF,N
 95   FORMAT(1H0,3HWF=,F8.3,5X,2HN=,I2)
      GO TO 67
 61   WRITE(20,68)
 68   FORMAT(1H0,43HEND OF CALCULATIONS FOR THE FIRST COMPONENT)
 67   READ(10,63)KEQ,F
 63   FORMAT(2F0.0)
      IF(KEQ.EQ.0.0) GO TO 69
      WRITE(20,64)KEQ,F
 64   FORMAT(1H1,20X,4HKEQ=,F8.3,10X,2HF=,F8.3)
      AF=(G/L)/KEQ
      WRITE(20,82)AF


 82   FORMAT(1H0,3HAF=,F8.3)
 60   READ(10,83)NTU,R
 83   FORMAT(2F0.0)
      IF(NTU.EQ.0.0) GO TO 61
      WRITE(20,84)NTU,R
 84   FORMAT(1H0,30X,4HNTU=,F8.3,20X,2HR=,F8.3)
C ROOTS OF AUXILARI EQUATION
      RT=NTU*(1.0-AF)
      WRITE(20,85)RT
 85   FORMAT(1H0,21HROOT OF AUXILARI EQN.,5X,3HRT=,E16.8)
      B(1)=0.0
      B(2)=R
      B(3)=1.0-R
      B(4)=0.0
      K(1,1)=1.0/AF
      K(1,2)=1.0
      K(1,3)=0.0
      K(1,4)=0.0
      K(2,1)=1.0
      K(2,2)=EXP(RT*WF)
      K(2,3)=-K(2,1)
      K(2,4)=-K(2,2)
      K(3,1)=-1.0/AF
      K(3,2)=-EXP(RT*WF)
      K(3,3)=-K(3,1)
```

```
      K(3,4)=-K(3,2)
      K(4,1)=0.0
      K(4,2)=0.0
      K(4,3)=(GS/G+1.0-1.0/AF)
      K(4,4)=(GS/G)*EXP(RT)
      WRITE(20,72)
 72   FORMAT(1H0,50X,13HK(I,J) MATRIX)
      WRITE(20,71) ((K(I,J),J=1,4),I=1,4)
 71   FORMAT(1H0,4(3X,E16.8))
      IN=1
      NA=N*N
      NB=N
      DO 15 I=1,N
      DO 15 J=1,N
 15   A(I+N*(J-1))=K(I,J)
C SUBROUTINE FOR SOLVING  SIMULTANEOUS LINEAR EQUATIONS
      CALL F4ACSL(A,B,N,NA,NB,IN,X,D,ID,IT,AA,BB,REINT)
      WRITE(20,16)
 16   FORMAT(1H0,10HARBITRARY CONSTANTS)
      DO 25 M=1,N
 25   WRITE(20,20)X(M)
 20   FORMAT(1X,5HX(M)=,E16.8)
      WRITE(20,30)IT
 30   FORMAT(1H0,21HNUMBER OF ITERATIONS=,I5)
      W=0.0
      WRITE(20,55)
 55   FORMAT(1H0,10X,16HGAS PHASE CONC.=,5X,20H(LIQ. PHASE CONC.)/K)
 35   IF(W.GT.WF)GO TO 40
C  TOP SECTION CONCENTRATIONS
      Y=(X(1)+X(2)*EXP(RT*W))*(F/G)
      YEQ=(X(1)/AF+X(2)*EXP(RT*W))*(F/G)*AF
      GO TO 45
C     BOTTOM SECTION CONCENTRATIONS
 40   Y=(X(3)+X(4)*EXP(RT*W))*(F/G)
      YEQ=(X(3)/AF+X(4)*EXP(RT*W))*(F/G)*AF
 45   WRITE(20,50)W,Y,YEQ
 50   FORMAT(1X,F5.3,5X,E16.8,5X,E16.8)
      IF(W.GT.1.0) GO TO 60



      W=W+0.05
      GO TO 35
 69   STOP
      END
```

REFERENCES

1. D. De Vault: J. Am. Chem. Soc., 65 (1943), 532.
2. A.T. James and A.J.P. Martin: Biochem. J., 50 (1952), 679.
3. F. Helfferich: J. of Chem. Ed., 41 (1964), 410.
4. A.J.B. Cruickshank and D.H. Everett: J. Chromatogr., 11 (1963), 289.
5. R.S. Henly, A. Rose and R.F. Sweeny: Anal.Chem., 36 (1964), 744.
6. C.H. Bosanquet in: "Gas Chromatography 1958", D.H. Desty (Ed.), Butterworths, London, 1958.
7. D.L. Peterson and F. Helfferich: J. Phy. Chem., 69 (1965), 1238.
8. M.J.E. Golay: Nature, 202 (1964), 489.
9. D.H. Desty, A. Goldup, G.R. Luchurst and W.T. Stanton: "Gas Chromatography", van Swaay (Ed.), Butterworths, London, 1962.
10. D.H. Everett and C.T.H. Stoddart: Trans. Faraday Soc., 57 (1961), 746.
11. D.H. Everett: Trans. Faraday Soc., 61 (1965), 1637.
12. J.R. Conder and J.H. Purnell: Trans. Faraday Soc., 64 (1968), 3100.
13. R.L. Martin: Anal. Chem., 33 (1961), 347.
14. R.L. Martin: Anal. Chem., 35 (1963), 116.
15. D.E. Martire, R.L. Pecsok and J.H. Purnell: Trans. Faraday Soc., 61 (1965), 2496.
16. D.E. Martire, R.L. Pecsok and J.H. Purnell: Nature, 203 (1964), 1279.
17. D.E. Martire: Anal. Chem., 36 (1965), 244.
18. R.L. Pecsok and A. de Yllane and A. Abdul-Karim: Anal. Chem., 36 (1964), 452.
19. J.R. Conder in: "Progress in Gas Chromatography", Vol.6, J.H. Purnell (Ed.), Interscience, London, 1968.
20. D.E. Martire and L.Z. Pollara in: "Advances in Chromatography", Vol.1., J.C. Giddings and R.A. Keller (Eds.), Marcel Dekker, New York, 1966.
21. A.J. Ashworth and D.H. Everett: Trans. Faraday Soc., 56 (1960), 1604.
22. A.J.B. Cruickshank, M.L. Windsor and C.L. Young: Proc. Roy. Soc., A295 (1966), 259.
23. P. Urone, J.F. Parcher in: "Advances in Chromatography", Vol.6, J.C. Giddings and R.A. Keller (Eds.), Marcel Dekker, New York, 1968.
24. P. Urone and J.F. Parcher: Anal. Chem., 38 (1966), 270.
25. V.G. Berezkin and V.M. Fateva: J. Chromatogr., 58 (1971), 73.
26. V.G. Berezkin: J. Chromatogr., 65 (1972), 227.
27. J.R. Conder, D.C. Locke and J.H. Purnell: J. Phys. Chem., 73 (1969),700.
28. D.F. Cadogan, J.R. Conder and J.H. Purnell: J. Phys. Chem., 73 (1969), 708.
29. D.E. Martire and R. Riedle: J. Phys. Chem., 72 (1968), 3478.
30. J.R. Conder: J. Chromatogr., 39 (1969), 273.

31. H. Liao and D.E. Martire: Anal. Chem., 44 (1972), 498.

32. J.R. Conder and J.H. Purnell: Trans. Faraday Soc., 65 (1969), 824.

33. J.R. Conder and J.H. Purnell: Trans. Faraday Soc., 65 (1969), 839.

34. E. Glueckauf: J. Chem. Soc., (1947), 1302.

35. E. Glueckauf: Nature, 156 (1945), 748.

36. R. Stock: Anal. Chem., 33 (1961), 1966.

37. C.J. Chen and J.F. Parcher: Anal. Chem., 43 (1971), 1738.

38. R.H. Peret and J.H. Purnell: J. Chromatogr., 7 (1962), 455.

39. D.H. James and C.G.S. Phillips: J. Chem. Soc., (1954), 1066.

40. P.E. Eberly Jr. and C.N. Kimberlin Jr.: Trans. Faraday Soc., 57 (1961), 1169.

41. R.A. Beebe and P.L. Evans: J. Phys. Chem., 7 (1966), 1009.

42. E. Cremer and H.F. Huber: "Gas Chromatography", Third International Symposium, N. Brenner (Ed.), Academic Press, 1962.

43. P.A. Sewel and R. Stock: J. Chromatogr., 50 (1970), 10.

44. D. Dollimore, G.R. Heal and D.R. Martin: J. Chromatogr., 50 (1970),209.

45. F.I. Stalkup and R. Kobayashi: A.I.Ch.E. Journal, 9 (1963), 121.

46. H.B. Gilmer and R. Kobayashi: A.I.Ch.E. Journal, 11 (1965), 702.

47. C.F. Chueh and W.T. Ziegler: A.I.Ch.E. Journal, 11 (1965), 508.

48. D.I. Lloyd: Ph.D. Thesis, Birmingham University, 1963.

49. M.G. Burnett: Anal. Chem., 35 (1963), 1567.

50. T. Katayama, E.K. Sung and E.L. Lightfoot: A.I.Ch.E. Journal, 11, (1965), 924.

51. P.C. Haarhoff and H.J. Van Der Linde: Anal. Chem., 37 (1965), 1742.

52. N. Dyson and A.B. Littlewood: Trans. Faraday Soc., 63 (1967), 1895.

53. J.F.K. Huber and R.G. Gerritze: J. Chromatogr., 58 (1971), 137.

54. J.W. Gibbs: "Collected Works", Vol.1, Longmans Green, New York, 1931.

55. G.N. Lewis and M. Randall: "Thermodynamics and the Free Energy of Chemical Substances", McGraw-Hill, New York, 1923.

56. R. Techno: Chem. Eng. Sci., 18 (1963), 27.

57. A.K. Hilmi: Ph.D. Thesis, Birmingham University, 1965.

58. J.R. Conder and J.H. Purnell: Trans. Faraday Soc., 64 (1968), 1505.

59. G. Scatchard and L.B. Tichnor: J. Am. Chem. Soc., 74 (1952), 3724.

60. K. Denbeigh: "The Principles of Chemical Equilibrium", Cambridge University Press, London, 1968.

61. J.M. Prausnitz: "Molecular Thermodynamics of Phase Equilibria", Prentice-Hall, 2nd Edition, Englewood Cliffs, N.J., 1969.

62. A.P. Coulborn and E.M. Schoenborn: Trans. Am. Inst. Chem. Engrs., 41 (1945), 421.

63. B.W. Gainey and C.L. Young: Trans. Faraday Soc., 64 (1968), 349.

64. D.L. Shafler and T.E. Daubert: Anal. Chem., 41 (1969), 1585.

65. N.V. Ible and B.F. Dodge: Chem. Eng. Sci., 2 (1953), 120.

66. J.J. Van Laar: Z. Physik. Chem., 72 (1910), 723.

67. J.H. Hildebrand and S.E. Wood: J. Chem. Phys., 1 (1933), 817.

68. J.H. Hildebrand and R.L. Scott: "Solubility of Non-electrolytes", 3rd Edition, Reinhold, New York, 1950.

69. G. Scatchard: Chem. Rev., 8 (1931), 321.

70. P.J. Flory: J. Chem. Phys., 9 (1941), 660.

71. M.L. Huggins: Ann. N.Y. Acad. Sci., 43 (1942), 1.

72. M. Margules: Sitzber. Akad. Wiss. Wisen. Math. Naturew., Klasse II, 104 (1895), 1243.

73. K. Wohl: Trans. Am. Inst. Chem. Engrs., 42 (1946), 215.

74. K. Wohl: Chem. Eng. Prog., 49 (1953), 218.

75. E. Hala, J. Pick, V. Fried and O. Vilim: "Vapour Liquid Equilibrium", Pergammon Press, London, 1958.

76. A.I.M. Keulemans: "Gas Chromatography", Reinhold, New York, 1959.

77. A.J. Ashworth and D.H. Everett: Trans. Faraday Soc., 56 (1960), 1609.

78. D.H. Everett and F.L. Swinton: Trans. Faraday Soc., 59 (1963), 2476.

79. D.H. Everett and R. Munn: Trans. Faraday Soc., 60 (1964), 1951.

80. S.H. Langer and J.H. Purnell: J. Phys. Chem., 67 (1963), 263.

81. S.H. Langer and J.H. Purnell: J. Phys. Chem., 70 (1966), 904.

82. G.M. Wilson: J. Am. Chem. Soc., 86 (1964), 127.

83. R.V. Orye and J.M. Prausnitz: Ind. Eng. Chem., 57 (1965), 18.

84. H. Renon and J.M. Prausnitz: A.I.Ch.E. Journal, 14 (1968), 135.

85. J.F. Heil and J.M. Prausnitz: A.I.Ch.E. Journal, 12 (1966), 678.

86. I.A. Wiehe, S. Dorai, C.G. Roder and A. Chandrasekhar: Chem. Eng. Sci., 26 (1971), 901.

87. R.K. Clark and H.H. Schmidt: J. Phys. Chem., 69 (1965), 3682.

88. W.C. Edmister, J.M. Prausnitz and K.C. Chow: A.I.Ch.E. Journal, 6 (1960), 214.

89. A.J.B. Cruickshank, B.W. Gainey and C.L. Young: Trans. Faraday Soc., 64 (1968), 337.

90. B.W. Gainey and C.L. Young: Trans. Faraday Soc., 65 (1969), 47.

91. R.F. Blank and J.M. Prausnitz: Ind. Eng. Chem. Fundam., 3 (1964), 1.

92. J.G. Helpinstill and M. Van Winkle: Ind. Eng. Chem. Proc. Des. Dev., 7 (1968), 213.

93. G.J. Pierotti, C.A. Deal and E.L. Derr: Ind. Eng. Chem., 51 (1959),95.

94. H.R. Null and D.A. Palmer: Chem. Engr. Prog., 65 (1969), 47.

95. H.R. Null: "Phase Equilibrium in Process Design", John Wiley, New York, 1970.

96. A.J.B. Cruickshank, M.L. Windsor and C.L. Young: Proc. Roy. Soc., A295 (1966), 271.

97. M.L. McGlashen and A.J.B. Potter: Proc. Roy. Soc., A267 (1962), 478.

98. G.H. Hudson and J.C. McCoubrey: Trans. Faraday Soc., 56 (1960), 761.

99. C.P. Hicks and C.L. Young: Trans. Faraday Soc., 64 (1968), 2675.

100. D.H. Everett, B.W. Gainey and C.L. Young: Trans. Faraday Soc., 64 (1968), 2667.

101. E.M. Dantzler, C.M. Knobler and M.L. Windsor: J. Chromatogr., 32 (1968), 433.

102. R.L. Pecsok and M.L. Windsor: Anal. Chem., 40 (1968), 1238.

103. C.R. Coan and A.D. King, Jr.: J. Chromatogr., 44 (1969), 429.

104. J.R. Conder and S.H. Langer: Anal. Chem., 39 (1967), 1461.

105. E.A. Guggenheim and C.J. Wormald: J. Chem. Phys., 42 (1965), 3775.

106. S. Brunaeur, P.H. Emmet and E. Teller: J. Am. Chem. Soc., 60(1938), 309.

107. F.M. Nelson and F.T. Eggerton: Anal. Chem., 30 (1958), 1387.

108. J.F. Roth and J. Ellwood: Anal. Chem., 31 (1959), 1738.

109. M.G. Farey and B.G. Tucker: Anal. Chem., 43 (1971), 367.

110. J.M. Coulson and J.F. Richardson: "Chemical Engineering Vol.2", Pergammon Press, Oxford, 1962, p.2.

111. J.H. Arnold: J. Chem. Phys., 1 (1933), 170.

112. L.A. Bromley and C.R. Wielke: Ind. Eng. Chem., 43 (1951), 1641.

113. Perry's Chemical Engineering Handbook, 4th Edition, McGraw-Hill, New York, 1963,

a - 3-229
b - 3-197
c - 3-214

114. B.L. Larger in: "Advances in Chromatography", Vol.1, J.C. Giddings and R.A. Keller (Eds.), Marcel Dekker, New York, 1965.

115. R. Kaider: "Vapour Phase Chromatography", Vol.3, Butterworths, London, 1963.

116. E.R. Adlard, M.A. Khan and B.T. Whitman in : "Gas Chromatography", M. Van Swaay (Ed.), Butterworths, London, 1962.

117. A. Hartkopf: J. Chromatog. Sci., 10 (1972), 145.

118. G.L. Roberts and S,J, Hawkes: J. Chromatog. Sci., 11 (1973), 130.

119. N.F. Brockmeir, R.W. McCoy and J.A. Meyer: Macromolecules, 5 (1972), 130.

120. D. Paterson, Y.B. Tewary, H.P. Schreiber and J.E. Guillet: Macromolecules, 4 (1971), 356.

121. D.F. Fritz and E. sz. Kovats: Anal. Chem., 45 (1973), 1175.

122. Handbook of Chemistry and Physics, 53rd Edition (1972-73), R.C. Weart (Ed.), Chemical Rubber Co., 1972.

123. J.H. Dymond and E.B. Smith: "Second Virial Coefficients of Gases", Clarendon Press, Oxford, 1969.

124. K.S. Pitzer and R.F. Curl, Jr.: J.Am. Chem. Soc., 79 (1957), 2369.

125. R.L. Halm and L.I. Stiel: A.I.Ch.E. Journal, 17 (1971), 259.

126. B.E. Eichinger and P.J. Flory: Trans. Faraday Soc., 64 (1968), 2035.

127. D. Paterson: J. Polym. Sci. Part C, No.16, (1968), 3379.

128. J.L. Gardon: J. Paint. Technology, 38 (1966), 43.

129. S.H. Langer and R.J. Sheeham in: "Progress in Gas Chromatography", Vol.6, J.H. Purnell (Ed.), Interscience, London, 1968.

130. A.N. Williams: Private Communication, University of Aston in Birmingham.

131. M.L. McGlashen and K.W. Morcom: Trans. Faraday Soc., 57 (1961), 581.

132. A.M. Bueche: J. Polym. Sci., 15 (1955), 97.

133. H. Burrel: Inter. Chem. Rev., 14 (1955), 3.

134. D. Mangaraj: Macromol. Chem., 65 (1963), 39.

135. K.B. Yerric and H.N. Beck: Rubber Chem. Tech., 37 (1964), 261.

136. F.P. Price, S.G. Martin and J.P. Bianchi: J. Polym. Sci., 22(1956),49.

137. C.L. Hussey and J.F. Parcher in: "Advances in Chromatography 1973", A. Zlatkis (Ed.), 8th International Symposium, Toronto, April 1973.

138. S. Bruin: Ind. Eng. Chem., Fundam., 9 (1970), 305.

139. D. Tassios: A.I.Ch.E. Journal, 17 (1971), 1367.

140. L.B. Schreiber and C.A. Eckert: Ind. Eng. Chem., Fundam., 10 (1971), 572.

141. D. Smith: Private Communication, University of Aston in Birmingham.

142. J.J. Van Deemter, F.J. Zuiderweg and A. Klinberg: Chem. Eng. Sci., 5 (1956), 271.

143. A. Klinberg and F. Sjenitzer: Chem. Eng. Sci., 5 (1956), 258.

144. R.M. Bethea and D.C. Bentsen: J. Chromatog. Sci., 10 (1972), 575.

145. J.C. Giddings: Anal. Chem., 35 (1963), 1338.

146. J.C. Giddings: Anal. Chem., 38 (1966), 490.

147. R.M. Bethea and F.S. Adams: Anal. Chem., 33 (1961), 832.

148. K.P. Hupe, U. Busch and K. Winde: J. Chromatog. Sci., 7 (1969), 1.

149. J.C. Giddings: J. Gas Chromatog., 1 (1963), 38.

150. J.C. Giddings: J. Gas Chromatog., 1 (1963), 12.

151. G.W.A. Rijinders in: "Advances in Chromatography", Vol.3, J.C. Giddings and R.A. Keller (Eds.), Marcel Dekker, New York, 1966.

152. V. Pretorius and K. De Clerk in: "Preparative Gas Chromatography", A. Zlatkis and V. Pretorius (Eds.), Wiley-Interscience, New York,1969.

153. L. Mir: J. Chromatog. Sci., 9 (1971), 436.

154. J. Naworski, Jr., D.R. Leonard and J.A. Williams, Jr.: J. Chromatog. Sci., 10 (1972), 153.

155. J. Albrecht and M. Verzele: J. Chromatog. Sci., 8 (1970), 586.

156. J. Albrecht and M. Verzele: J. Chromatog. Sci., 9 (1971), 745.

157. D.A. Craven: J. Chromatog. Sci., 8 (1970), 540.

158. J.R. Conder and J.H. Purnell: Chem. Eng. Sci., 25 (1970), 353.

159. J.R. Conder: Symposium on "Novel Separation Techniques", Instn. Chem. Engrs., London, Jan. 1973.

160. K. De Clerk and V. Pretorius: Sep. Sci., 6 (1971), 401.

161. K.P. Hupe: J. Chromatog. Sci., 9 (1971), 11.

162. J.M. Ryan and G.L. Dienes: Drug and Cosmetic Industry, 99 (1966), 60.

163. J.M. Ryan, R.S. Timmins and J.F. O'Donnell: Chem. Eng. Prog., 64, (1968), 53.

164. J.M. Ryan: Chem. Engrng., May, 19 (1969), 170.

165. A.B. Carel, R.E. Clement and G. Perkins Jr.: J. Chromatog. Sci., 7 (1969), 218.

166. G.R. Fitch, M.E. Probert and P.F. Tiley: J. Chem. Soc., (1962),4875.

167. P.E. Barker and D. Critcher: Chem. Eng. Sci., 13 (1960), 82.

168. P.E. Barker and D. Lloyd: Symposium on "The Less Common Means of Separation", 1963, Instn. Chem. Engrs., London, 1964, 68.

169. P.E. Barker and D.H. Huntington: J. Gas Chromatog., 4 (1966), 59.

170. P.E. Barker and S. Al-Madfai: J. Chromatog. Sci., 7 (1969), 425.

171. P.E. Barker and D.H. Huntington in: "Gas Chromatography 1966", Littlewood (Ed.), Institute of Petroleum, London, 1967.

172. P.E. Barker and R.E. Deeble: Anal. Chem., 45 (1973), 1121.

173. D.H. Huntington: Ph.D. Thesis, University of Birmingham, 1966.

174. S. Al-Madfai: Ph.D. Thesis, University of Birmingham, 1969.

175. P.F. Tiley: J. Appl. Chem., 17 (1967), 131.

176. B.D. Smith and W.K. Brinkley: A.I.Ch.E. Journal, 6 (1960), 44.

177. D.W. Pritchard, M.E. Probert and P.F. Tiley: Chem. Eng. Sci., 26 (1971), 2063.

178. T.H. Chilton and A.P. Colburn: Ind. Eng. Chem., 27 (1935), 255.

179. R.E. Deeble: Private Communication, University of Aston in Birmingham.

180. M.V. Sussman, K.N. Astil, R. Rombach, S.S. Chen and A.A. Cerullo: "Recent Advances in Separation Techniques", A.I.Ch.E., Symposium Series, No.120, 68 (1972), 72.

181. E.J. Tuthil: J. Chromatog. Sci., 8 (1970), 285.

182. Brit. Patent Appl. No. 5764/68 and 44375/68.

183. D.T. Sawyer and G.L. Hargrave in: "Progress in Gas Chromatography", Vol.6, J.H. Purnell (Ed.), John Wiley, New York, 1968.

184. A.J.P. Martin: Analyst, 81 (1956), 52.

185. A.J.P. Martin in: "Vapour Phase Chromatography", D.H. Desty (Ed.), Butterworths, London, 1957.

186. A.J.P. Martin and R.L.M. Synge: Biochem. J., 35 (1941), 1358.

187. J.R. Anderson and K.H. Napier: Australian J. Chem., 10 (1957),250.

188. J.R. Anderson: J. Am. Chem. Soc., 78 (1956), 5692.

189. A.P. Kudchadker, G.A. Alani and B.J. Zwolinski: Chem. Rev., 68 (1968), 659.

190. I.F. Golubev: "Viscosity of Gases and Gas Mixtures", Israel Programme for Scientific Translations, Jerusalem, 1970.

191. C.R. Wilke: J. Chem. Phys., 18 (1950), 517.

192. W.D. Lansing and E.O. Kraemer: J. Am. Chem. Soc., 57 (1935), 1369.

193. H. Mark: J. Am. Chem. Soc., 65 (1943), 2319.

194. R. Houwink: J. Pract. Chem., 57 (1940), 15.

195. H. Batzer: Macromol. Chem., 10 (1953), 13.

196. S.R. Rafikov, S.H. Pavlova and I.I. Iverdokheboua: "Determination of Molecular Weights and Polydispersity of High Polymers", Israel Programme for Scientific Translations, Jerusalem, 1964.

197. M. Kuroto and W.H. Stockmayer: Adv. Polym. Sci., 3 (1963), 196.

198. J. Brandrup and E.H. Immergut: "Polymer Handbook", John Wiley, New York, 1966.

199. P. Flory: J.Am. Chem. Soc., 58 (1936), 1877.

200. K.S. Pitzer: J. Am. Chem. Soc., 77 (1955), 3427.

201. E.M. Dantzler and C.M. Knobler: J. Phys. Chem., 75 (1969), 1341.

202. J.P. O'Connell and J.M. Prausnitz: Ind. Eng. Chem., Proc. Des. Dev., 6 (1967), 245.

203. K.A. Kobe and R.E. Lynn, Jr.: Chem. Rev., 52 (1953), 117.

204. J.J. Carberry and R.H. Bretton: A.I.Ch.E. Journal, 4 (1958), 367.

205. J.F. Wehner and R.H. Williams: Chem. Eng. Sci., 6 (1956), 89.

206. C.A. Slescher, Jr.: A.I.Ch.E. Journal, 5 (1959), 146.

207. T. Miyauchi and T. Vermeulen: Ind. Eng. Chem., Fundam., 2 (1963),113.

208. P.V. Danckwerts: Chem. Eng. Sci., 2 (1953), 1.

209. J.W. Hiby in: "The Interaction between Fluids and Particles", R.A. Rottenburg (Ed.), Instn. Chem. Engrs., London, 1962.

210. K.W. McHenry, Jr. and R.H. Wilhelm: A.I.Ch.E. Journal, 3 (1957), 83.

NOMENCLATURE

A_{ij}	Constants in the Margules, Van Laar and Wilson Equations.
A_L	Liquid surface area.
A_S	Solid surface area.
a	Product collection rate of Component A from top off-take, Mark-Houwink constant, Mass transfer area per unit length.
a_c	Column cross sectional area occupied by gas.
a_L	Bulk liquid concentration of solute.
B_{ii}	Second virial coefficient of component i.
B_{ij}	Cross second virial coefficient of i.j mixture.
B*	Reduced second virial coefficient (BP_c/RT_c)
b	Product collection rate of component B from top off-take.
c	Gas phase concentration.
C_i	Inlet gas phase concentration.
C_t	Total processing cost per unit time.
D_g	Diffusivity in the gas phase.
D_s	Diffusivity in the liquid phase.
d_c	Column diameter.
d_p	Mean particle diameter.
E	Total diffusivity in the gas phase (Molecular diffusivity and Eddy diffusivity).
F(o)	Volumetric flow rate of pure carrier gas reduced to column outlet pressure.
F(y)	Total volumetric flow rate of carrier gas reduced to column outlet pressure.
f	Fugacity.
f_n	External feed concentration to n^{th} plate.

G	Molar Gibbs Energy, Volumetric gas flow rate at mean column conditions, Volumetric gas flow rate in the separating section.
G^E	Excess molar Gibbs energy.
G_b	Volumetric gas flow rate of bottom off-take.
G_{ij}	Constants in the NRTL and Heil equations.
G_s	Volumetric gas flow rate in the stripping section.
$\bar{g}$	Partial molar Gibbs energy.
$\bar{g}^E$	Excess partial molar Gibbs energy of mixing.
g_{ij}	Constants in the Heil and NRTL equations - a measure of the interactions between the i-j pair of molecules.
H^E	Excess molar enthalpy of mixing.
h	Height of a theoretical plate.;
$\bar{h}^E$	Excess partial molar enthalpy of mixing.
J_n^m	Correction factor for gas phase compressibility $\frac{n}{m}\frac{(p_i/p_o)^m-1}{(p_i/p_o)-1}$
K	Partition coefficient (q/c).
K_a	Liquid surface adsorption coefficient.
K_Ga	Overall gas phase mass transfer coefficient.
K_L	Bulk liquid partition coefficient.
K_s	Solid surface adsorption coefficient.
k	Mass ratio $K\frac{V_L}{V_g}$
L,l	Column length.
M	Molecular weight.
N	Number of theoretical plates.
N_D	Flux of molecules due to axial diffusion.
N_{OG},N_t	Number of transfer units.
n	Number of moles of the liquid phase, Number of carbon atoms in the molecular chain.

n_i	Number of moles of component, i, Number of methylene groups in the component, i.
P	Pressure.
P^o	Vapour pressure.
P_c	Critical pressure.
P_e	Peclet number.
P_r	Reduced pressure (P/P_c).
$\|P\|$	Parochor contribution to P_c.
ΔP	Eduljee contribution to P_c.
p_i	Column inlet pressure.
p_o	Column outlet pressure.
Q_r	Preparative column efficiency (throughput per unit time).
q	Liquid phase concentration.
R	Gas constant, Resolution (x/4), Fraction of feed in vapour phase.
$[R_D]$	Molar refraction contribution to P_c.
r	Size ratio of liquid phase molecules to solute molecules.
S^E	Excess molar entropy of mixing.
s	Number of segments per polysegmented molecule.
$\bar{s}^E$	Excess partial molar entropy of mixing.
T,t	Temperature.
T_b	Boiling point temperature.
T_c	Critical temperature.
T_r	Reduced temperature.
ΔT	Eduljee contribution to T_c
$\bar{u}$	Mean superficial velocity in the column.
u_i	Inlet velocity to the column.

$\bar{V}$	Partial molar volume.
V^o	Molar volume of pure component.
V_b	Molar volume of a component at its boiling point.
V_c	Critical Volume.
V_G	Volume of a plate occupied by gas.
V_g	Column gas hold-up.
V_L	Volume of liquid phase in the column, Volume of a plate occupied by liquid phase.
V_N	Net retention volume $(V_R - V_g)$
V_N^o	Corrected net retention volume.
V_R'	Corrected retention volume $(J_3^2 V_R)$.
V_m	Volume of gas adsorbed when the surface of the adsorbent is covered with a single layer of molecules.
V_n	Total plate volume $(V_G + KV_L)$.
W	Feed rate of solute to the column.
w	Accentric factor, Dimensionless length term.
w_H	Accentric factor of a polar molecule's homomorph.
x	Mole fraction in the liquid phase.
Δx	Distance between two peak maxima.
y	Mole fraction in the gas phase.
y_o	Mole fraction in the gas phase measured at column outlet pressure.
z	Number of nearest neighbour sites to a given segment of the large molecule in a solution containing different size molecules.

Greek

α	Separation factor $(K_2/K_1, K_2 \; K_1)$
α'	Stripping factor (G/LK).
α_{ij}	Constant in the NRTL equation.

δ	Solubility parameter, Factor allowing for the effect of finite column length on the range of separation.
β	Term for the effect of gas phase non-ideality on the net retention volume ($(2B_{12}-\bar{V}_1)/RT$), Factor allowing for the effect of concentration on the partition coefficient.
γ	Activity coefficient.
ϕ	Volume fraction in the liquid phase.
ϕ_{max}, ϕ_{min}	Operating G/L in the separating section which are the maximum and minimum values to allow products of the required purity to be achieved.
$\Gamma_2^{(1)}$	Excess liquid surface concentration.
Γ	Dimensionless gas phase concentration.
φ	Surface tension, Dimensionless liquid phase concentration.
ρ	Size ratio of solute molecules to liquid phase molecules, Density.
μ	Chemical potential, Dipole moment, Absolute viscosity.
τ	Polar part of the solubility parameter.
T_{ij}	Constants in the NRTL and Heil equations.
η	Constant in the O'Connell-Prausnitz equation.
χ_{ij}	Interaction parameter between the i-j pair of molecules.
λ	Non-polar part of the solubility parameter.
λ_{ij}	Constant in the Wilson equation.
σ	Standard deviation of a gaussian peak.

Subscripts

L	Liquid state.
V	Vapour state.
o	Pure state.
∞	Infinite dilution.

Other symbols are defined in the thesis.